

UNIVERSITY OF CYPRUS



FACULTY OF ENGINEERING
DEPARTMENT OF ARCHITECTURE

«RECONFIGURABLE RIGID-BAR LINKAGE STRUCTURES
BASED ON A DUAL EFFECTIVE CRANK–SLIDER APPROACH»

M.Sc. DISSERTATION

CONSTANTINA THEOKLI

NICOSIA
MAY 2021

CONSTANTINA THEOKLI

CONSTANTINA THEOKLI

Dedicated to my family

© Constantina Thekli

CONSTANTINA THEOKLI

«RECONFIGURABLE RIGID-BAR LINKAGE STRUCTURES BASED
ON A DUAL EFFECTIVE CRANK–SLIDER APPROACH»

by

Constantina Theokli

Thesis supervisor:

Dr. Marios C. Phocas, Professor

Department of Architecture, University of Cyprus

Examination committee:

Dr. Marios C. Phocas, Professor

Department of Architecture, University of Cyprus

Dr. Aimilios Michael, Assistant Professor

Department of Architecture, University of Cyprus

Dr. Eftychios Christoforou, Assistant Professor

Department of Mechanical and Manufacturing Engineering, University of Cyprus

CONSTANTINA THEOKLI

SPECIAL THANKS

It is a genuine pleasure to express my deep gratitude to my thesis supervisor, Dr. Marios C. Phocas, Professor at the Department of Architecture of the University of Cyprus. His prompt inspirations, timely advice and constant encouragement have been of substantial importance for the development of this thesis. His guidance, ideas and feedback have been invaluable.

I am also very grateful to Dr. Eftychios Christoforou, Assistant Professor at the Department of Mechanical and Manufacturing Engineering, University of Cyprus, for the valuable advices given to me for the successful development of the thesis. I would also like to thank Konstantinos Petrou, M.Sc. student at the Department of Mechanical and Manufacturing Engineering of the University of Cyprus, for the fruitful cooperation in the last years.

Finally, I would like to thank my family and friends for providing me with constant support and continuous encouragement throughout my years of study.

CONSTANTINA THEOKLI

ABSTRACT

Deployable structures have been used throughout history, but it was not until the beginning of the twentieth Century that there was an emergency of thought inspired by the speed and technological advances of the Industrial Revolution. This type of structures is considered as a special case within the broader class of adaptive and morphing structures, which are characterized by their ability to change shape. In this context, adaptability, as a post-design reflection progress, refers to a framework within which variable and fixed parameters are defined in such a way that customization and optimization are enhanced at various levels.

The current research focuses on the design and analysis of a reconfigurable structure and the investigation of its morphological and kinetic behavior. It refers to the Effective Crank–Slider reconfiguration approach, namely a kinematics approach that stepwise reduces a planar system to an externally actuated 1-DOF system, in order to adjust each joint angle of the planar system from an initial, to a target position. Two control system configurations are proposed following horizontal and vertical actuation of the structure. The structure consists of aluminum bars, interconnected via joints and sliders. At midspan the structural linkage is further supported on diagonals positioned within the system to form a V- or X-shape according to the reconfiguration requirements of the system. In the first alternative, the V-diagonals are rigidly supported on the structural grid at midspan and pin connected with a horizontal member on the top. On the top of the structure, a linear actuator and a sliding block are applied that allow movement of the structure. In the second alternative, the X-diagonals are pin supported on the structural grid and connected with the beam of the linkage at midspan. The diagonals consist of four telescopic round hollow sections with an actuator attached to each one, that control the kinematics of the linkage. Each internal joint of the linkage is equipped with brakes, whereas in each reconfiguration step, two joints are released. Through movement of the slider in each step, the selected joint angles adjustment may provide symmetrical or non-symmetrical configurations of the system.

Initially, the typologies of deployable and reconfigurable lightweight structures are presented. The analysis of the proposed systems is based on the initial and target position of the corresponding

planar linkages. In following, aspects of construction design of the proposed spatial structure are presented, referring to the system supports, the members and their joint connections, as well as the actuation components that enable horizontal or vertical reconfigurations. Subsequently, the related control concept applied and motion planning alternatives are investigated. Among different feasible sequences, the ones with less required steps are selected and investigated with regard to the highest maximum brake torques and slider displacements. The corresponding spatial structure envelope consists of ETFE membranes with integrated thin photovoltaic films applied on two longitudinal rows on each side. In a simulation analysis are derived the solar irradiance and the energy production by the photovoltaic units in the initial and selected target positions of the system. The case study refers to Larnaca, Cyprus, and Stockholm, Sweden, and the solstices occur annually, on the 21st of December, March, June and September.

The overall aim of the study is the development and investigation of a reconfigurable system, achieving specific symmetrical and non-symmetrical configurations with as few reconfiguration steps as possible. The kinematics approach applied provides maximum flexibility and endurance with minimum required actuation energy. The photovoltaic units integrated with the flexible building envelope enable high levels of energy production, exceeding the performance of a corresponding fixed shape building.

ΠΕΡΙΛΗΨΗ

Οι αναπτυσσόμενες αναδιπλούμενες δομικές κατασκευές έχουν χρησιμοποιηθεί καθ' όλη την πάροδο του χρόνου μέχρι σήμερα, αλλά η ύπαρξη τους γίνεται πιο έντονη στις αρχές του εικοστού αιώνα όπου η τεχνολογία εξελίσσεται ραγδαία με την πρόοδο της Βιομηχανικής Επανάστασης. Αυτός ο τύπος δομικών κατασκευών θεωρείται ως μια ειδική περίπτωση στην ευρύτερη τυπολογία των προσαρμοστικών δομών, οι οποίες έχουν την ικανότητα να αλλάζουν σχήμα. Στη συγκεκριμένη περίπτωση, η προσαρμοστικότητα, ως πρόοδος αντανάκλασης μετά το σχεδιασμό, αναφέρεται σε ένα πλαίσιο εντός του οποίου οι μεταβλητές και σταθερές παράμετροι ορίζονται με τέτοιο τρόπο ώστε η προσαρμογή και η βελτιστοποίηση να ενισχύονται σε διάφορα επίπεδα.

Η παρούσα μελέτη επικεντρώνεται στο σχεδιασμό και στην ανάλυση μιας αναδιπλούμενης δομικής κατασκευής και στη διερεύνηση της μορφολογικής και κινητικής της συμπεριφοράς. Συγκεκριμένα αναφέρεται στην αναδιάρθρωση ενός ενεργοποιητή κίνησης, δηλαδή μία κινηματική προσέγγιση που μειώνει σταδιακά ένα επίπεδο σύστημα σε ένα σύστημα ενός βαθμού ελευθερίας, όπου ενεργοποιείται εξωτερικά προκειμένου να προσαρμόζεται κάθε γωνιά σύνδεσης του επίπεδου συστήματος από την αρχική μορφή του φορέα. Η δομή του πρωτεύοντα στατικού φορέα του συστήματος αποτελείται από ράβδους αλουμινίου σε σειρά, συνδεδεμένες με μηχανισμούς άρθρωσης και ενεργοποιητές κίνησης. Στο μέσο της κατασκευής, ο δομικός φορέας υποστηρίζεται περαιτέρω με διαγώνιες ράβδους είτε σε σχήμα V, είτε σε σχήμα X σύμφωνα με τις απαιτήσεις της αναδιάρθρωσης του συστήματος. Στην πρώτη εναλλακτική, οι V-διαγώνιοι στηρίζονται άκαμπτα στο δομικό πλέγμα στο μέσο του ανοίγματος της κατασκευής και συνδέονται αρθρωτά με οριζόντιο μέλος στο άνω μέρος. Στην κορυφή εφαρμόζεται ένας γραμμικός ενεργοποιητής και στοιχείο ολίσθησης που επιτρέπουν την κίνηση της δομής. Στη δεύτερη περίπτωση, οι X-διαγώνιοι στηρίζονται αρθρωτά στο δομικό πλέγμα και συνδέονται με τη δοκό του συστήματος στα μέσα του στοιχείου. Οι διαγώνιοι αποτελούνται από τέσσερα τηλεσκοπικά στρογγύλες, κοίλες διατομές με ένα ενεργοποιητή προσαρμοσμένο στο καθένα για τον έλεγχο της κίνησης της δομής. Κάθε εσωτερική άρθρωση του συνδέσμου είναι εξοπλισμένη με φρένα, ενώ σε κάθε βήμα αναδιαμόρφωσης, απελευθερώνονται δύο αρθρώσεις. Σε κάθε βήμα

ο ενεργοποιητής κίνησης μπορεί να δημιουργήσει συμμετρικές και μη συμμετρικές μορφές του συστήματος ανάλογα με τις επιλεγμένες ρυθμίσεις.

Αρχικά, αναλύονται οι έννοιες και οι τυπολογίες αναδιπλούμενων και ελαφριών κατασκευών. Η ανάλυση των προτεινόμενων συστημάτων βασίζεται στην αρχική και τελική μορφή του χωρικού συστήματος. Στη συνέχεια, παρουσιάζονται πτυχές του κατασκευαστικού σχεδιασμού της χωρικής δομής, όπου γίνεται αναφορά στα στηρίγματα του συστήματος, στα μέλη και στις συνδέσεις τους, καθώς και στα στοιχεία ενεργοποίησης που επιτρέπουν οριζόντιες ή κάθετες αναδιαμορφώσεις. Στην ενότητα αυτή, εξετάζονται η ιδέα ελέγχου που έχει τύχει εφαρμογής και εναλλακτικές σεναρίων κίνησης για την επίτευξη συγκεκριμένων μορφών του μοντέλου. Για τις μορφές αυτές επιλέγονται και διερευνώνται τα σενάρια με τα λιγότερα απαιτούμενα βήματα με κριτήριο τις υψηλότερες μέγιστες ροπές φρένων και μετατοπίσεις του ενεργοποιητή. Το κέλυφος του δομικού φορέα της χωρικής κατασκευής αποτελείται από μεμβράνες ETFE και λεπτές μεμβράνες φωτοβολταϊκών, τα οποία εφαρμόζονται σε δυο σειρές από κάθε πλευρά. Βάσει ανάλυσης με προσομοίωση, προκύπτει η ηλιακή ακτινοβολία και η παραγωγή ενέργειας από τις φωτοβολταϊκές μεμβράνες στην αρχική και επιλεγμένες τελικές μορφές του συστήματος. Η περίπτωση μελέτης αναφέρεται στην Λάρνακα, Κύπρο, και στη Στοκχόλμη, Σουηδία, κατά τα ηλιοστάσια ετησίως, στις 21 Δεκεμβρίου, Μαρτίου, Ιουνίου και Σεπτεμβρίου.

Γενικότερο στόχο της μελέτης αποτελεί η ανάπτυξη και η διερεύνηση ενός προσαρμοστικού συστήματος δομικής κατασκευής, επιτυγχάνοντας συγκεκριμένες συμμετρικές και μη συμμετρικές μορφές με όσο το δυνατό λιγότερα βήματα μετασχηματισμού. Η μέθοδος κινηματικής επιφέρει μέγιστη ευελιξία και αντοχή με ελάχιστη δυνατή απαιτούμενη ενέργεια ενεργοποίησης της κίνησης. Οι φωτοβολταϊκές μονάδες που είναι ενσωματωμένες στο εύκαμπτο περίβλημα του κτιρίου επιτρέπουν υψηλά επίπεδα παραγωγής ενέργειας, υπερβαίνοντας την απόδοση ενός αντίστοιχου κτιρίου σταθερού σχήματος.

CONTENTS

ABSTRACT	9
ΠΕΡΙΛΗΨΗ	11
FIGURES CATALOGUE	15
TABLES CATALOGUE	21
APPENDIX	22
CHAPTER 1 INTRODUCTION	23
1.1 RECONFIGURABLE STRUCTURES	23
1.2 PROTOTYPE DEVELOPMENTS.....	23
1.2.1 Scissor-like elements	24
1.2.2 Tensegrity Structures.....	32
1.2.3 Bar Linkages.....	44
1.3 MOTIVATION AND THESIS STRUCTURE.....	52
CHAPTER 2 DUAL RECONFIGURABLE SYSTEMS	55
2.1 CONTROL SEQUENCES	55
2.1.1 Sequence 1a (S1 _a).....	56
2.1.2 Sequence 1b (S1 _b).....	57
2.1.3 Sequence 1c (S1 _c).....	58
2.1.4 Sequence 1d (S1 _d).....	60
2.1.5 Sequence 1e (S1 _e).....	60
2.1.6 Sequence 1f (S1 _f).....	61
2.1.7 Sequence 2a (S2 _a).....	61

CONTENTS

2.1.8 Sequence 3a (S3 _a).....	63
Sequence 3b (S3 _b).....	64
Sequence 3c (S3 _c):.....	65
CHAPTER 3 CONSTRUCTION DESIGN.....	67
3.1 STRUCTURAL SYSTEM.....	67
3.2 ENVELOPE STRUCTURE.....	79
CHAPTER 4 KINEMATICS ANALYSIS.....	83
4.1 LINKAGE JOINTS.....	83
4.2 MOTION ANALYSIS.....	85
4.3 NUMERICAL RESULTS.....	87
CHAPTER 5 ENERGY APPROACH.....	91
5.1 STRUCTURE USAGE.....	91
5.2 ENERGY APPROACH.....	91
CHAPTER 6 CONCLUSIONS.....	113
APPENDIX.....	115
REFERENCES.....	237

FIGURES CATALOGUE

Figure 1.1 Evolution of self-deployable structures [1.4]	24
Figure 1.2 Scissor hinge systems: a) Translational, b) curvilinear system	25
Figure 1.3 Simple form of scissor-like elements	26
Figure 1.4 Deployability condition for a scissor-like case system	26
Figure 1.5 Scissor-like elements categories: a) Center scissor-pair, b) Off-center scissor-pair, c) Angulated scissor-pair [1.1].....	27
Figure 1.6 Double curved shape structure [1.5].....	28
Figure 1.7 Construction stages of the deployable stage [1.6]	29
Figure 1.8 Deployable structure of the stage floor	30
Figure 1.9 Construction details of deployable stage.....	31
Figure 1.10 The Rolling Bridge, Grand Union Canal Paddington Basin, London [1.7]	31
Figure 1.11 Tensegrity patents: a) Fuller's patent [1.1]; b) Snelson's patent [1.1]	32
Figure 1.12 Configuration of T-prism – Simplex [1.11]	34
Figure 1.13 Icosahedric tensegrity system: a) Side view; b) Top view [1.11]	34
Figure 1.14 Cuboctahedric circuit tensegrity system [1.23].....	35
Figure 1.15 Diamond tensegrity	36
Figure 1.16 Corresponding transformation from and back to doubled-up octahedron.....	36
Figure 1.17 a) Octahedral structure b) planar view of corresponding 3-struts single layer tensegrity system	37
Figure 1.18 Planar view of 6-struts two-layer tensegrity system.....	37
Figure 1.19 Planar view of 9-struts three-layer tensegrity system.....	37

Figure 1.20 Zig-zag structure, Z type configuration: a) Side view; b) Top view 38

Figure 1.21 Top view of tensegrity structure: a) Folded structure showing the numbering of mid-span nodes; b) Deployed structure connected at mid-span as well as x, y and z conventions 40

Figure 1.22 Deployment motion and actuation components of the tensegrity-ring footbridge system [1.9]..... 41

Figure 1.23 ¼ scale ring-module tensegrity footbridge system [1.9] 42

Figure 1.24 5-module tensegrity structure: a) Experimental setup; b) 3-module structure center joint; c) 5-module structure center joint..... 43

Figure 1.25 Plan view: Geometric principle of tensegrity modules 44

Figure 1.26 The basic 4-bar linkage mechanism 46

Figure 1.27 Stepwise reconfiguration of the 9-bar system. Direct actuation approach (Sequence I) and Cable-driven actuation approach (Sequence II) [1.16] 47

Figure 1.28 Experimental setup of direct and cable-driven actuation method of the bar-linkage [1.16]..... 48

Figure 1.29 Joint connection of experimental setup 48

Figure 1.30 Isometric view of the 3-dimensional hybrid reconfigurable structure [1.17]..... 49

Figure 1.31 Horizontal structure of two adjacent linear prototype units and members connections design [1.17] 50

Figure 1.32 Effective crank-slider approach, which is the basis for the stepwise deployment and reconfigurations of the n -bar linkage 51

Figure 1.33 Experimental deployment of the linkage to the first target position [1.15]..... 52

Figure 1.34 Experimental reconfiguration of the linkage from the first to the second target position [1.15]..... 52

Figure 1.35 Experimental deployment of the linkage to the second target position [1.15]..... 52

Figure 2.1 Structure Configurations	56
Figure 2.2 Selected feasible motion sequence 1a, Scale 1:200.....	57
Figure 2.3 Structure Configurations	57
Figure 2.4 Selected feasible motion sequence 1b, Scale 1:200	58
Figure 2.5 Structure Configurations	59
Figure 2.6 Selected feasible motion sequence 1c, Scale 1:200.....	59
Figure 2.7 Structure Configurations	62
Figure 2.8 Selected feasible motion sequence 2a, Scale 1:200.....	63
Figure 2.9 Structure Configurations	64
Figure 2.10 Selected feasible motion sequences in relation to the systems, Scale 1:200.....	64
Figure 3.1 Planar bar linkage structure with horizontal reconfigurability, Scale 1:50.....	68
Figure 3.2 Planar bar linkage structure with vertical reconfigurability, Scale 1:50	69
Figure 3.3 Spatial structure with horizontal reconfigurability, composed of two actuation linkages and intermediate bare linkages.....	70
Figure 3.4 Spatial structure with vertical reconfigurability, composed of two actuation linkages and intermediate bare linkages.....	70
Figure 3.5 Connection principle of beams of structural grid, Scale 1:10	71
Figure 3.6 Linkage beam support connection principle with the structural grid of the system, Scale 1:10	72
Figure 3.7 Linkage beams connection principle, Scale 1:10	73
Figure 3.8 Support principle of V-diagonals to the structural grid, Scale 1:10	74

Figure 3.9 Linear motion actuator connection principle to the planar actuation linkage for horizontal reconfigurability, Scale 1:22.5.....	75
Figure 3.10 Support principle of X-diagonals to the structural grid, Scale 1:20.....	76
Figure 3.11 Linear motion actuator connection principle to the planar actuation linkage for vertical reconfigurability, Scale 1:20.....	77
Figure 3.12 Construction design principle of secondary structure to the planar linkages of the spatial system, Scale 1:10.....	78
Figure 3.13 ETFE roof from below and inflated cushions fixed to a cable structure that easily deform to define the desired warped surface in an industry building.....	79
Figure 3.14 Spatial structure with vertical reconfigurability and ETFE membrane.....	81
Figure 3.15 Spatial structure with horizontal reconfigurability and ETFE membrane.....	81
Figure 3.16 Construction design of ETFE membrane support.....	82
Figure 4.1 Structure Configurations.....	84
Figure 4.2 Structure Configurations.....	85
Figure 4.3 Structure Configurations.....	85
Figure 4.4 Commands ‘Angle’ and ‘Lock’ from standard mates list.....	86
Figure 4.5 Definition of motor and gravity.....	86
Figure 4.6 Specifying the model steps in the timeline view.....	87
Figure 4.7 Example for calculation of torque graph using the ‘result’ command.....	87
Figure 4.8 Brake torques of Sequence 1.....	88
Figure 4.9 Brake torques of Sequence 2.....	88
Figure 4.10 Brake torques of Sequence 3.....	89

Figure 5.1 Thin-film solar cell application	92
Figure 5.2 Transparency of a Photovoltaic System [5.1].....	93
Figure 5.3 Structure of a Photovoltaic Cell [5.3].....	94
Figure 5.4 Average min and max temperatures in Larnaca, Cyprus [5.8].....	95
Figure 5.5 Average sun hours over the year in Larnaca, Cyprus [5.8].....	95
Figure 5.6 Average min and max temperatures in Stockholm, Sweden [5.8]	96
Figure 5.7 Average sun hours over the year in Stockholm, Sweden [5.8]	96
Figure 5.8 Cyprus’s sun path diagrams on 21st of December at 12:00 am (site orientation: 0°) .	98
Figure 5.9 Cyprus’s sun path diagrams on 21st of June at 12:00 am (site orientation: 0°)	98
Figure 5.10 Sweden’s sun path diagrams on 21st of December at 12:00 am (site orientation: 0°)	98
Figure 5.11 Sweden’s sun path diagrams on 21st of June at 12:00 am (site orientation: 0°)	98
Figure 5.12 Solar irradiance on 21st of March at 12:00 am (site orientation: 0°)	99
Figure 5.13 Solar irradiance on 21st of March at 12:00 am (site orientation: 90°)	99
Figure 5.14 Solar irradiance on 21st of June at 12:00 am (site orientation: 0°)	100
Figure 5.15 Solar irradiance on 21st of June at 12:00 am (site orientation: 90°)	100
Figure 5.16 Solar irradiance on 21st of September at 12:00 am (site orientation: 0°).....	101
Figure 5.17 Solar irradiance on 21st of September at 12:00 am (site orientation: 90°).....	101
Figure 5.18 Solar irradiance on 21st of December at 12:00 am (site orientation: 0°)	102
Figure 5.19 Solar irradiance on 21st of December at 12:00 am (site orientation: 90°)	103
Figure 5.20 Energy production of photovoltaic system (site orientation: 0°).....	104
Figure 5.21 Energy production of photovoltaic system (site orientation: 90°).....	104
Figure 5.22 Solar irradiance on 21st of March at 12 am (Site orientation: 0°).....	105

Figure 5.23 Solar irradiance on 21st of March at 12 am (Site orientation: 90°).....	105
Figure 5.24 Solar irradiance on 21st of June at 12 am (Site orientation: 0°).....	106
Figure 5.25 Solar irradiance on 21st of June at 12 am (Site orientation: 90°).....	106
Figure 5.26 Solar irradiance on 21st of September at 12 am (Site orientation: 0°).....	107
Figure 5.27 Solar irradiance on 21st of September at 12 am (Site orientation: 90°).....	107
Figure 5.28 Solar irradiance on 21st of December at 12 am (Site orientation: 0°).....	108
Figure 5.29 Solar irradiance on 21st of December at 12 am (Site orientation: 90°).....	109
Figure 5.30 Energy production of photovoltaic system (Site orientation: 0°).....	109
Figure 5.31 Energy production of photovoltaic system (Site orientation: 90°).....	110
Figure 5.32 Overall energy production of photovoltaic system in Larnaca and Stockholm	111

TABLES CATALOGUE

Table 2. 1 Scheduling table for feasible control sequence 1a.....	56
Table 2.2 Scheduling tables for feasible control sequence 1b.....	58
Table 2.3 Scheduling tables for feasible control sequence 1c.....	59
Table 2.4 Scheduling tables for control sequence 1d.....	60
Table 2.5 Scheduling tables for control sequence 1e.....	60
Table 2.6 Scheduling tables for control sequence 1f.....	61
Table 2.7 Scheduling tables for feasible control sequence 2a.....	62
Table 2.8 Scheduling tables for feasible control sequence 3a.....	64
Table 2.9 Scheduling tables for control sequence 3b.....	65
Table 2.10 Scheduling tables for control sequence 3c.....	65
Table 4. 1 Maximal brake torques.....	89
Table 4. 2 Maximal displacement of sliding block.....	90
Table 5.1 ETFE membrane and BIPV System characteristics.....	97

APPENDIX

Appendix 1 Scenarios of Sequence 2115

Appendix 2: Sun Paths151

Appendix 3: Simulation Results of Solar Irradiance and Energy Production.....173

CONSTANTINA THEOKLI

CHAPTER 1 INTRODUCTION

1.1 Reconfigurable Structures

The interactive relation of society, technology and architecture expanded the area of research, design and application of static structures aiming at transformability and adaptability. The necessity for an architecture that is not static, instead it has the ability to adapt in time through systems with embedded kinetic mechanisms was initially demonstrated by Zuk and Clark [1.1]. Their respective classification was based on the technical processes to be followed for achieving any implied transformations.

Furthermore, technological and conceptual advances that took place in the last 30 years have enabled kinematics to be implemented in functioning prototypes for reconfigurable robotic environments [1.2]. The significance of buildings and components with variable mobility, location, or geometry that constitute timely adaptable systems as to differing external loading, functional and environment conditions, is internationally acknowledged [1.3]. In this context, adaptability, as a post-design reflection progress, refers to a framework within which variable and fixed parameters are defined in such a way that customization and optimization are enhanced at various levels.

Building reconfigurations in particular are directly related to the properties of their integrative parts, the structure and the building envelope. The development of the structure kinetic operability is significant in two aspects; the structural mechanism that enables different geometrical configurations of its components through among others, folding, sliding, expanding and transforming in size and shape, and the control system that directs the structure towards specified transformations, through pneumatic, chemical, magnetic, natural or mechanical processes. The human body may be considered as the most representative example of dynamically interactive living organisms.

1.2 Prototype Developments

In the 1950s, the aerospace industry took an interest in deployable structures, and today probably dominates the research in this field. Deployable structures have found many uses in the industry. Large structures such as satellites, telescopes and antennas have to be packaged in much smaller volumes in spacecraft and once in space they are deployed. This type of structures can be considered of being a special case within the broader class of adaptive and morphing structures, which are characterized by their ability to change shape. They are converted from a closed compact form to a predetermined expanded configuration, based on their geometrical, material and mechanical properties. The kinematics of the system is usually based on a single degree of freedom transformation.

The conception of deployable structures looks towards two different uses in two different contexts. The first is the erection of the structure, i.e. kinematics, and the second is the static and functional behavior when deployed, Fig.1.1.

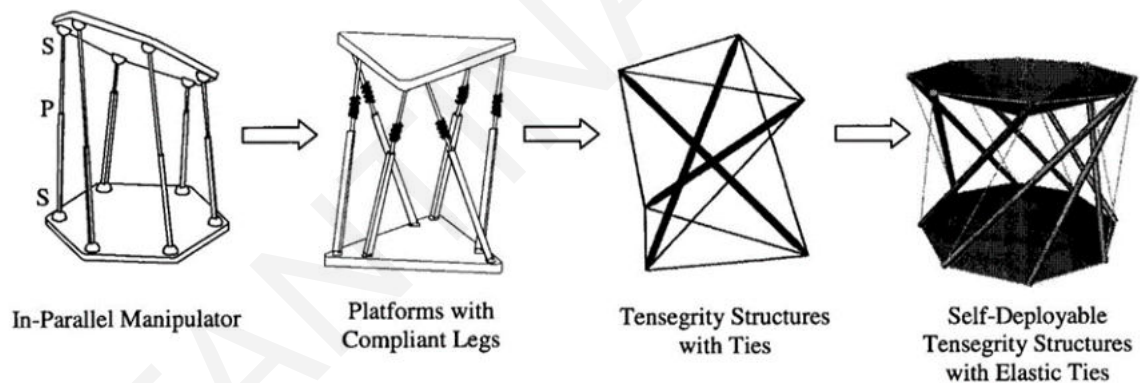


Figure 1.1 Evolution of self-deployable structures [1.4]

1.2.1 Scissor-like elements

Scissor-like elements comprise one of the most common types of deployable structures. This technique is an evolution of the old history and technology knowledge from the history of the lever mechanism. Many terms have been developed through the years, in order to describe scissor structure units: From Pinero's studies on this topic, the early term "Pantograph" in 1961, to Gante's

term “scissor-like elements”, until today’s researcher’s use of the term “Pivot-hinge structure unit” [1.5]. Pinero invented a scissor mechanism, in which each rod has three pivot joints, one on each end and one between the two ends; the center pivots are spread apart, thus lengthening the mechanism, as a whole to a planar pattern, Fig. 1.2.

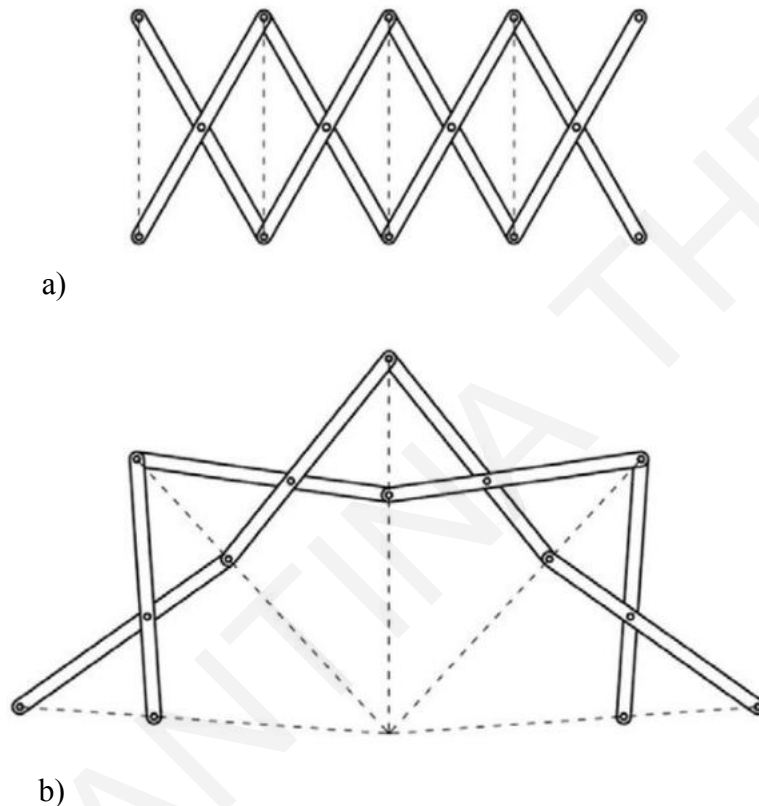


Figure 1.2 Scissor hinge systems: a) Translational, b) curvilinear system

Pinero realized that, if the internal pivot point on a rod is not at the midpoint, then it is possible to create a shell-shaped surface. Following Pinero, Gante’s work referred to the structural behavior of the scissor-hinge structures in analytical and numerical way and the development of methods for their combined geometric and structural design [1.5]. However, Gante’s research concentrated on structures that are transformed between two predefined geometries, an open and a closed one, without attempting to provide additional geometric flexibility in an intermediate shape state.

One of the most important requirements of scissor-hinge structures is that the configuration is able to be contracted into a compact shape. Fig. 1.3 shows a basic scissor-hinge structure. In Fig. 1.4, it can be deduced that in compact shape, the three elements will have one dimension and $C_0, B_0, A_1, C_1, B_1, A_2, C_2, B_2, A_3, C_3, B_3$ will be collinear. The application of the above condition, results to the sum of the lengths of the bar segments on either side of any scissor-like element been equal to the sum of the lengths of the corresponding bar segments of the adjacent scissor-like elements $(a_{i-1}) + (b_{i-1}) = a_i + b_i$.

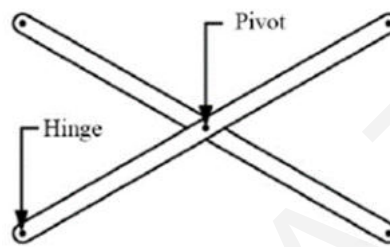


Figure 1.3 Simple form of scissor-like elements

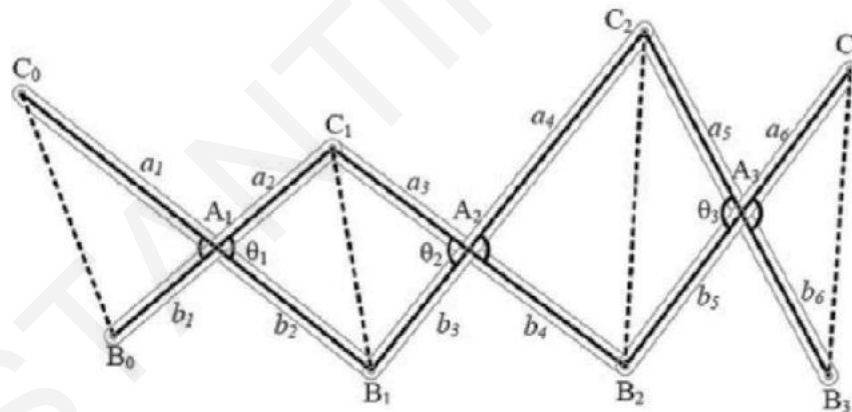


Figure 1.4 Deployability condition for a scissor-like case system

The geometry of a scissor structure depends on the geometry and connection of the scissor modules. Changes in the length of the bars or the location of the pivot points are some parameters that affect the system's shape as well. There are two categories of scissor-hinge structures, based on the properties of the lines connecting their intersection points.

The first category refers to translational scissor-hinge structures, which can only slide without any rotation. This condition is met, if all axes connect the pairs of hinges between adjacent structures and are parallel to each other. The second category consists of curvilinear scissor-hinge structures, whereas the above axes intersect at one or more points and are rotated around their intersection points during deployment. In both of these groups, it is possible to obtain contracted, deployed, or some semi-deployed intermediate forms. Furthermore, in expanding the capabilities of planar scissor structures, a new primary element has been proposed, i.e., the modified scissor-like elements. The Modified scissor-like element is placed in-between the symmetrical scissors and enables higher geometric transformation capability. The three categories are shown in Fig. 1.5.

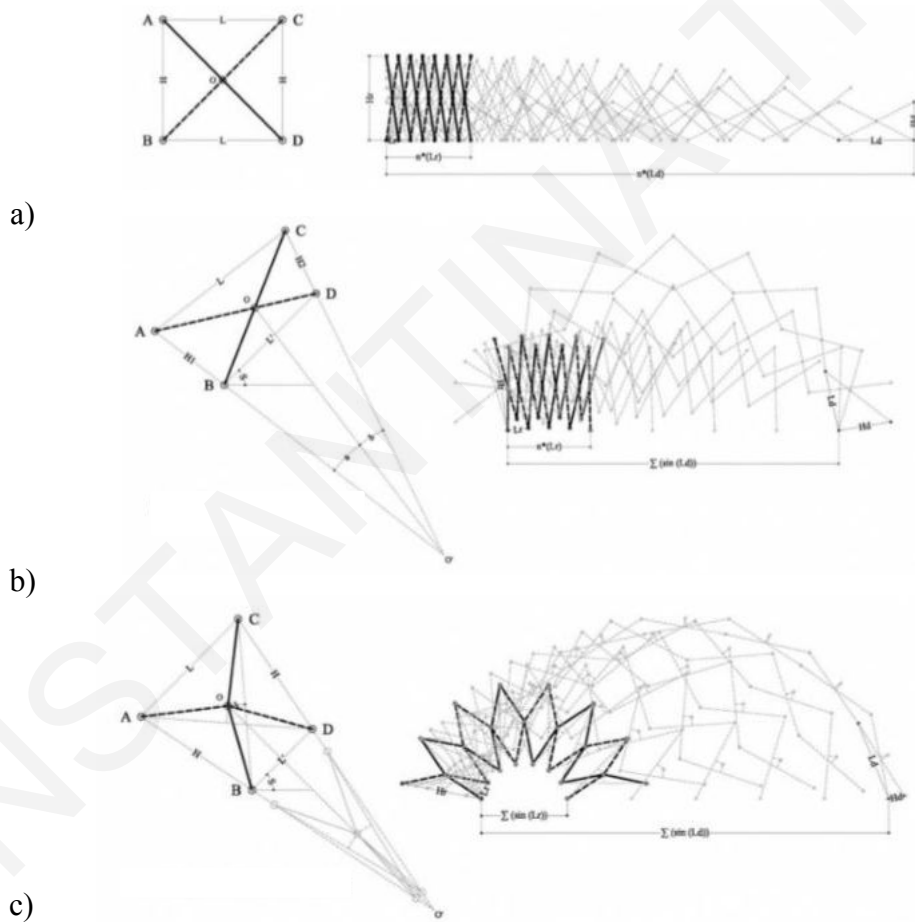


Figure 1.5 Scissor-like elements categories: a) Center scissor-pair, b) Off-center scissor-pair, c) Angulated scissor-pair [1.1]

By extension, scissor gridshells allow easy applications in different environments and functional requirements. Scissor-like gridshells follow the same principles as linear scissor structures. The final form of the shell is determined by the joint assemblage and position. The shell is constructed as planar surfaces of various scissor modules connected to the hinges. The position of the pivots and the length of the bars are important factors for the control of the final geometry of the shell. Scissor-like gridshells can be related to the post-formed shell, as they are first designed and constructed as flat surfaces, which later reach the final form through the scissors' transformations. Actuators in predefined points of the structure, control and provide the motion of the structural surfaces.

In principle, spatial scissor structures are based on combinations of planar scissor modules connected to each other in different ways. The prototype shown in Fig. 1.6 was defined as a cross valut shape with four main frames, connected to the ground. There are four main connections between the main vertical frames, which act as hinges in the plane of each frame. At the intersection points, the scissors are replaced by the scissor-like elements and the actuators are placed on these four points of connection. The spatial structure develops double curved shapes with a minimum number of actuators increasing the feasibility of this kind of applications.

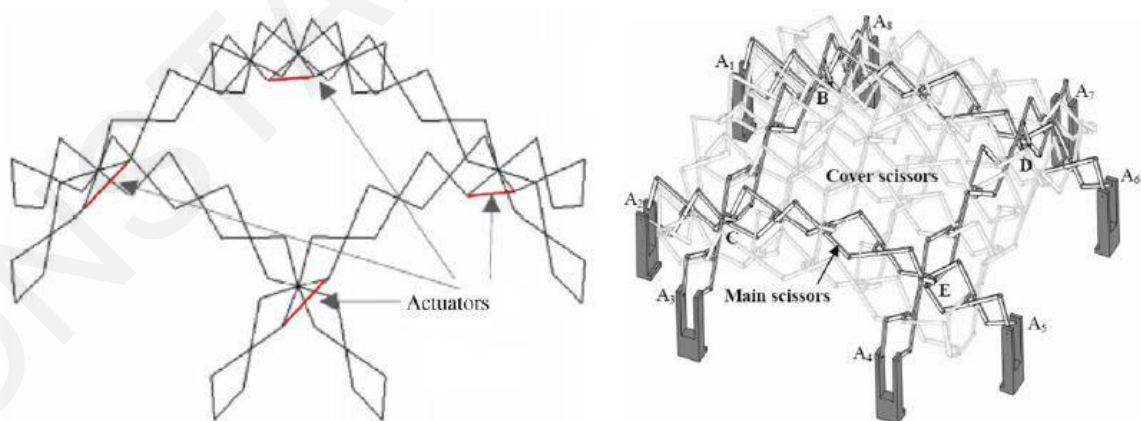


Figure 1.6 Double curved shape structure [1.5]

1.2.1.1 Deployable Stage

The deployable stage shown in Fig. 1.7 was designed by the team SmiA in the frame of a research in the Polytechnic University of Catalonia, in Barcelona [1.6]. The research describes the design process for a deployable, movable stage that can be adapted to different spaces and uses, like cultural events with the characteristics of lightness, adaptability, low energy and limited cost.

The research was based on the study of scissor systems, folding, and in particular, the design of folding-membrane deployable structures. The project consists of a half-circle platform that folds horizontally with the help of structural link bars. The main elements of the structure are the floor elements, the folding floor mechanism, the scissor arches and the membrane. The shell of the stage is divided in five sections attached to the deployable scissor arches, forming a hemispherical dome when lifted. In addition, the overall structure is a half-circumference, radially divided into five equal parts that generate six axes, made of the main beams that support the floor and the arches. The articulated scissor system, which connects the six beams causes the floor to unfold. Each axis is articulated by scissors that allow the rotation of the main axes, from the central point following the trajectory of the half circumference, resembling the opening of a fan.

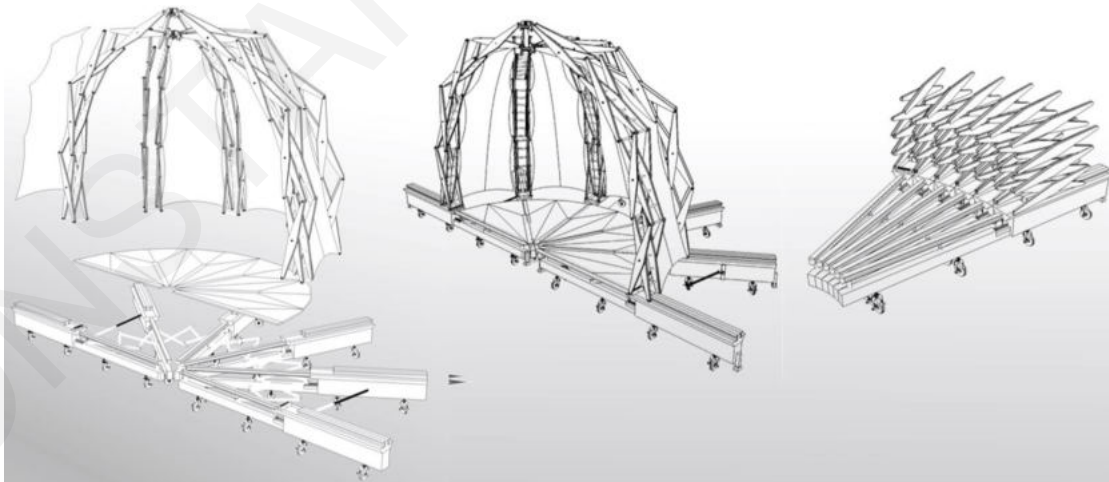


Figure 1.7 Construction stages of the deployable stage [1.6]

The specific characteristics of the system used in this structure corresponds to ten articulated straight eccentric scissors. This type of system generates curves that depend on the eccentricity between each bar that composes the scissors. Every two scissors articulate one of the major axes of the stage in plan. These axes are the beams that support the arches; the beam is articulated by hinges on the ends, allowing the rotation movement to achieve the opening.

The arches on the six axes consist of four double scissor modules, where three of them are asymmetric. The symmetrical scissor is placed at the base of the arch, containing the joint for the support base and the wheels. On the side axes, rolling of the scissors is enabled for inducing bending of the arches. The membrane unfolds and closes through the zip attached to the two sections with the help of the hydraulic cylinder.

In the deployment process, the stage is transported and unfolded to the site and then fixed to the floor, Figs 1.8, 1.9. The six main beams carry the wheels underneath that allow the movement of the stage from one place to another. The beams turn radially with the help of two hydraulic cylinders and the joints between. On the other hand, when the beams are fixed to their position, the unfolding of the arches takes place along with the assembly of the membrane.



Figure 1.8 Deployable structure of the stage floor

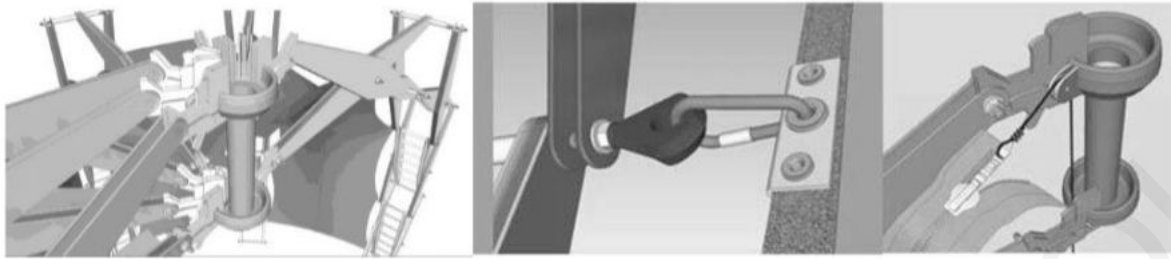


Figure 1.9 Construction details of deployable stage

1.2.1.2 Rolling Bridge

The Rolling Bridge was designed by the award-winning Heatherwick Studio, and was completed in 2004 at Grand Union Canal Paddington Basin, London [1.7]. The studio was commissioned to design a pedestrian bridge to span an inlet of the Grand Union Canal and provide an access route for workers and residents. Also, the bridge needed to open to allow access for the boats.

The concept of the design was inspired by the dinosaur *Apatosaurus* from the film *Jurassic Park*. The animators simulated the animal's flesh by using steel mechanisms covered in silicon rubber to imitate the natural movement and flexibility. It is a twelve-meter bridge and was made from eight triangular segments, which fold towards each other, forming an octagonal sculpture that stands on one side of the canal towpath as shown in Fig. 1.10.

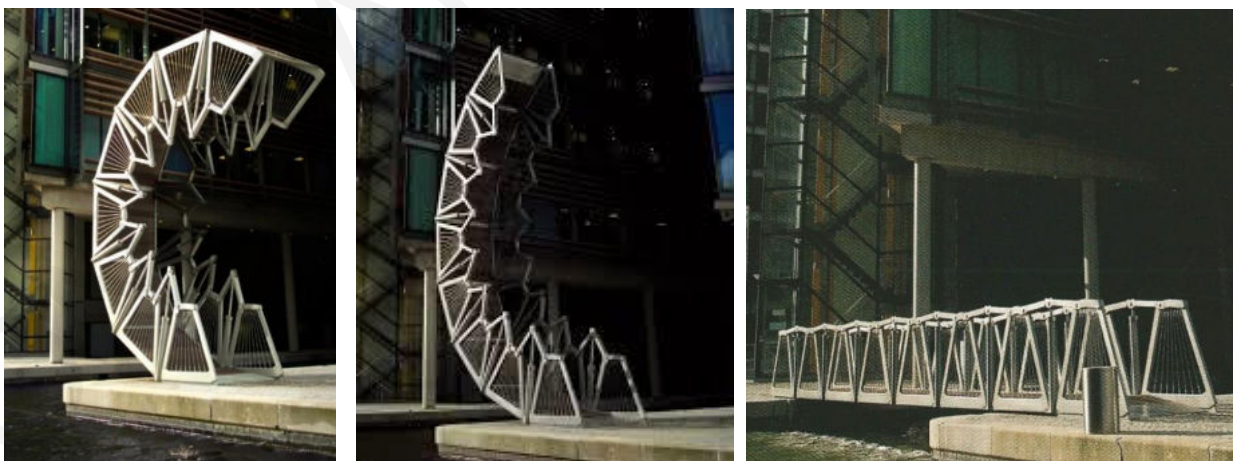


Figure 1.10 The Rolling Bridge, Grand Union Canal Paddington Basin, London [1.7]

As the rams open out of their vertical posts, they extend to the hand rails upwards. The pivoted sections are drawn toward each other and they create a slow curling motion. The bridge has the advantage to stop at any interval.

1.2.2 Tensegrity Structures

The term tensegrity was first introduced by the American inventor and engineer Richard Buckminster Fuller in 1962, referring to the combination of tensional and integrity [1.1]. Tensegrity systems consist of continuous elements in tension, like cables, and discontinuous elements in compression, i.e., bars. Buckminster Fuller described tensegrity structures in a more romantic approach as “islands of compression in a sea of tension”.

While Fuller was the first inventor of the term, the sculptor Kenneth Snelson was claiming the lead with his novel structure X-Piece, Fig. 1.11 [1.1]. Snelson played an essential role in the development of the structural systems, working with pieces composed of rigid and flexible components. In 1976, Pugh developed a more precise definition. A tensegrity system is established, when a set of discontinuous compressive components interacts with a set of continuous tensile components to define a stable volume in space [1.8].

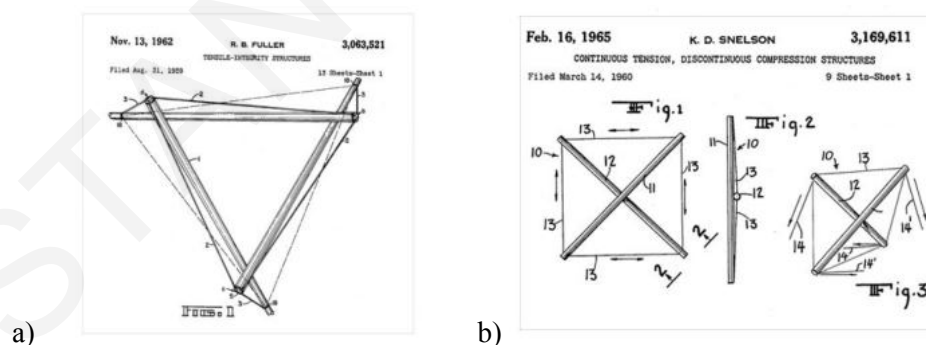


Figure 1.11 Tensegrity patents: a) Fuller's patent [1.1]; b) Snelson's patent [1.1]

Computational technology advances have provided appropriate tools for the study of these structures and the definition of the geometrical and mechanical principles governing them.

Tensegrity structures are impressive, rigid, particularly durable and extremely interesting, because of their integrity resembling a cluster of floating rods. These lightweight systems have a very lively behavior, despite the requirement for high pretension of the tension-only members for stability. When the structures are deployed from a closed form, the systems reach an open form, with the least minimum energy, offering optimized conditions in the mass and load transfer. Also, these systems are efficient, because of the energy reserved in the tendons in the form of tension. In these systems, only small amounts of external energy are required to activate their movement. However, despite their flexibility, tensegrity systems have very limited practical use.

Tensegrity prism (T-prism)

The T-prism was invented by Karl Ioganson in Moscow in 1921 [1.9]. It is the simplest and one of the most instructive members of the tensegrity family. The T-prism has 9 tendons and 3 struts and belongs to a subclass of prismatoids. It has been called tensegrity prism or T-prism as it can be considered as a twisted prism consisting of two triangular faces twisted with respect to each other.

Tensegrity structures are designed by keeping the lengths of tendons and struts constant, and determining the lengths of another set of tendons. When one end of the prism is twisted relative to the other, the rectangular sides of the prism become non-planar quadrilaterals. Thus, two opposite angles of each quadrilateral become obtuse and acute. For the structure to be stable and prestressed, the prism is twisted in such a way that the distance between the obtuse angles is least (an intermediate stage of twisting) and hence, a completely stable T-prism is formed [1.10].

The simplest example of the rhombic configuration is the "simplex" as shown in Fig. 1.12, which is obtained when three compressed members of equal length are inserted in a prismatic unit of nine tensioned members of equal length. Simplex gives birth to the "icosahedric tensegrity system", Fig. 1.13, by coupling two of these systems. The icosahedric tensegrity consists of six struts and twenty-four cables. The struts are parallel to one another, two by two. The equilibrium geometry depends on the distance between two parallel struts [1.11].



Figure 1.12 Configuration of T-prism – Simplex [1.11]

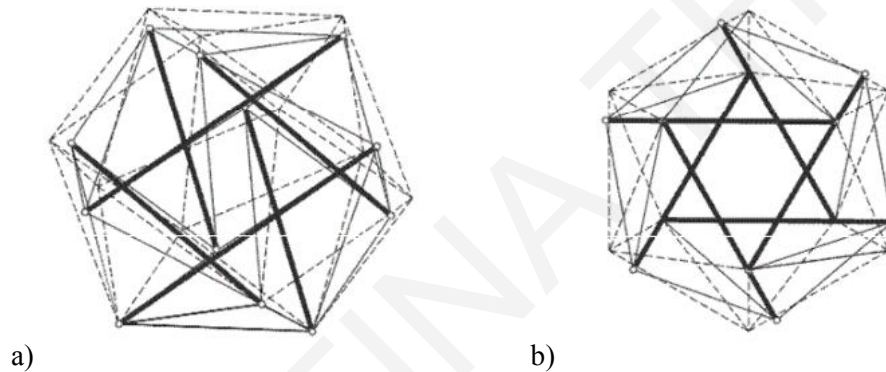


Figure 1.13 Icosahedric tensegrity system: a) Side view; b) Top view [1.11]

Circuit cells were originally used by Fuller, who called the system, "basketry tensegrity". The essential characteristic of this second pattern is the existence of continuous compressed components. Its construction can be derived from a rhombic configuration system with three layers each composed of four struts, when an opposite pair of cables are forced towards one another. Consequently, the resulted system consists of discontinuous compressed circuits and its cable set geometry fits with a cuboctahedron, Fig. 1.14. Other circuit systems can be derived from known polyhedral geometries. In these systems, the number of cables ensures the stability of a node. They comprise four connections by node. According to Pugh, a circuit system is more rigid than a rhombic one with the same number of struts [1.11].

Circuit systems can be related to geodesic tensegrity systems. The geometric generation of these systems relies on the division of triangular or square faces of polyhedra. This breakdown is characterized by the number of generated segments of the edges of the initial polyhedron, which is called "breakdown frequency". The edges of each triangle are divided into equal numbers of equal parts and the lines drawn between the points define a grid on each face. A circuit system can be based on a geodesic system in which the faces of the initial polyhedron are subdivided to a frequency, which is a multiple of two.

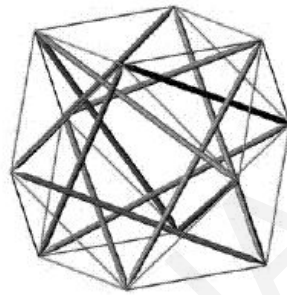


Figure 1.14 Cuboctahedric circuit tensegrity system [1.23]

Diamond tensegrity

Diamond tensegrity, also known as T-icosahedron, is depicted in Fig. 1.15. These tensegrities are characterized by the fact that each triangle of tendons is connected to the adjacent one via a strut and two interconnecting tendons [1.10]. It was first exhibited in 1949 by Buckminster Fuller [1.9] and is one of a few tensegrities which have mirror symmetry. This structural type is classified as a 'diamond' because each of its struts is surrounded by a diamond form of four tendons, which are supported by two adjacent struts.

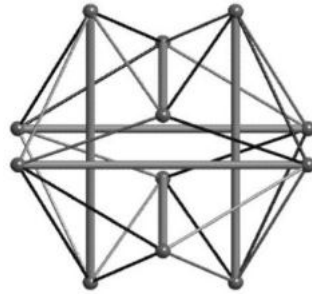


Figure 1.15 Diamond tensegrity

Diamond tensegrity has 6 struts and 24 tendons with tendon to strut lengths ratio of 0.612 [1.11]. If the quadrilaterals nested with struts are changed to squares, then the tendons form a cuboctahedron network. Fig. 1.16 illustrates the change on a system of tendons, from an octahedral arrangement to a cuboctahedron and backwards. Small arrows indicate the direction of movement of the struts and of the corresponding pair of opposite points of the quadrilateral as the tendon system goes through transformations [1.10].

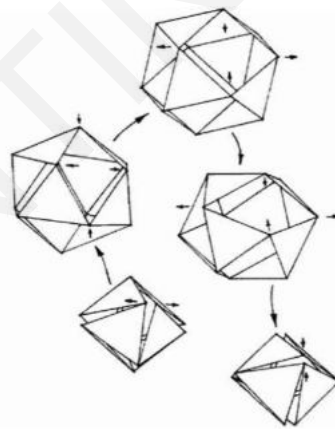


Figure 1.16 Corresponding transformation from and back to doubled-up octahedron

Opening the octahedral structure carefully from one end gives a single layer diamond structure as depicted in Fig. 1.17. New tensegrity structures with spherical symmetry can be generated by addition of new layers of struts and tendons and joining both ends of each layer. Planar views of tensegrity systems based on this approach are depicted in Figs 1.18 and 1.19.

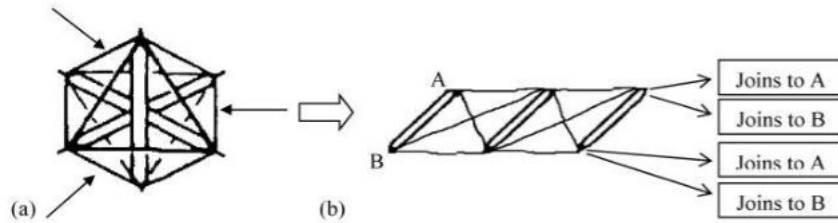


Figure 1.17 a) Octahedral structure b) planar view of corresponding 3-struts single layer tensegrity system

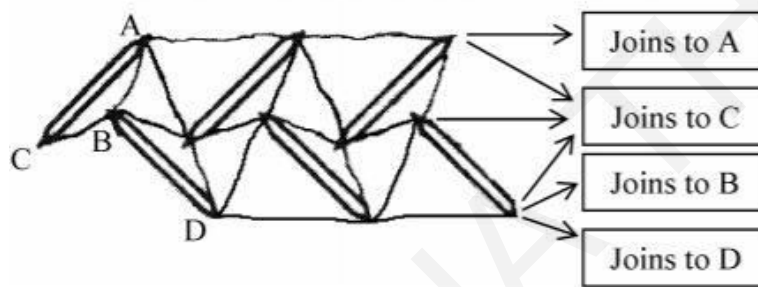


Figure 1.18 Planar view of 6-struts two-layer tensegrity system

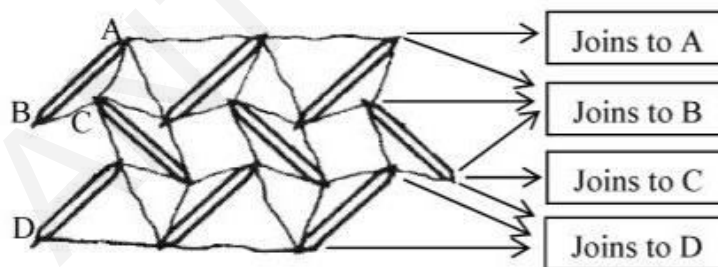


Figure 1.19 Planar view of 9-struts three-layer tensegrity system

Zig-zag tensegrity

The zig-zag is counterpart of the diamond T-icosahedron, Fig. 1.20. Although both structures have 6 struts, the major difference is that T-tetrahedron has four tendon triangles, whereas the T-icosahedron has eight of them. In general, zig-zag structures with Z type configuration are simpler

and less rigid, due to their lower number of tendons than their diamond counterparts with rhombic configuration [1.10].

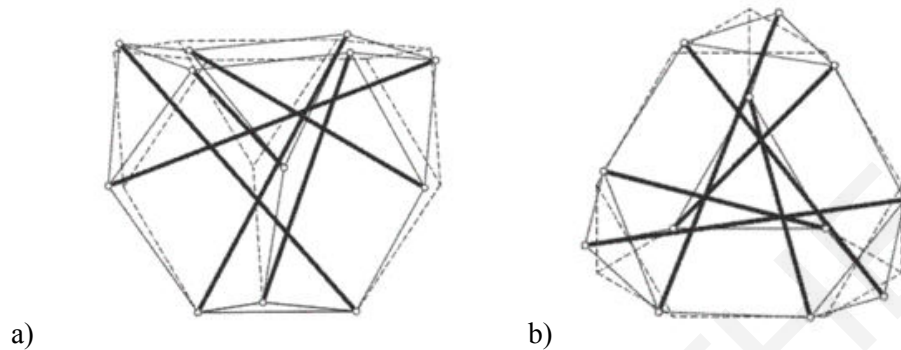


Figure 1.20 Zig-zag structure, Z type configuration: a) Side view; b) Top view

The spatial definition of individual tensegrity modules, which are stable by themselves, permits an exceptional capacity to create systems by joining them together. This connection implies the option of the endless extension of the assembled piece. By extension, tensegrity gridshells are considered to be closer to the category of lattice gridshells, as the assembly and erection of the structure takes place directly on site. It's easier for tensegrity surfaces to be constructed in modules and interconnected, in order to create the surfaces of a shell. This is achievable with the use of actuators that control the structure's behavior, in order to adapt to changing environments. Also, they develop a system of interconnections between compression and tension members; thus a nonlinear analysis of form-finding methods is important to be carried out, in order for the optimal form to be designed.

1.2.2.1 Transformable tensegrity-ring footbridge

The aim of the development of a transformable tensegrity-ring footbridge is the shape transformations of a multiple-degree-of-freedom (DOF), $\frac{1}{4}$ scale tensegrity footbridge system using continuous active cables and springs [1.8]. Shape transformations such as deployment and shape corrections are conducted using the same remote actuation scheme. During the complexity of the shape transformation task and the large solution space, a stochastic search algorithm is

combined with a modified dynamic relaxation algorithm to identify the right actuation steps for each active cable, in order to obtain the desired shape transformation.

The structure is composed of steel struts that are hollow tubes with a 28 mm diameter and 1.5 mm thickness, steel cables with a cross sectional area of 11 mm^2 and spring steel elements with stiffness of 2 kN/m at the support and 2.9 kN/m at other locations. The structure contains two types of cables, non-continuous and continuous cables. Non-continuous cables are composed of one segment and they end at the joints that define the segment. A continuous cable has at least one intermediate joint between its two end joints. Intermediate joints allow cable sliding. The end of the continuous cable located at the support, is rolled and attached to drums. The length is changed through winding or unwinding the cable on the drum. The end nodes are placed on rail-supports, where the supports are blocked in the three directions, when the two bridge halves are connected and prestressed.

Spring elements, have maximum length, when the structure is folded. Deployment is controlled through increasing length of continuous cables; springs contribute since they progressively release their elastic deformation energy during deployment. The combination of continuous cables and springs is an actuation scheme that reduces the number of actuators required for deployment and has the advantage of actuators located only at the supports.

The pentagonal tensegrity-ring module is deployable, if the cable lengths can be adjusted. During deployment, the length of the x-cables controls folding, while the layer cables control unfolding. However, actions on both cable groups are required to obtain stable configurations, Fig. 1.21.

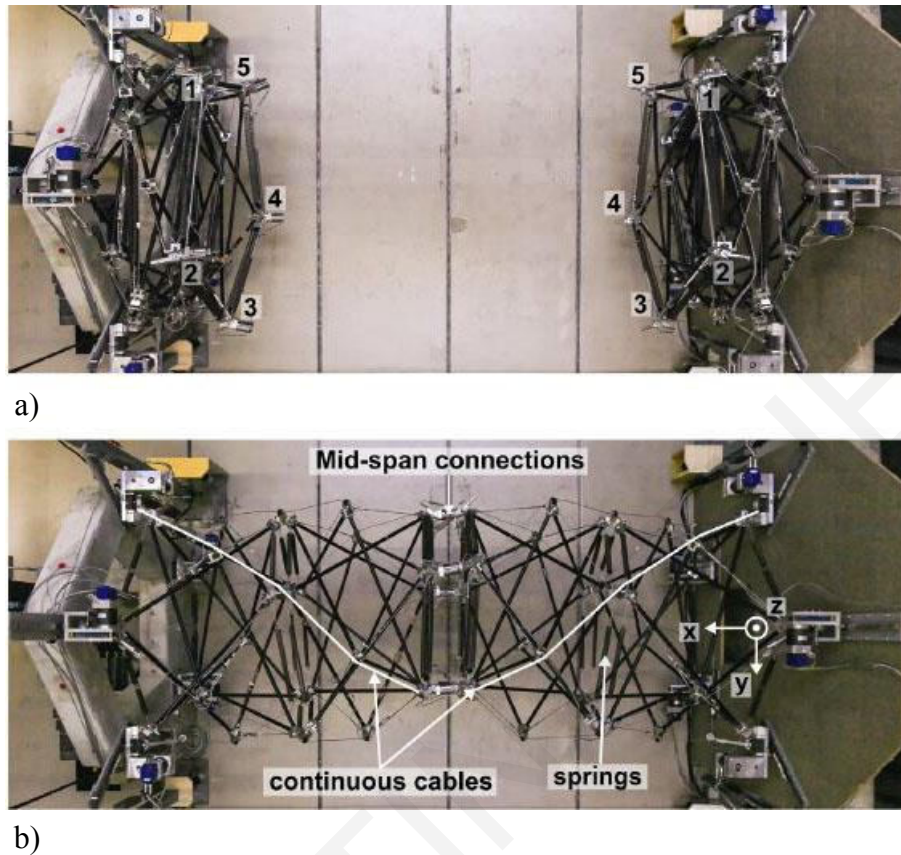


Figure 1.21 Top view of tensegrity structure: a) Folded structure showing the numbering of mid-span nodes; b) Deployed structure connected at mid-span as well as x, y and z conventions

The design and control of the tensegrity system with continuous cables and spring elements are employed resulting in a 5-actuator system, Fig. 1.22. Actuators can thus be placed on the supports since continuous cables run through the boundary nodes. Springs allow length changes without requiring any actuation devices. Also, spring length changes are driven by actions on other elements. In this study, springs replace layer cables, so the length changes are driven by actions of the continuous active x-cables. On the other hand, springs are elongated in the folded configuration and contracted in the unfolded configurations allowing spring energy to be used for unfolding. Springs are thus in low energy state in the unfolded configuration reducing the risk of energy bursts under service.

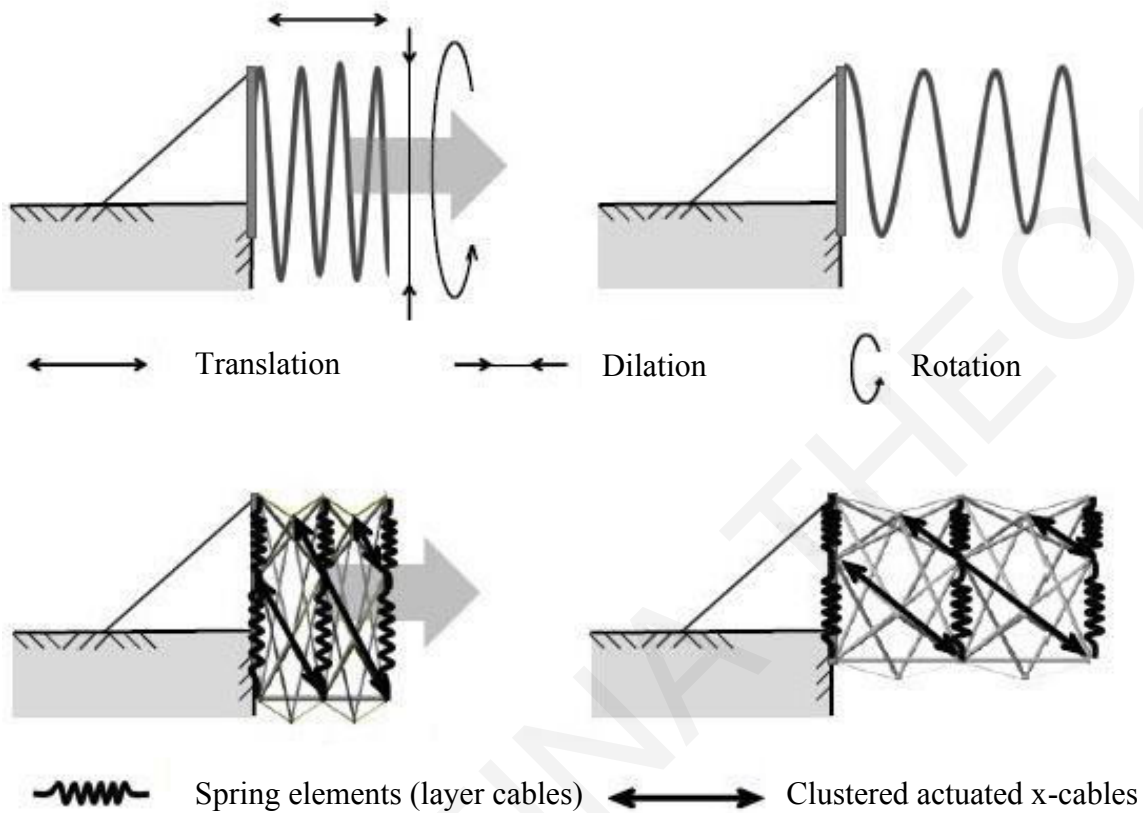


Figure 1.22 Deployment motion and actuation components of the tensegrity-ring footbridge system [1.9]

Although the shape transformation for deployment of the tensegrity-ring system involves modifying several DOF, it is found feasible with the same length change applied in all 5 active continuous x-cables. A single actuator connected to the 5 active cables is sufficient for the deployment of each half of the tensegrity footbridge system. Single actuator configurations do not allow adjustments in the shape of the system, unless the actuator controls individually every cable.

The experimental testing of the prototype verified that the actuation scheme with active cables and spring elements is applicable for both, large transformations such as deployment, as well as small shape changes, such as deployment corrections, Fig. 1.23. Actuation steps differ according to the desired shape changes. In all cases, the efficiency of using advanced computing methods for shape

control of active deployable tensegrity systems has potentials in the shape control of other tensegrity systems as well.

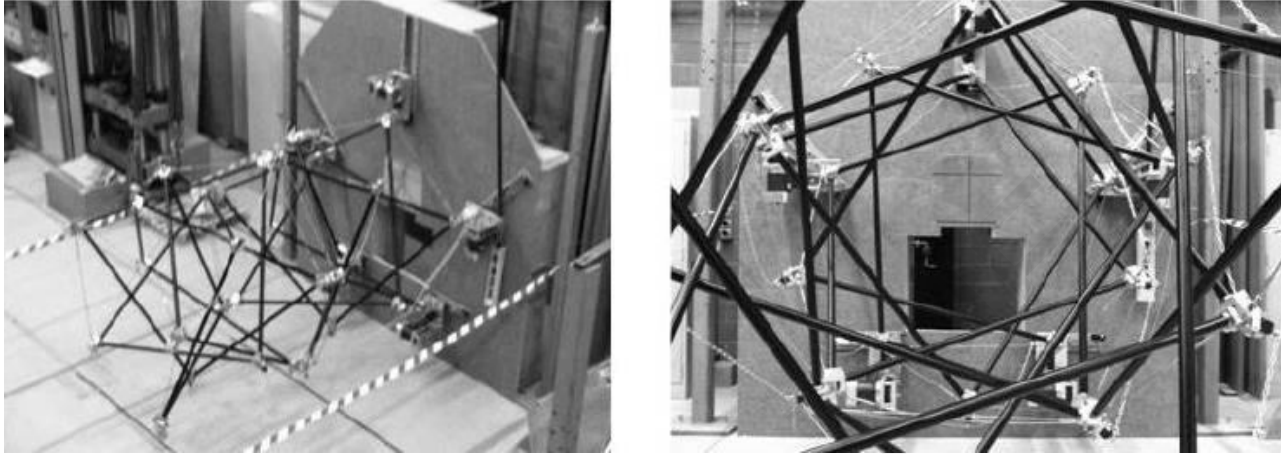


Figure 1.23 $\frac{1}{4}$ scale ring-module tensegrity footbridge system [1.9]

1.2.2.2 Tensegrity gridshell, EPFL

A full-scaled adjustable tensegrity prototype was designed and built for the Swiss National exhibition, by the Applied Computing and Mechanics Laboratory at EPFL, supervised by Ian Smith [1.10]. The structure is based on a tensegrity typology and consists of three modules creating a surface made of struts and cables. Each module is made of 6 struts and 24 cables, Fig. 1.24. There is a central joint for the reduction of the buckling length of compression members, thus allowing a smaller cross-section of the struts. Also, telescopic struts are used to control the geometry. Stainless steel cables of 6 mm diameter used to form a double layered structure and lateral cables for the connection of two layers. Two different cable lengths are in each layer, the first one forming three isosceles triangles and the other one, forming an isometric triangle in center. The 6 struts in each module meet the central joint, due to assembly requirements. The end of the specific struts consists of a nut rod system, to enable length changes in the strut. Fiberglass reinforced polyester tubes are used for the struts offering a minimal diameter for the movement of the threaded rod and sufficient buckling strength.

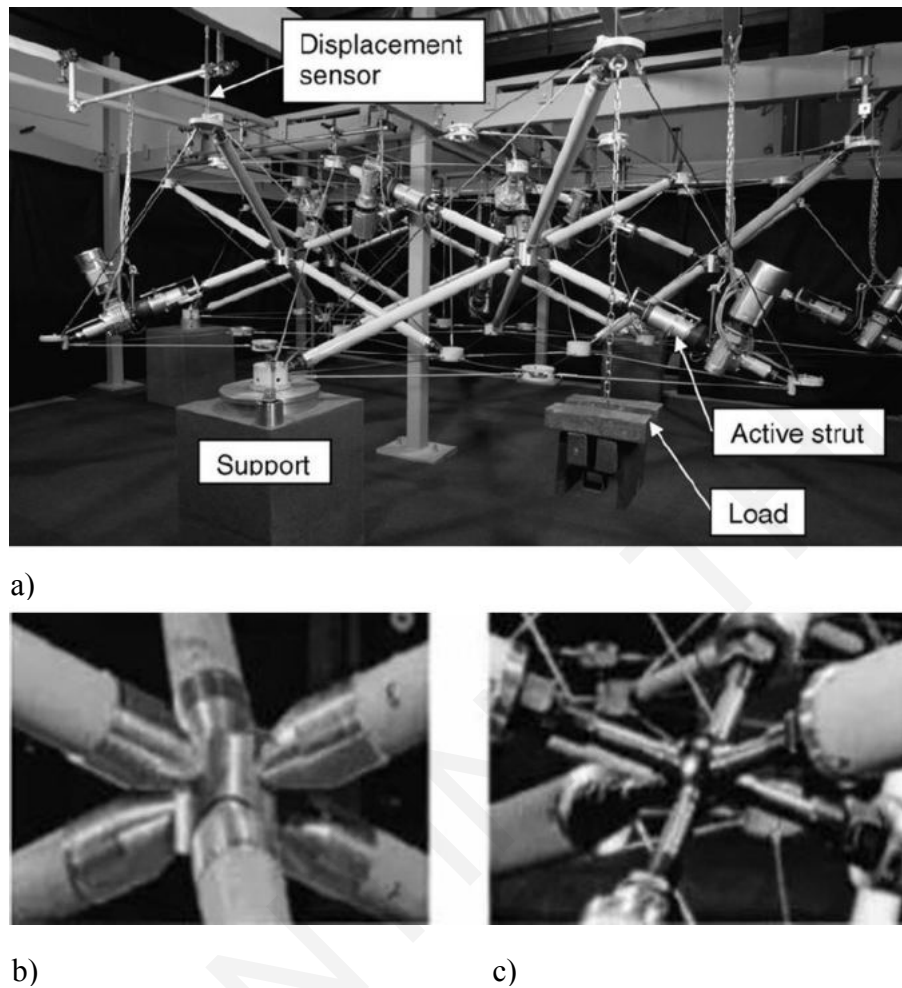


Figure 1.24 5-module tensegrity structure: a) Experimental setup; b) 3-module structure center joint; c) 5-module structure center joint

The assembly method of the structure requires building the modules individually and then connecting them depending on the desired configurations and self-stress value, Fig. 1.25. The self-stress value is controlled by changing the telescopic struts length. The assembly method is considered difficult, due to the non-equilibrium state of the structure. For that reason, the modules are assembled independently and connected afterwards creating the final form. The sequence of the struts lengthening is very crucial, as the asymmetrical sequence can lead to imbalance and cause the collapsing of the system. Also, is used a dynamic simulation, to check the cable's optimal

tension values. The main factors that affect the structure's adjustability are the number of the telescopic struts and the range of movement individually.

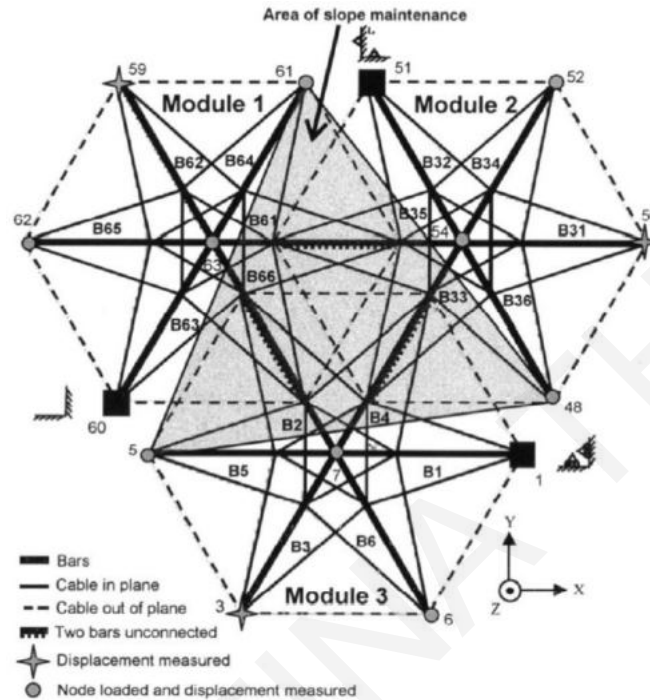


Figure 1.25 Plan view: Geometric principle of tensegrity modules

1.2.3 Bar Linkages

Bar linkages are highly effective in creating structures that deploy or transform, allowing flexibility and low energy consumption during motion. In structural terms, closely related to deployable and reconfigurable modular structures are linkage-based systems. In previous years, the kinematics of reconfigurable rigid structures composed of a series of n -bar linkages, with either direct and cable-driven actuation have been investigated in simulations and experimentally [1.3]. The transformations of the systems were based on the use of only one or two actuators at the supports of each n -bar linkage using a sequence of motion steps through selectively releasing a number of joints of the primary members, in order to reduce the system to a 1-DOF mechanism and thus adjust the system joints to the desired values.

A linkage is a collection of interconnected components, called links. The physical connection between two links is called a joint. This definition is general enough to encompass gears and cams, where the joint is formed by direct contact between two gear teeth or between a cam and follower. Bar linkages have two elementary joints, the rotary hinge and the joint and the linear or rotating actuator. These joints allow 1-DOF movement between the two links that they connect. The configuration variable for a hinge is the angle measured around its axis between the two links.

1.2.3.1 Effective 4-bar mechanism

The ‘effective 4-bar mechanism’ is an alternative control approach that requires only one motion actuator along with electromagnetic or hydraulic brakes installed on each joint. The members connected between them by locked joints form an ‘effective link’. Alternatively to a rotational or linear actuator attached on the pin support, the actuation system may include two actuators and two corresponding independent continuous cables that generate control torques at the joints when tensioned, as well as brakes installed on the joints. The four joint angles defining the mechanism’s configuration are not independent and the 4-bar mechanism is effectively a 1-DOF system. One joint is adjusted in each reconfiguration step, while the rest 3 unlocked joints remain passive, Fig. 1.26.

A typical application of the 4-bar mechanism in machine design involves a single motor actuator constantly rotating link-1. Its motion is transferred via link-2 to link-3 that performs a back-and-forth rotation. In this case, the three moving links are termed ‘crank’, ‘coupler’ and ‘rocker’, respectively, and link-4 is the ‘ground’. The rotational motion characteristics of the 4-bar linkage members are specified by a simple formula called ‘Grashof’s condition’ and depend on the relative lengths of the links [1.3].

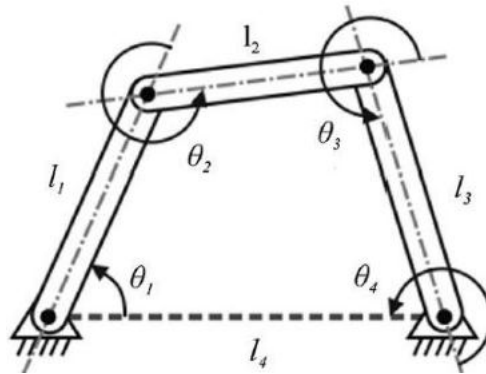
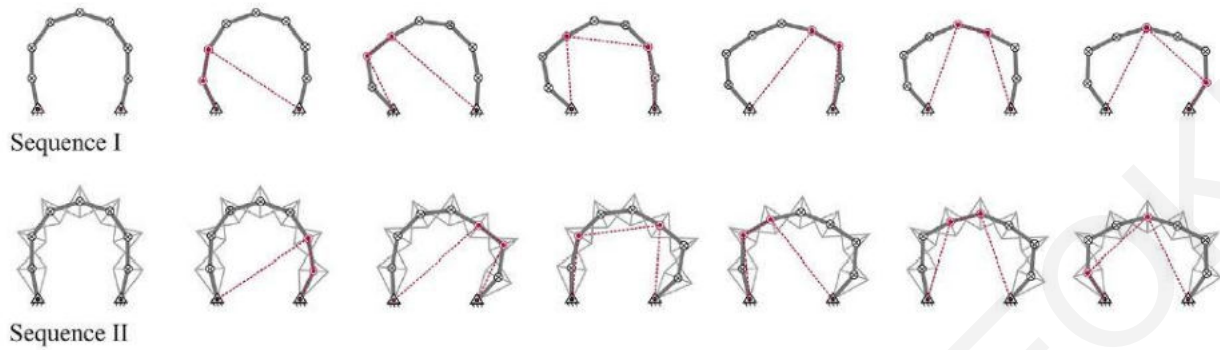


Figure 1.26 The basic 4-bar linkage mechanism

Reconfigurable Bar Linkage Structure

The basic reconfigurable bar linkage structure can be appropriately configured to implement a direct or cable-driven actuation method based on the effective 4-bar mechanism [1.16]. In the direct actuation method, one linear motion actuator is connected to the ground and the first bar of the pin supported linkage. In the cable-driven method, on either side of the structure, there are two linear motion actuators connected to the cables, whose base is attached to a rotational ground joint.

Two symmetric postures were selected for the initial and final configurations of the system. The initial configuration is $\theta_i = [102, 168, 144, 144, 144, 144, 144, 168, 102]^T$ degrees and the target configuration is $\theta_f = [124, 144, 120, 168, 148, 168, 120, 144, 124]^T$ degrees (internal n -bar angles). Usually, a reconfiguration between an initial and final position can be realized via alternative sequences. An optimal one may be selected based on specific criteria, like maximum brake torques, cable length variation etc. Fig. 1.27 shows the reconfiguration steps of two sequences applied for the linkage system.



\triangle : pivoted-to-the-ground unlocked joint, \triangle : pivoted-to-the-ground locked joint, \odot : unlocked joint, \otimes : unlocked joint,

Figure 1.27 Stepwise reconfiguration of the 9-bar system. Direct actuation approach (Sequence I) and Cable-driven actuation approach (Sequence II) [1.16]

In the experimental setup, the operation of the actuators is based on a 12 V DC motor and a lead-screw mechanism that generates the linear motion, Fig. 1.28. The brake system includes a cylindrical aluminum block with a symmetrical array of holes on its curved surface for locking the joint when the two stopper pins are inserted in the holes, Fig. 1.29. The main drawback of this approach is that locking the joint is limited to a set of fixed, discrete positions (120° , 144° and 168° internal joint angles) and introduces an extra motion planning constraint. All the joints are installed with brakes except the base joints. The spring-loaded pins of the brake system maintain a joint at a locked position and they are released upon activating their electromagnets. This ensures a fail-safe operation of the brakes system. On each joint, the pair of electromagnets is wired in parallel to lock/release the joint simultaneously with the same control signal. The controlled operation involves a set of corresponding relays that receive control signals from the controller. The sensors are potentiometer type, providing absolute measurements of the joint angles. There is no need for initialization through a homing procedure during system start-up or following a power failure. The positions sensors are installed on every joint except of the two at the base.

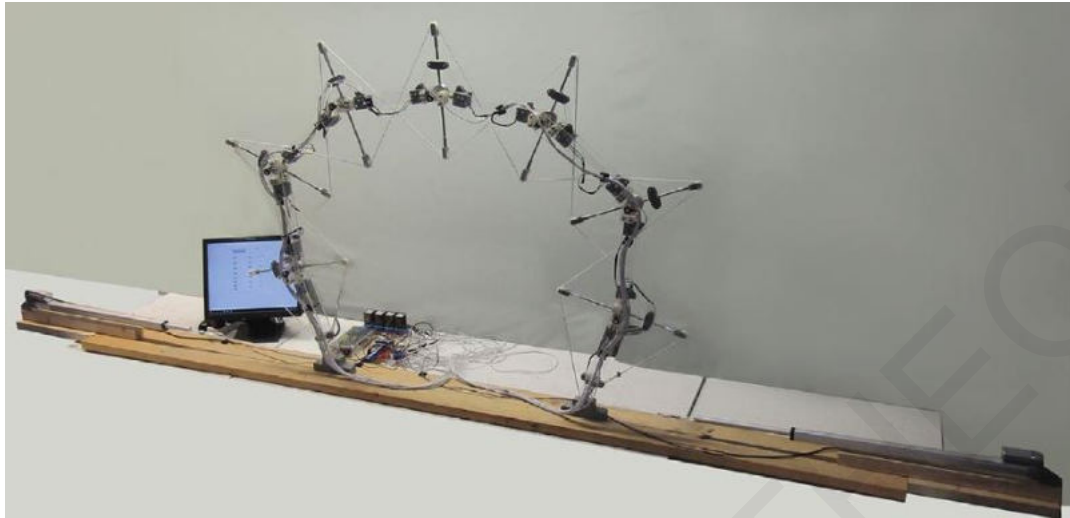


Figure 1.28 Experimental setup of direct and cable-driven actuation method of the bar-linkage [1.16]



Figure 1.29 Joint connection of experimental setup

Reconfigurable Hybrid Bar Linkage Structure

The reconfigurable hybrid linkage structure developed in [1.11] refers to a primary system consisting of hinge-connected beams, stabilized through a strengthening system of struts and continuous diagonal cables with closed circuit. Fig. 1.30 shows the spatial system. The structure

may obtain different geometries that define different configuration states, through modification of the cable's length.

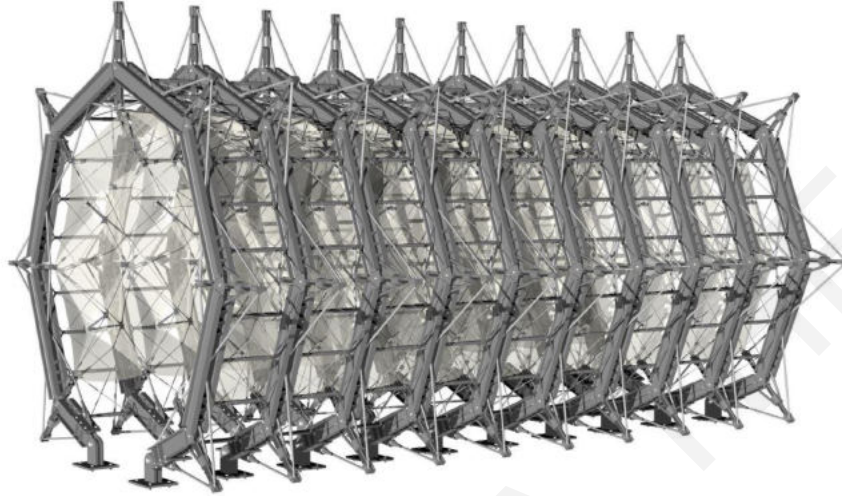


Figure 1.30 Isometric view of the 3-dimensional hybrid reconfigurable structure [1.17]

The proposed reconfiguration concept of each planar linkage system based on the effective 4-bar mechanism requires only two single motion actuators per basic component linkage tensioning each corresponding cable at the structural supports, as well as hydraulic brakes at the joints. Transformations of the n -bar linkage take place through appropriate control of shape sequences, such that for each individual intermediate motion step involved, a 1-DOF, 4-bar mechanism is realized through selective locking of $(n-4)$ joints. Motion planning of the structure is concerned with generating appropriate motion patterns and selecting the most appropriate one according to specific criteria as for example the braking torques in the primary joints, the cables axial forces and the required size of cable adjustments involved in each motion sequence. The integrative development of the kinetic structure, the construction design of the components and their connections and its control mechanism have been conducted following nonlinear processes of design and optimization while aiming at sustainability and effective use of resources, Fig. 1.31.

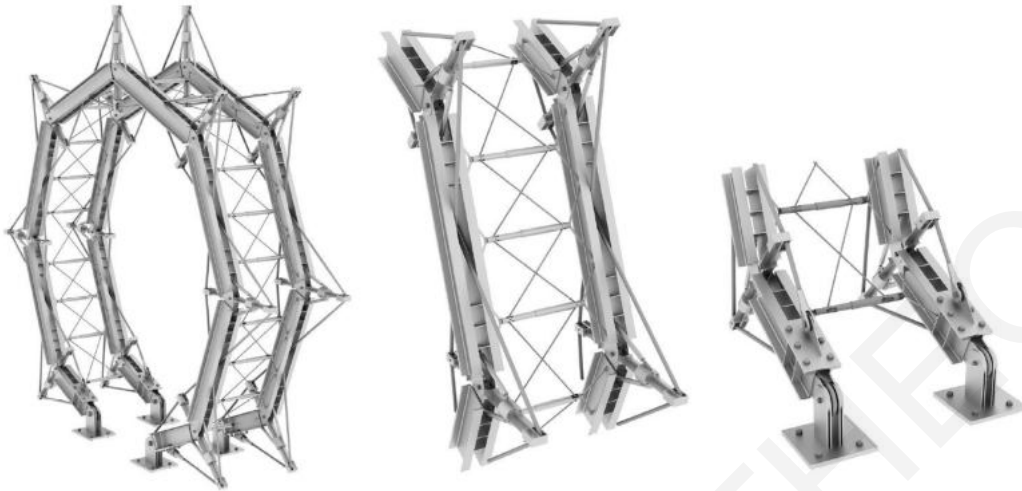


Figure 1.31 Horizontal structure of two adjacent linear prototype units and members connections design [1.17]

1.2.3.2 Effective Crank Slider mechanism

In this control approach, the basic and kinematics element is again a planar linkage comprised of serially connected rigid links with pivot joints between them. All joints are equipped with electromagnetic or hydraulic brakes. One end of the chain connects to the ground through a pivot joint and the other side is pinned to a linear sliding block, constituting the mechanism a closed kinematic chain. A linear actuator is considered acting on the sliding block. An alternative or supplementary rotational actuation can be considered with regard to the base pivot joint.

During the stepwise adjustments, each step involves selectively releasing one intermediate joint, by releasing the corresponding brake of the linkage in addition to the pin joints at the supports, constituting the mechanism a generic 1-DOF system, namely an ‘effective crank-slider’ system, Fig. 1.32. An appropriate control sequence can be used for stepwise reconfigurations induced by the linear actuator.

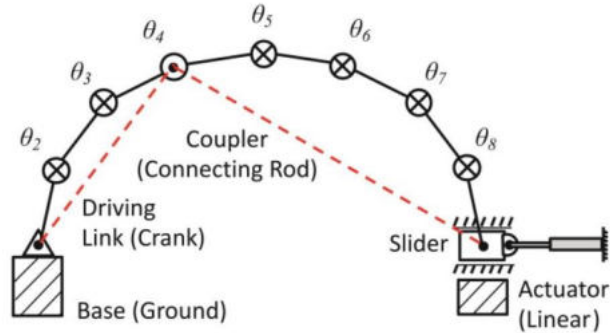


Figure 1.32 Effective crank-slider approach, which is the basis for the stepwise deployment and reconfigurations of the n -bar linkage

Deployable and Reconfigurable Bar Linkage Structure

The deployment and reconfiguration approach of a linkage structure developed in [1.12], refers to the ability of a system to erect from an initial to a target position and further adjust its shape through its motion control with computational assistance. This study presents a conceptually analogous approach for deployment and reconfiguration purposes compared to the effective 4-bar approach, applied to a different class of modular linkage structures with one of the pin supports connected to an actuated sliding block.

Motion planning requires to consider the kinematics of the basic crank-slider mechanism and its singular configurations. The specific mechanism when fully extended or retracted reaches its limit positions, where the slider may not move any further. The linear motion actuator performs the actual reconfiguration, while the controller receives feedback information from the sensors regarding the current position of the joints. In the experimental setup, actuation of the system is based on an electric linear actuator (12V DC, 150 cm travel) connected to the sliding block.

The investigations conducted involve simulation of the system kinematics and experimental verification of selected motion sequences with a prototype model in scale 1:10. Figs 1.33-1.35 show the experimental deployment and reconfiguration of a linkage based on the effective crank-slider approach. The results demonstrate the feasibility of the proposed concept and reveal the potential of transformable structures.

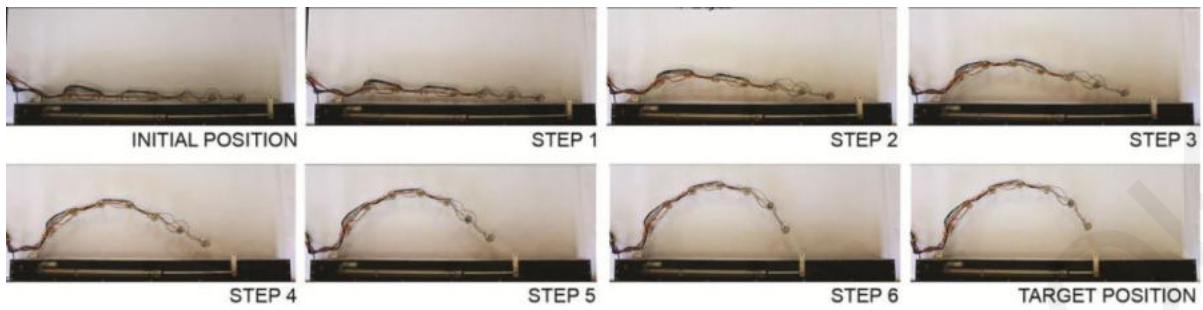


Figure 1.33 Experimental deployment of the linkage to the first target position [1.15]

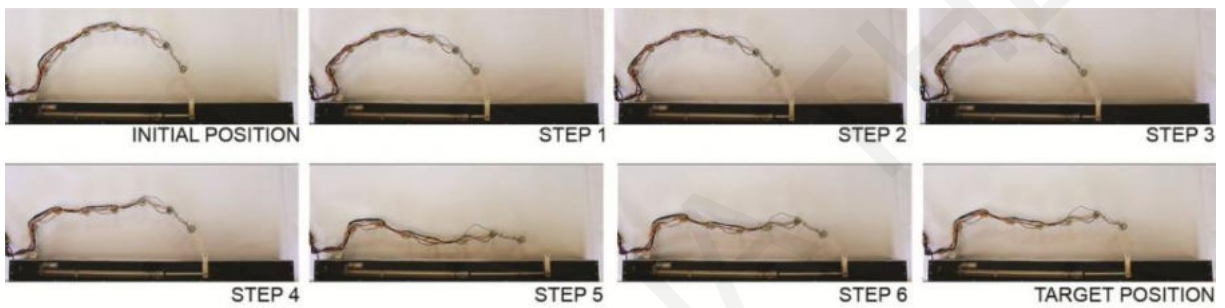


Figure 1.34 Experimental reconfiguration of the linkage from the first to the second target position [1.15]

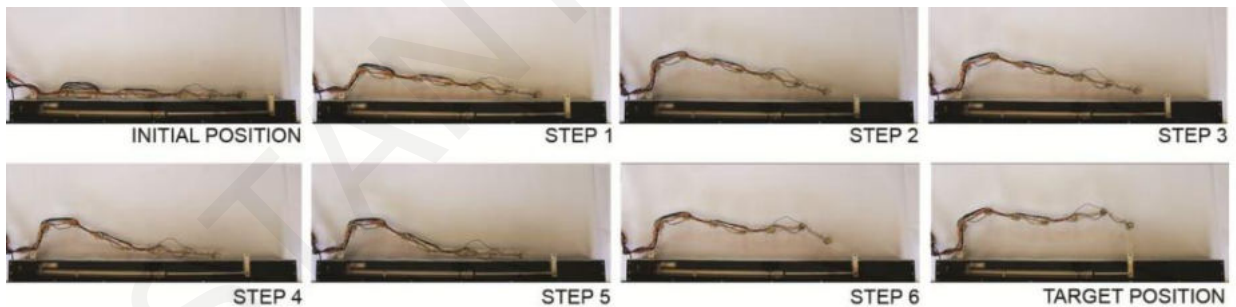


Figure 1.35 Experimental deployment of the linkage to the second target position [1.15]

1.3 Motivation and Thesis Structure

Transformable systems rely on embedded computation and the replacement of primary members with actuators. Unavoidably, the employment of actuation components on the primary structure

often leads to increased structural weight, complex mechanisms and energy-inefficient operation. Furthermore, deployable structures developed and implemented so far, are limited to specific target configurations. In this respect, linkage-based systems, which comprise continuous series of 1-dimensional, rigid bars interconnected by lower-order pairs, constitute promising systems towards the development of reconfigurable modular structures with enhanced shape flexibility and controllability. Along these lines, the present Thesis aims at the development and investigation of a reconfigurable system that is capable to achieve numerous symmetrical and non-symmetrical configurations with as few reconfiguration steps as possible. The kinematics approach applied based on the effective crank–slider method provides maximum flexibility and endurance with minimum required actuation energy. The photovoltaic units integrated with the flexible building envelope enable high levels of energy production, exceeding the performance of a corresponding fixed shape building.

Initially, the typologies of deployable and reconfigurable lightweight structures are presented. The kinematics of the system is usually based on a SDOF system transformation. The analysis focuses on three structural typologies, namely, scissor-like, tensegrity systems and rigid-bar linkages.

The second chapter, focuses on the design and analysis of a reconfigurable structure and the investigation of its kinetic behavior. The effective crank–slider reconfiguration approach is applied in the system’s motion planning, which stepwise reduces the planar system to an externally actuated 1-DOF mechanism, in order to adjust each joint angle of the planar system from an initial to a target position. Among different feasible sequences, the ones with less required steps are selected and investigated.

In Chapter 3, the construction design of the structure is presented. The design refers to the system supports, the members and their joint connections, as well as the actuation components that enable horizontal or vertical reconfigurations. The Chapter deals also with the building envelope that consists of ETFE membranes and thin photovoltaic films applied on two longitudinal rows on each side.

Chapter 4 focuses on the kinematics of the reconfigurable structure. The analysis includes the motion analysis of the structure using the FEA software Solidworks. The results obtained refer to the maximum brake torques and slider displacements in the selected reconfiguration sequences.

In the last Chapter, a simulation analysis provides the solar irradiance and the energy production by the photovoltaic units for the initial and three target positions of the building. The case study refers to the solstices annually with regard to Larnaca, Cyprus, and Stockholm, Sweden.

The final chapter of the Thesis includes the conclusions of the study.

CHAPTER 2 DUAL RECONFIGURABLE SYSTEMS

The current research focuses on the design and analysis of a reconfigurable structure and the investigation of its kinetic behavior. It refers to the Effective Crank–Slider reconfiguration approach, namely a kinematics approach that stepwise reduces a planar system to an externally actuated 1-DOF system, in order to adjust each joint angle of the planar system from an initial to a target position. Through movement of the slider in each step, the selected joint angles adjustment may provide symmetrical or non-symmetrical configurations of the system. Two control system configurations are proposed following horizontal and vertical actuation of the structure.

Firstly, in the initial position of the system, the linkages and the joints of the structure remain locked. During the sequences for implementing the required shape adjustment, there are locked and unlocked brakes in the joints. Also, the movement of the slider, in each step induces symmetrical and non-symmetrical forms. In the specific dual kinematics mechanisms investigated, the adjustment of two angles in each step provides symmetrical system forms and the adjustment of one angle in each step, non-symmetrical forms. At the same time, during each step, the angles are adjusted to complete the target position. The first and the last joint of the structure are pivoted to the ground. The left and the right joints of the slider are the only joints of the system without brakes. The brakes are used for the activation and the deactivation of the joints. There are many sequences that can provide the target position. Once a joint has been adjusted, the respective joint will be locked in the following steps of the reconfiguration. In the tables below, all feasible and non-feasible sequences investigated are presented.

2.1 Control sequences

Sequence 1 leads to a symmetrical system form and the movement of the slider is vertical. During the slider's movement, there are two locked joints and two adjusted angles, in each step. The target position is completed, after two steps.

2.1.1 Sequence 1a (S1a)

All the joints in the Initial position (STEP 0) are locked and the height of the structure is 4.50 m. The first and the last joints are locked. In the first step, the slider moves the structure by 51.64 cm to the bottom, so that the joint 3 and 7 are currently adjusted. In the last step, the joints 1 and 9 are unlocked and the joints 3 and 7 are locked. The slider moves the structure 78.64 cm to the top, so that the target position is achieved (STEP 2), Fig. 2.1, Table 2.1.

STEP 0 $[\theta_1, \theta_2, \theta_3, \theta_4, H_5, \theta_6, \theta_7, \theta_8, \theta_9] = [98^\circ, 143.60^\circ, 143.42^\circ, 155^\circ, 0\text{m}, 155^\circ, 143.42^\circ, 143.60^\circ, 98^\circ]$

STEP 1 $[\theta_1, \theta_2, \theta_3, \theta_4, H_5, \theta_6, \theta_7, \theta_8, \theta_9] = [98^\circ, 149.08^\circ, 120^\circ, 172.92^\circ, -0.5164\text{m}, 172.92^\circ, 120^\circ, 149.08^\circ, 98^\circ]$

STEP 2 $[\theta_1, \theta_2, \theta_3, \theta_4, H_5, \theta_6, \theta_7, \theta_8, \theta_9] = [67.32^\circ, 203.02^\circ, 120^\circ, 149.66^\circ, +0.7864\text{m}, 149.66^\circ, 120^\circ, 203.02^\circ, 67.32^\circ]$

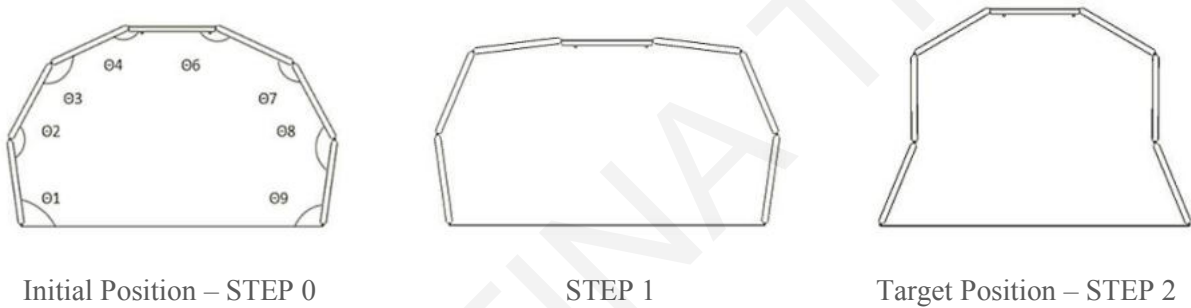


Figure 2.1 Structure Configurations

Table 2.1 Scheduling table for feasible control sequence 1a

	J ₁	J ₂	J ₃	J ₄	J ₅	J ₆	J ₇	J ₈	J ₉
Step 1									
Step 2									

: pivoted-to-the-ground unlocked joint, : pivoted-to-the-ground locked joint, : unlocked joint, : locked joint,
 : effective link, : slider, : currently adjustment

In Step 1 where the joints 1 and 9 are locked, the ground level is replaced to the joints 2 and 8. Also, in Step 2, joints 3 and 7 are unlocked, so that the two linkages between joints 2 and 4 move as one. The same happens with the joints 6 and 8, Fig. 2.2.

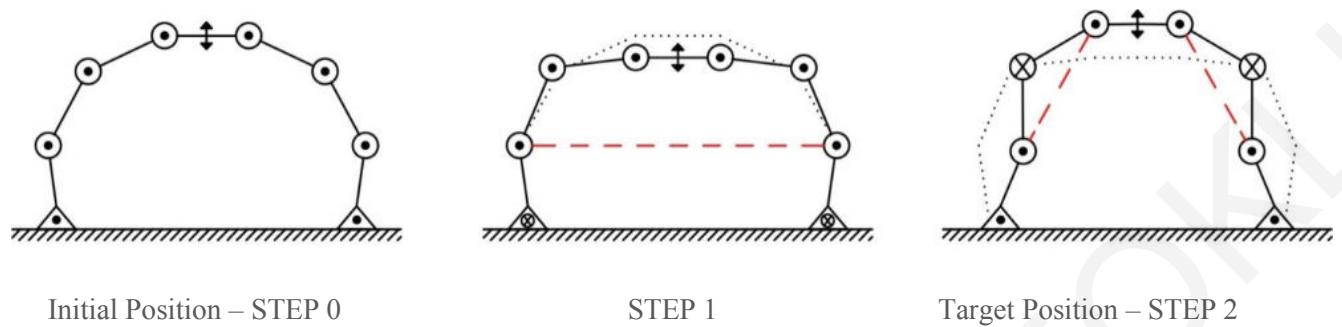


Figure 2.2 Selected feasible motion sequence 1a, Scale 1:200

2.1.2 Sequence 1b (S1_b)

All the joints of the system in the initial position (STEP 0) are locked and the height of the structure is 4.50 m. The joints 2 and 8 are locked. In the first step, the slider moves the structure by 66.50 cm to the ground, so that the joints 3 and 7 are currently adjusted. In the last step, the joints 2 and 8 are unlocked and the joints 3 and 7 are locked. The slider moves the structure 93.50 cm to the top, so that the target position is achieved (STEP 2), Fig. 2.3, Table 2.2.

STEP 0 $[\theta_1, \theta_2, \theta_3, \theta_4, H_5, \theta_6, \theta_7, \theta_8, \theta_9] = [98^\circ, 143.60^\circ, 143.42^\circ, 155^\circ, 0\text{m}, 155^\circ, 143.42^\circ, 143.60^\circ, 98^\circ]$

STEP 1 $[\theta_1, \theta_2, \theta_3, \theta_4, H_5, \theta_6, \theta_7, \theta_8, \theta_9] = [100.77^\circ, 143.60^\circ, 120^\circ, 175.63^\circ, -0.665\text{m}, 175.63^\circ, 120^\circ, 143.60^\circ, 100.77^\circ]$

STEP 2 $[\theta_1, \theta_2, \theta_3, \theta_4, H_5, \theta_6, \theta_7, \theta_8, \theta_9] = [67.32^\circ, 203.02^\circ, 120^\circ, 149.66^\circ, +0.935\text{m}, 149.66^\circ, 120^\circ, 203.02^\circ, 67.32^\circ]$

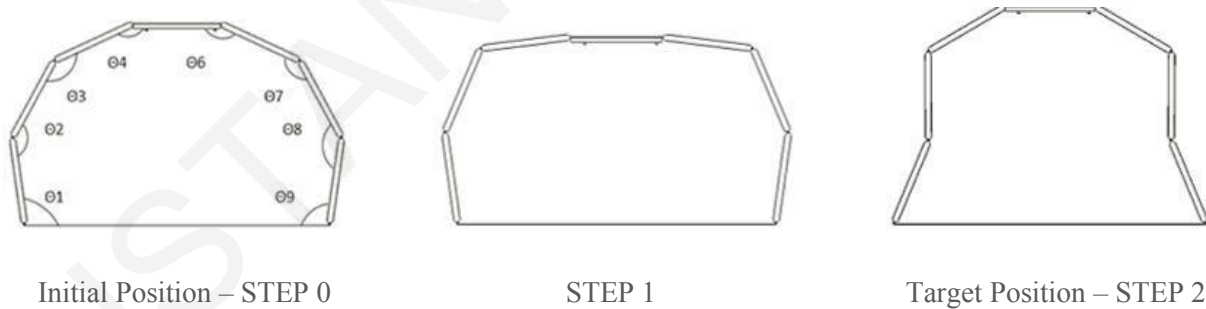


Figure 2.3 Structure Configurations

Table 2.1 Scheduling tables for feasible control sequence 1b

	J ₁	J ₂	J ₃	J ₄	J ₅	J ₆	J ₇	J ₈	J ₉
Step 1									
Step 2									

: pivoted-to-the-ground unlocked joint, : pivoted-to-the-ground locked joint, : unlocked joint, : locked joint,
 : effective link, : slider, : currently adjustment

In step 1, joints 2 and 8 are locked, so that the two linkages between joints 1 and 3 move as one. The same happens with the joints 7 and 9. In the final step, the joints 3 and 7 are locked, so that the links between them move as one. The form is symmetrical for both sides of the system. The joints 3 and 7 are locked, so that the links between them move as one, Fig. 2.4.

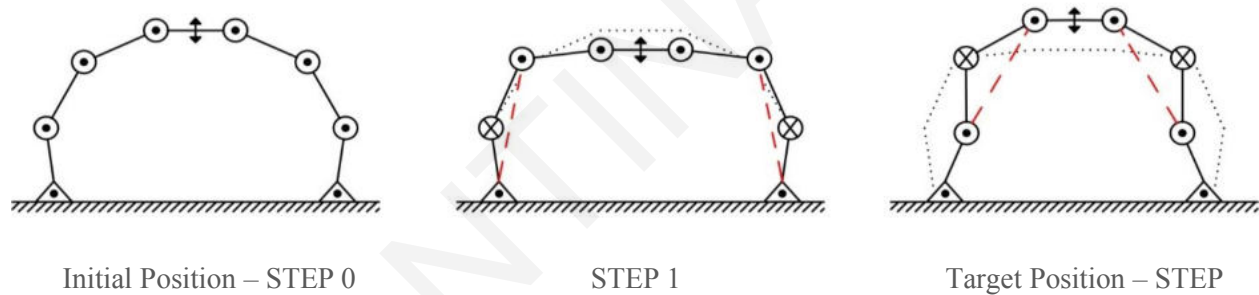


Figure 2.4 Selected feasible motion sequence 1b, Scale 1:200

2.1.3 Sequence 1c (S1c)

All the joints in the Initial position (STEP 0) are locked and the height of the structure is 4.50 m. In the first step, the joints 3 and 7 are locked and the slider moves the structure by 64.90 cm to the top, so that the first and the last joints are currently adjusted. In the second step, the joints 1 and 9 are locked and all others are unlocked. The slider moves the structure 93.50 cm to the bottom in achieving the target position (STEP 2), Fig. 2.5, Table 2.3.

$$STEP\ 0\ [\theta_1, \theta_2, \theta_3, \theta_4, H_5, \theta_6, \theta_7, \theta_8, \theta_9] = [98^\circ, 143.60^\circ, 143.42^\circ, 155^\circ, 0m, 155^\circ, 143.42^\circ, 143.60^\circ, 98^\circ]$$

$$STEP\ 1\ [\theta_1, \theta_2, \theta_3, \theta_4, H_5, \theta_6, \theta_7, \theta_8, \theta_9] = [67.32^\circ, 194.14^\circ, 143.42^\circ, 135.12^\circ, +0.6487m, 135.12^\circ, 143.42^\circ, 194.14^\circ, 67.32^\circ]$$

STEP 2 $[\theta_1, \theta_2, \theta_3, \theta_4, H_5, \theta_6, \theta_7, \theta_8, \theta_9] = [67.32^\circ, 203.02^\circ, 120^\circ, 149.66^\circ, -0.3787\text{m}, 149.66^\circ, 120^\circ, 203.02^\circ, 67.32^\circ]$

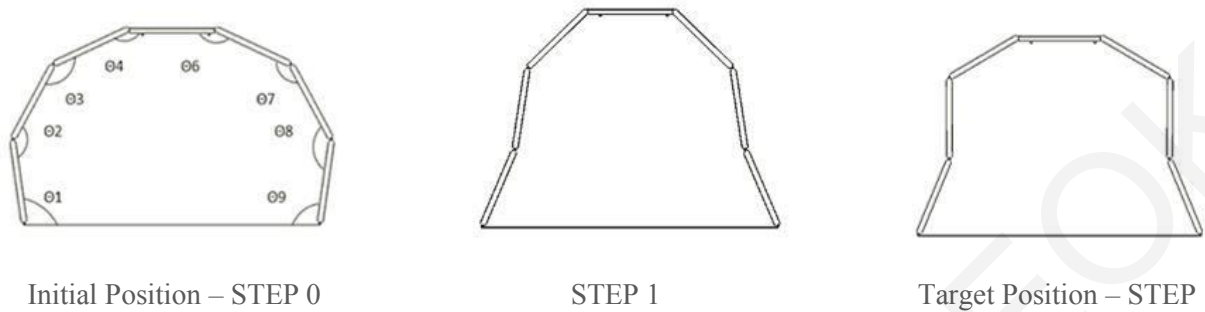


Figure 2.5 Structure Configurations

Table 2.2 Scheduling tables for feasible control sequence 1c

	J ₁	J ₂	J ₃	J ₄	J ₅	J ₆	J ₇	J ₈	J ₉
Step 1									
Step 2									

: pivoted-to-the-ground unlocked joint, : pivoted-to-the-ground locked joint, : unlocked joint, : locked joint,
 : effective link, : slider, : currently adjustment

In Step 1, the joints 3 and 7 are locked, so that the two linkages between joints 2 and 4 move as one. The same happens with the joints 7 and 9. In the third step, where the joints 1 and 9 are locked, the ground level is replaced to the joints 2 and 8, Fig. 2.6.

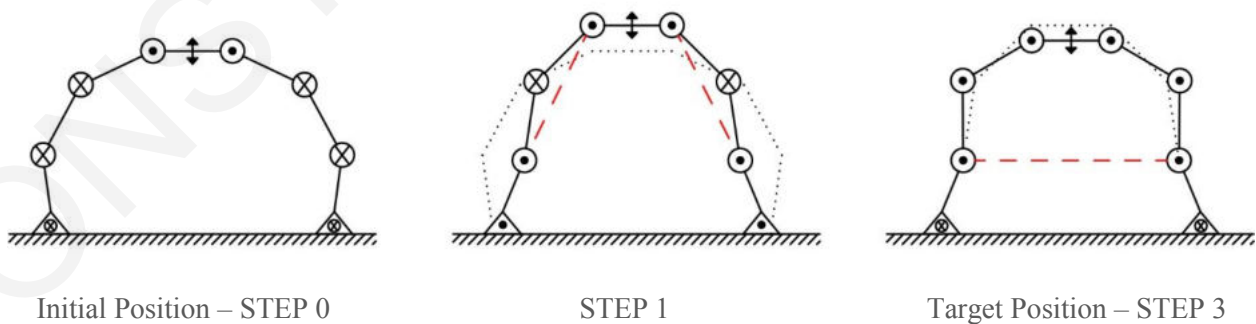


Figure 2.6 Selected feasible motion sequence 1c, Scale 1:200

2.1.4 Sequence 1d (S1d)

All the joints in the Initial position (STEP 0) are locked and the height of the structure is 4.50 m. In the first step, the joints 2 and 8 are currently adjusted and joints 1 and 9 are locked. In the second step, the joints 2 and 8 are locked and all others are unlocked. It is not possible to complete the configuration because of a singularity, Table 2.4.

Table 2.3 Scheduling tables for control sequence 1d

	J ₁	J ₂	J ₃	J ₄	J ₅	J ₆	J ₇	J ₈	J ₉
Step 1									
Step 2									

: pivoted-to-the-ground unlocked joint, : pivoted-to-the-ground locked joint, : unlocked joint, : locked joint,
 : effective link, : slider, : currently adjustment

2.1.5 Sequence 1e (S1e)

In this case, there are two locked and two adjusted joints in each step, but it is not possible to complete the configuration, because of a singularity. If there were more steps, the target position would be completed, Table 2.5.

Table 2.4 Scheduling tables for control sequence 1e

	J ₁	J ₂	J ₃	J ₄	J ₅	J ₆	J ₇	J ₈	J ₉
Step 1									
Step 2									

: pivoted-to-the-ground unlocked joint, : pivoted-to-the-ground locked joint, : unlocked joint, : locked joint,
 : effective link, : slider, : currently adjustment

2.1.6 Sequence 1f (S1f)

All the joints in the Initial position (STEP 0) are locked and the height of the structure is 4.50 m. In the first step, the joints 2 and 8 are currently adjusted and joint 3 and 7 are locked. In the second step, the joints 2 and 8 are locked and all others are currently adjusted. It is not possible to complete the configuration, because of a singularity. If there were more steps, the target position could be completed, Table 2.6.

Table 2.5 Scheduling tables for control sequence 1f

	J ₁	J ₂	J ₃	J ₄	J ₅	J ₆	J ₇	J ₈	J ₉
Step 1									
Step 2									

: pivoted-to-the-ground unlocked joint,
 : pivoted-to-the-ground locked joint,
 : unlocked joint,
 : locked joint,
 : effective link,
 : slider,
 : currently adjustment

2.1.7 Sequence 2a (S2a)

Sequence 2 leads to a non-symmetrical form, where the slider's movement is horizontal. In every step, there are two locked and one adjusted joint. The sequence consists of three steps to complete the target position. All the joints in the Initial position (STEP 0) are locked and the height of the structure is 4.50 m. In the first step, the joints 3 and 8 are locked and joint 7 is currently adjusted. The slider destination is on the right, for 47.86 cm. In the second step, the joints 3 and 8 are unlocked and the joints 1 and 7 are locked. Also, joint 3 is adjusted and the slider moves the structure to the left, by 97.12 cm. In the last step, all the joints are adjusted and the joints 3 and 7 are locked. The target position is achieved, Fig. 2.7, Table 2.7.

$$STEP 0 [\theta_1, \theta_2, \theta_3, \theta_4, H_5, \theta_6, \theta_7, \theta_8, \theta_9] = [98^\circ, 143.60^\circ, 143.42^\circ, 155^\circ, 0m, 155^\circ, 143.42^\circ, 143.60^\circ, 98^\circ]$$

$$STEP 1 [\theta_1, \theta_2, \theta_3, \theta_4, H_5, \theta_6, \theta_7, \theta_8, \theta_9] = [84.53^\circ, 156.85^\circ, 143.42^\circ, 155.2^\circ, +0.4786m, 156.75^\circ, 134^\circ, 143.6^\circ, 105.65^\circ]$$

$$STEP 2 [\theta_1, \theta_2, \theta_3, \theta_4, H_5, \theta_6, \theta_7, \theta_8, \theta_9] = [84.53^\circ, 172.18^\circ, 105^\circ, 162.65^\circ, -0.9712m, 157.66^\circ, 134^\circ, 168.86^\circ, 79.48^\circ]$$

$$STEP 3 [\theta_1, \theta_2, \theta_3, \theta_4, H_5, \theta_6, \theta_7, \theta_8, \theta_9] = [62^\circ, 218.19^\circ, 105^\circ, 154.81^\circ, +0.377m, 158.38^\circ, 134^\circ, 156.32^\circ, 91.30^\circ]$$

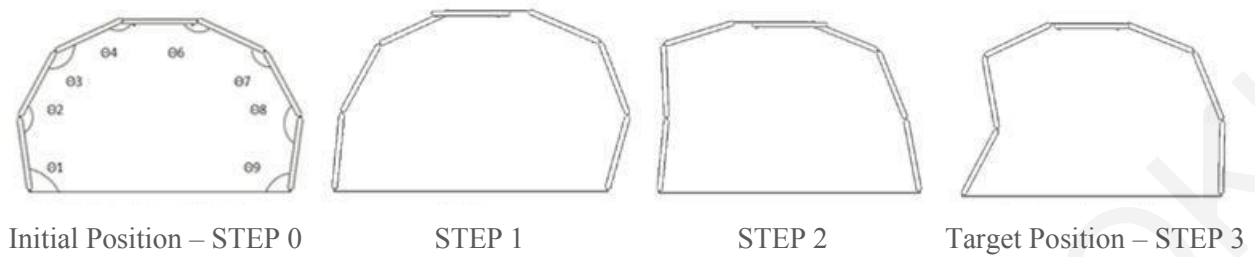


Figure 2.7 Structure Configurations

Table 2.6 Scheduling tables for feasible control sequence 2a

	J ₁	J ₂	J ₃	J ₄	J ₅	J ₆	J ₇	J ₈	J ₉
Step 1									
Step 2									
Step 3									

: pivoted-to-the-ground unlocked joint,
 : pivoted-to-the-ground locked joint,
 : unlocked joint,
 : locked joint,
 - - - : effective link,
 : slider,
 : currently adjustment

In Step 1, the joints 3 and 8 are locked, so that the two linkages between joints 2 and 4 move as one. The same happens with the joints 7 and 9. In the second step, the joints 1 and 7 are locked, and the ground level is replaced to the joints 2 and 9. Also, the links between joints 6 and 8 act as one. In the final Step the joints 3 and 7 are locked, so that the links between joints 2 and 4 and joints 6 and 8, move as one, Fig. 2.8.

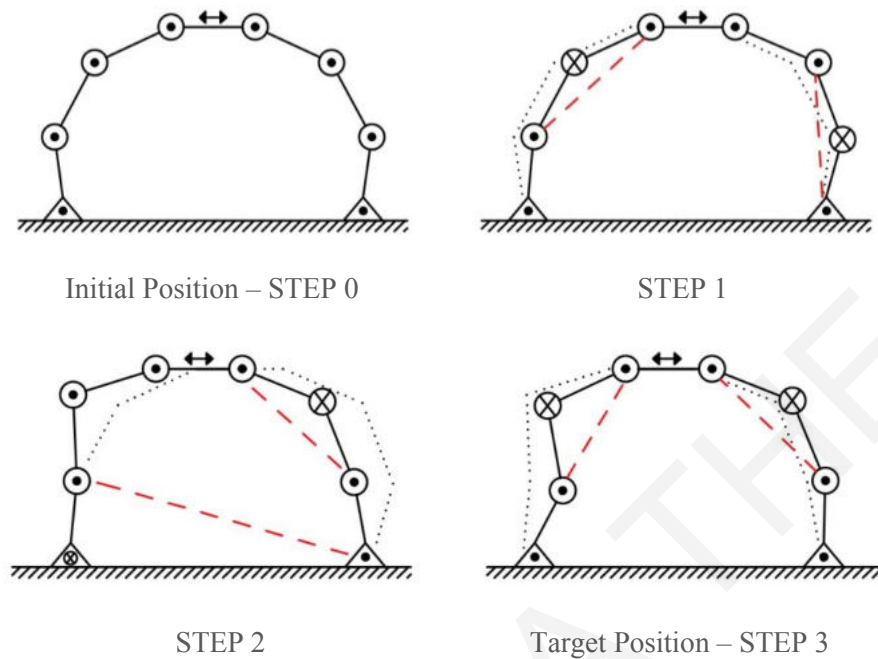


Figure 2.8 Selected feasible motion sequence 2a, Scale 1:200

For each sequence there are many combinations to complete the target position, but sometimes there are singularities and the target position cannot be achieved. The sequences orders determined are presented in Appendix 1.

2.1.8 Sequence 3a (S3a)

Sequence 3 leads to a symmetrical form and the movement of the slider is vertical. During the slider's movement, there are two locked joints and two adjusted joints. Following one step, the final position is completed. In Step 1, all the joints are currently adjusted except the joints 3 and 7 that are locked, Fig. 2.9, Table 2.8.

$$STEP 0 [\theta_1, \theta_2, \theta_3, \theta_4, H_5, \theta_6, \theta_7, \theta_8, \theta_9] = [98^\circ, 143.60^\circ, 143.42^\circ, 155^\circ, 0m, 155^\circ, 143.42^\circ, 143.60^\circ, 98^\circ]$$

$$STEP 1 [\theta_1, \theta_2, \theta_3, \theta_4, H_5, \theta_6, \theta_7, \theta_8, \theta_9] = [120^\circ, 101.70^\circ, 143.42^\circ, 174.88^\circ, -1.3445m, 174.88^\circ, 143.42^\circ, 101.7^\circ, 120^\circ]$$

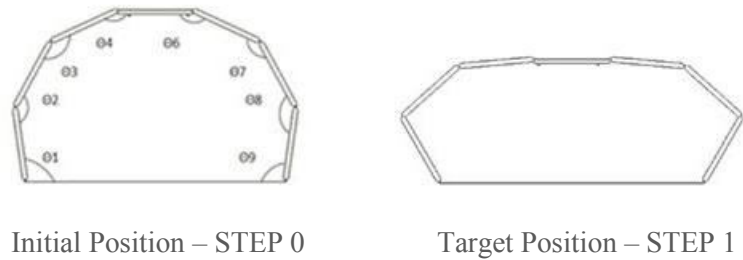


Figure 2.9 Structure Configurations

Table 2.7 Scheduling tables for feasible control sequence 3a

	J ₁	J ₂	J ₃	J ₄	J ₅	J ₆	J ₇	J ₈	J ₉
Step 1									

: pivoted-to-the-ground unlocked joint,
 : pivoted-to-the-ground locked joint,
 : unlocked joint,
 : locked joint,

 - - - : effective link,
 : slider,
 : currently adjustment

In Step 1, the joints 3 and 7 are locked, so that the two linkages between joints 2 and 4 move as one. The same happens with the joints 6 and 8, Fig. 2.10.

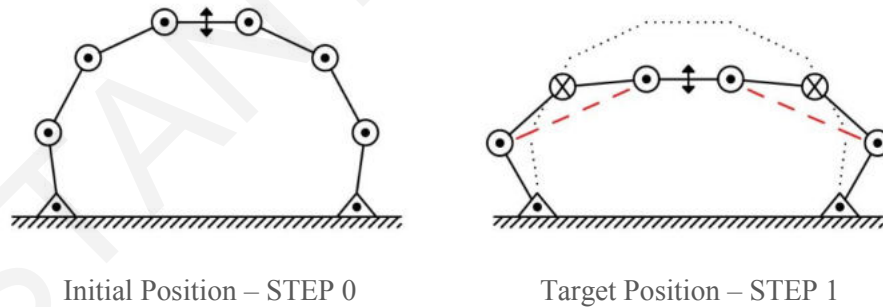


Figure 2.10 Selected feasible motion sequences in relation to the systems, Scale 1:200

Sequence 3b (S3_b)

In Step 1, all the joints are currently adjusted expect the joints 2 and 7, which are locked. It is not possible to complete the configuration because of a singularity, Table 2.9.

Table 2.8 Scheduling tables for control sequence 3b

	J ₁	J ₂	J ₃	J ₄	J ₅	J ₆	J ₇	J ₈	J ₉
Step 1									

: pivoted-to-the-ground unlocked joint,
 : pivoted-to-the-ground locked joint,
 : unlocked joint,
 : locked joint,
 : effective link,
 : slider,
 : currently adjustment

Sequence 3c (S3c):

In Step 1, all the joints are currently adjusted expect the joints 1 and 9, which are locked. It is not possible to complete the configuration because of a singularity. If there were more steps, the target position could be completed, Table 2.10.

Table 2.9 Scheduling tables for control sequence 3c

	J ₁	J ₂	J ₃	J ₄	J ₅	J ₆	J ₇	J ₈	J ₉
Step 1									

: pivoted-to-the-ground unlocked joint,
 : pivoted-to-the-ground locked joint,
 : unlocked joint,
 : locked joint,
 : effective link,
 : slider,
 : currently adjustment

Among possible sequences to achieve specific symmetrical and non-symmetrical configurations, the ones with the least reconfiguration steps have been investigated, since the kinematics approach applied provides maximum flexibility and endurance with minimum required actuation energy.

CONSTANTINA THEOKLI

CHAPTER 3 CONSTRUCTION DESIGN

The current chapter refers to the structural and construction design of the planar and spatial linkage structure. Main parameters that influence the design refer to the supports of each linkage, the members and their joint connections, as well as the actuation components that are integrated within the system to enable horizontal or vertical transformations. In this framework, two alternatives have been developed, based on the integration of a horizontal and four vertical linear motion actuators respectively. In both cases, the primary planar linkage consists of seven hinge connected beams supported on a structural grid that serves as the floor structure. The structural grid has an overall length of 7 m in span direction, and it is supported on honeycomb columns with variable height to accommodate any height differences of the ground level. At midspan, the structural linkage is further supported on diagonals positioned within the system to form a V- or X-shape according to the reconfiguration requirements of the system.

3.1 Structural System

In the first alternative, the V-diagonals are rigidly supported on the structural grid at midspan and hinge interconnected with a horizontal member on the top, below the beam of the linkage at midspan, Fig. 3.1. A linear motion actuator is positioned above the linkage beam and connected on one side with the latter and on the other side, with the member interconnecting the V-diagonals. Thus, operation by the actuator provides relative displacements of the linkage to its support elements at midspan. The V-diagonals consist of round hollow profiles of \varnothing 140/10 mm.

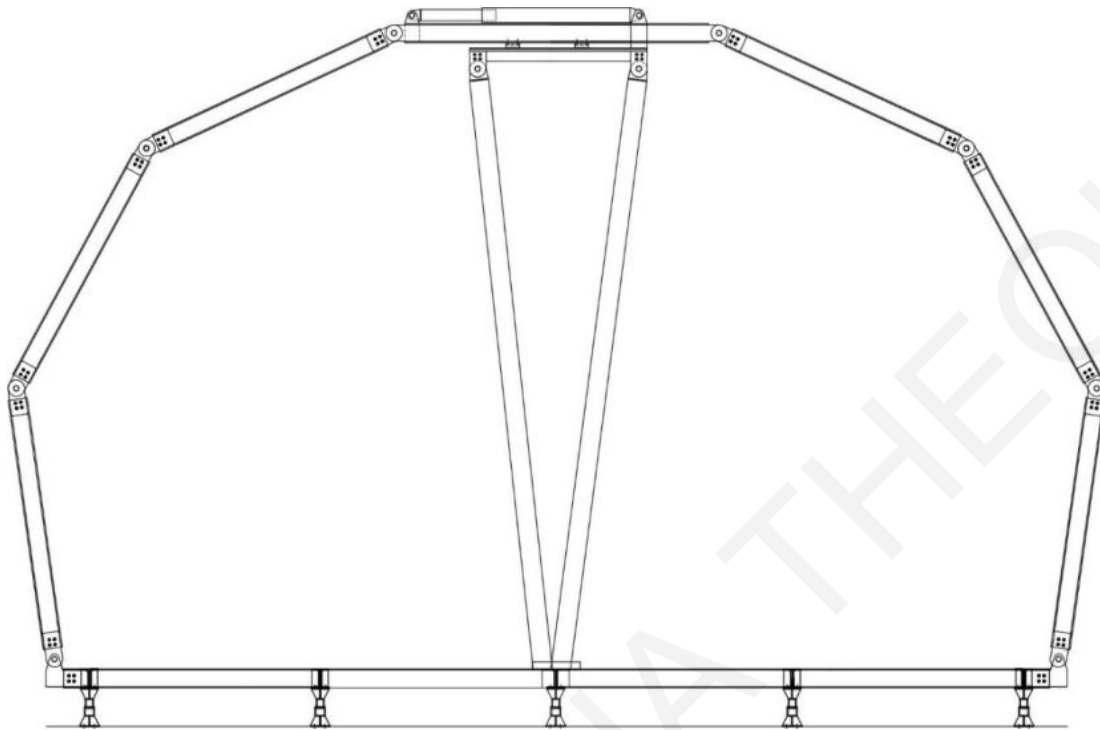


Figure 3.1 Planar bar linkage structure with horizontal reconfigurability, Scale 1:50

In the second alternative, the X-diagonals are hinge supported on the structural grid and the beam of the linkage at midspan, Fig. 3.2. The diagonals consist of four telescopic round hollow sections of $\varnothing 140/10$ mm and $\varnothing 120/7$ mm that are interconnected at mid-length through flat steel plates of 10 mm thickness. The joint connection of the steel plates has a certain travel distance provided by the longitudinal holes of the elements that primary serves assembly issues.

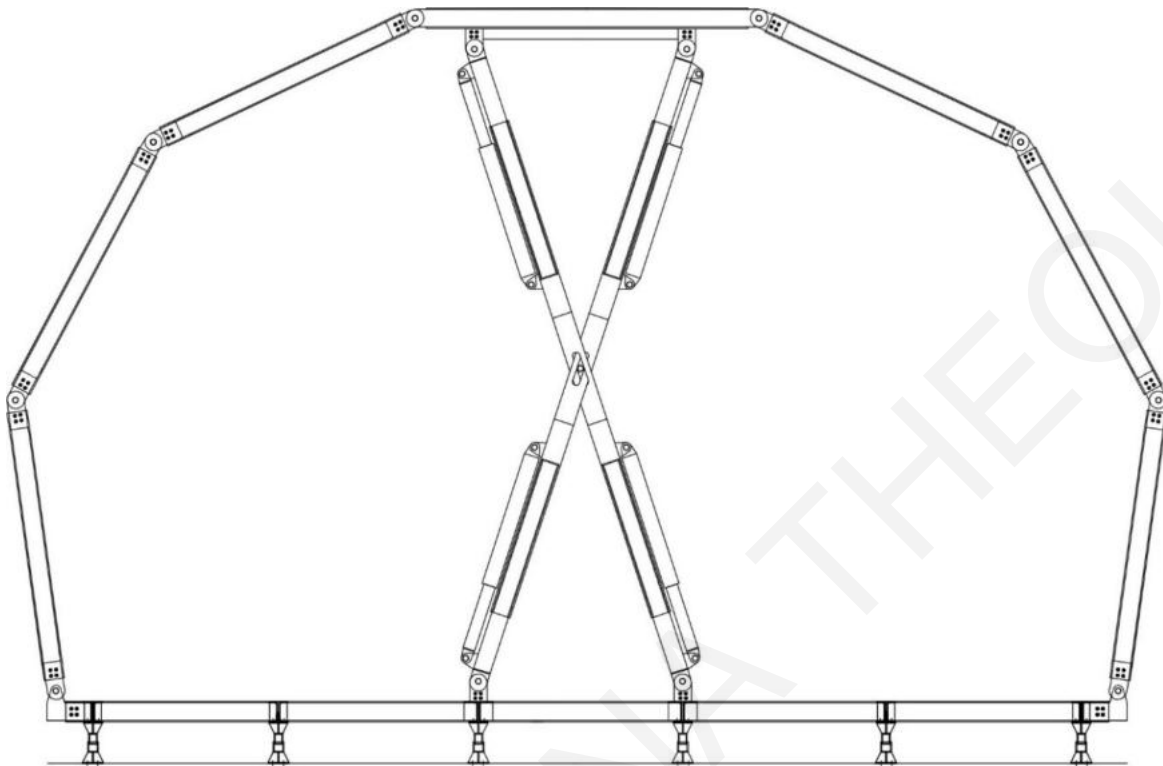


Figure 3.2 Planar bar linkage structure with vertical reconfigurability, Scale 1:50

The spatial system is composed of 10 planar bar linkages arranged at relative distance of 2.0 m in the longitudinal direction, Figs 3.3, 3.4. In each spatial system only the first and last linkage are actively controlled by the linear actuation and supported at midspan by the diagonals. This arrangement requires nevertheless that the ‘bare linkages’ follow any reconfiguration of the system provided by the ‘actuation linkages’ through their rigid connection to the latter along the circumference of the spatial system. Hence, the diaphragm is ensured through secondary beams, hinge connected with the linkage members at both ends, and prestressed cable diagonals. The structural composition principle of linearly adding planar systems to provide the spatial system enables uniform, identical and synchronous reconfigurations of the system in span direction. The differentiation in the system composition in actuation and bare planar linkages enables minimization of the number of actuation elements (i.e., actuators) used and preservation of minimum self-weight of the structure. Furthermore, expandability of the spatial structure in both

directions is possible, depending on the number of members of the bar linkages, the number and position of the actuation and bare linkages and the structural grid.

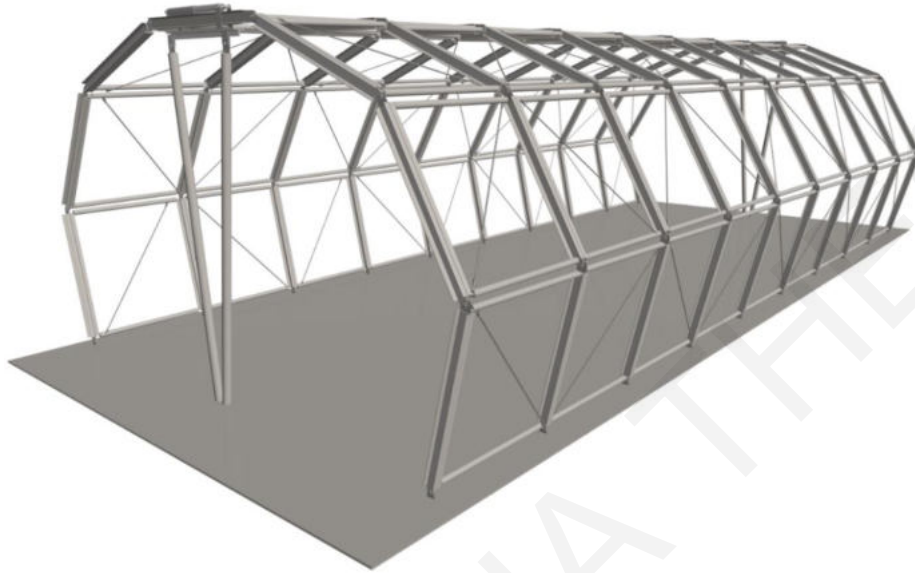


Figure 3.3 Spatial structure with horizontal reconfigurability, composed of two actuation linkages and intermediate bare linkages

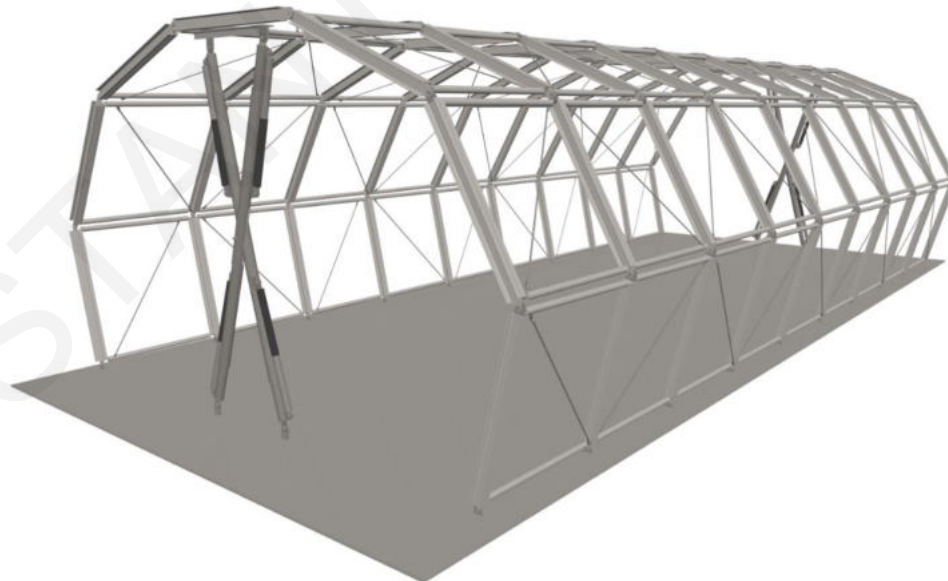


Figure 3.4 Spatial structure with vertical reconfigurability, composed of two actuation linkages and intermediate bare linkages

The construction design of the members connections is based on the members modularity and favors flexibility and clarity of the structure operability. The structural grid is composed of partly rigidly connected beams in both horizontal directions. The beams consist of double UPN 140/60 sections interconnected through cross-shaped steel plates of 10 mm thickness, as shown in Fig. 3.5.

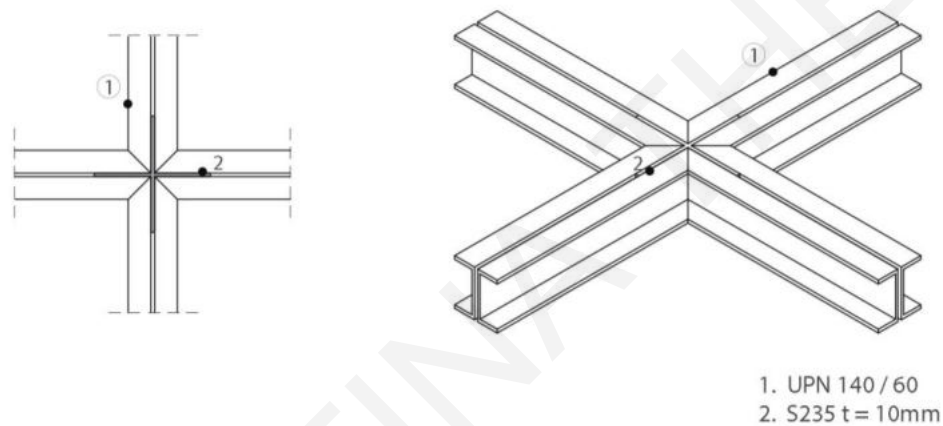


Figure 3.5 Connection principle of beams of structural grid, Scale 1:10

The beams of each linkage are hinge connected to the structural grid through a steel plate of 10 mm thickness connected with the horizontal beam and two plates that extend from the linkage beam webs, as shown in Fig. 3.6. Thus, the supports of the linkages allow rotations of the members in span direction.

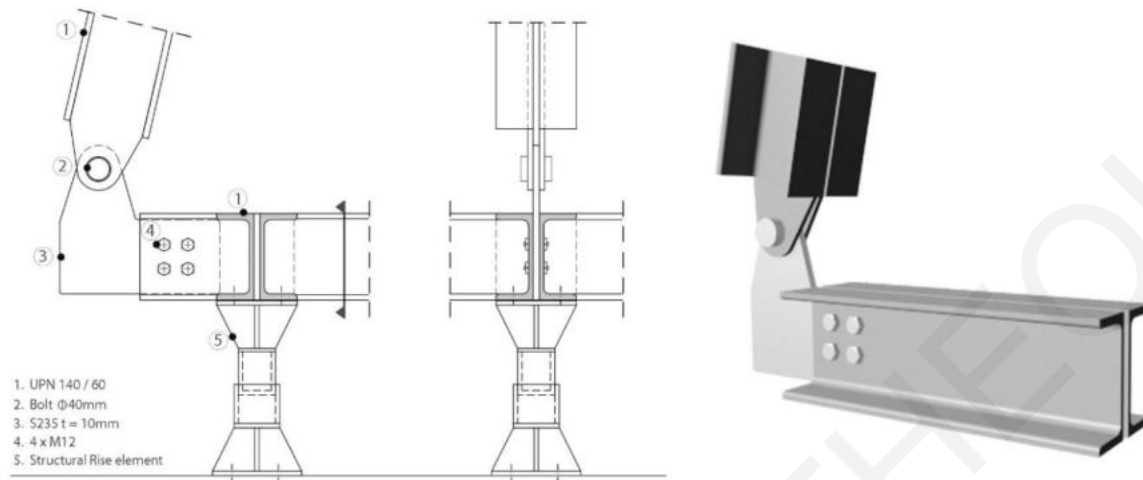


Figure 3.6 Linkage beam support connection principle with the structural grid of the system, Scale 1:10

The beams of the linkage are interconnected through a steel plate of 10 mm thickness inserted between the UPN sections of the beam and two steel plates of 10 mm thickness each that extend from the other beam's web, as shown in Fig. 3.7. Note that the actuation beams on the joints (electromagnetic brakes or pneumatic actuators) are not included in Fig. 3.7.

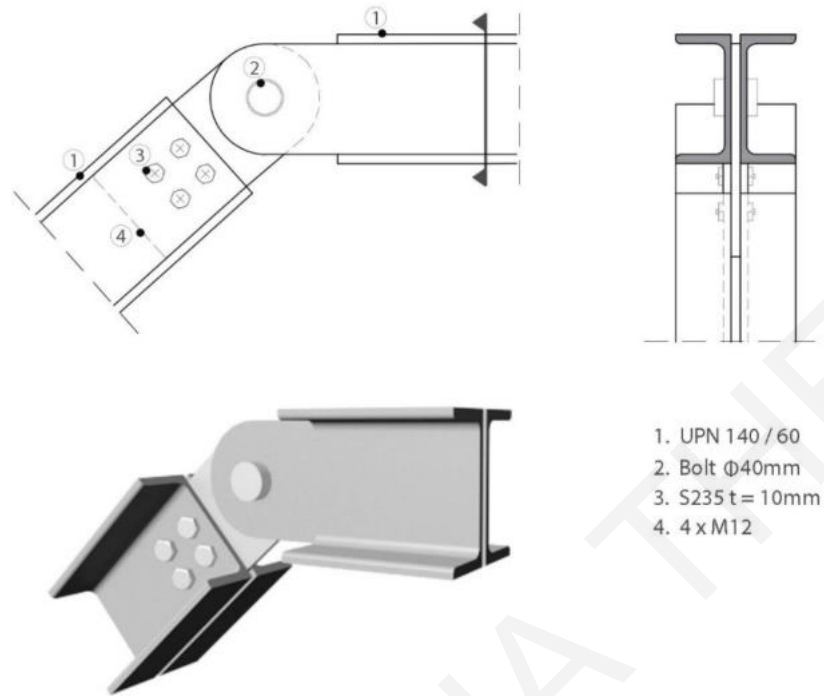


Figure 3.7 Linkage beams connection principle, Scale 1:10

The connection of the V-diagonals at midspan of the system in the alternative with horizontal actuation takes place over two horizontal steel plates, whereas the lower one is connected to the structural grid joint and the upper one, welded to the diagonals as shown in Fig. 3.8.

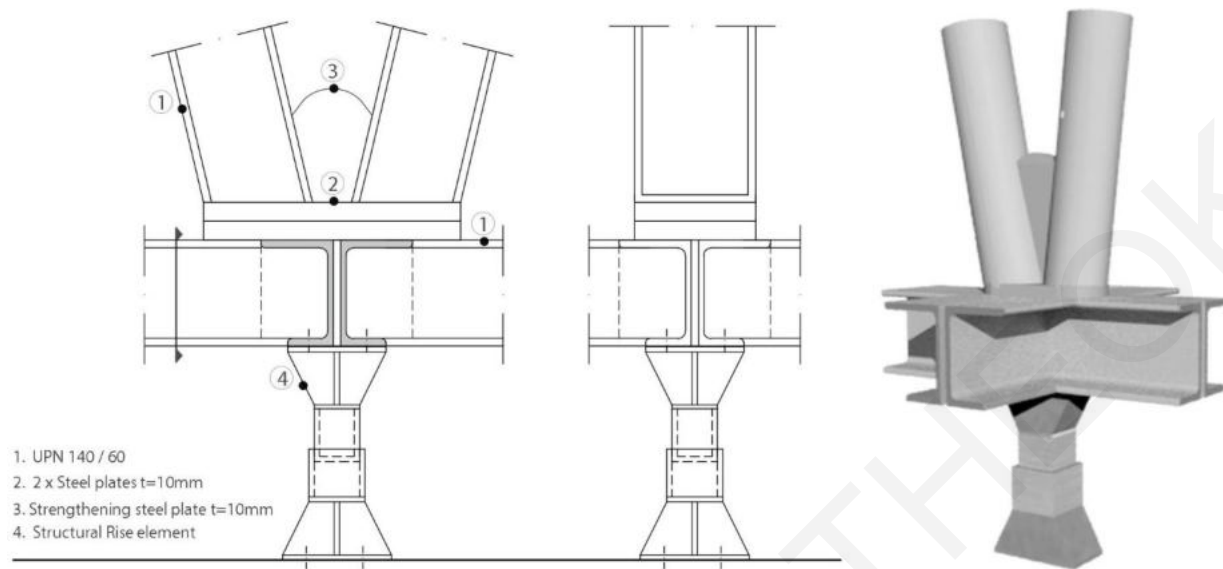


Figure 3.8 Support principle of V-diagonals to the structural grid, Scale 1:10

The integration of the linear motion actuator with the actuation linkage is shown in Fig. 3.9. The actuators ends are connected to the horizontal structural members (i.e., the linkage beam and the diagonals interconnecting member on each side respectively) through steel plates of 10 mm thickness. The linkage beam may role on the interconnecting member with a section of T 140/140 mm over specially formed sliding elements.

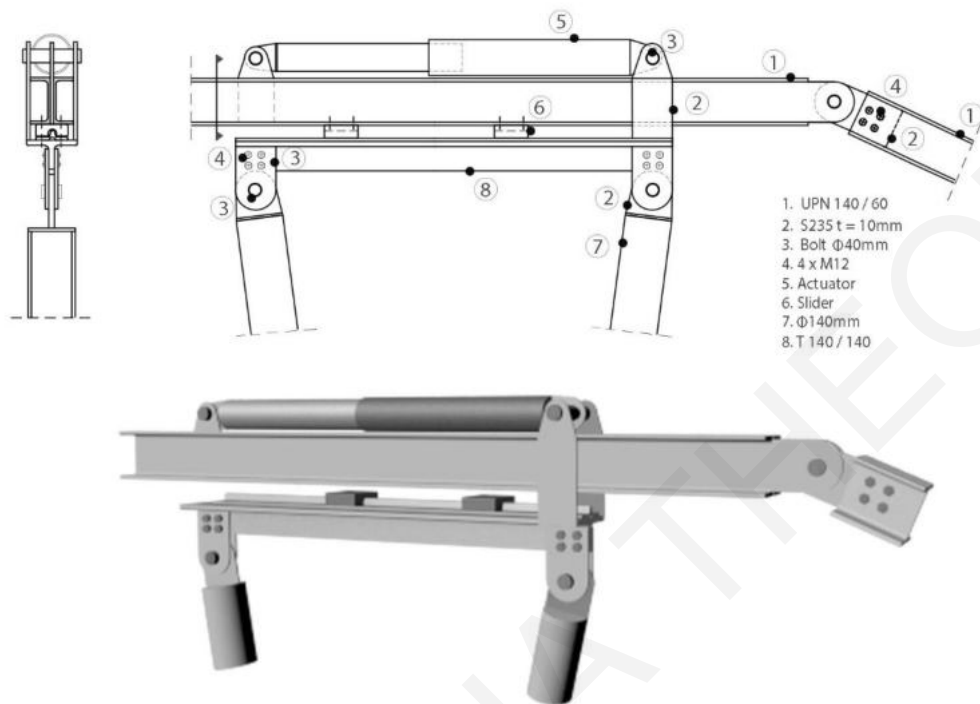


Figure 3.9 Linear motion actuator connection principle to the planar actuation linkage for horizontal reconfigurability, Scale 1:22.5

The connection of the X-diagonals at midspan of the system in the alternative with vertical actuation takes place over steel plates of 10 mm thickness that are welded with the structural grid and the diagonals respectively, as shown in Fig. 3.10. Thus, the connection joints allow rotations of the diagonals in span direction.

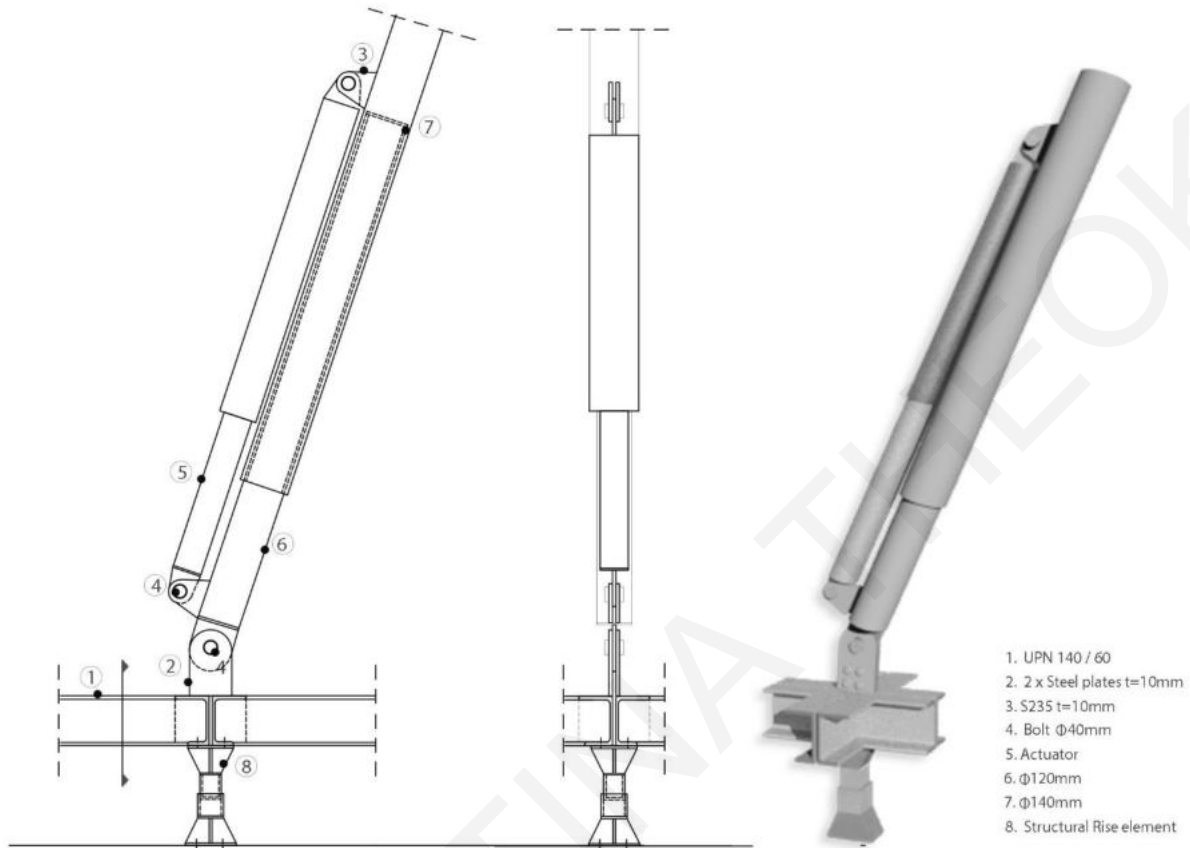


Figure 3.10 Support principle of X-diagonals to the structural grid, Scale 1:20

In this alternative, the diagonals are directly connected through steel plates to their interconnecting beam that is rigidly connected to the linkage beam. The actuators are connected to the telescopic diagonals, on one end, to the large round hollow section, and on the other end, to the small round hollow section, as shown in Fig. 3.11.

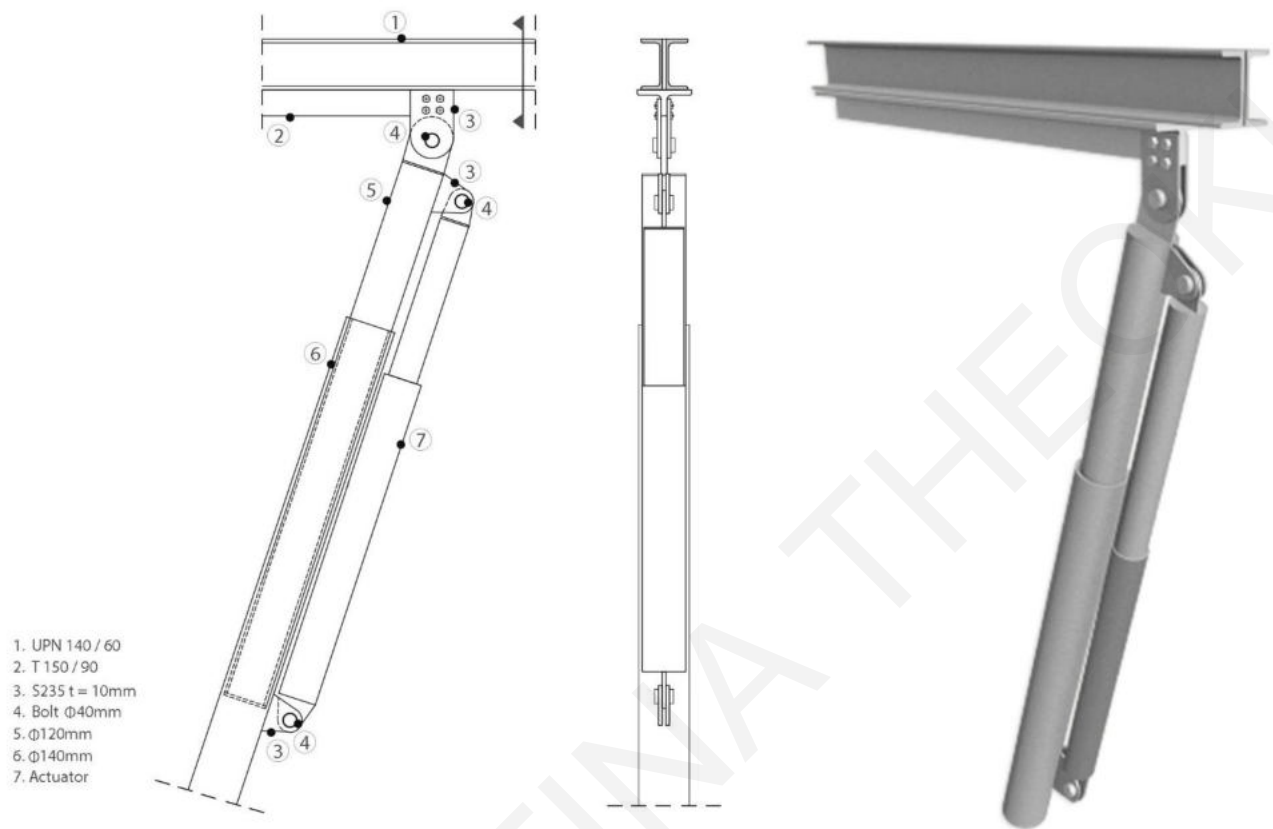


Figure 3.11 Linear motion actuator connection principle to the planar actuation linkage for vertical reconfigurability, Scale 1:20

The rigid connection of the planar bar linkages in the longitudinal direction of the spatial system takes place through secondary compression members, of round hollow sections of $\varnothing 76.1/10$ mm, placed in pairs on both sides of the joint connections of the linkage beams, and cable diagonals of $\varnothing 20$ mm diameter. The compression members are hinge connected to the linkage beams over steel plates of 10 mm thickness, welded to the secondary members and the web of the linkage beam sections. The connection joints allow rotations of the secondary members in vertical direction to the linkage beams. The cable elements are anchored on RODAN elements, RDN12, hinge connected to the secondary members sections, Fig. 3.12.

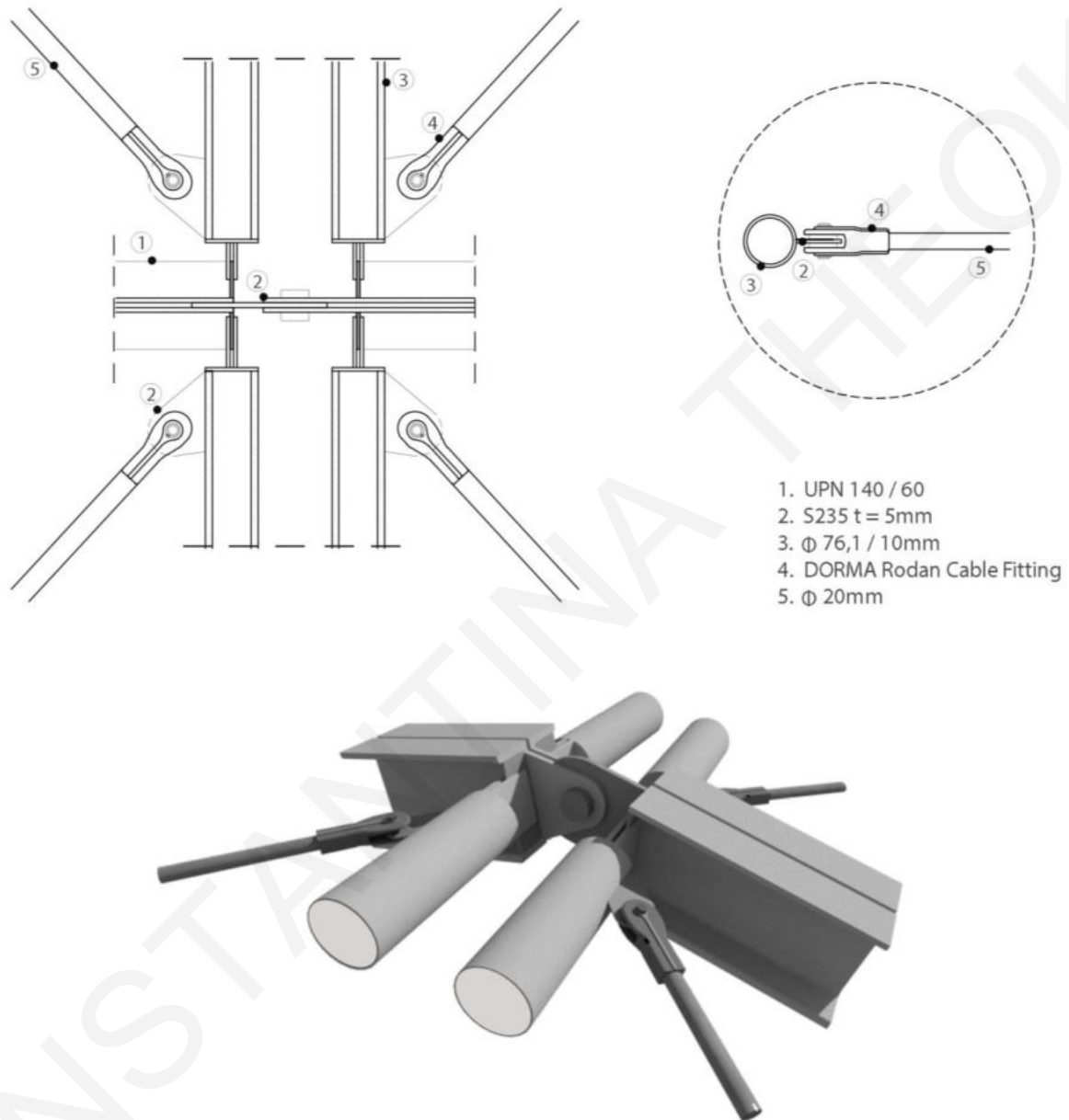


Figure 3.12 Construction design principle of secondary structure to the planar linkages of the spatial system, Scale 1:10

3.2 Envelope Structure

The building envelope is required to provide roofing to the variable space of the structure, while deforming elastically in response to the shape adjustments of the primary structure. In the specific case example, the envelope should have at the material level, good mechanical properties, i.e., elasticity, strength and durability. In principle, coated polyester textiles of THV, Polytetrafluoroethylene, and noncoated PTFE are mostly suitable for adaptable structures. These materials are foldable with good UV stability and light transmittance properties in the range of 15-40 % [3.1]. At the structural level the envelope should have low self-weight, structural efficiency, capability to cover the respective span spaces with only elastic deformations and minimal stress interactions with the primary structure. In addition, the envelope is required to be flexible, in order to accommodate the member structure.

ETFE, ethylene tetrafluoroethylene, has been known since 1940s, when a US patent for the substance was granted to DuPont. Unlike its close relation Teflon (PTFE), which was an accidental spin-off, ETFE was the result of DuPont's research program to develop an insulation material for industrial machinery that was resistant to friction and abrasion, immune to radiation and effective at both extremely high and low temperatures. ETFE is also used in the chemical industry, as shown in Fig. 3.13 whereas one of the most stable known chemical compounds has been widely adopted for applications in hostile environments, such as filters and linings for acid and alkaline baths.



Figure 3.13 ETFE roof from below and inflated cushions fixed to a cable structure that easily deform to define the desired warped surface in an industry building

In the architecture field, ETFE was sparked by the first oil crisis in 1973-74, when Europe began to focus on harvesting solar energy to replace fossil fuels. Extruded ETFE film was developed at Hoechst, where researchers significantly advanced production techniques and market applications, including use as a replacement for glass in greenhouses and in metallized form, for thermal solar collectors. ETFE showed no change in its optical or mechanical properties and these results provided the assurance that paved the way for architectural applications [3.2].

ETFE films, also known as ETFE fabric membranes, can be heat-sealed, thermoformed, and laminated to various substrates. TCI offers ETFE to create tensile membrane structures with exceptional transparency, elasticity, and durability around the world. It can be purchased in clear, printed, or colored varieties, all of which maintain excellent chemical, weather, and stress-crack resistance and low flammability. ETFE is currently one of the most sustainable materials on the market, since it can be 100 % recycled after its long service life [4.3].

In the specific case example, the envelope is required to be flexible in order to accommodate for cases of dissimilar configurations assumed by any adjacent n-bar linkages that constitute the primary member structure. At the lower and upper longitudinal row of the spatial structure on each side, ETFE membranes have been placed. The membrane units have overall dimensions in plane of 2.0 x 2.0 m and the envelope is positioned at a distance of 20 cm underneath the primary structure for preserving continuity in the cover material. In the two lower rows on each side and the upper one, in the longitudinal direction of the spatial structure, thin strips of ETFE membranes have been applied. The ETFE membranes are placed at the bar linkage connection zones defined by the secondary members. In principle, the adjacent ETFE membranes are interconnected on the beams that consist of double UPN 140/60 sections. In addition, membrane units are to be supported on a steel plate of 10 mm thickness, and fixed through the membrane clips. Furthermore, photovoltaic membranes have been applied in the two upper rows on each side, in the longitudinal direction of the spatial structure, as further described in Chapter 5.



Figure 3.14 Spatial structure with vertical reconfigurability and ETFE membrane



Figure 3.15 Spatial structure with horizontal reconfigurability and ETFE membrane

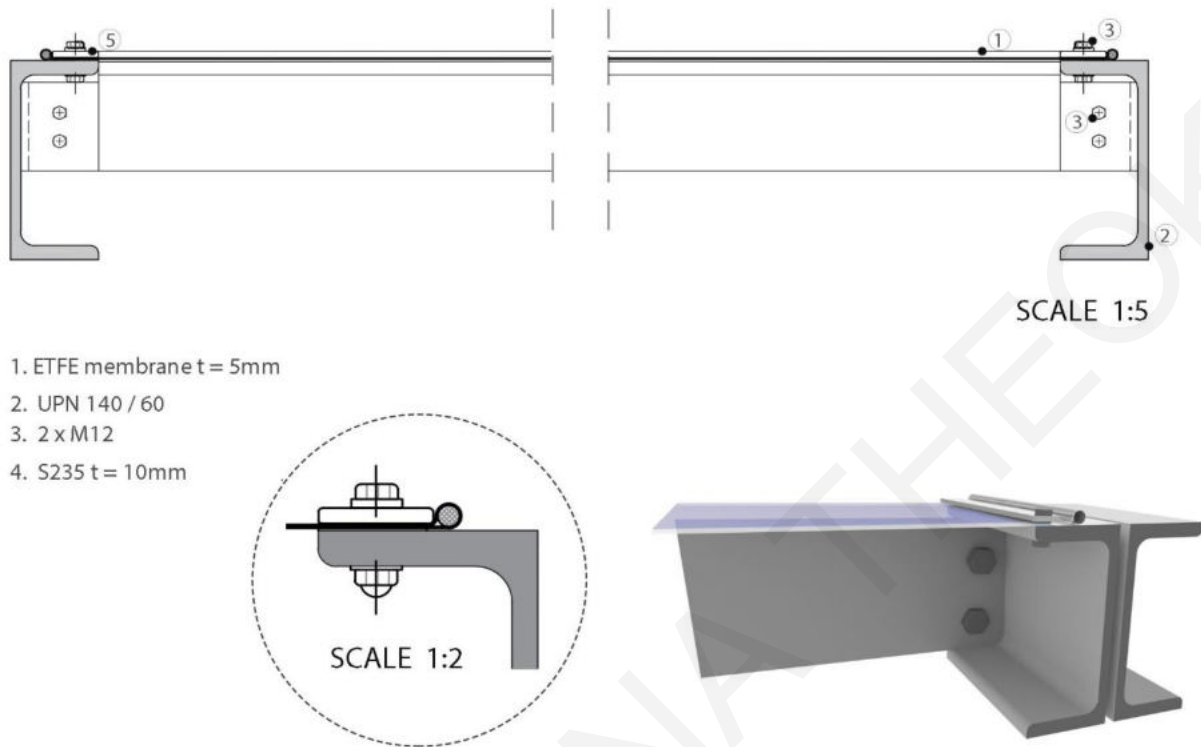


Figure 3.16 Construction design of ETFE membrane support

CHAPTER 4 KINEMATICS ANALYSIS

The numerical analysis of the structure was based on its kinematics based on the crank–slider approach. In the current stage, the analysis focuses on the motion analysis of the structure using the FEA software Solidworks. Following the preliminary stage of determining the control sequences for implementing the required shape adjustments and the construction design, a new model has been created based on the same geometric characteristics and dimensions of the basic system. In addition, the members and the materials of the structure have been defined. Also, the simulation includes the brake torques analysis, based on the self-weight and the material stresses. The model was created twice, a model for the case of the horizontal and one for the vertical actuation motion.

The model was designed in the 3D drawing interface of the software program and then all the data needed for the simulation were entered into the database (input data). First of all, in the drawing interface, the members of the structure were designed and then, with the assembly method, the initial position was developed. The linkages were connected with pins and the linkages with steel plates, nuts and bolts, according to the software library. Also, the linkage for the actuator's position was created, and with the assembly method, the actuator was selected for the structure's motion. The same procedure was followed for the modelling of the horizontal and vertical actuated system.

4.1 Linkage Joints

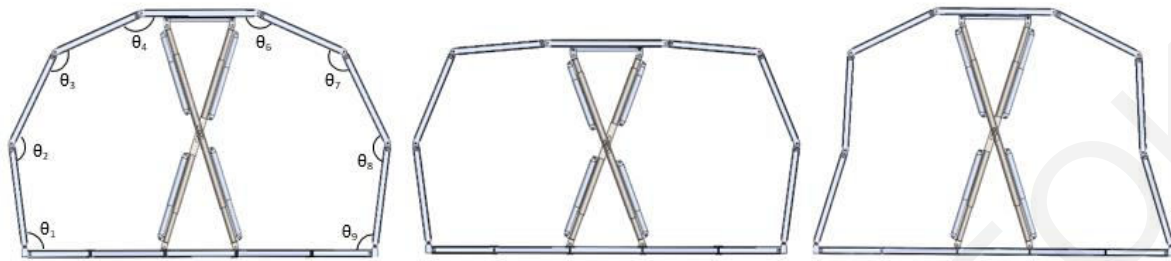
Following the modelling of the horizontal and vertical motion system, the joint angles have been determined as below for the initial, intermediate and target positions of the systems, according to the respective selected motion sequences. After redefining the angles, the spatial models of the structure were created within the software interface, and a motion analysis was conducted, Figs 4.1-4.3.

Sequence 1a (S1_a)

STEP 0 [$\theta_1, \theta_2, \theta_3, \theta_4, H_5, \theta_6, \theta_7, \theta_8, \theta_9$] = [98°, 144.6°, 139°, 158.4°, 0m, 158.4°, 139°, 144.6°, 98°]

STEP 1 [$\theta_1, \theta_2, \theta_3, \theta_4, H_5, \theta_6, \theta_7, \theta_8, \theta_9$] = [98°, 148.25°, 118.5°, 175.3°, -0.5164m, 175.3°, 118.5°, 148.25°, 98°]

STEP 2 $[\theta_1, \theta_2, \theta_3, \theta_4, H_5, \theta_6, \theta_7, \theta_8, \theta_9] = [72.3^\circ, 194.65^\circ, 118.5^\circ, 154.5^\circ, +0.7864\text{m}, 154.5^\circ, 118.5^\circ, 194.65^\circ, 72.3^\circ]$



Initial Position – STEP 0

STEP 1

Target Position – STEP 2

Figure 4.1 Structure Configurations

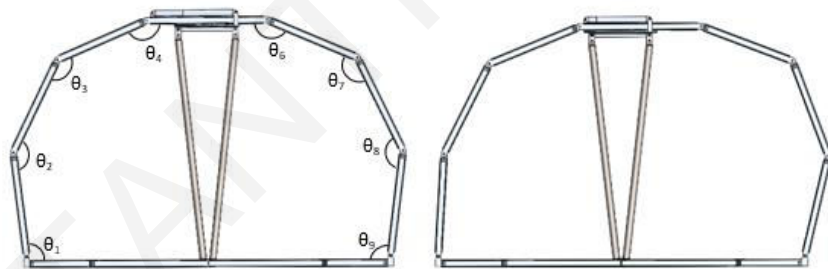
Sequence 2a (S2a)

STEP 0 $[\theta_1, \theta_2, \theta_3, \theta_4, H_5, \theta_6, \theta_7, \theta_8, \theta_9] = [98^\circ, 144.6^\circ, 139^\circ, 158.4^\circ, 0\text{m}, 158.4^\circ, 139^\circ, 144.6^\circ, 98^\circ]$

STEP 1 $[\theta_1, \theta_2, \theta_3, \theta_4, H_5, \theta_6, \theta_7, \theta_8, \theta_9] = [86.8^\circ, 155.48^\circ, 139^\circ, 158.7^\circ, +0.4786\text{m}, 159.85^\circ, 131.13^\circ, 144.6^\circ, 104.4^\circ]$

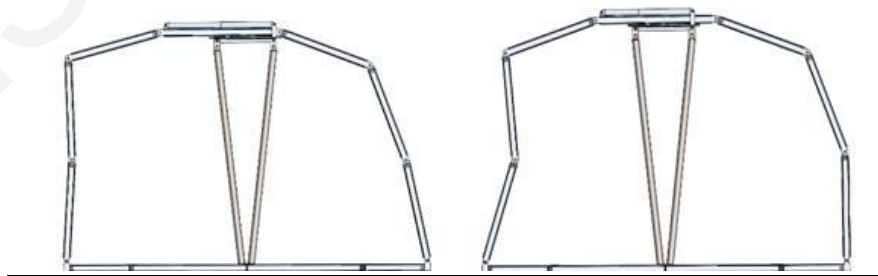
STEP 2 $[\theta_1, \theta_2, \theta_3, \theta_4, H_5, \theta_6, \theta_7, \theta_8, \theta_9] = [86.8^\circ, 185.6^\circ, 102^\circ, 165.57^\circ, -0.9407\text{m}, 160.2^\circ, 131.13^\circ, 171^\circ, 77.7^\circ]$

STEP 3 $[\theta_1, \theta_2, \theta_3, \theta_4, H_5, \theta_6, \theta_7, \theta_8, \theta_9] = [71.65^\circ, 203.94^\circ, 102^\circ, 162.4^\circ, +0.377\text{m}, 161.2^\circ, 131.13^\circ, 157.8^\circ, 89.85^\circ]$



Initial Position – STEP 0

STEP 1



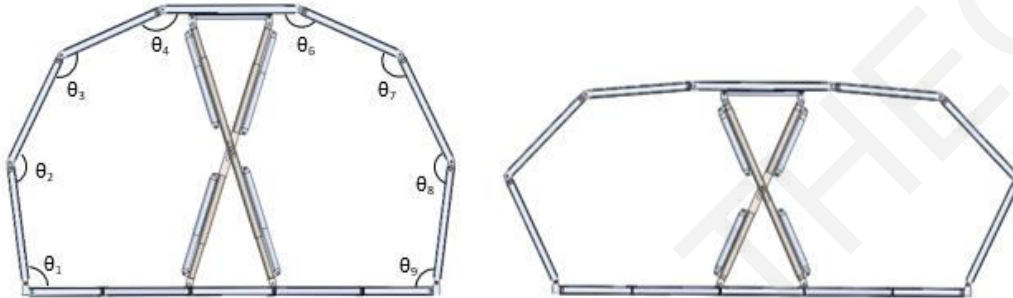
STEP 2

Target Position STEP 3

Figure 4.2 Structure Configurations**Sequence 3a (S3_a)**

STEP 0 [$\theta_1, \theta_2, \theta_3, \theta_4, H_5, \theta_6, \theta_7, \theta_8, \theta_9$] = [98°, 144.6°, 139°, 158.4°, 0m, 158.4°, 139°, 144.6°, 98°]

STEP 1 [$\theta_1, \theta_2, \theta_3, \theta_4, H_5, \theta_6, \theta_7, \theta_8, \theta_9$] = [116.8°, 107.6°, 140.15°, 175.5°, -1.15m, 175.5°, 140.15°, 107.6°, 116.8°]



Initial Position – STEP 0

Target Position - STEP 1

Figure 4.3 Structure Configurations**4.2 Motion Analysis**

The torques determination in the joints throughout the transformation process is significant for the reconfiguration of the structure. This stage is divided into three sub-stages. First of all, the calculation process includes the definition of the angles of the joints for the initial and target positions, then the positions of the linkages need to be locked by the mates list, Fig. 4.4.

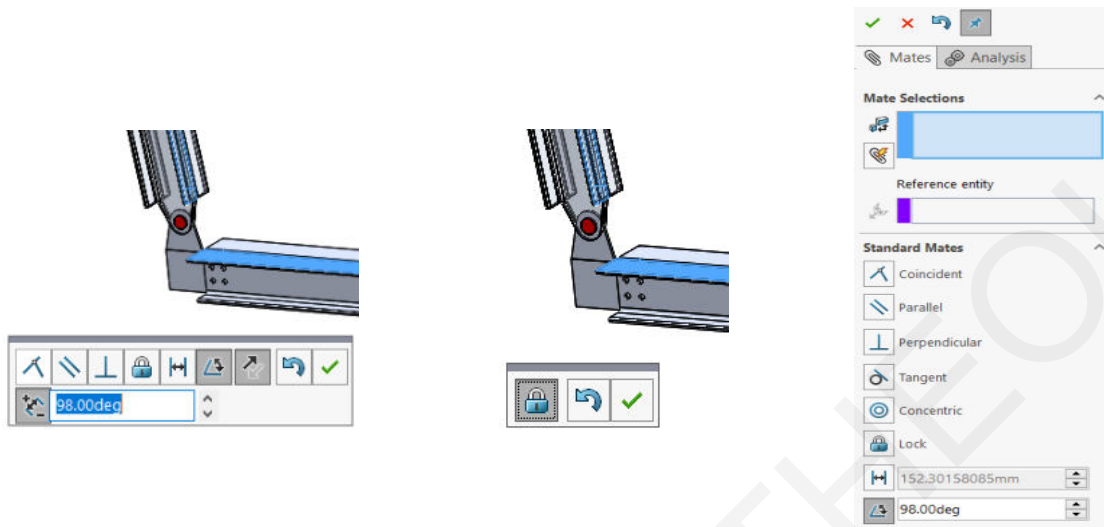


Figure 4.4 Commands ‘Angle’ and ‘Lock’ from standard mates list

The second stage is to select the type (servo motor) of the linear actuator from the library and the direction of the model (e.g., gravity). The direction of weight is defined based on the x, y, z axes, whereas in this model the direction is downwards corresponding to the y-axis, Fig. 4.5.

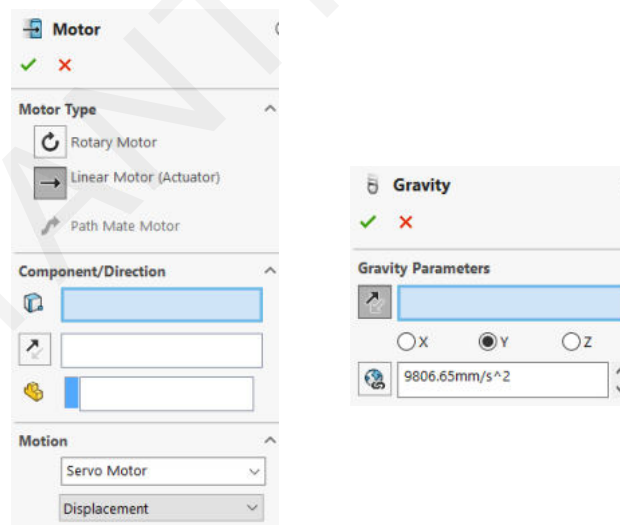


Figure 4.5 Definition of motor and gravity

The last step is about the actuator's displacement. According to the timeline data, the actuator is activated, and the steps of the displacement and the respective time, defined, Fig. 4.6.

Tasks		Triggers			Actions					Time	
Name	Description	Trigger	Condition	Time/Delay	Feature	Action	Value	Duration	Profil	Start	End
Task1		Time		0s	LinearMotor2	On				0s	0s
Task2		Task1	Task Start	<None>	LinearMotor2	Change	478.4mm	10s		0s	10s
Task3		Task2	Task Start	<None>	Joint (2)	On				0s	0s
Task4		Task2	Task Start	<None>	Joint (10)	Off				0s	0s
Task5		Task2	Task End	<None>	LinearMotor2	Change	-940.7mm	10s		10s	20s
Task6		Task5	Task Start	<None>	Joint (2)	On				10s	10s
Task7		Task5	Task Start	<None>	Joint (10)	Off				10s	10s
Task8		Task5	Task End	<None>	LinearMotor2	Change	377mm	10s		20s	30s
Task9		Task8	Task Start	<None>	Joint (2)	On				20s	20s
Task10		Task8	Task Start	<None>	Joint (10)	Off				20s	20s

Figure 4.6 Specifying the model steps in the timeline view

The actuator's movement to the top or the right of the structure is signed with the symbol "+", in contrast to the movement to the bottom or the left side of the structure that is signed with the symbol "-". The velocity of the actuator movement is defined as the ratio of displacement over time (Dx/Dt). In addition, all the steps of the structure have been defined, so that the torques on the joints are calculated and presented in the Results interface of the software in graphs, Fig. 4.7.

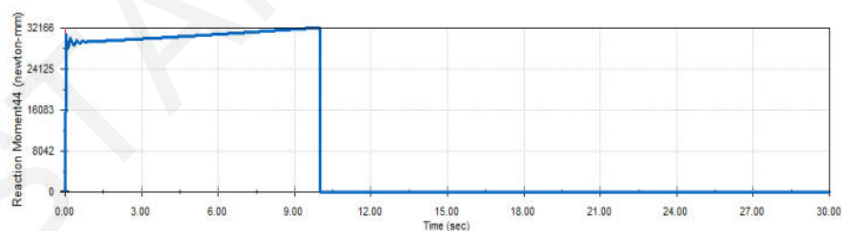


Figure 4.7 Example for calculation of torque graph using the 'result' command

4.3 Numerical Results

The system configurations, as well as the brake torques and the displacements of the actuator have been determined, based on the horizontal and vertical actuation systems. Among different feasible sequences, the ones with less required steps are selected and investigated with regard to the highest maximum brake torques and slider displacements. Figs 4.8-4.10 illustrate the reaction moments on the joints, in each sequence. The reconfiguration steps have a duration 10 seconds.

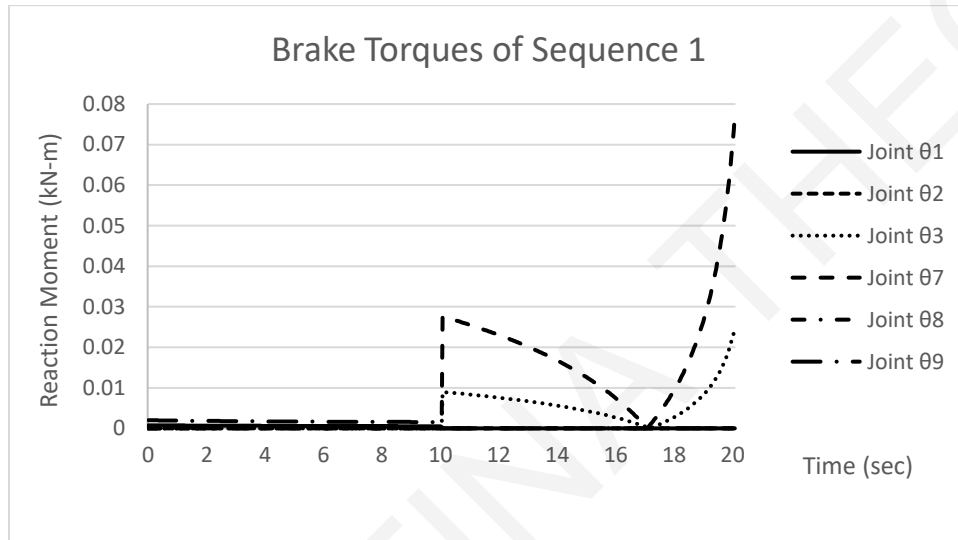


Figure 4.8 Brake torques of Sequence 1

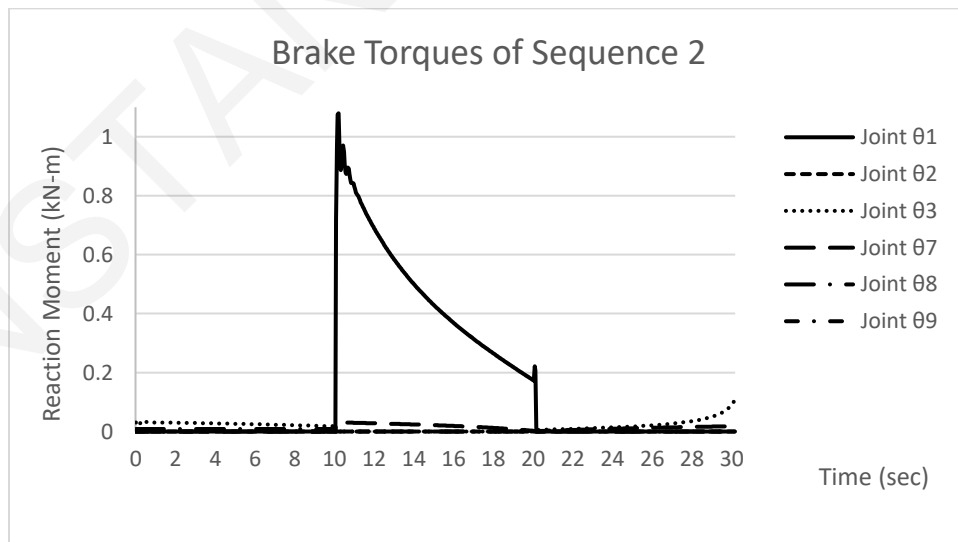


Figure 4.9 Brake torques of Sequence 2

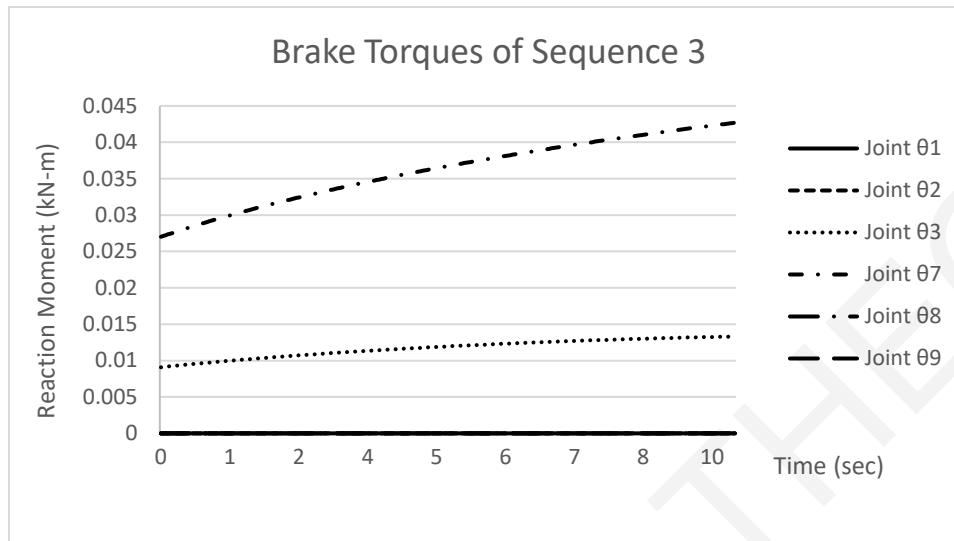


Figure 4.10 Brake torques of Sequence 3

Table 4.1 shows the maximal brake torques on the joints, in each sequence. The maximum brake torques are registered in Sequence 2 and the minimum, in Sequence 3. The respective highest maximum value in Sequence 1 is around 7.7 kNcm. In Sequences 2 and 3, the highest values amount to 108 and 4.3 kNcm, respectively. Moreover, in Sequence 2 is present the highest value of braking torque in all sequences; it is more possible to appear a deformation in the Sequence 2.

Table 4. 1 Maximal brake torques

	Joint 1 θ_1 [kN.cm]	Joint 2 θ_2 [kN.cm]	Joint 3 θ_3 [kN.cm]	Joint 7 θ_7 [kN.cm]	Joint 8 θ_8 [kN.cm]	Joint 9 θ_9 [kN.cm]	Max Torque [kN.cm]
Seq. 1	0.076	0	2.475	7.734	0	0.199	7.734
Seq. 2	107.944	0	10.220	3.111	0.913	0	107.944
Seq. 3	0	0	1.331	4.269	0	0	4.269

The displacements of the sliding block have been recorded as shown in Table 4.2. The maximum displacement in Sequences 1 and 2 is around 80 and 95 cm respectively. In Sequence 3, the respective value amounts to 115 cm. Thus, Sequence 3 has the highest value of the sliding block displacement, in contrast to Sequence 1, which has the lowest. In addition, Sequence 3 requires

more energy for the sliding block displacement than the other Sequences. The results indicate that it is preferable to eventually select a sequence with more steps, in achieving minimum displacements of the sliding block.

Table 4. 2 Maximal displacement of sliding block

	Displacement STEP 1 [cm]	Displacement STEP 2 [cm]	Displacement STEP 3 [cm]	Maximum Displacement [cm]
Seq. 1	51.64	78.64	-	78.64
Seq. 2	47.86	94.07	37.70	94.07
Seq. 3	115	-	-	115

CHAPTER 5 ENERGY APPROACH

5.1 Structure Usage

Earthquakes, pandemics, conflicts and environmental disasters have challenged architects, planners, designers and engineers. In this respect, temporary structures may adapt to the type of disaster (i.e., refugee migration, earthquakes, pandemics, etc.) quickly and efficiently, suiting both the circumstances and the location in which they are implemented. The crisis of epidemics constitutes an increasing risk and the communication of disease, a contemporary point of reference. Furthermore, the spread of infectious diseases can be so pervasive that they move from a local outbreak to a globally affected pandemic.

The proposed structure may be used for emergency situations, like the COVID-19 pandemic. The main usage of the structure is to create a space for doctors and the community during the performance of Covid tests and/or to inform the citizens about related measures taken during the pandemic. The size of the structure is appropriate to follow all sanitary protocols, and encourage people to keep social distancing measures. A clear threshold of sanitary protocols for both people and goods will additionally reinforce the inside of the building as a clean zone. As COVID-19 can be transmitted through airborne particles, proper quantities of fresh air in the interior space must be ensured for the users. Thus, the operable openings of the structure can supplement air dilution.

5.2 Energy Approach

Photovoltaic systems that are fully integrated into an architectural application, such as the BIPV system, can be applied during the design study, the construction, or upgrade of the structure. BIPV technologies can aesthetically upgrade the building and turn it into a high-efficiency infrastructure for solar energy production.

Thin-film solar cells were originally introduced in the 1970s by researchers at the Institute of Energy Conversion at the University of Delaware in the United States. The technology

continuously improved so that in the early 21st Century the global thin-film photovoltaic market was growing at an unprecedented rate and was forecast to continue to grow. Several types of thin-film solar cells are widely used because of their relatively low cost and their efficiency in producing electricity. Thin film solar cell technology has recently seen some radical advancement as a result of new materials and innovations in device structures [5.1].

Amorphous silicon thin-film cells are the oldest and most mature type of thin-films. They are made of nanocrystalline silicon, unlike typical solar-cell wafers. Amorphous silicon is cheaper to manufacture than crystalline silicon and most other semiconducting materials. Amorphous silicon is also popular, because it is abundant, non-toxic and relatively inexpensive. However, the average efficiency is very low, less than 10 % [5.2].

Applications of thin-film solar cells began in the 1980s with small strips that were used for calculators and watches. Throughout the early 21st Century the potential for thin-film applications increased greatly, because of their flexibility, which facilitates their installation on curved surfaces, as well as their use in building-integrated photovoltaics, Fig. 5.1 [5.1]. Sheets of thin-films may be used to generate electricity increasingly in places where other photovoltaic cells cannot be used, such as on curved surfaces on buildings, cars, or even, clothing to charge handheld devices. Such uses could help to achieve a sustainable energy future.

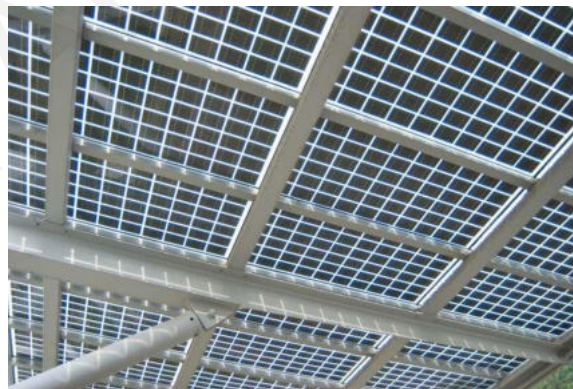


Figure 5.1 Thin-film solar cell application

If there is a long distance between the cells of the PV modules, there will be more transparency of the modules, Fig. 5.2. This allows sunlight to pass through the PV, providing at the same time, protection from rain and cold [5.4].

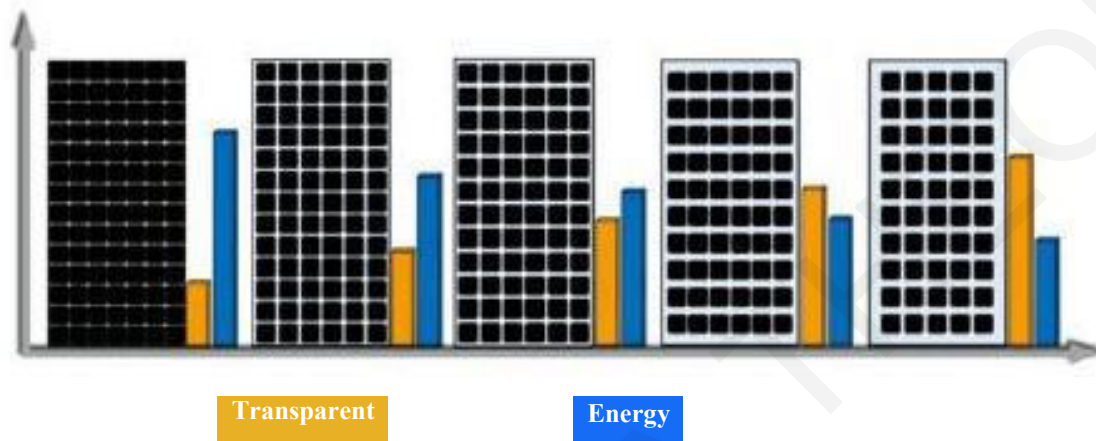


Figure 5.2 Transparency of a Photovoltaic System [5.1]

The corresponding envelope of the spatial structure consists of integrated thin photovoltaic films on two longitudinal rows, on each side of the structure, in place of the ETFE membranes. The photovoltaics application is based on the elements' exposure to the sun. The PV thin films, have the advantage that the distance between the cells can be adjusted and the light transmittance can change in achieving shading inside of the building. The irradiation levels and the PV systems performance were calculated through the platform of PV-sites [5.5], based on the weather conditions of Cyprus and Sweden, as these are provided by the weather data of the Energy Plus platform [5.6].

In principle, thin-film technologies reduce the amount of active material in a cell. The majority of film panels have 2-3 percentage points lower conversion efficiencies than crystalline silicon. Cadmium telluride (CdTe), copper indium gallium selenide (CIGS) and amorphous silicon (a-Si) are three thin-film technologies often used for outdoor applications. Fig. 5.3 shows a typical structure of a photovoltaic thin film cell.

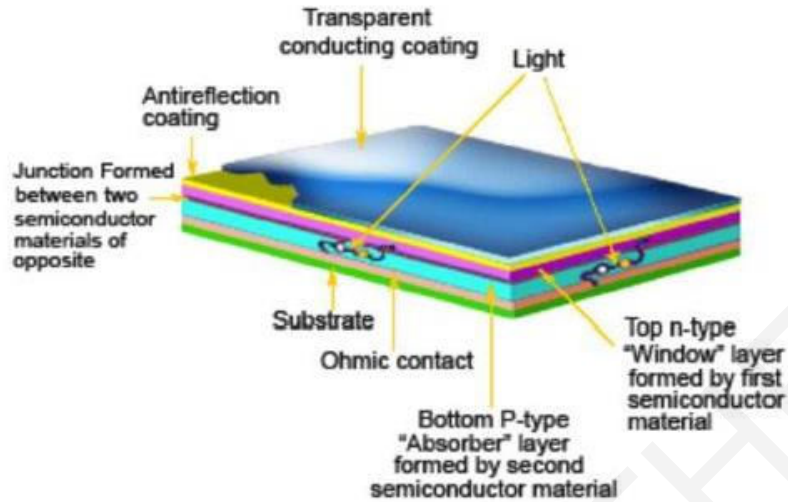


Figure 5.3 Structure of a Photovoltaic Cell [5.3]

The analysis is based on the climatic conditions of Larnaca, Cyprus (latitude: 34.923096 and Longitude: 33.634045), where for almost 8 months of the year, the sky is clear and there is high solar radiation [5.7, 5.8]. The analysis results show that the building integration of PV systems can contribute to the conversion of an existing low energy performance structure to an energy efficiency standards structure. According to the Department of Meteorology of Cyprus [5.7], the region of Larnaca has mild winters and warm to hot summers, with temperatures ranging from 7 to 33° C, respectively, Fig. 5.4. Also, the sun hours do not reach rates under the 180 hours during the winter months, Fig. 5.5.

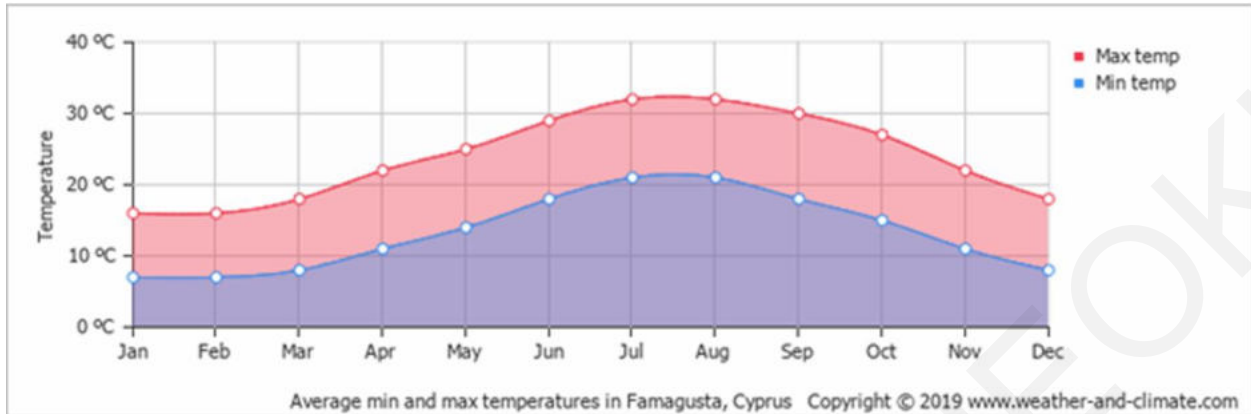


Figure 5.4 Average min and max temperatures in Larnaca, Cyprus [5.8]

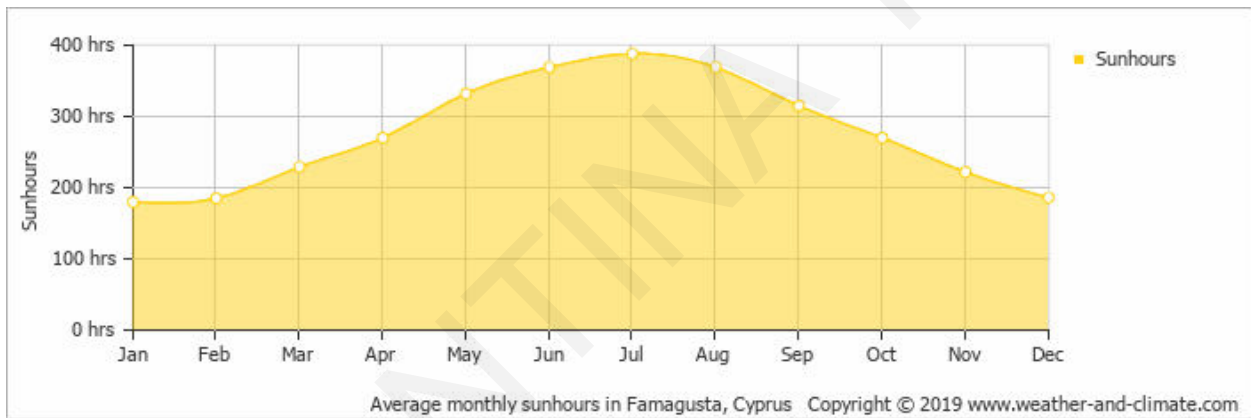


Figure 5.5 Average sun hours over the year in Larnaca, Cyprus [5.8]

The analysis results also refer to the climatic conditions of Stockholm, Sweden (latitude: 59.334591 and Longitude: 18.063240), a humid continental climate [5.9]. The city of Stockholm has cold winters and mild summers, with temperatures ranging from -2 to 22° C, respectively, Fig. 5.6. Also, the sun hours do not exceed 300 hours during summer months and 150 hours during winter months, Fig. 5.7.

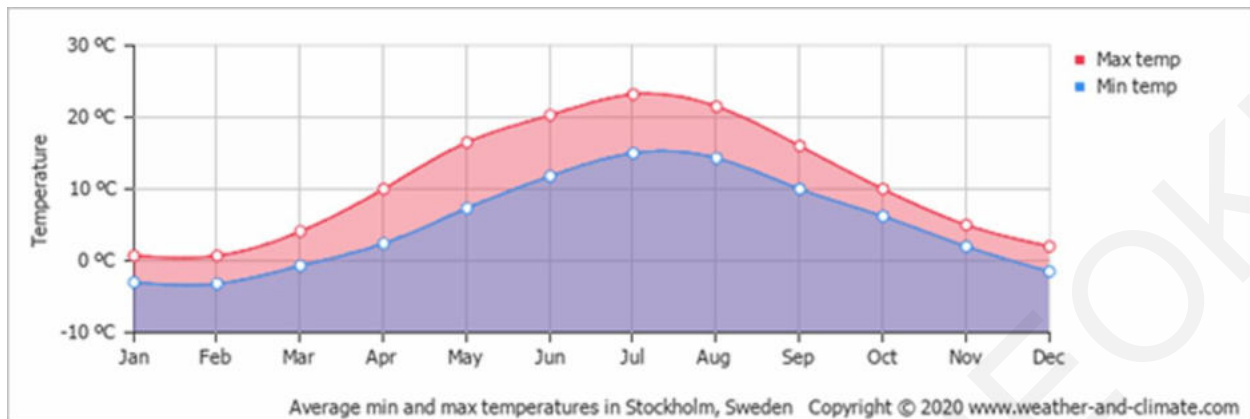


Figure 5.6 Average min and max temperatures in Stockholm, Sweden [5.8]



Figure 5.7 Average sun hours over the year in Stockholm, Sweden [5.8]

The simulation analysis provided the irradiance measurements and energy production by the PV system. Solar irradiance is the total amount of solar energy falling on a surface and it can be related to the area under solar irradiance versus the time curve [5.9]. Measurements or estimation of the solar irradiation (i.e., solar energy in Wh/m^2) in a specific location, is significant in studying the optimal design and predicting the performance and efficiency of a PV system [5.10-5.12]. The study conducted refers to the calculation of the direct, diffuse and indirect irradiance. The case study refers to the solstices that occur annually, on the 21st of December, March, June and September.

The model in its different configurations was designed in the 3D drawing interface of the software PVsits and the data needed for the simulation was entered into the database (input data). From the PV system library, the PV system selected is mono-Si, transparent BIPV system and the modules of 1.0 x 2.0 m dimensions and 5 mm thickness of the thin films. The Power of the PV System is 230 Wp, for each module. Also, was selected one inverter for each PV side of the system of 5 kW power.

Table 5.1 ETFE membrane and BIPV System characteristics

Transparent BIPV system		ETFE membrane	
Technology	mono-Si	Specific Gravity	1.74
Dimensions	1.0 x 2.0 m	Water Absorption %	< 0.03
Active layer	60 cells	Tensile Strength (psi)	7000
Peak Power	230 Wp	Elongation at Break %	300
NOCT	45° C	Initial Tear Strength	500
Voltage at Open Circuit (V _{oc})	36.9 V	Continuous Use Temp (°C)	165
Voltage at Maximum Power (V _{mpp})	258.8 V	Melt Point	260
Efficiency level	15 %	Refractive Index	1.4
Transparency	21 %	Light Transmission %	65

5.2.1 Simulation Results

The direct, diffuse and indirect solar irradiance have been calculated in each month of the year, on the 21st day at 12:00 am. Specifically, the analysis of the results focuses on the solstices that occur on the 21st of December, March, June and September 2020, in Cyprus and Sweden for 2 different site orientations, namely of 0° and 90°, Figs 5.8-5.11. In the simulation analysis is derived also the energy production by the photovoltaic units with regard to the initial and three target positions of the building obtained through the respective motion sequences.

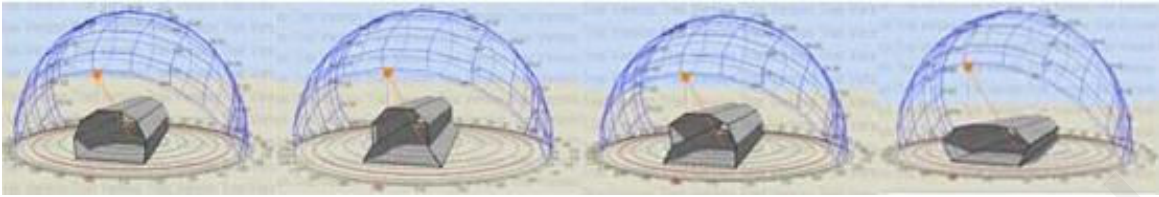


Figure 5.8 Cyprus's sun path diagrams on 21st of December at 12:00 am (site orientation: 0°)

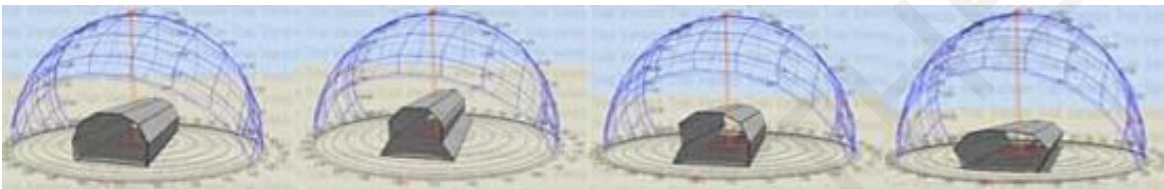


Figure 5.9 Cyprus's sun path diagrams on 21st of June at 12:00 am (site orientation: 0°)

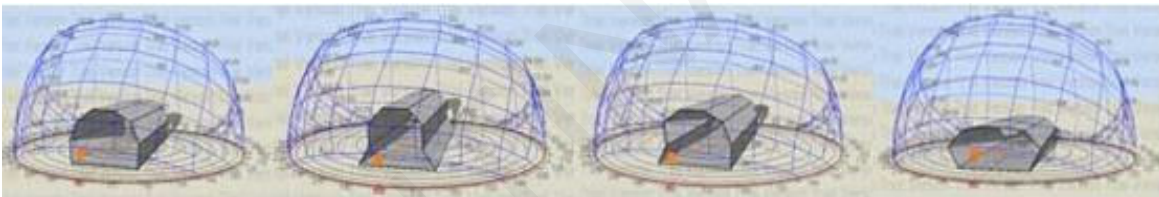


Figure 5.10 Sweden's sun path diagrams on 21st of December at 12:00 am (site orientation: 0°)



Figure 5.11 Sweden's sun path diagrams on 21st of June at 12:00 am (site orientation: 0°)

Figs 5.12 and 5.13 present the solar irradiance on the 21st of March for the site of Larnaca and an orientation of 0° and 90° respectively. The photovoltaic system gathers the highest rate of diffuse and indirect solar irradiance at the initial position of the building, while the other positions induce

a similar amount of solar irradiance. On the other hand, building position C yields the highest amount of solar irradiance, in contrast to the initial position that corresponds to the lowest respective value.

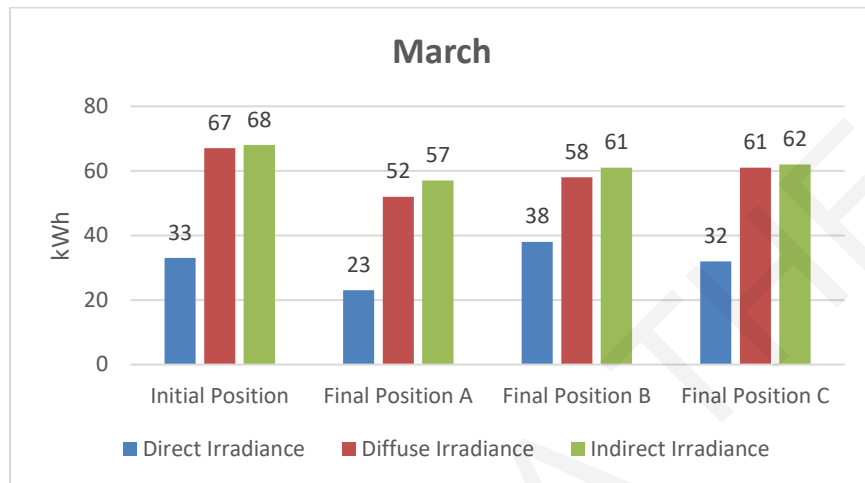


Figure 5.12 Solar irradiance on 21st of March at 12:00 am (site orientation: 0°)

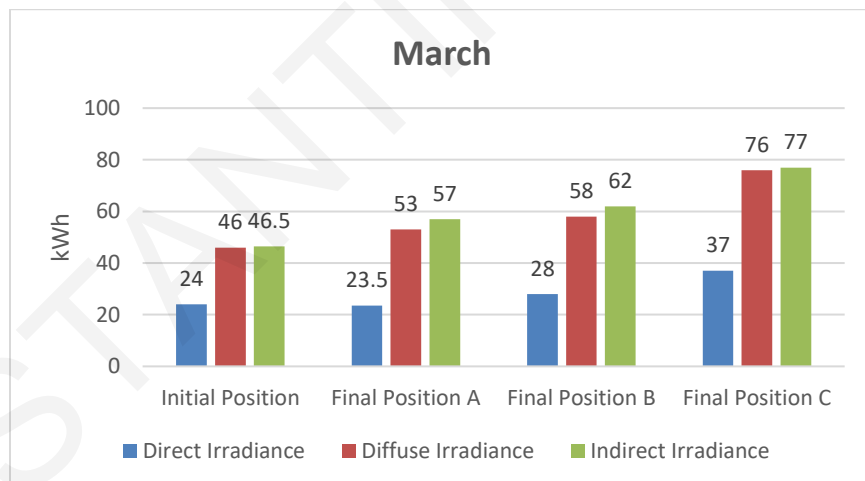


Figure 5.13 Solar irradiance on 21st of March at 12:00 am (site orientation: 90°)

On the 21st of June at 12:00 am, all solar irradiances have highest value at the initial position of the building and a site orientation of 0°, Figs 5.14, 5.15. In the case of an orientation of 90°, the initial position of the building yields the lowest values of solar irradiance. Furthermore, the total

solar irradiance of 288 kWh registered at the final position C of the building and 90° site orientation is the highest. The lowest total solar irradiance of 247 kWh refers to an initial building position and a site orientation of 0°.

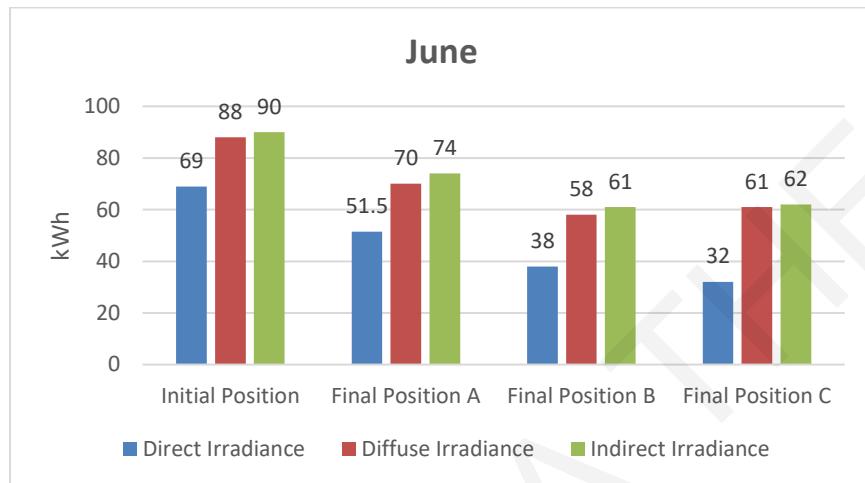


Figure 5.14 Solar irradiance on 21st of June at 12:00 am (site orientation: 0°)

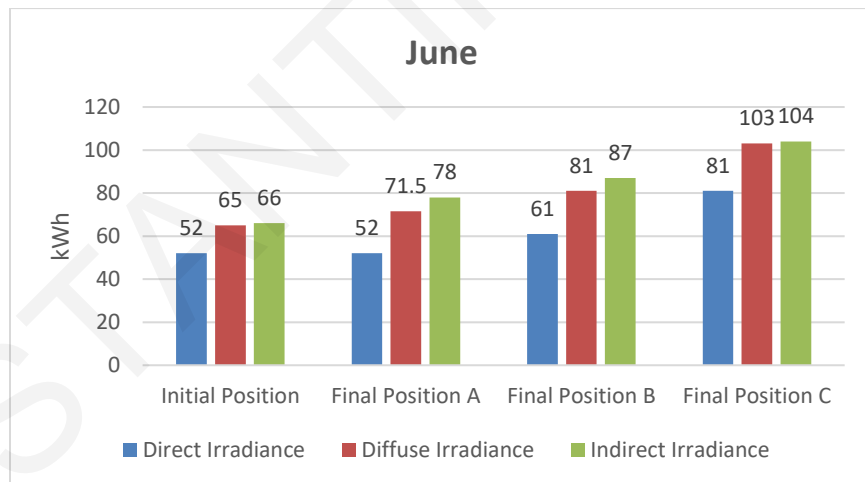


Figure 5.15 Solar irradiance on 21st of June at 12:00 am (site orientation: 90°)

On the 21st of September, the initial building position induces the highest solar irradiances at a site orientation of 0°, while the respective values at the building position C are close to the former,

Fig. 5.16. The building position A induces the lowest values of solar irradiances, 48 kWh of direct irradiance, 60 kWh diffuse irradiance and 66 kWh indirect irradiance. At a site orientation of 90°, the initial building position induces the lowest respective values, in contrast to the building position C, that induces the highest ones, Fig. 5.17. Comparatively, the corresponding values at the initial building position are the highest at a site orientation of 0°.

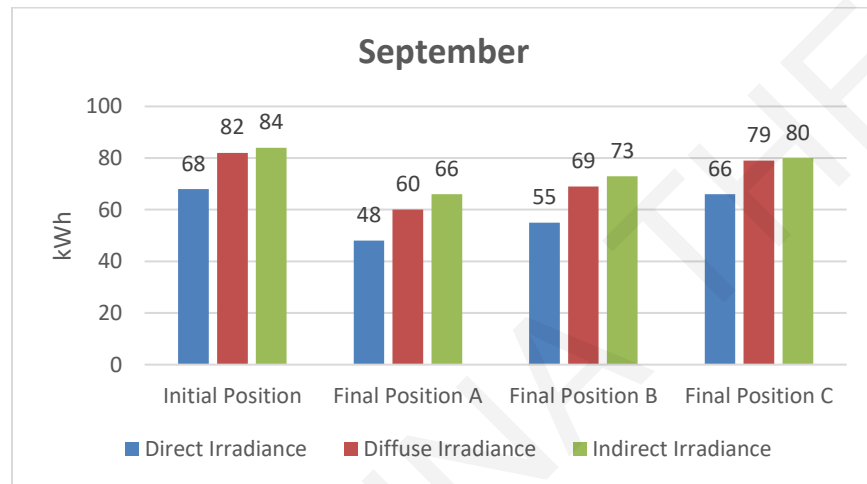


Figure 5.16 Solar irradiance on 21st of September at 12:00 am (site orientation: 0°)

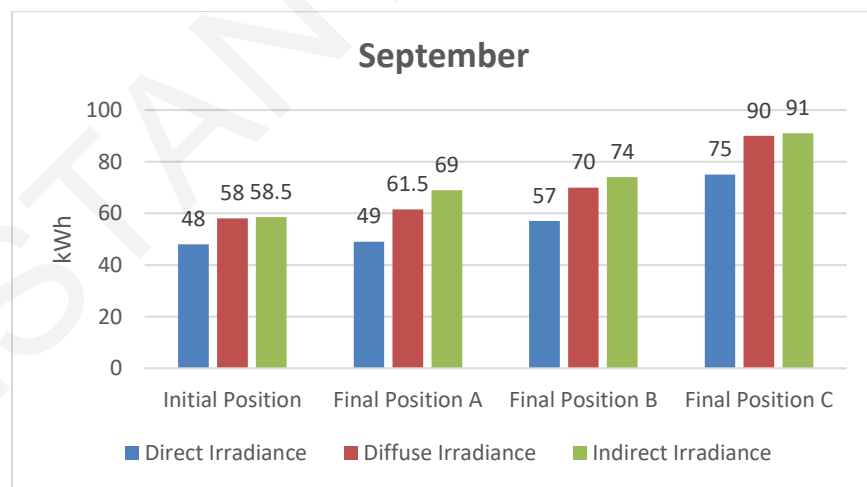


Figure 5.17 Solar irradiance on 21st of September at 12:00 am (site orientation: 90°)

On the 21st of December, the amount of direct solar irradiance is very low in all variables of the building position and site orientation, in contrast to the respective values of indirect solar irradiance. In addition, the values of the solar irradiance induced at the building positions A and B are the same, at both orientations. The solar irradiance at a site orientation of 90° has a maximum value at the building position C. The initial building position induces the highest solar irradiance values at a site orientation of 0° , whereas it induces the lowest respective values at a site orientation of 90° , Figs 5.18, 5.19.

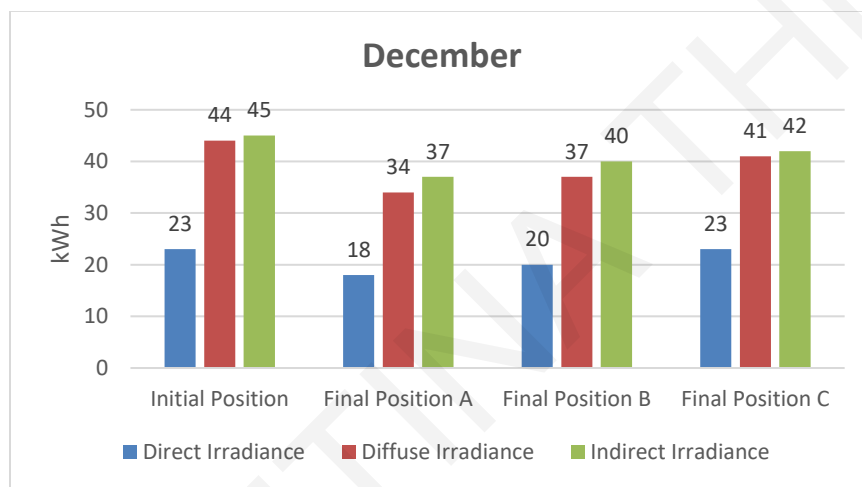


Figure 5.18 Solar irradiance on 21st of December at 12:00 am (site orientation: 0°)

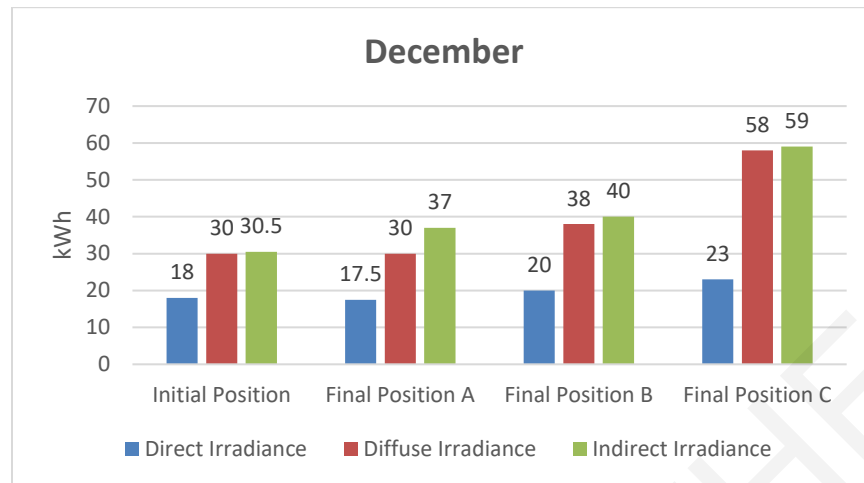


Figure 5.19 Solar irradiance on 21st of December at 12:00 am (site orientation: 90°)

Based on the analysis results for the site location of Larnaca, Cyprus, the values obtained with regard to the solar irradiation are the highest in the case of the 21st of June, and the lowest, in the case of the 21st of December. Accordingly, all three types of solar irradiation at the building position A have the lowest values at a site orientation of 0°. The respective solar irradiances are the highest at the building position C and a site orientation of 90°, for the case of the 21st of September. Hereby, the direct solar irradiance developed the lowest values compared to the other two types; this applies to all building positions and site orientations. The highest comparative values refer to the indirect solar irradiance. In conclusion, the initial position of the building at a site orientation of 0° induces the highest solar irradiation, whereas, at site orientation 90°, it induces the lowest respective values.

The amount of energy production by the photovoltaic system was investigated for the same dates, building position and site orientation variables, Figs 5.20, 5.21. As expected, the 21st of June provides the highest respective values, in contrast to the 21st of December, which corresponds to the lowest respective values. In addition, the rates of energy production at the final building position on the 21st of December, are close enough, to approximately 5 kWh. The photovoltaic

system produces comparatively higher energy amounts at the initial building position and a site orientation of 0°, as well as at the building position C and a site orientation of 90°.

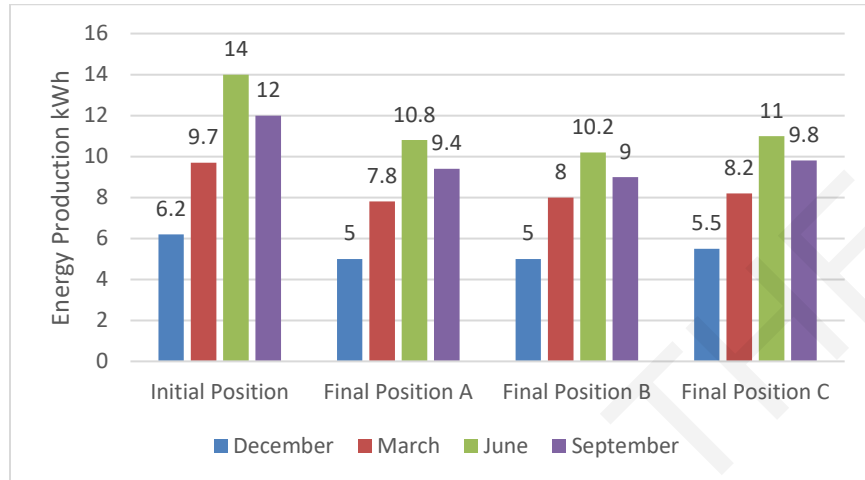


Figure 5.20 Energy production of photovoltaic system (site orientation: 0°)

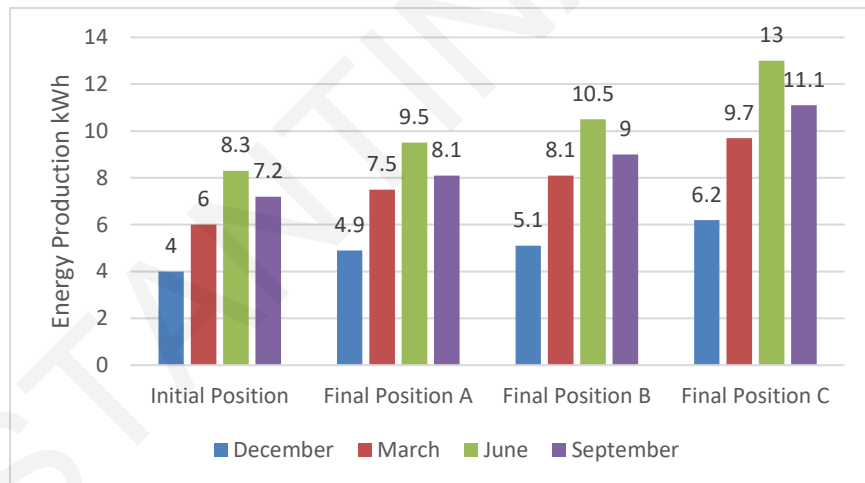


Figure 5.21 Energy production of photovoltaic system (site orientation: 90°)

Subsequently, the simulation analysis referred to Stockholm, Sweden, at the corresponding site orientations of 0° and 90°. On the 21st of March at 12:00 am, at a site orientation of 0°, the indirect irradiance value at the initial building position is slightly higher than the respective value at the final building position C. All other values of solar irradiance at the final building position C are

higher than the corresponding values at the initial building position. The total values of solar irradiance at all building positions are similar, Figs 5.22, 5.23.

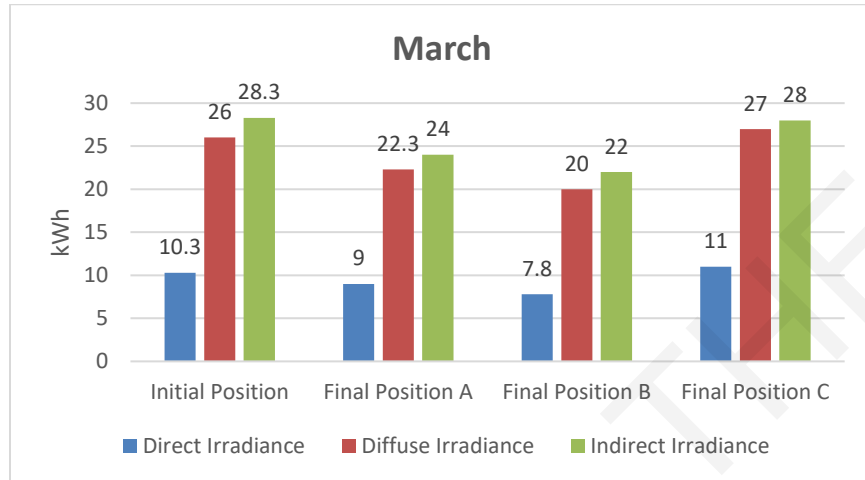


Figure 5.22 Solar irradiance on 21st of March at 12 am (Site orientation: 0°)

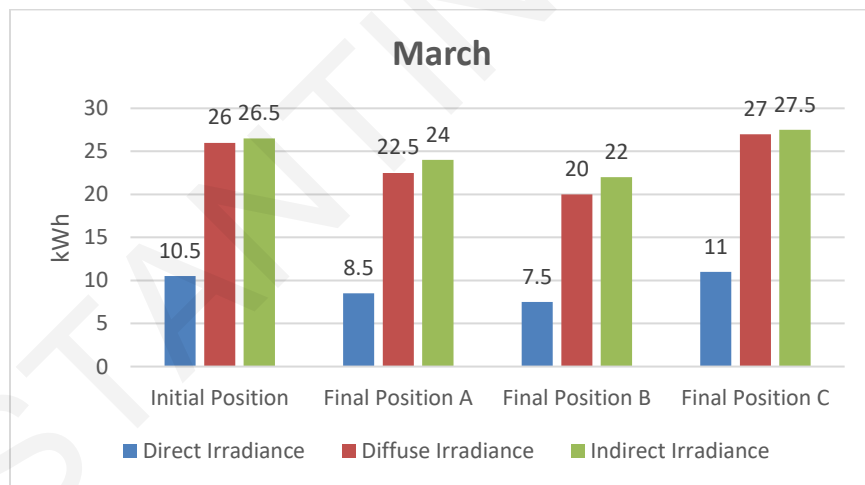


Figure 5.23 Solar irradiance on 21st of March at 12 am (Site orientation: 90°)

On the 21st of June, the direct irradiances at all building positions and site orientations are similar. In addition, indirect irradiance at the initial building position and at a site orientation of 0° is higher than the corresponding value at the final building position C. At the latter building position, the

highest values at both orientations were registered, in contrast to the corresponding values at the final building positions A and B, Figs 5.24, 5.25. Also, the indirect irradiance amount at the final building position B and a site orientation of 0° is significantly lower than the corresponding amount at the final building position B and a site orientation of 90° , i.e., with values of 36.5 and 46 kWh respectively.

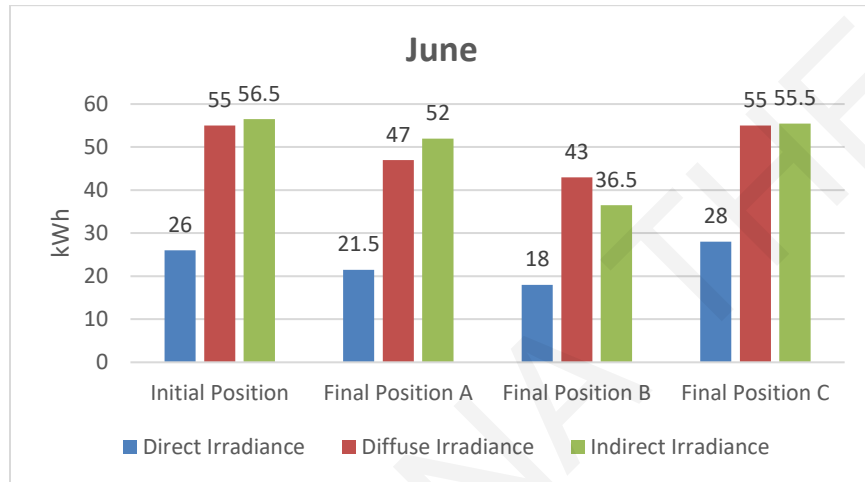


Figure 5.24 Solar irradiance on 21st of June at 12 am (Site orientation: 0°)

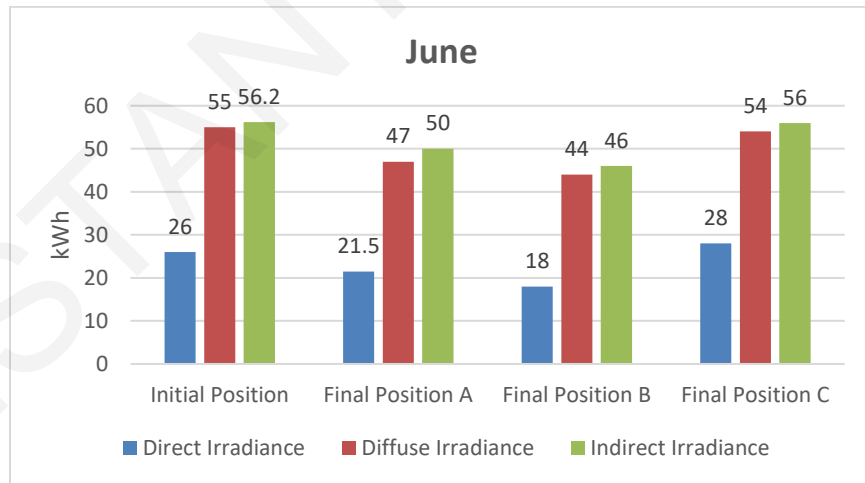


Figure 5.25 Solar irradiance on 21st of June at 12 am (Site orientation: 90°)

On the 21st of September at 12:00 am, the final building position C gathers the highest amount of solar irradiance, Figs 5.26, 5.27. Alongside, all values of solar irradiance at the initial building position and a site orientation of 0° are much higher than the corresponding values at a site orientation of 90°. The final building position B at both orientations collects the lowest total solar irradiance in contrast to the final building position C.

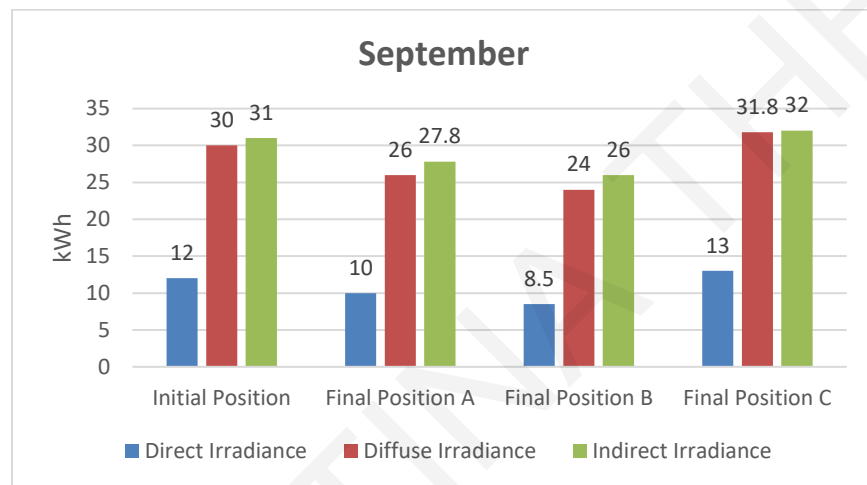


Figure 5.26 Solar irradiance on 21st of September at 12 am (Site orientation: 0°)

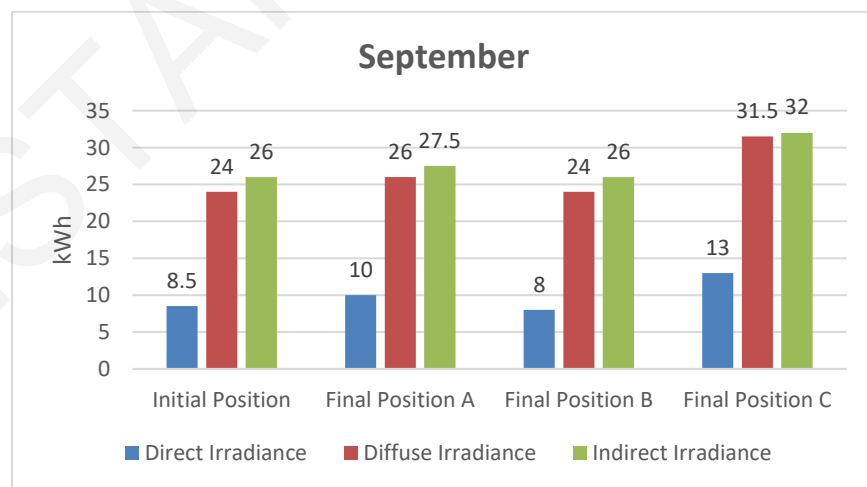


Figure 5.27 Solar irradiance on 21st of September at 12 am (Site orientation: 90°)

On the 21st of December at 12:00 am, the solar irradiances at all building positions and orientations are similar, Figs 5.28, 5.29. The direct irradiance values at both orientations are very low, in contrast to the indirect irradiances, which occupy the highest values of solar energy. Additionally, the total solar irradiance at the final building position A and a site orientation of 90° is higher than at the other final building positions. Furthermore, the direct irradiance at the final building positions and a site orientation of 0° is lower than the corresponding values of direct irradiance at the final building positions and a site orientation of 90° .

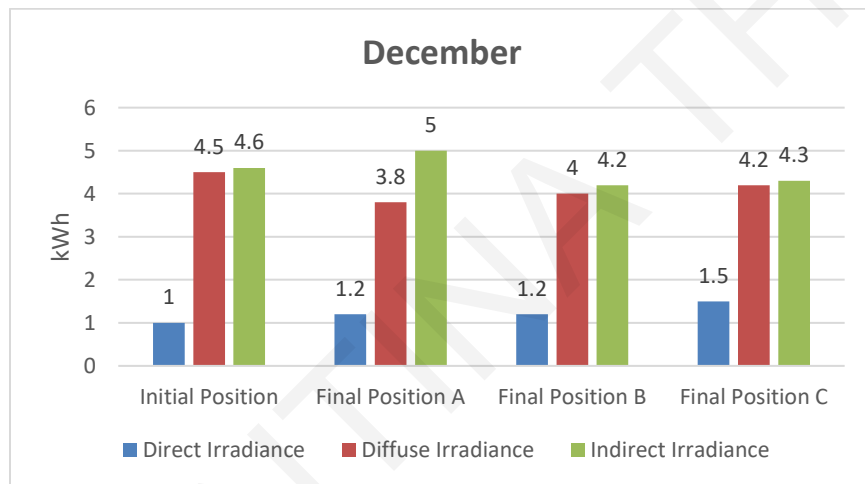


Figure 5.28 Solar irradiance on 21st of December at 12 am (Site orientation: 0°)

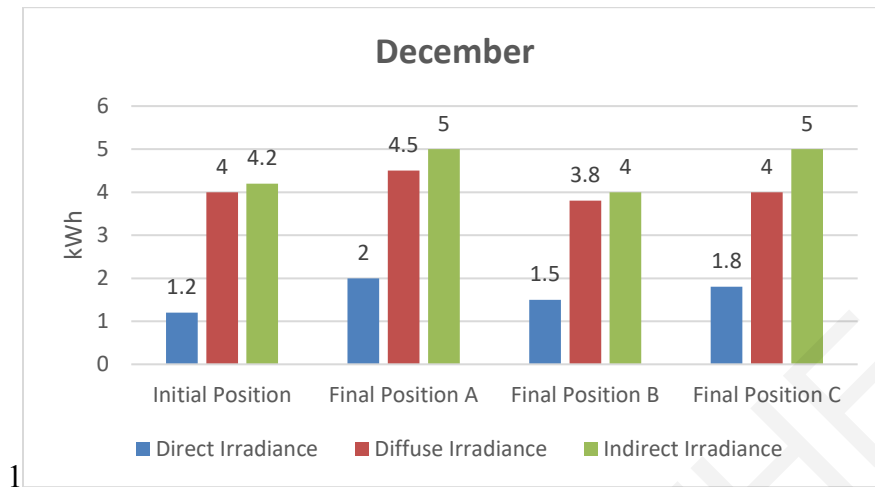


Figure 5.29 Solar irradiance on 21st of December at 12 am (Site orientation: 90°)

At the final building position C, the highest rates of energy production are achieved at both orientations, Figs 5.30, 5.31. In particular, the energy production at the initial building position and a site orientation of 0° is relatively high in contrast to the corresponding site orientation of 90°. Also, the amount of energy production in December at both orientations is practically negligible, whereas the amount of energy production in June has the highest rate.

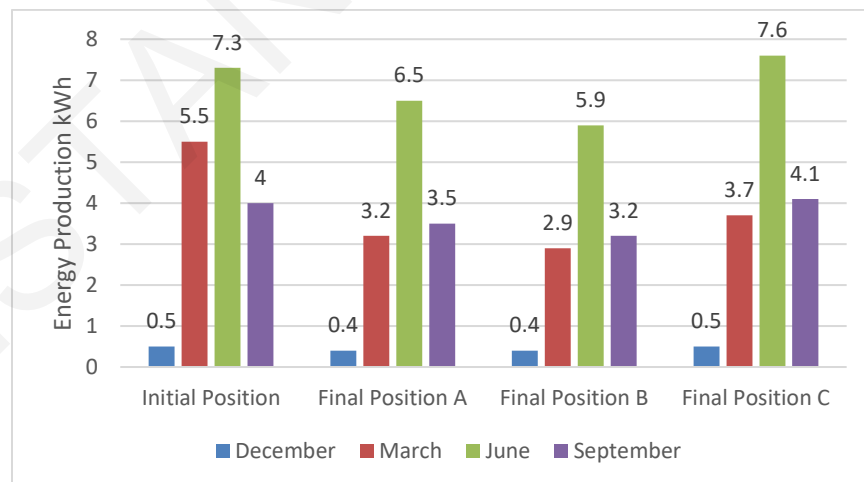


Figure 5.30 Energy production of photovoltaic system (Site orientation: 0°)

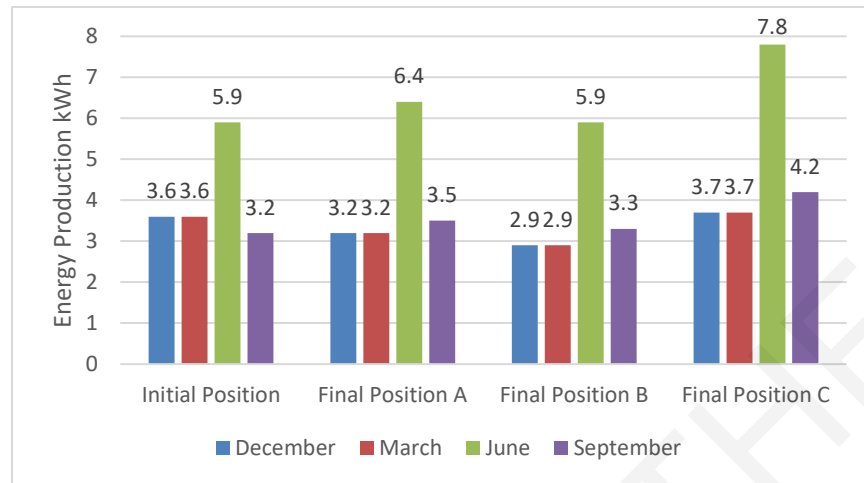


Figure 5.31 Energy production of photovoltaic system (Site orientation: 90°)

The analysis verified at first place that in Larnaca there is more solar irradiance and correspondingly, energy production than in Stockholm, Fig. 5.32. Overall, the total energy production in Larnaca, is higher at a site orientation of 0° in contrast to the respective value obtained in Stockholm, i.e., 141.6 and 67 kWh respectively. Comparing further the two geographic locations, the initial building position in Larnaca gathers the highest total solar irradiance at a site orientation of 0° in all analysis cases. Additionally, the final building position C collects the highest energy at a site orientation of 90° in all analysis cases. On the other hand, in Stockholm, at all building positions, higher values of solar irradiance are obtained at a site orientation of 0°, except for the cases of the 21st of March and June. In Stockholm, at the initial building position, the highest total solar irradiance is achieved at a site orientation of 0° in all analysis cases. Alongside, the final building positions B and C in both cities occupy comparatively higher energy production values at a site orientation of 90°. Furthermore, the obtained total solar irradiance at the final building position A in Larnaca, in all analysis cases, is higher at a site orientation of 0° compared to the corresponding final building position in Stockholm, which gathers the highest energy at a site orientation of 90°.

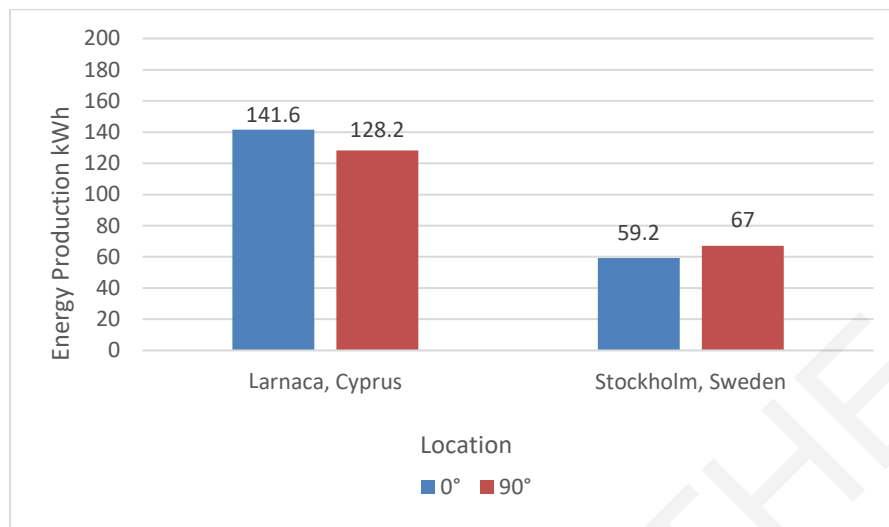


Figure 5.32 Overall energy production of photovoltaic system in Larnaca and Stockholm

CONSTANTINA THEOKLI

CHAPTER 6 CONCLUSIONS

In the current study the design and analysis of a reconfigurable structure and the investigation of its kinetic behavior have been conducted. The kinematics applied are based on the Effective Crank–Slider reconfiguration approach, namely a kinematics approach that stepwise reduces a planar system to an externally actuated 1-DOF system, in order to adjust each joint angle of the planar system from an initial to a target position. During a motion sequence for implementing the required shape adjustment, there are locked and unlocked brakes in the joints. Once a joint has been adjusted, this will be locked in the following steps of the reconfiguration. Through movement of the slider in each step, the selected joint angles adjustment may provide symmetrical or non-symmetrical configurations of the system. Among different feasible sequences, the ones with less required steps are selected and investigated with regard to the highest maximum brake torques and slider displacements. The kinematics approach applied provides maximum flexibility and endurance with minimum required actuation energy.

A building envelope of ETFE and photovoltaic membranes was applied in the longitudinal direction of the spatial structure. The photovoltaic units integrated with the flexible building envelope enable high levels of energy production, exceeding the performance of a corresponding fixed shape building. The simulation analysis provided the irradiance measurements and energy production by the photovoltaic system. The case study focused on the solstices annually, i.e., on the 21st of December, March, June and September, at 12 am, in Cyprus and Sweden for 2 different site orientations, namely of 0° and 90° . In the simulation analysis was also derived the energy production by the photovoltaic units with regard to the initial and three target positions of the building obtained through the respective motion sequences.

The analysis illustrates that Larnaca gathers higher amounts of solar irradiance and results in higher energy production than Stockholm. In particular, in Larnaca, the total energy production is higher at a site orientation of 0° . In all analysis cases the initial building position in Larnaca has the highest total solar irradiance at a site orientation of 0° . Also, all building positions in Stockholm resulted in higher values of solar irradiance at a site orientation of 0° , except for the cases of the 21st of March and June. Alongside, the final building positions B and C in both cities occupy

comparatively higher energy production values at a site orientation of 90° . Furthermore, the obtained total solar irradiance at the final building position A in Larnaca, in all analysis cases, is higher at a site orientation of 0° , whereas the same final building position in Stockholm, gathers the highest energy at a site orientation of 90° .

In terms of future work, the numerical analysis of further motion sequences and the automated selection of favorable ones according to specific criteria, such as maximum brake torques and slider displacements may be conducted. From an energy perspective, a further parameter to be investigated is the natural lighting levels of the building, which can also affect the visual comfort of the users. Also, a Life-Cycle-Cost Analysis is considered to be significant, with regard to the production of the components of the system, the erection and assemblage of the structure, as well as the operation of the kinetic structure and the building.

APPENDIX

Appendix 1 Scenarios of Sequence 2

Sequence Order 2a (S2_a)

	J ₁	J ₂	J ₃	J ₄	J ₅	J ₆	J ₇	J ₈	J ₉
Step 1									
Step 2									
Step 3									

	J ₁	J ₂	J ₃	J ₄	J ₅	J ₆	J ₇	J ₈	J ₉
Step 1									
Step 2									
Step 3									

	J ₁	J ₂	J ₃	J ₄	J ₅	J ₆	J ₇	J ₈	J ₉
Step 1									
Step 2									
Step 3									

	J ₁	J ₂	J ₃	J ₄	J ₅	J ₆	J ₇	J ₈	J ₉
Step 1									
Step 2									
Step 3									

Sequence Order 2b (S2_b)

	J ₁	J ₂	J ₃	J ₄	J ₅	J ₆	J ₇	J ₈	J ₉
Step 1									
Step 2									
Step 3									

	J ₁	J ₂	J ₃	J ₄	J ₅	J ₆	J ₇	J ₈	J ₉
Step 1									
Step 2									
Step 3									

Sequence Order 2c (S2_c)

	J ₁	J ₂	J ₃	J ₄	J ₅	J ₆	J ₇	J ₈	J ₉
Step 1									
Step 2									
Step 3									

	J ₁	J ₂	J ₃	J ₄	J ₅	J ₆	J ₇	J ₈	J ₉
Step 1									
Step 2									
Step 3									

Sequence Order 2d (S2d)

	J ₁	J ₂	J ₃	J ₄	J ₅	J ₆	J ₇	J ₈	J ₉
Step 1									
Step 2									
Step 3									

	J ₁	J ₂	J ₃	J ₄	J ₅	J ₆	J ₇	J ₈	J ₉
Step 1									
Step 2									
Step 3									

	J ₁	J ₂	J ₃	J ₄	J ₅	J ₆	J ₇	J ₈	J ₉
Step 1									
Step 2									
Step 3									

	J ₁	J ₂	J ₃	J ₄	J ₅	J ₆	J ₇	J ₈	J ₉
Step 1									
Step 2									
Step 3									

Sequence Order 2e (S2_e)

	J ₁	J ₂	J ₃	J ₄	J ₅	J ₆	J ₇	J ₈	J ₉
Step 1									
Step 2									
Step 3									

	J ₁	J ₂	J ₃	J ₄	J ₅	J ₆	J ₇	J ₈	J ₉
Step 1									
Step 2									
Step 3									

	J ₁	J ₂	J ₃	J ₄	J ₅	J ₆	J ₇	J ₈	J ₉
Step 1									
Step 2									
Step 3									

	J ₁	J ₂	J ₃	J ₄	J ₅	J ₆	J ₇	J ₈	J ₉
Step 1									
Step 2									
Step 3									

Sequence Order 2f (S2f)

	J ₁	J ₂	J ₃	J ₄	J ₅	J ₆	J ₇	J ₈	J ₉
Step 1									
Step 2									
Step 3									

	J ₁	J ₂	J ₃	J ₄	J ₅	J ₆	J ₇	J ₈	J ₉
Step 1									
Step 2									
Step 3									

	J ₁	J ₂	J ₃	J ₄	J ₅	J ₆	J ₇	J ₈	J ₉
Step 1									
Step 2									
Step 3									

	J ₁	J ₂	J ₃	J ₄	J ₅	J ₆	J ₇	J ₈	J ₉
Step 1									
Step 2									
Step 3									

Sequence Order 2g (S_{2g})

	J ₁	J ₂	J ₃	J ₄	J ₅	J ₆	J ₇	J ₈	J ₉
Step 1									
Step 2									
Step 3									

	J ₁	J ₂	J ₃	J ₄	J ₅	J ₆	J ₇	J ₈	J ₉
Step 1									
Step 2									
Step 3									

	J ₁	J ₂	J ₃	J ₄	J ₅	J ₆	J ₇	J ₈	J ₉
Step 1									
Step 2									
Step 3									

	J ₁	J ₂	J ₃	J ₄	J ₅	J ₆	J ₇	J ₈	J ₉
Step 1									
Step 2									
Step 3									

Sequence Order 2h (S2_h)

	J ₁	J ₂	J ₃	J ₄	J ₅	J ₆	J ₇	J ₈	J ₉
Step 1									
Step 2									
Step 3									

	J ₁	J ₂	J ₃	J ₄	J ₅	J ₆	J ₇	J ₈	J ₉
Step 1									
Step 2									
Step 3									

	J ₁	J ₂	J ₃	J ₄	J ₅	J ₆	J ₇	J ₈	J ₉
Step 1									
Step 2									
Step 3									

	J ₁	J ₂	J ₃	J ₄	J ₅	J ₆	J ₇	J ₈	J ₉
Step 1									
Step 2									
Step 3									

Sequence Order 2i (S2_i)

	J ₁	J ₂	J ₃	J ₄	J ₅	J ₆	J ₇	J ₈	J ₉
Step 1									
Step 2									
Step 3									

	J ₁	J ₂	J ₃	J ₄	J ₅	J ₆	J ₇	J ₈	J ₉
Step 1									
Step 2									
Step 3									

	J ₁	J ₂	J ₃	J ₄	J ₅	J ₆	J ₇	J ₈	J ₉
Step 1									
Step 2									
Step 3									

	J ₁	J ₂	J ₃	J ₄	J ₅	J ₆	J ₇	J ₈	J ₉
Step 1									
Step 2									
Step 3									

Sequence Order $2j$ (S_{2j})

	J ₁	J ₂	J ₃	J ₄	J ₅	J ₆	J ₇	J ₈	J ₉
Step 1									
Step 2									
Step 3									

	J ₁	J ₂	J ₃	J ₄	J ₅	J ₆	J ₇	J ₈	J ₉
Step 1									
Step 2									
Step 3									

	J ₁	J ₂	J ₃	J ₄	J ₅	J ₆	J ₇	J ₈	J ₉
Step 1									
Step 2									
Step 3									

	J ₁	J ₂	J ₃	J ₄	J ₅	J ₆	J ₇	J ₈	J ₉
Step 1									
Step 2									
Step 3									

Sequence Order 2k (S2_k)

	J ₁	J ₂	J ₃	J ₄	J ₅	J ₆	J ₇	J ₈	J ₉
Step 1									
Step 2									
Step 3									

	J ₁	J ₂	J ₃	J ₄	J ₅	J ₆	J ₇	J ₈	J ₉
Step 1									
Step 2									
Step 3									

	J ₁	J ₂	J ₃	J ₄	J ₅	J ₆	J ₇	J ₈	J ₉
Step 1									
Step 2									
Step 3									

	J ₁	J ₂	J ₃	J ₄	J ₅	J ₆	J ₇	J ₈	J ₉
Step 1									
Step 2									
Step 3									

Sequence Order 2I (S2i)

	J ₁	J ₂	J ₃	J ₄	J ₅	J ₆	J ₇	J ₈	J ₉
Step 1									
Step 2									
Step 3									

	J ₁	J ₂	J ₃	J ₄	J ₅	J ₆	J ₇	J ₈	J ₉
Step 1									
Step 2									
Step 3									

	J ₁	J ₂	J ₃	J ₄	J ₅	J ₆	J ₇	J ₈	J ₉
Step 1									
Step 2									
Step 3									

	J ₁	J ₂	J ₃	J ₄	J ₅	J ₆	J ₇	J ₈	J ₉
Step 1									
Step 2									
Step 3									

Sequence Order 2m (S2_m)

	J ₁	J ₂	J ₃	J ₄	J ₅	J ₆	J ₇	J ₈	J ₉
Step 1									
Step 2									
Step 3									

	J ₁	J ₂	J ₃	J ₄	J ₅	J ₆	J ₇	J ₈	J ₉
Step 1									
Step 2									
Step 3									

	J ₁	J ₂	J ₃	J ₄	J ₅	J ₆	J ₇	J ₈	J ₉
Step 1									
Step 2									
Step 3									

	J ₁	J ₂	J ₃	J ₄	J ₅	J ₆	J ₇	J ₈	J ₉
Step 1									
Step 2									
Step 3									

Sequence Order $2n$ (S_{2n})

	J ₁	J ₂	J ₃	J ₄	J ₅	J ₆	J ₇	J ₈	J ₉
Step 1									
Step 2									
Step 3									

	J ₁	J ₂	J ₃	J ₄	J ₅	J ₆	J ₇	J ₈	J ₉
Step 1									
Step 2									
Step 3									

	J ₁	J ₂	J ₃	J ₄	J ₅	J ₆	J ₇	J ₈	J ₉
Step 1									
Step 2									
Step 3									

	J ₁	J ₂	J ₃	J ₄	J ₅	J ₆	J ₇	J ₈	J ₉
Step 1									
Step 2									
Step 3									

Sequence Order 2o (S2o)

	J ₁	J ₂	J ₃	J ₄	J ₅	J ₆	J ₇	J ₈	J ₉
Step 1									
Step 2									
Step 3									

	J ₁	J ₂	J ₃	J ₄	J ₅	J ₆	J ₇	J ₈	J ₉
Step 1									
Step 2									
Step 3									

	J ₁	J ₂	J ₃	J ₄	J ₅	J ₆	J ₇	J ₈	J ₉
Step 1									
Step 2									
Step 3									

	J ₁	J ₂	J ₃	J ₄	J ₅	J ₆	J ₇	J ₈	J ₉
Step 1									
Step 2									
Step 3									

Sequence Order 2p (S2p)

	J ₁	J ₂	J ₃	J ₄	J ₅	J ₆	J ₇	J ₈	J ₉
Step 1									
Step 2									
Step 3									

	J ₁	J ₂	J ₃	J ₄	J ₅	J ₆	J ₇	J ₈	J ₉
Step 1									
Step 2									
Step 3									

	J ₁	J ₂	J ₃	J ₄	J ₅	J ₆	J ₇	J ₈	J ₉
Step 1									
Step 2									
Step 3									

	J ₁	J ₂	J ₃	J ₄	J ₅	J ₆	J ₇	J ₈	J ₉
Step 1									
Step 2									
Step 3									

Sequence Order $2q$ (S_{2q})

	J ₁	J ₂	J ₃	J ₄	J ₅	J ₆	J ₇	J ₈	J ₉
Step 1									
Step 2									
Step 3									

	J ₁	J ₂	J ₃	J ₄	J ₅	J ₆	J ₇	J ₈	J ₉
Step 1									
Step 2									
Step 3									

	J ₁	J ₂	J ₃	J ₄	J ₅	J ₆	J ₇	J ₈	J ₉
Step 1									
Step 2									
Step 3									

	J ₁	J ₂	J ₃	J ₄	J ₅	J ₆	J ₇	J ₈	J ₉
Step 1									
Step 2									
Step 3									

Sequence Order $2r$ (S_{2r})

	J ₁	J ₂	J ₃	J ₄	J ₅	J ₆	J ₇	J ₈	J ₉
Step 1									
Step 2									
Step 3									

	J ₁	J ₂	J ₃	J ₄	J ₅	J ₆	J ₇	J ₈	J ₉
Step 1									
Step 2									
Step 3									

	J ₁	J ₂	J ₃	J ₄	J ₅	J ₆	J ₇	J ₈	J ₉
Step 1									
Step 2									
Step 3									

	J ₁	J ₂	J ₃	J ₄	J ₅	J ₆	J ₇	J ₈	J ₉
Step 1									
Step 2									
Step 3									

Sequence Order 2s (S2s)

	J ₁	J ₂	J ₃	J ₄	J ₅	J ₆	J ₇	J ₈	J ₉
Step 1									
Step 2									
Step 3									

	J ₁	J ₂	J ₃	J ₄	J ₅	J ₆	J ₇	J ₈	J ₉
Step 1									
Step 2									
Step 3									

	J ₁	J ₂	J ₃	J ₄	J ₅	J ₆	J ₇	J ₈	J ₉
Step 1									
Step 2									
Step 3									

	J ₁	J ₂	J ₃	J ₄	J ₅	J ₆	J ₇	J ₈	J ₉
Step 1									
Step 2									
Step 3									

Sequence Order 2t (S2_t)

	J ₁	J ₂	J ₃	J ₄	J ₅	J ₆	J ₇	J ₈	J ₉
Step 1									
Step 2									
Step 3									

	J ₁	J ₂	J ₃	J ₄	J ₅	J ₆	J ₇	J ₈	J ₉
Step 1									
Step 2									
Step 3									

	J ₁	J ₂	J ₃	J ₄	J ₅	J ₆	J ₇	J ₈	J ₉
Step 1									
Step 2									
Step 3									

	J ₁	J ₂	J ₃	J ₄	J ₅	J ₆	J ₇	J ₈	J ₉
Step 1									
Step 2									
Step 3									

Sequence Order 2u (S2_u)

	J ₁	J ₂	J ₃	J ₄	J ₅	J ₆	J ₇	J ₈	J ₉
Step 1									
Step 2									
Step 3									

	J ₁	J ₂	J ₃	J ₄	J ₅	J ₆	J ₇	J ₈	J ₉
Step 1									
Step 2									
Step 3									

	J ₁	J ₂	J ₃	J ₄	J ₅	J ₆	J ₇	J ₈	J ₉
Step 1									
Step 2									
Step 3									

	J ₁	J ₂	J ₃	J ₄	J ₅	J ₆	J ₇	J ₈	J ₉
Step 1									
Step 2									
Step 3									

Sequence Order $2v$ (S_{2v})

	J ₁	J ₂	J ₃	J ₄	J ₅	J ₆	J ₇	J ₈	J ₉
Step 1									
Step 2									
Step 3									

	J ₁	J ₂	J ₃	J ₄	J ₅	J ₆	J ₇	J ₈	J ₉
Step 1									
Step 2									
Step 3									

	J ₁	J ₂	J ₃	J ₄	J ₅	J ₆	J ₇	J ₈	J ₉
Step 1									
Step 2									
Step 3									

	J ₁	J ₂	J ₃	J ₄	J ₅	J ₆	J ₇	J ₈	J ₉
Step 1									
Step 2									
Step 3									

Sequence Order 2w (S2_w)

	J ₁	J ₂	J ₃	J ₄	J ₅	J ₆	J ₇	J ₈	J ₉
Step 1									
Step 2									
Step 3									

	J ₁	J ₂	J ₃	J ₄	J ₅	J ₆	J ₇	J ₈	J ₉
Step 1									
Step 2									
Step 3									

	J ₁	J ₂	J ₃	J ₄	J ₅	J ₆	J ₇	J ₈	J ₉
Step 1									
Step 2									
Step 3									

	J ₁	J ₂	J ₃	J ₄	J ₅	J ₆	J ₇	J ₈	J ₉
Step 1									
Step 2									
Step 3									

Sequence Order 2x (S2_x)

	J ₁	J ₂	J ₃	J ₄	J ₅	J ₆	J ₇	J ₈	J ₉
Step 1									
Step 2									
Step 3									

	J ₁	J ₂	J ₃	J ₄	J ₅	J ₆	J ₇	J ₈	J ₉
Step 1									
Step 2									
Step 3									

	J ₁	J ₂	J ₃	J ₄	J ₅	J ₆	J ₇	J ₈	J ₉
Step 1									
Step 2									
Step 3									

	J ₁	J ₂	J ₃	J ₄	J ₅	J ₆	J ₇	J ₈	J ₉
Step 1									
Step 2									
Step 3									

Sequence Order 2y (S_{2y})







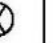

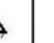





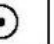










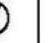

	J ₁	J ₂	J ₃	J ₄	J ₅	J ₆	J ₇	J ₈	J ₉
Step 1									
Step 2									
Step 3									







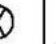

















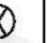


	J ₁	J ₂	J ₃	J ₄	J ₅	J ₆	J ₇	J ₈	J ₉
Step 1									
Step 2									
Step 3									







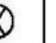
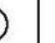
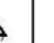






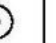
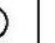









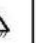
	J ₁	J ₂	J ₃	J ₄	J ₅	J ₆	J ₇	J ₈	J ₉
Step 1									
Step 2									
Step 3									







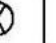
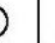
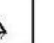






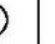








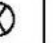


	J ₁	J ₂	J ₃	J ₄	J ₅	J ₆	J ₇	J ₈	J ₉
Step 1									
Step 2									
Step 3									

Sequence Order 2z (S2z)

	J ₁	J ₂	J ₃	J ₄	J ₅	J ₆	J ₇	J ₈	J ₉
Step 1									
Step 2									
Step 3									

	J ₁	J ₂	J ₃	J ₄	J ₅	J ₆	J ₇	J ₈	J ₉
Step 1									
Step 2									
Step 3									

	J ₁	J ₂	J ₃	J ₄	J ₅	J ₆	J ₇	J ₈	J ₉
Step 1									
Step 2									
Step 3									

	J ₁	J ₂	J ₃	J ₄	J ₅	J ₆	J ₇	J ₈	J ₉
Step 1									
Step 2									
Step 3									

Sequence Order 2aa (S2_{aa})

	J ₁	J ₂	J ₃	J ₄	J ₅	J ₆	J ₇	J ₈	J ₉
Step 1									
Step 2									
Step 3									

	J ₁	J ₂	J ₃	J ₄	J ₅	J ₆	J ₇	J ₈	J ₉
Step 1									
Step 2									
Step 3									

	J ₁	J ₂	J ₃	J ₄	J ₅	J ₆	J ₇	J ₈	J ₉
Step 1									
Step 2									
Step 3									

	J ₁	J ₂	J ₃	J ₄	J ₅	J ₆	J ₇	J ₈	J ₉
Step 1									
Step 2									
Step 3									

Sequence Order 2ab (S2_{ab})

	J ₁	J ₂	J ₃	J ₄	J ₅	J ₆	J ₇	J ₈	J ₉
Step 1									
Step 2									
Step 3									

	J ₁	J ₂	J ₃	J ₄	J ₅	J ₆	J ₇	J ₈	J ₉
Step 1									
Step 2									
Step 3									

	J ₁	J ₂	J ₃	J ₄	J ₅	J ₆	J ₇	J ₈	J ₉
Step 1									
Step 2									
Step 3									

	J ₁	J ₂	J ₃	J ₄	J ₅	J ₆	J ₇	J ₈	J ₉
Step 1									
Step 2									
Step 3									

Sequence Order 2ac (S2_{ac})

	J ₁	J ₂	J ₃	J ₄	J ₅	J ₆	J ₇	J ₈	J ₉
Step 1									
Step 2									
Step 3									

	J ₁	J ₂	J ₃	J ₄	J ₅	J ₆	J ₇	J ₈	J ₉
Step 1									
Step 2									
Step 3									

	J ₁	J ₂	J ₃	J ₄	J ₅	J ₆	J ₇	J ₈	J ₉
Step 1									
Step 2									
Step 3									

	J ₁	J ₂	J ₃	J ₄	J ₅	J ₆	J ₇	J ₈	J ₉
Step 1									
Step 2									
Step 3									

Sequence Order 2ad (S2_{ad})

	J ₁	J ₂	J ₃	J ₄	J ₅	J ₆	J ₇	J ₈	J ₉
Step 1									
Step 2									
Step 3									

	J ₁	J ₂	J ₃	J ₄	J ₅	J ₆	J ₇	J ₈	J ₉
Step 1									
Step 2									
Step 3									

	J ₁	J ₂	J ₃	J ₄	J ₅	J ₆	J ₇	J ₈	J ₉
Step 1									
Step 2									
Step 3									

	J ₁	J ₂	J ₃	J ₄	J ₅	J ₆	J ₇	J ₈	J ₉
Step 1									
Step 2									
Step 3									

Sequence Order 2ae (S2_{ae})

	J ₁	J ₂	J ₃	J ₄	J ₅	J ₆	J ₇	J ₈	J ₉
Step 1									
Step 2									
Step 3									

	J ₁	J ₂	J ₃	J ₄	J ₅	J ₆	J ₇	J ₈	J ₉
Step 1									
Step 2									
Step 3									

	J ₁	J ₂	J ₃	J ₄	J ₅	J ₆	J ₇	J ₈	J ₉
Step 1									
Step 2									
Step 3									

	J ₁	J ₂	J ₃	J ₄	J ₅	J ₆	J ₇	J ₈	J ₉
Step 1									
Step 2									
Step 3									

Sequence Order 2af (S2af)

	J ₁	J ₂	J ₃	J ₄	J ₅	J ₆	J ₇	J ₈	J ₉
Step 1									
Step 2									
Step 3									

	J ₁	J ₂	J ₃	J ₄	J ₅	J ₆	J ₇	J ₈	J ₉
Step 1									
Step 2									
Step 3									

	J ₁	J ₂	J ₃	J ₄	J ₅	J ₆	J ₇	J ₈	J ₉
Step 1									
Step 2									
Step 3									

	J ₁	J ₂	J ₃	J ₄	J ₅	J ₆	J ₇	J ₈	J ₉
Step 1									
Step 2									
Step 3									

Sequence Order 2ag (S2_{ag})

	J ₁	J ₂	J ₃	J ₄	J ₅	J ₆	J ₇	J ₈	J ₉
Step 1									
Step 2									
Step 3									

	J ₁	J ₂	J ₃	J ₄	J ₅	J ₆	J ₇	J ₈	J ₉
Step 1									
Step 2									
Step 3									

	J ₁	J ₂	J ₃	J ₄	J ₅	J ₆	J ₇	J ₈	J ₉
Step 1									
Step 2									
Step 3									

	J ₁	J ₂	J ₃	J ₄	J ₅	J ₆	J ₇	J ₈	J ₉
Step 1									
Step 2									
Step 3									

Sequence Order 2ah (S2_{ah})

	J ₁	J ₂	J ₃	J ₄	J ₅	J ₆	J ₇	J ₈	J ₉
Step 1									
Step 2									
Step 3									

	J ₁	J ₂	J ₃	J ₄	J ₅	J ₆	J ₇	J ₈	J ₉
Step 1									
Step 2									
Step 3									

	J ₁	J ₂	J ₃	J ₄	J ₅	J ₆	J ₇	J ₈	J ₉
Step 1									
Step 2									
Step 3									

	J ₁	J ₂	J ₃	J ₄	J ₅	J ₆	J ₇	J ₈	J ₉
Step 1									
Step 2									
Step 3									

Sequence Order 2ai (S2_{ai})

	J ₁	J ₂	J ₃	J ₄	J ₅	J ₆	J ₇	J ₈	J ₉
Step 1									
Step 2									
Step 3									

	J ₁	J ₂	J ₃	J ₄	J ₅	J ₆	J ₇	J ₈	J ₉
Step 1									
Step 2									
Step 3									

	J ₁	J ₂	J ₃	J ₄	J ₅	J ₆	J ₇	J ₈	J ₉
Step 1									
Step 2									
Step 3									

	J ₁	J ₂	J ₃	J ₄	J ₅	J ₆	J ₇	J ₈	J ₉
Step 1									
Step 2									
Step 3									

Sequence Order 2aj (S2_{aj})

	J ₁	J ₂	J ₃	J ₄	J ₅	J ₆	J ₇	J ₈	J ₉
Step 1									
Step 2									
Step 3									

	J ₁	J ₂	J ₃	J ₄	J ₅	J ₆	J ₇	J ₈	J ₉
Step 1									
Step 2									
Step 3									

	J ₁	J ₂	J ₃	J ₄	J ₅	J ₆	J ₇	J ₈	J ₉
Step 1									
Step 2									
Step 3									

	J ₁	J ₂	J ₃	J ₄	J ₅	J ₆	J ₇	J ₈	J ₉
Step 1									
Step 2									
Step 3									

Sequence Order 2ak (S2_{ak})

	J ₁	J ₂	J ₃	J ₄	J ₅	J ₆	J ₇	J ₈	J ₉
Step 1									
Step 2									
Step 3									

	J ₁	J ₂	J ₃	J ₄	J ₅	J ₆	J ₇	J ₈	J ₉
Step 1									
Step 2									
Step 3									

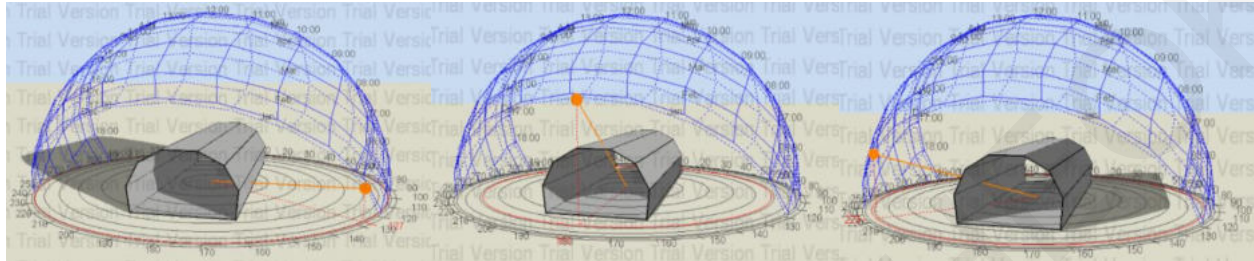
	J ₁	J ₂	J ₃	J ₄	J ₅	J ₆	J ₇	J ₈	J ₉
Step 1									
Step 2									
Step 3									

	J ₁	J ₂	J ₃	J ₄	J ₅	J ₆	J ₇	J ₈	J ₉
Step 1									
Step 2									
Step 3									

Appendix 2: Sun Paths

Larnaca, Cyprus – Site Orientation 0°, Initial Position

21st of December

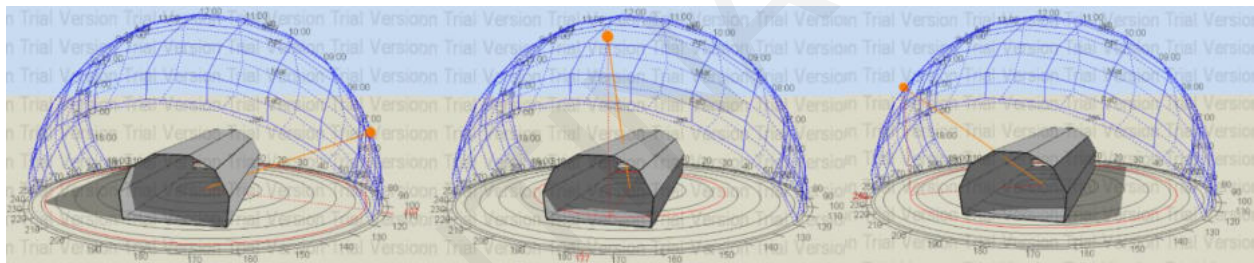


08:00

12:00

15:00

21st of March

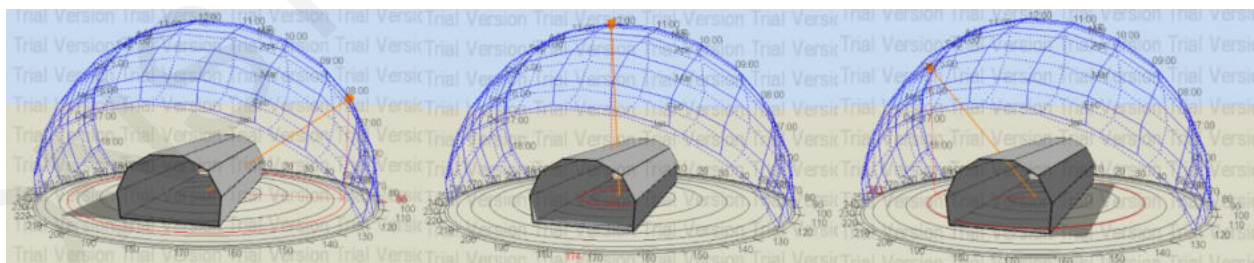


08:00

12:00

15:00

21st of June



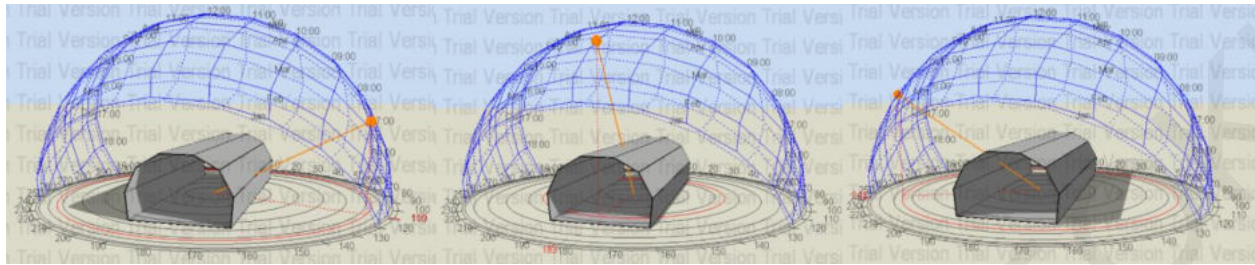
08:00

12:00

15:00

APPENDIX

21st of September



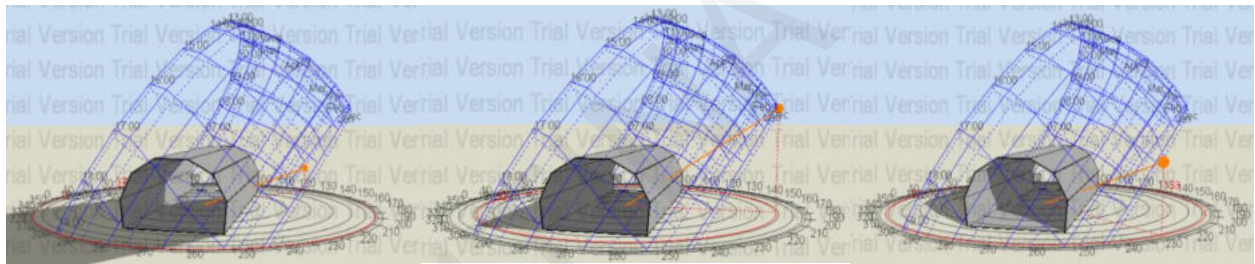
08:00

12:00

15:00

Larnaca, Cyprus – Site Orientation 90°, Initial Position

21st of December

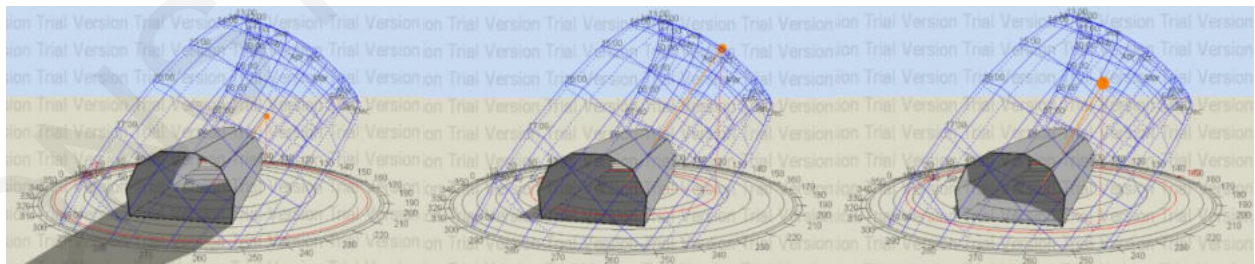


08:00

12:00

15:00

21st of March

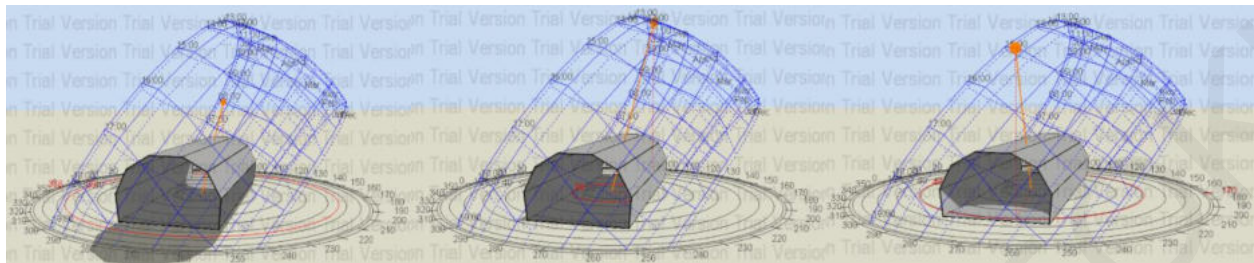


08:00

12:00

15:00

21st of June

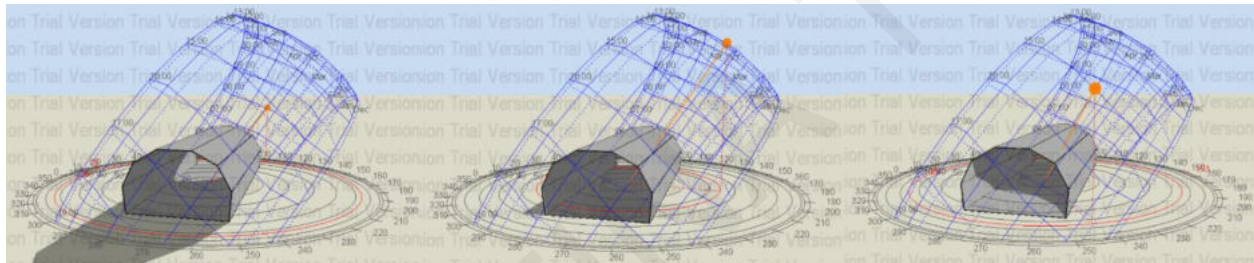


08:00

12:00

15:00

21st of September



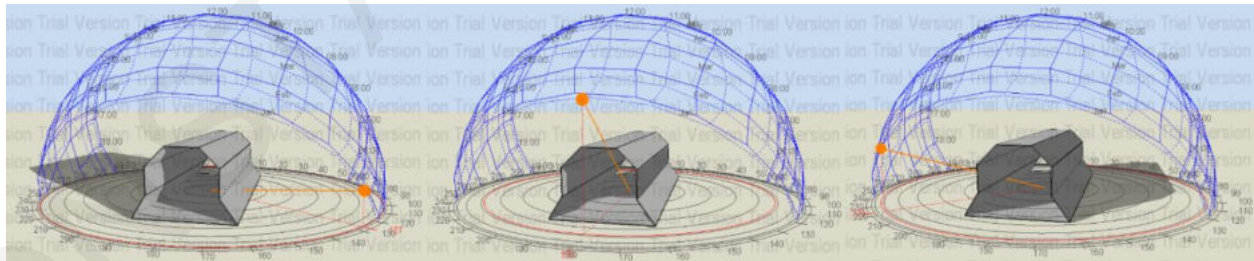
08:00

12:00

15:00

Larnaca, Cyprus – Site Orientation 0°, Final Position A

21st of December



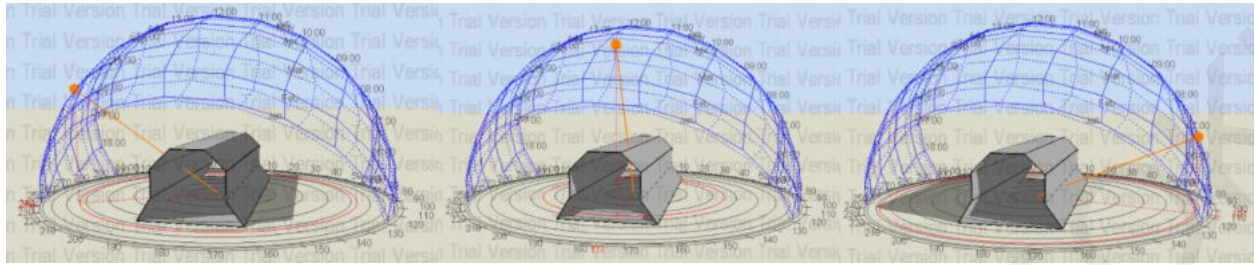
08:00

12:00

15:00

APPENDIX

21st of March

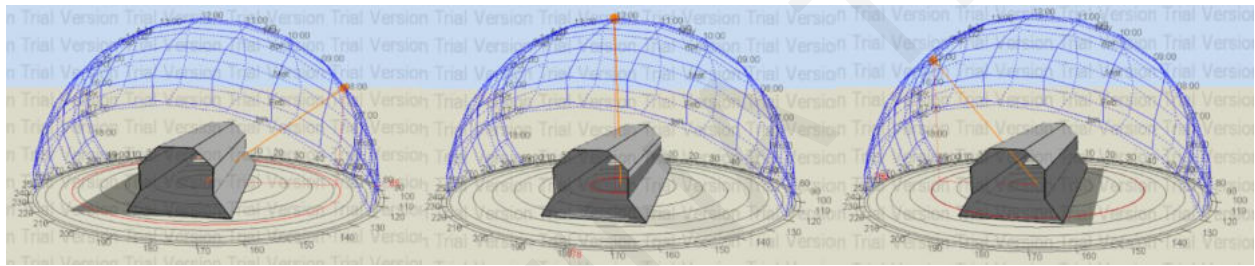


08:00

12:00

15:00

21st of June

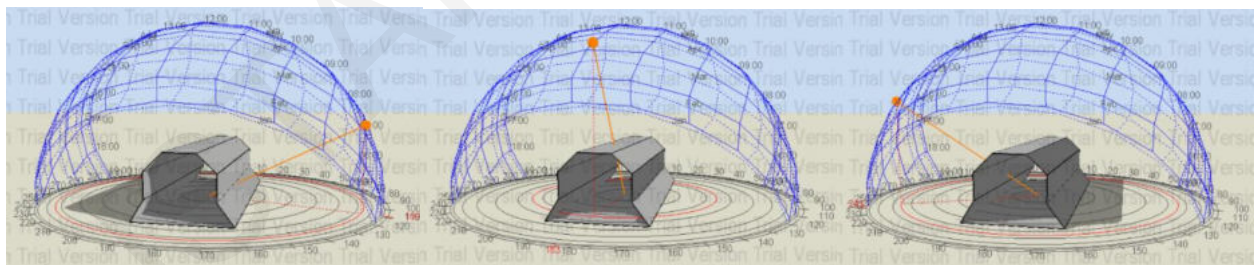


08:00

12:00

15:00

21st of September



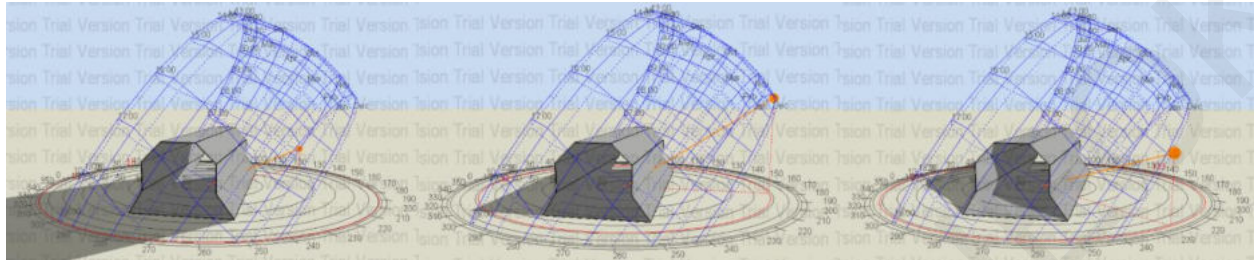
08:00

12:00

15:00

Larnaca, Cyprus – Site Orientation 90°, Final Position A

21st of December

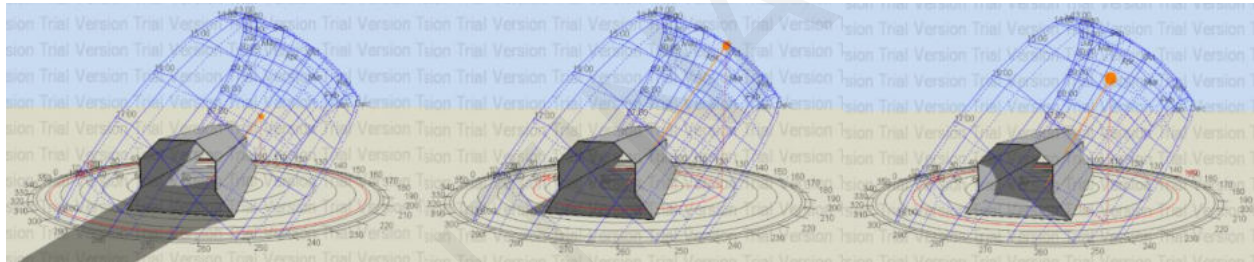


08:00

12:00

15:00

21st of March

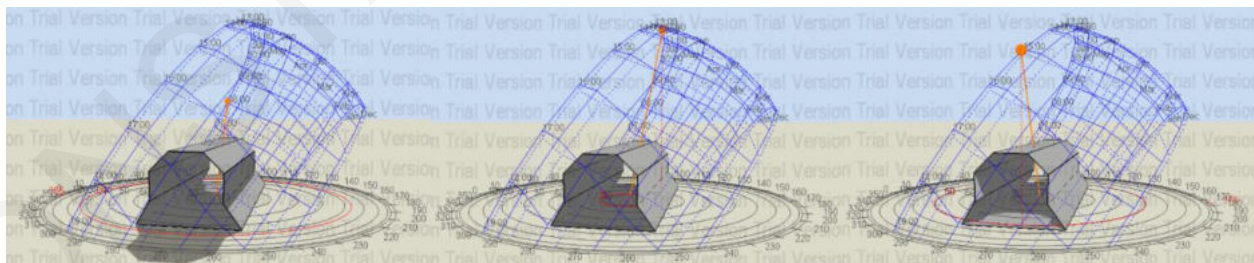


08:00

12:00

15:00

21st of June



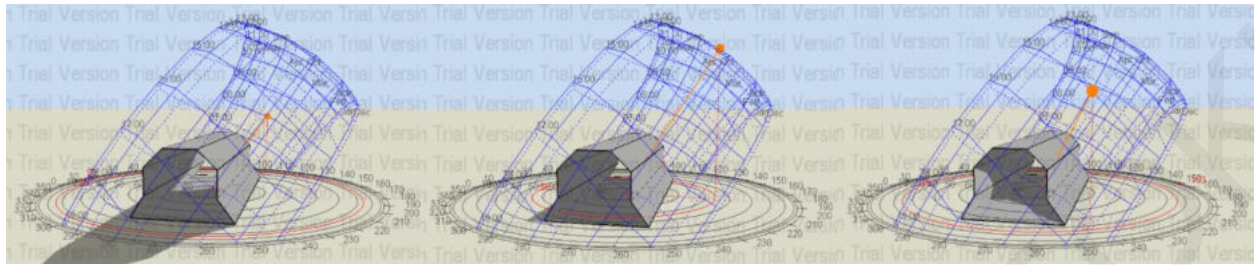
08:00

12:00

15:00

APPENDIX

21st of September



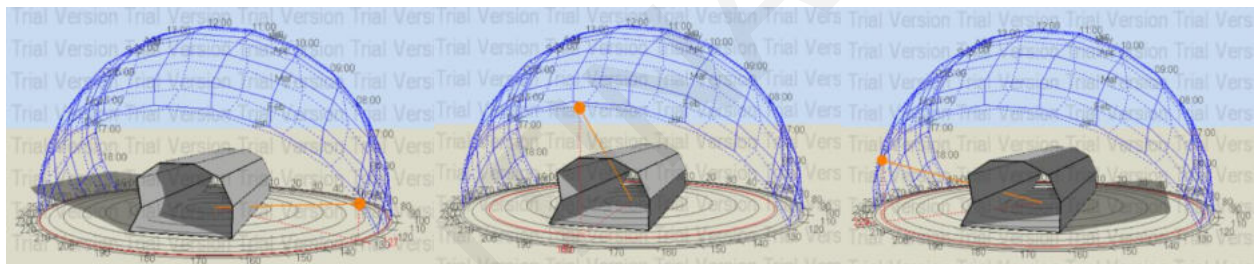
08:00

12:00

15:00

Larnaca, Cyprus – Site Orientation 0°, Final Position B

21st of December

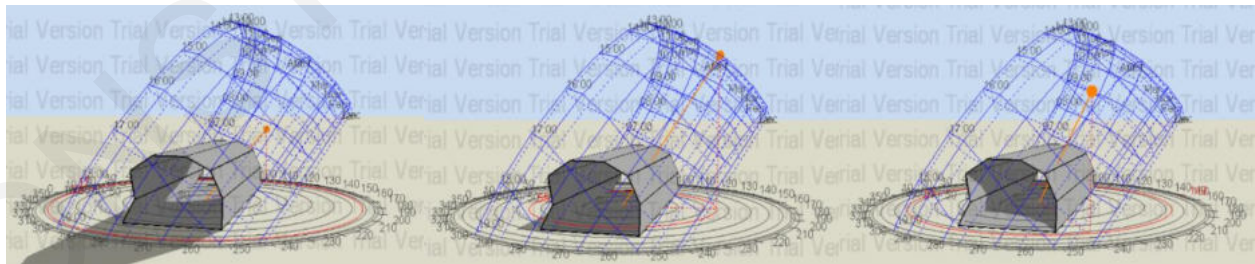


08:00

12:00

15:00

21st of March

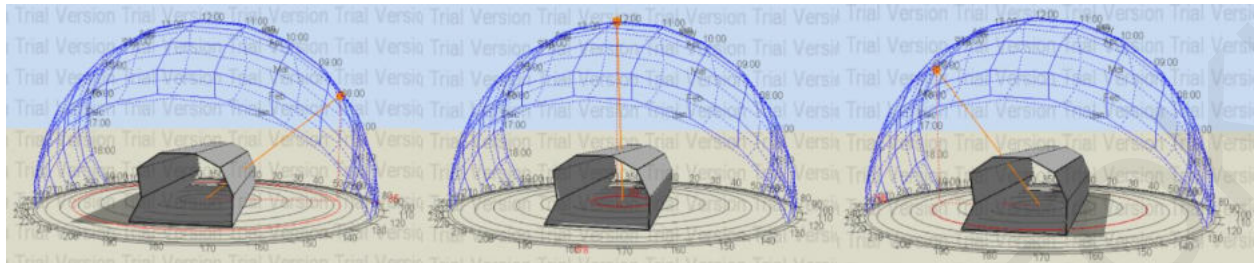


08:00

12:00

15:00

21st of June

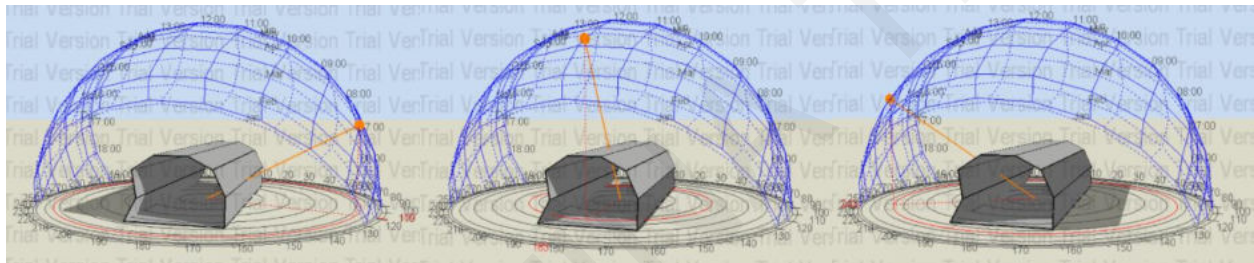


08:00

12:00

15:00

21st of September



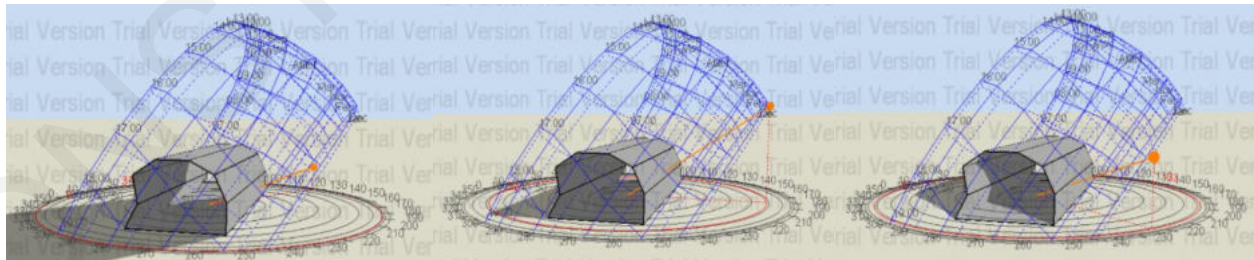
08:00

12:00

15:00

Larnaca, Cyprus – Site Orientation 90°, Final Position B

21st of December

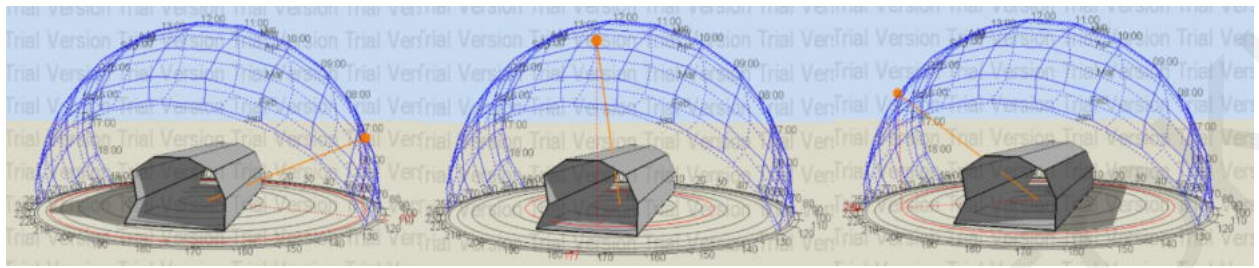


08:00

12:00

15:00

21st of March

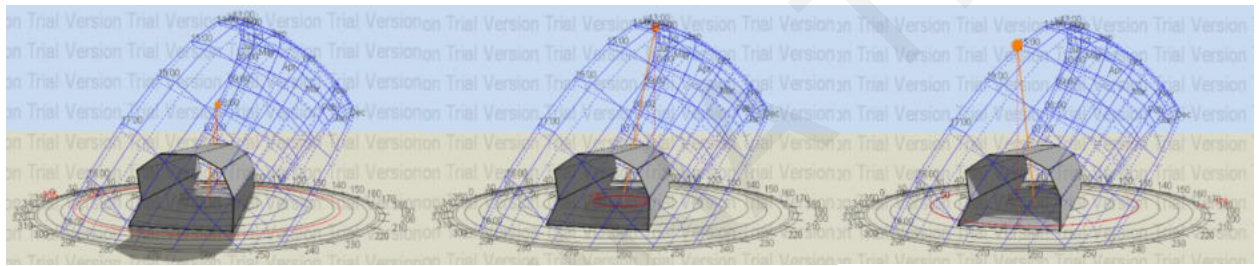


08:00

12:00

15:00

21st of June

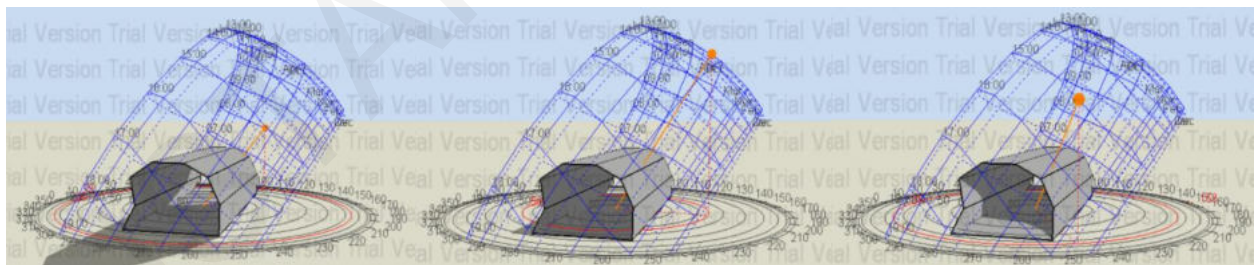


08:00

12:00

15:00

21st of September



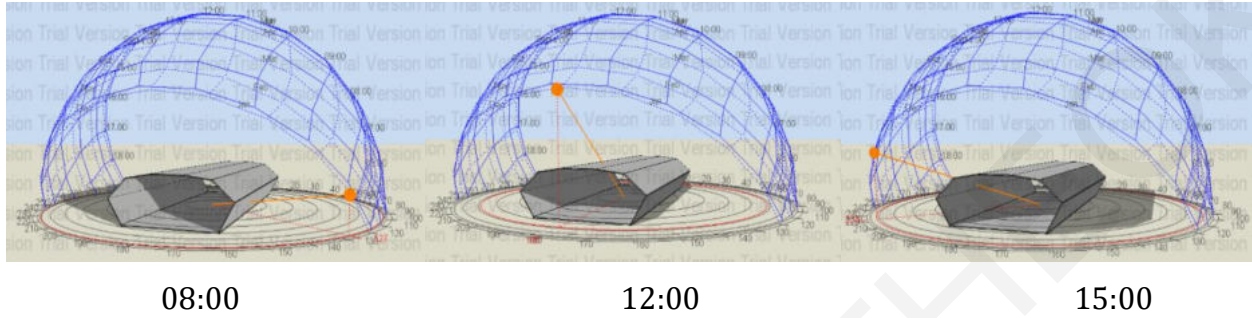
08:00

12:00

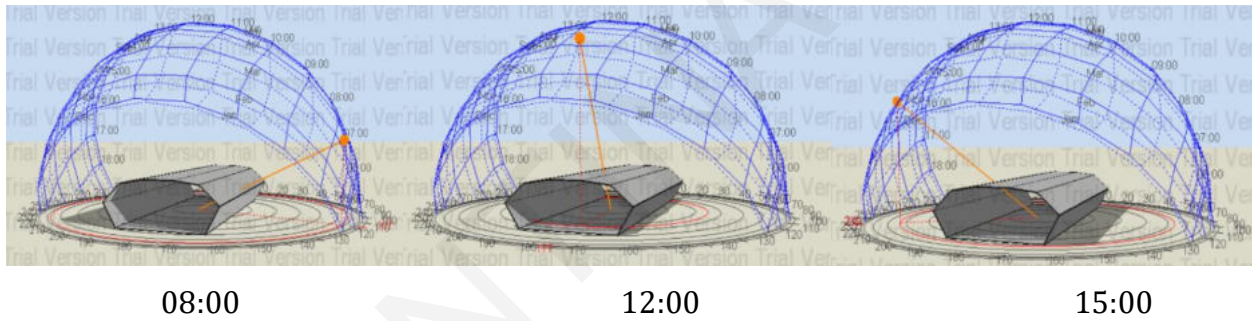
15:00

Larnaca, Cyprus – Site Orientation 0°, Final Position C

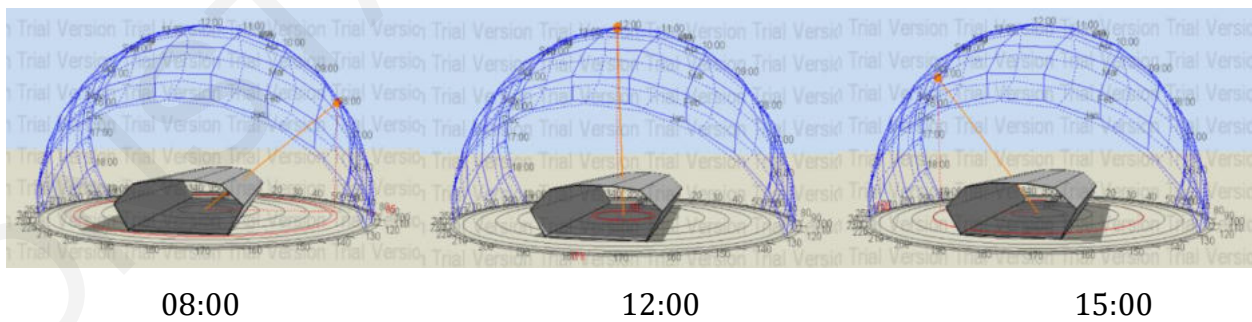
21st of December



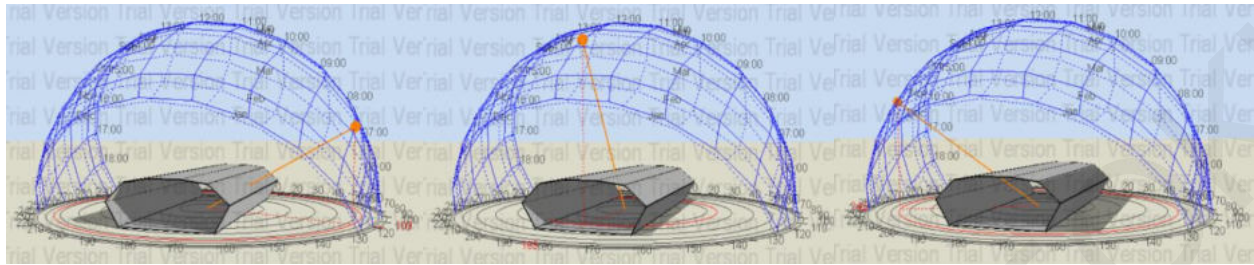
21st of March



21st of June



21st of September



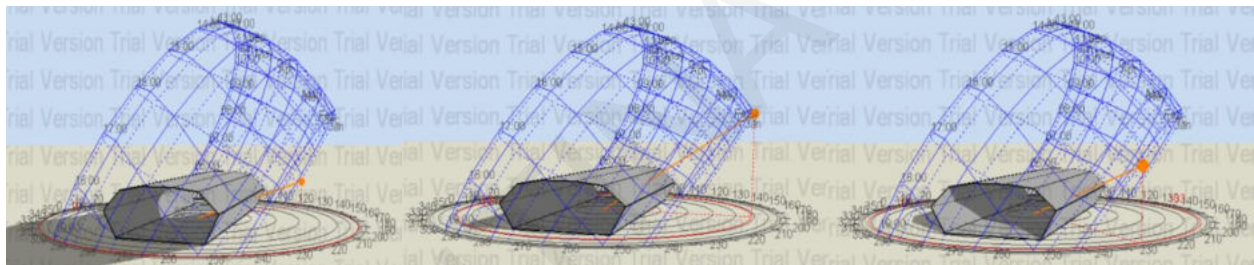
08:00

12:00

15:00

Larnaca, Cyprus – Site Orientation 90°, Final Position C

21st of December

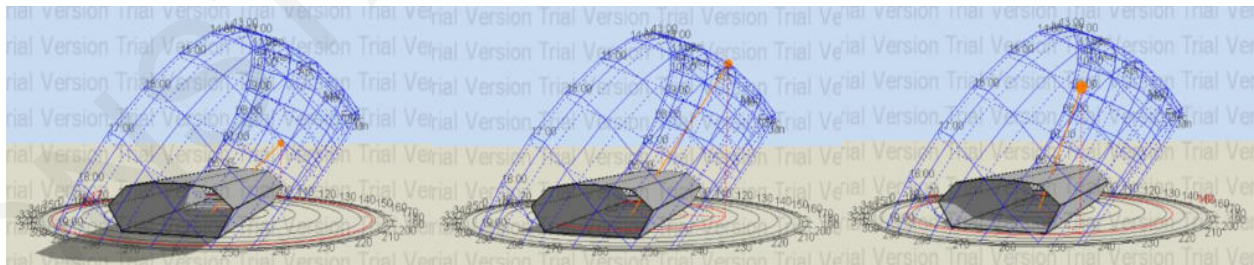


08:00

12:00

15:00

21st of March



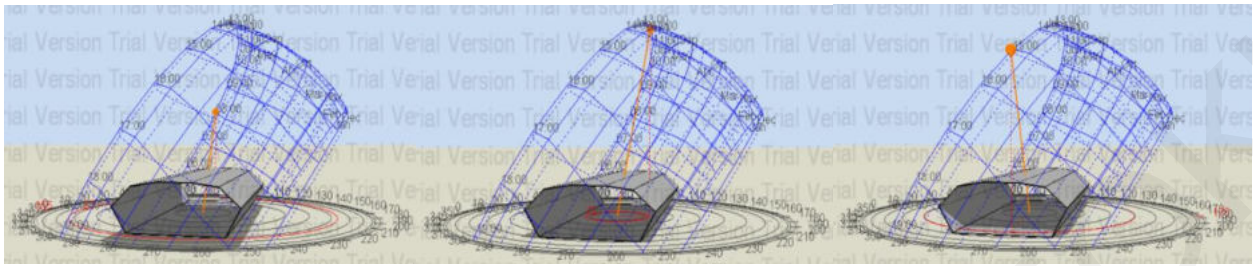
08:00

12:00

15:00

APPENDIX

21st of June

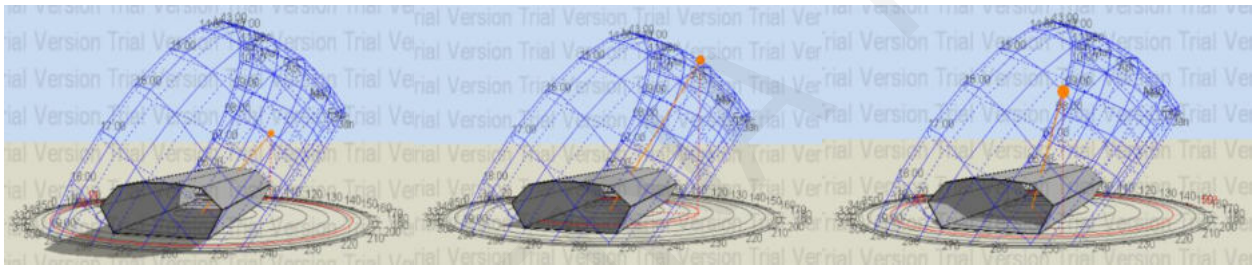


08:00

12:00

15:00

21st of September



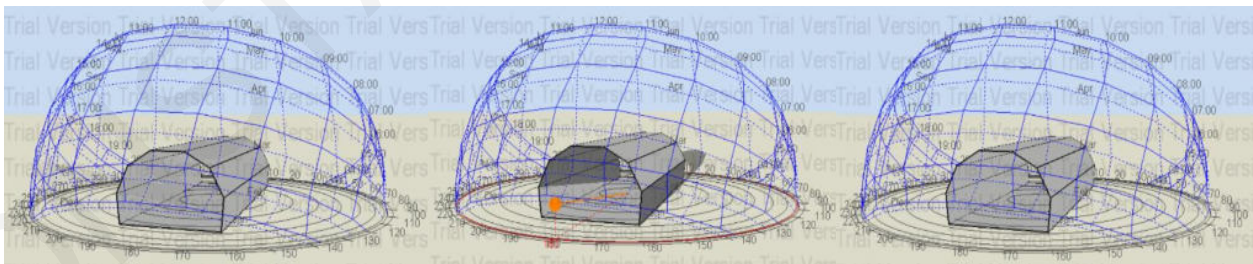
08:00

12:00

15:00

Stockholm, Sweden – Site Orientation 0°, Initial Position

21st of December



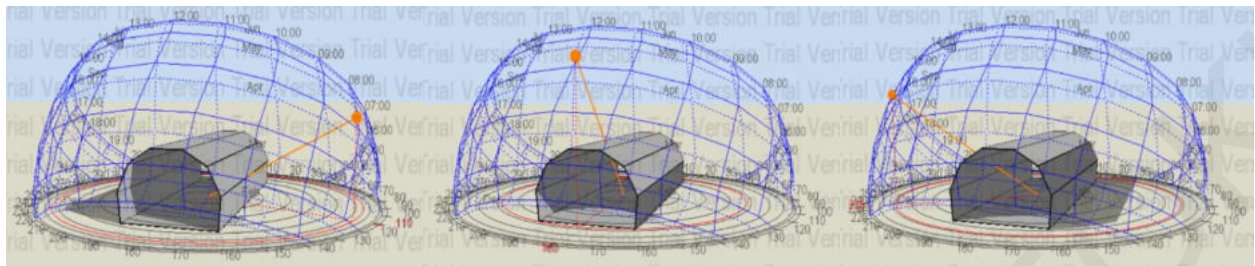
08:00

12:00

15:00

APPENDIX

21st of March

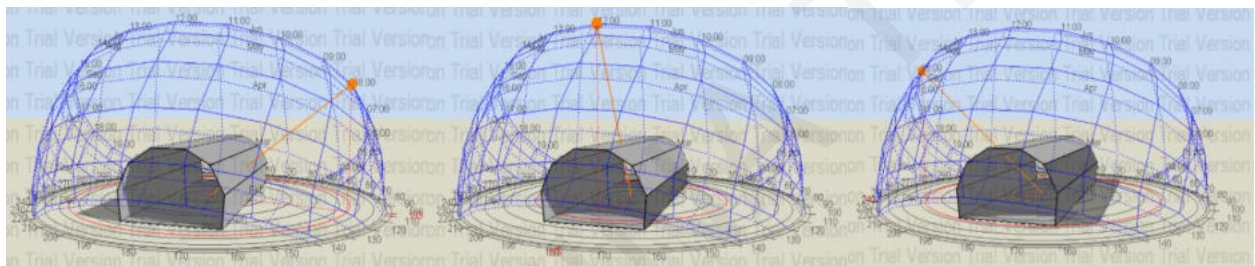


08:00

12:00

15:00

21st of June

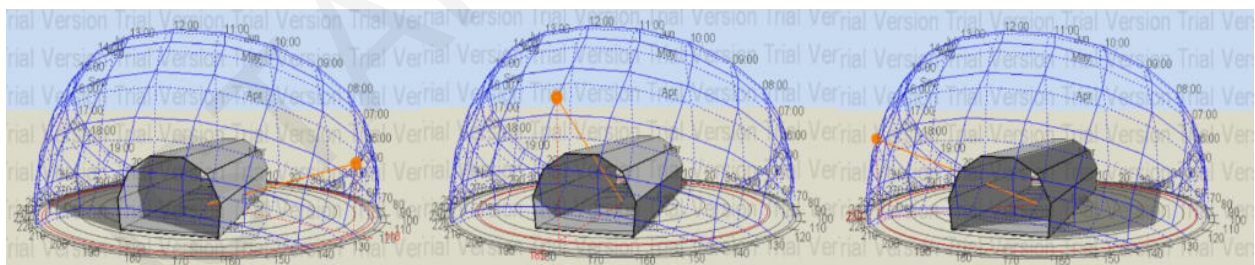


08:00

12:00

15:00

21st of September



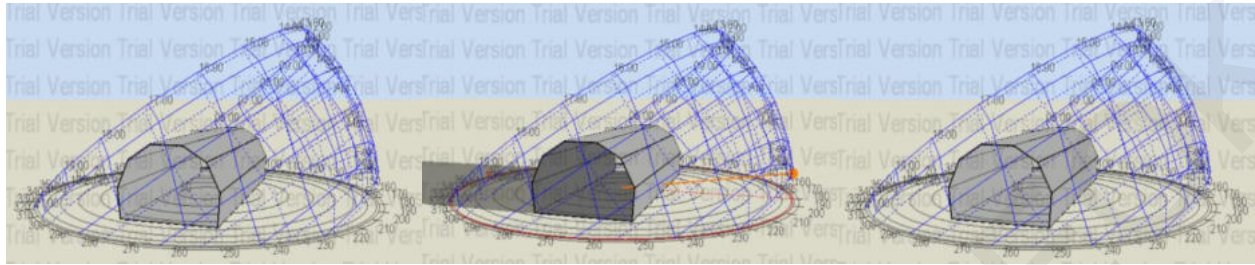
08:00

12:00

15:00

Stockholm, Sweden – Site Orientation 90°, Initial Position

21st of December

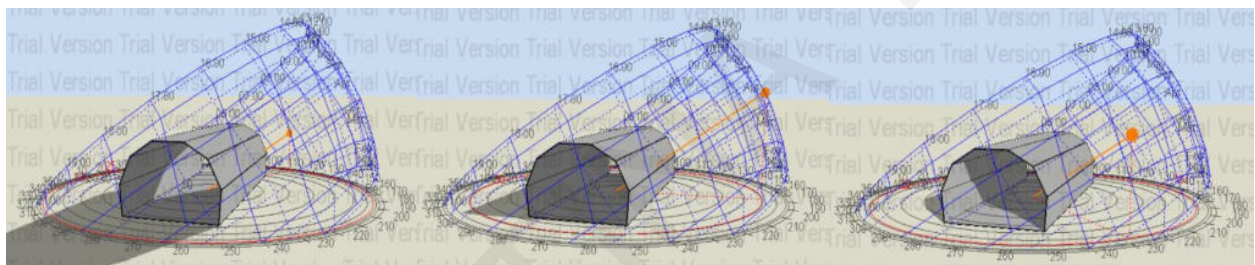


08:00

12:00

15:00

21st of March

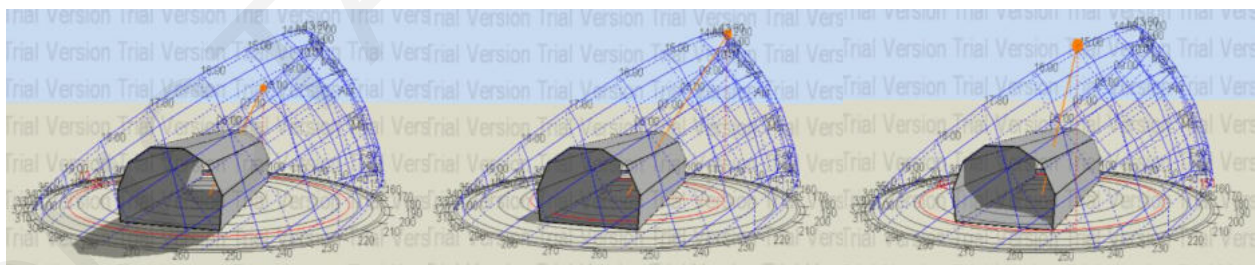


08:00

12:00

15:00

21st of June

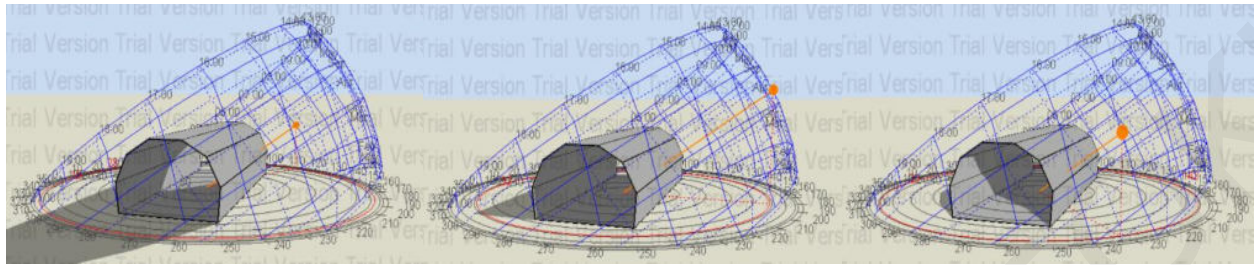


08:00

12:00

15:00

21st of September



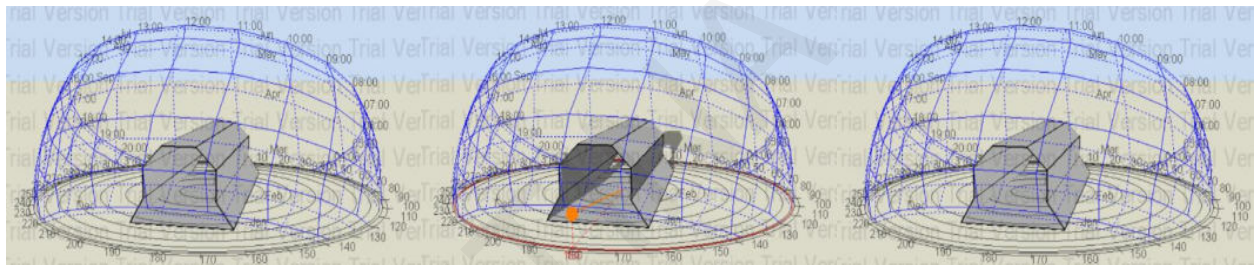
08:00

12:00

15:00

Stockholm, Sweden – Site Orientation 0°, Final Position A

21st of December

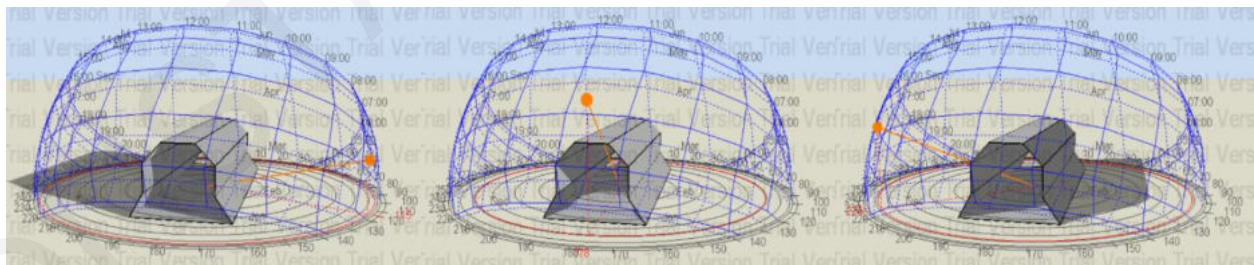


08:00

12:00

15:00

21st of March

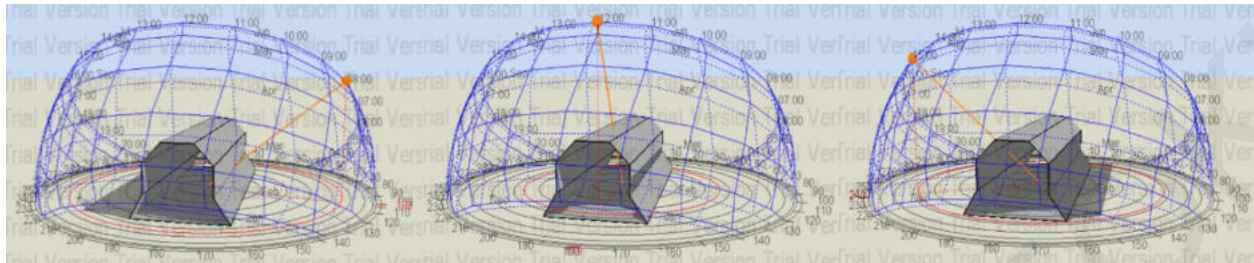


08:00

12:00

15:00

21st of June

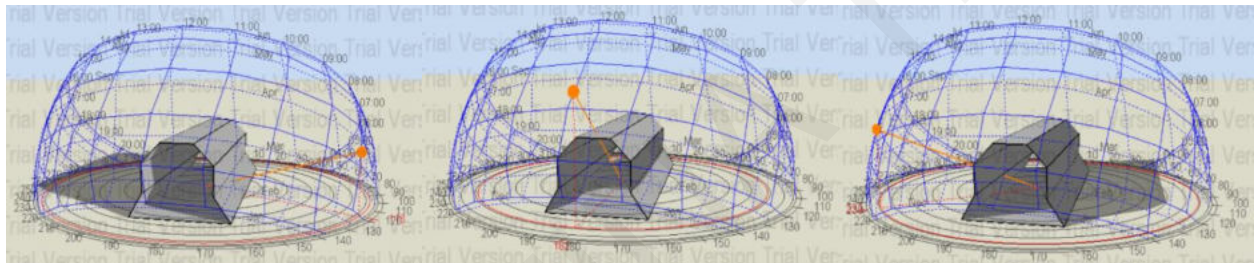


08:00

12:00

15:00

21st of September



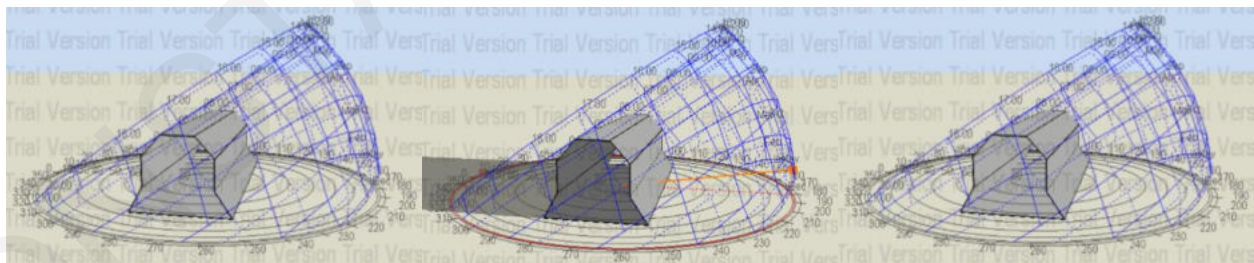
08:00

12:00

15:00

Stockholm, Sweden – Site Orientation 90°, Final Position A

21st of December



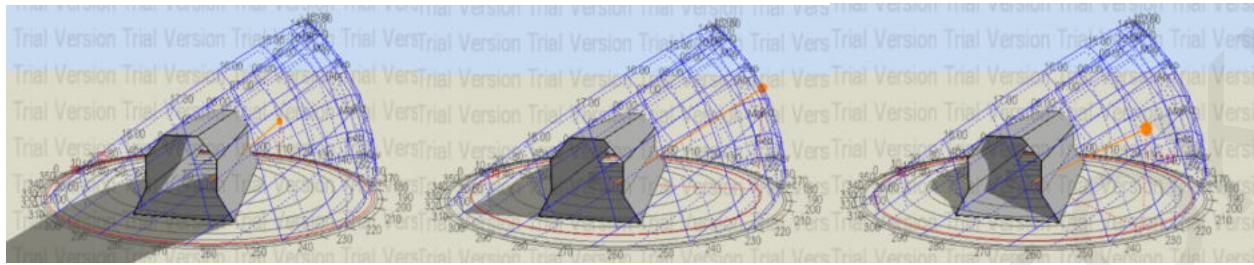
08:00

12:00

15:00

APPENDIX

21st of March

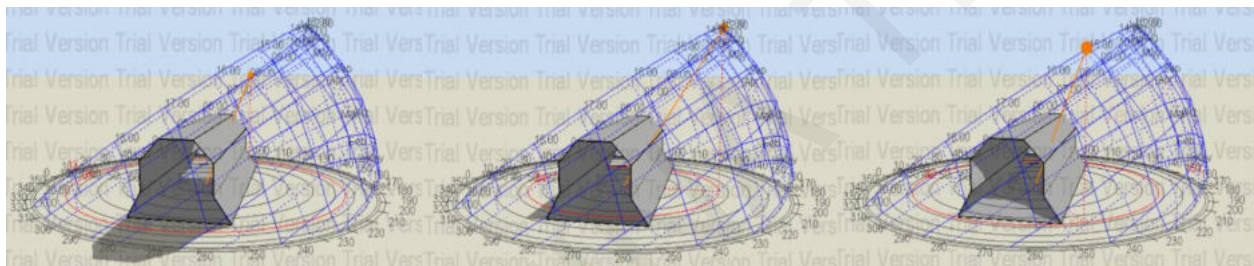


08:00

12:00

15:00

21st of June

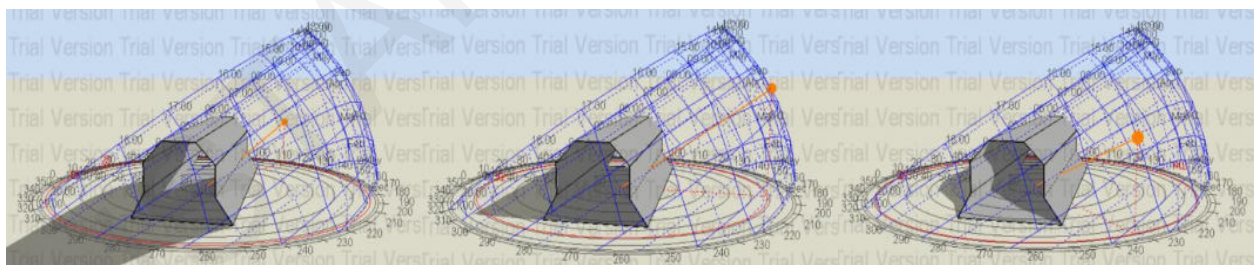


08:00

12:00

15:00

21st of September



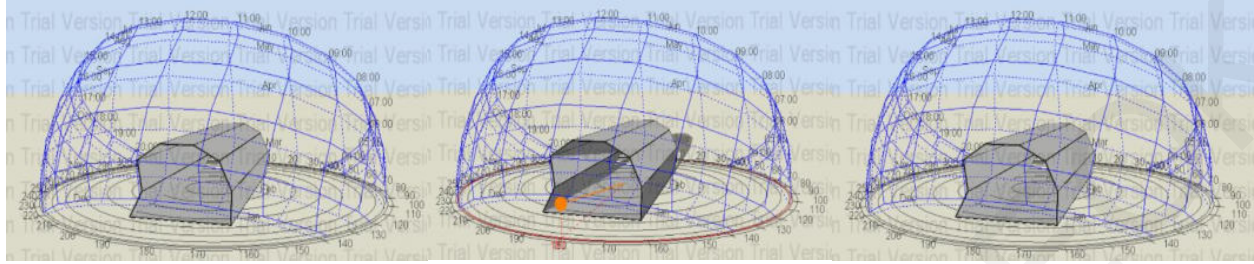
08:00

12:00

15:00

Stockholm, Sweden – Site Orientation 0°, Final Position B

21st of December

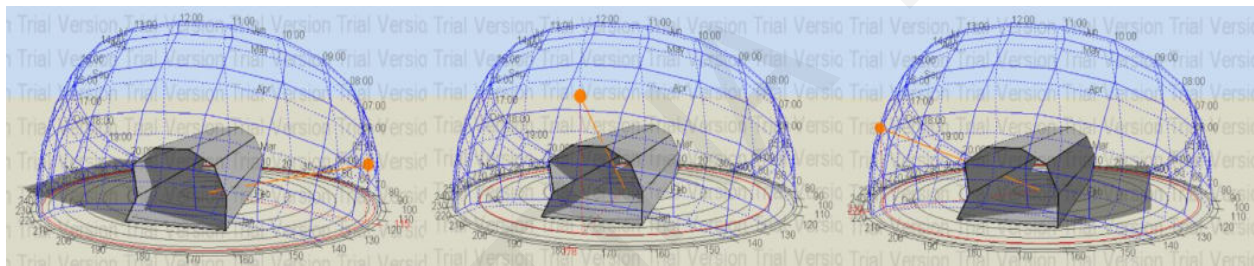


08:00

12:00

15:00

21st of March

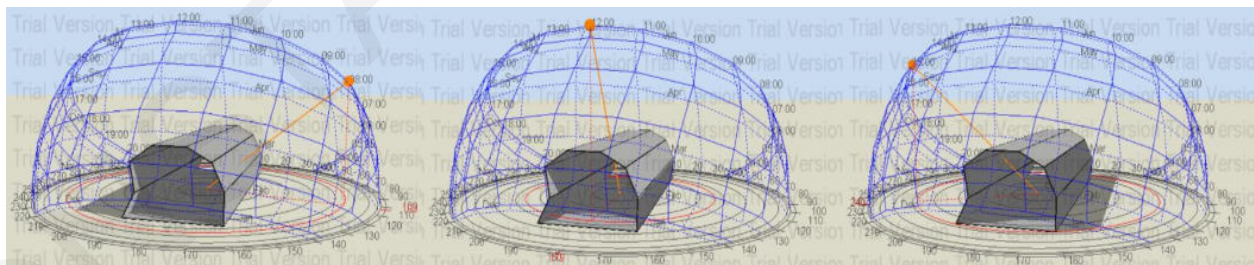


08:00

12:00

15:00

21st of June

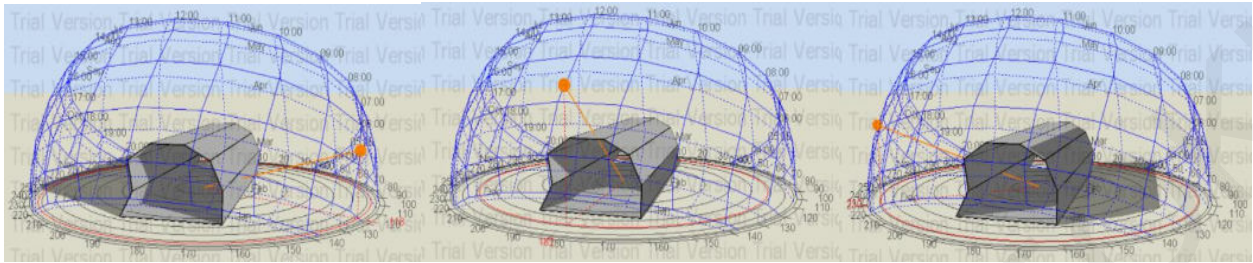


08:00

12:00

15:00

21st of September



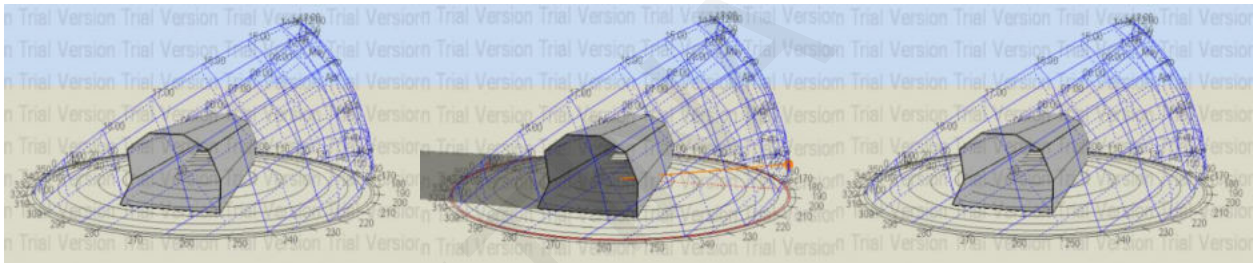
08:00

12:00

15:00

Stockholm, Sweden – Site Orientation 90°, Final Position B

21st of December

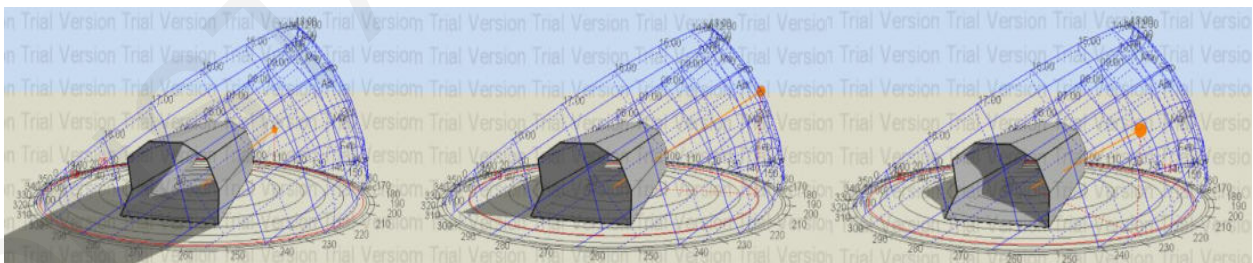


08:00

12:00

15:00

21st of March



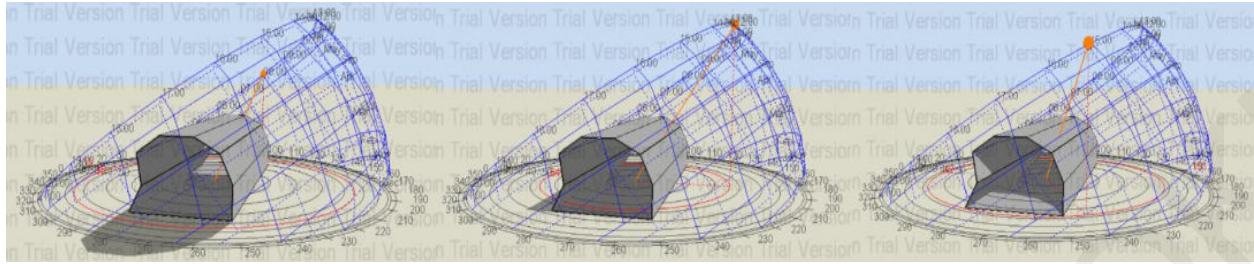
08:00

12:00

15:00

21st of June

APPENDIX

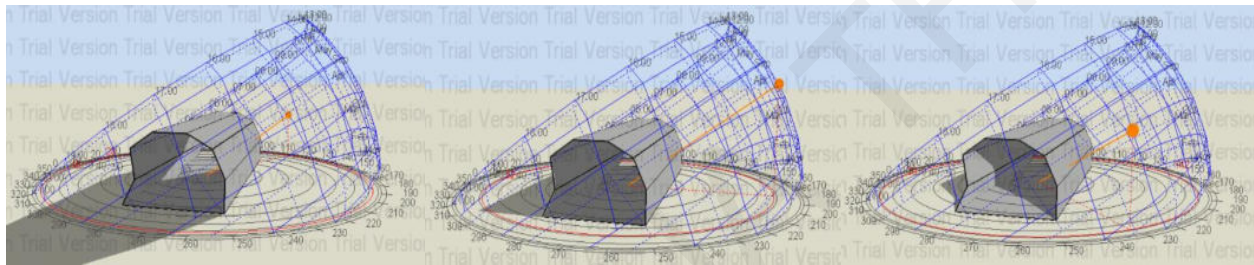


08:00

12:00

15:00

21st of September



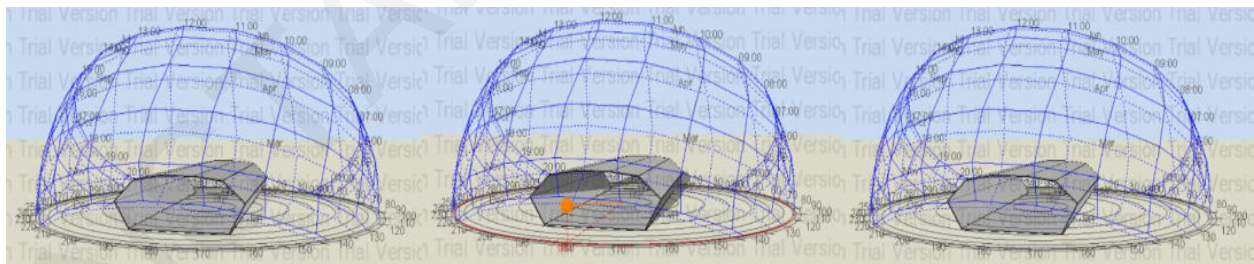
08:00

12:00

15:00

Stockholm, Sweden – Site Orientation 0°, Final Position C

21st of December



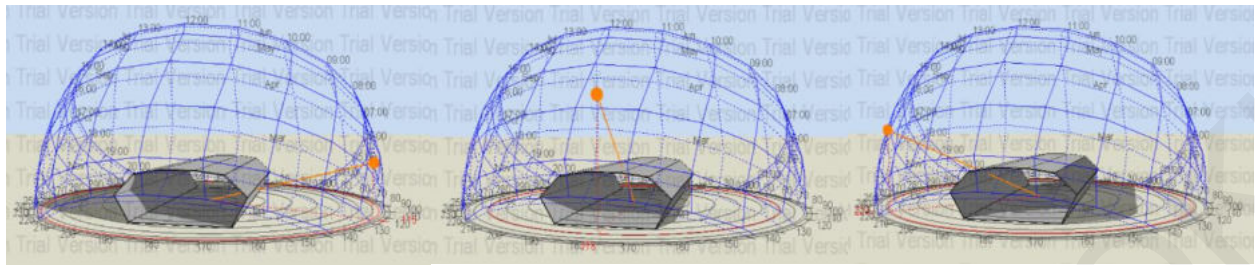
08:00

12:00

15:00

21st of March

APPENDIX

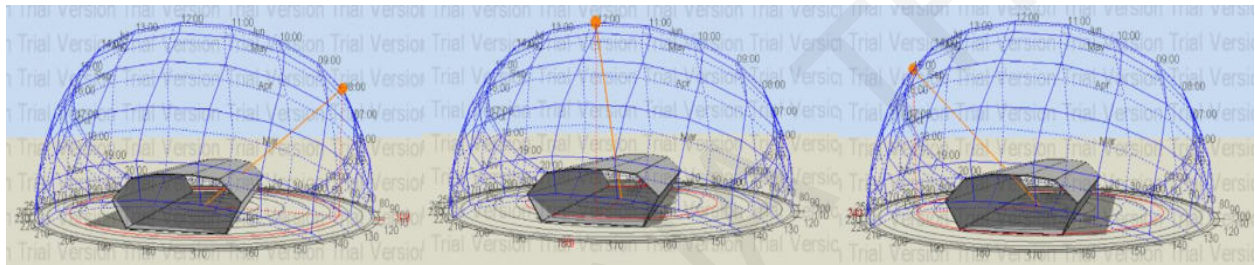


08:00

12:00

15:00

21st of June

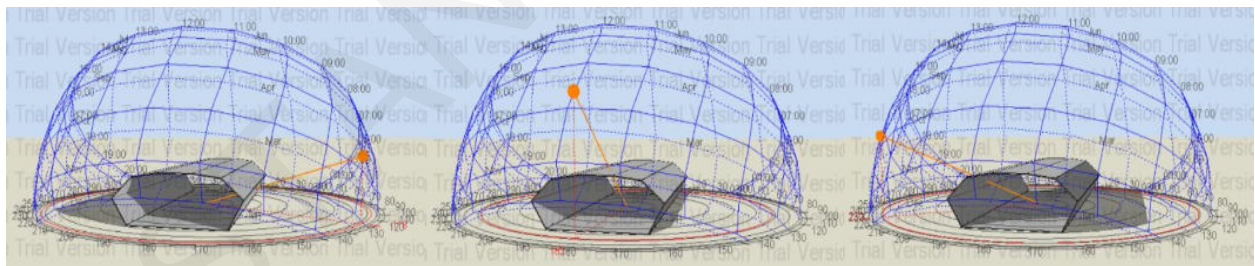


08:00

12:00

15:00

21st of September



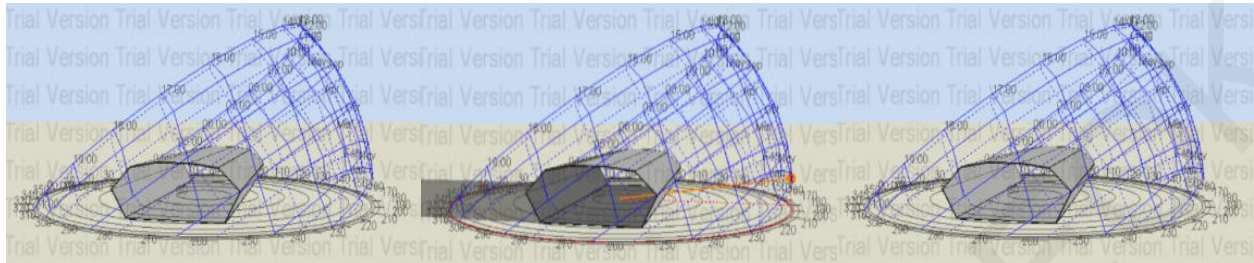
08:00

12:00

15:00

Stockholm, Sweden – Site Orientation 90°, Final Position C

21st of December

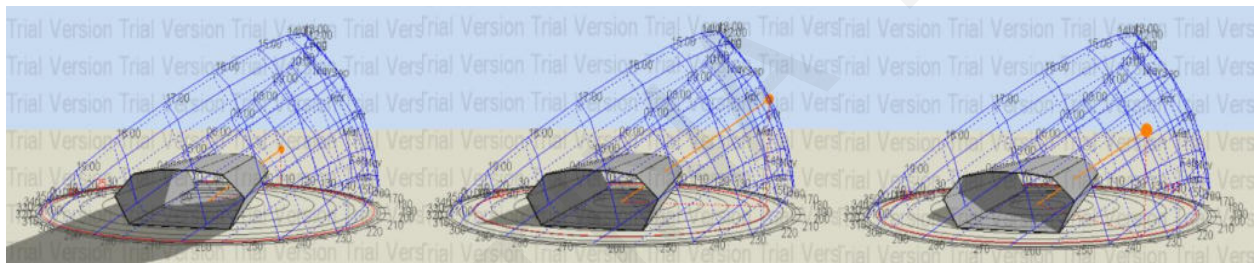


08:00

12:00

15:00

21st of March

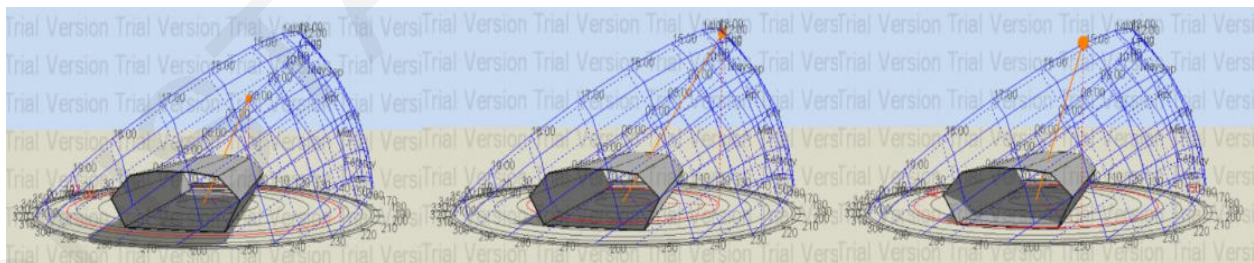


08:00

12:00

15:00

21st of June

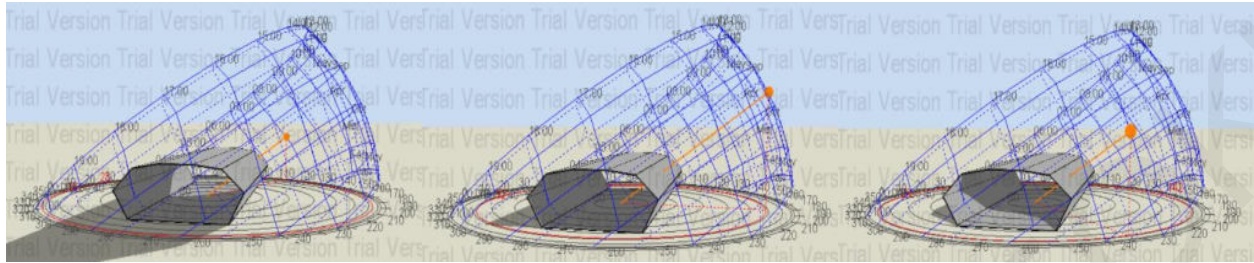


08:00

12:00

15:00

21st of September



08:00

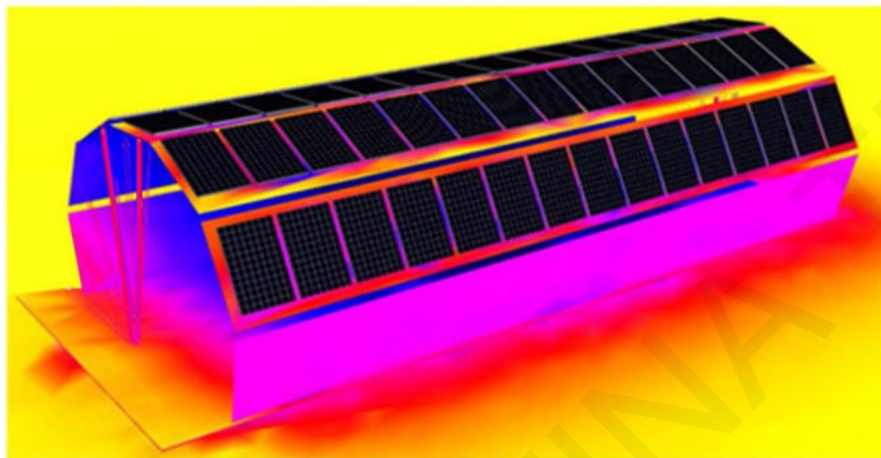
12:00

15:00

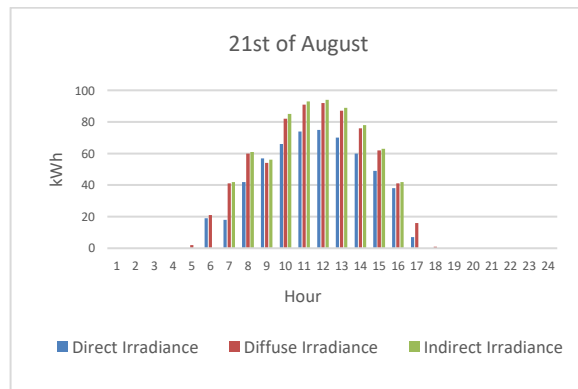
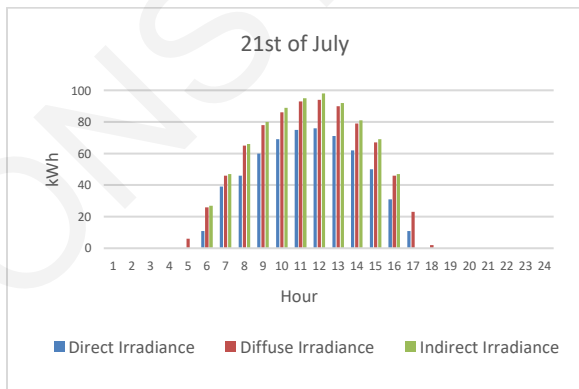
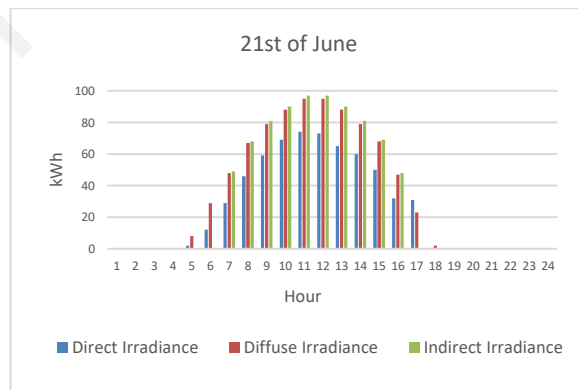
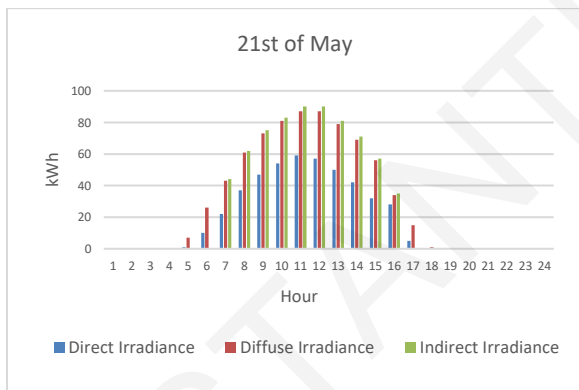
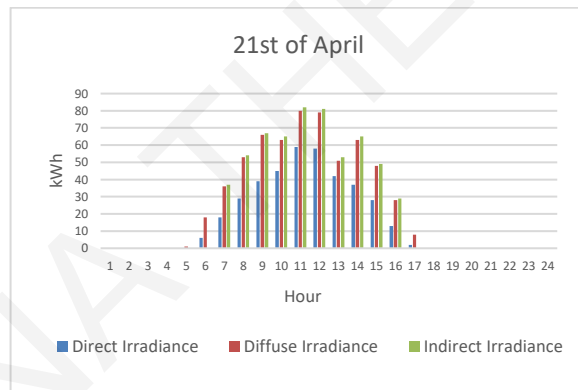
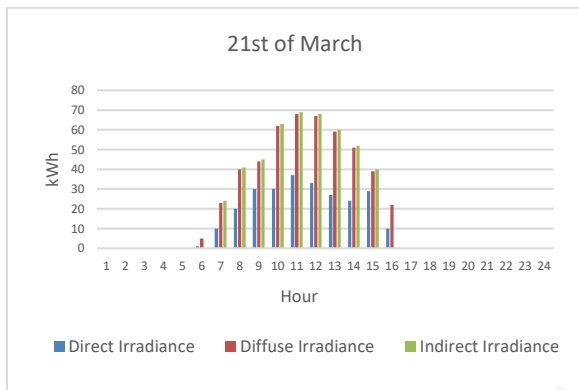
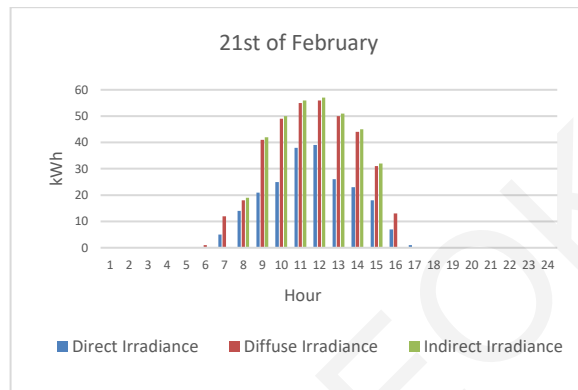
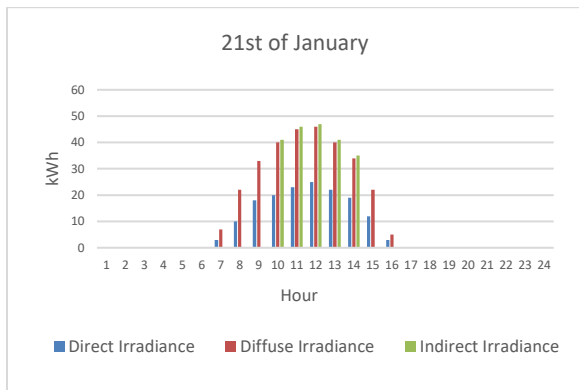
Appendix 3: Simulation Results of Solar Irradiance and Energy Production

A. Site Location: Larnaca, Cyprus, Site Orientation 0°

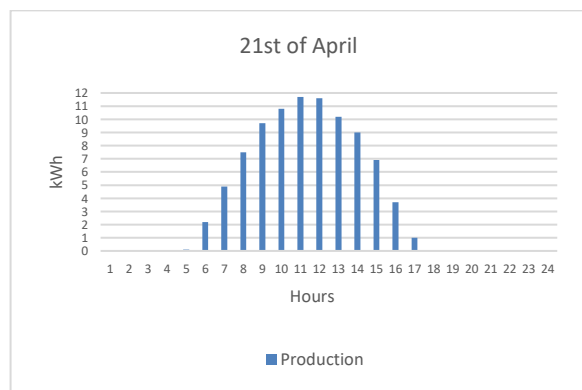
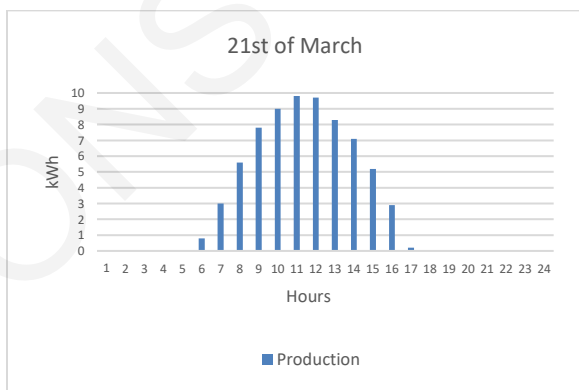
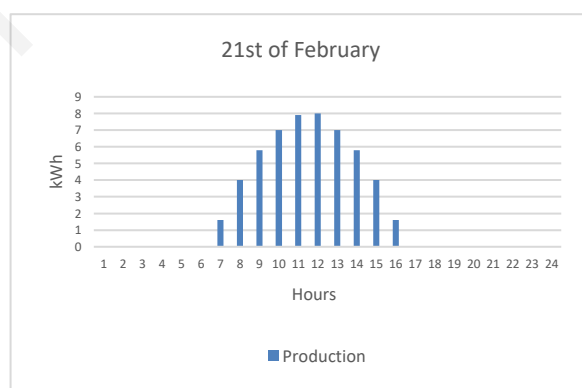
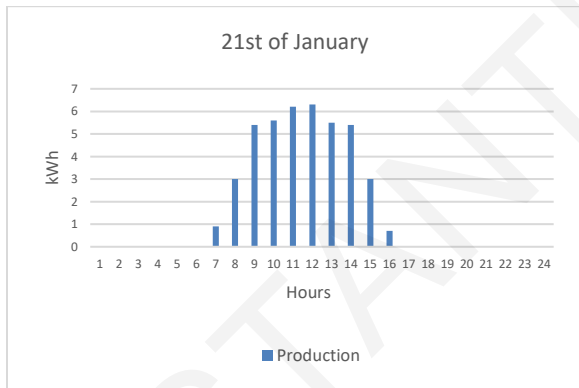
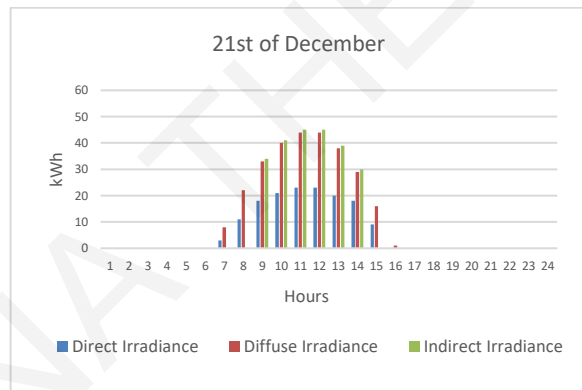
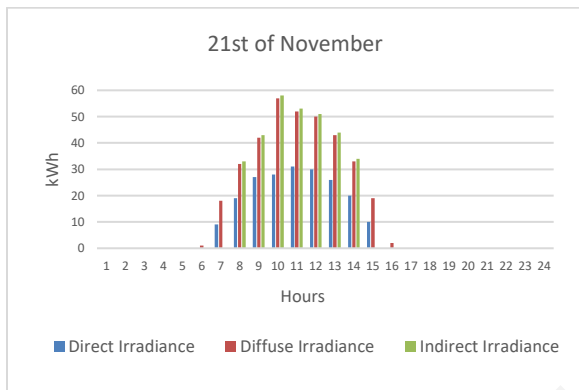
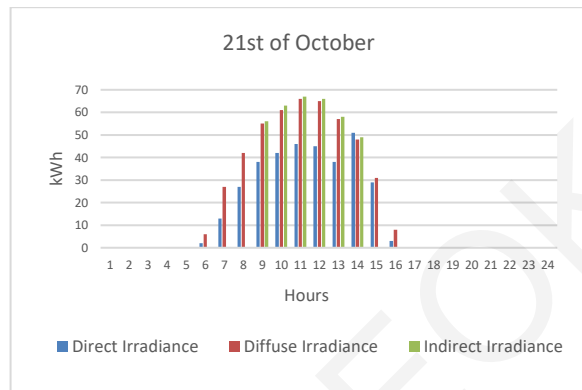
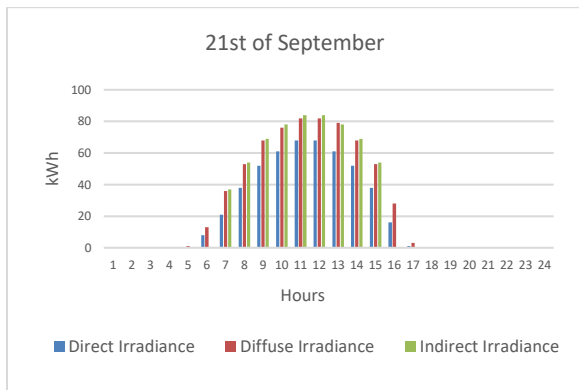
Initial Position

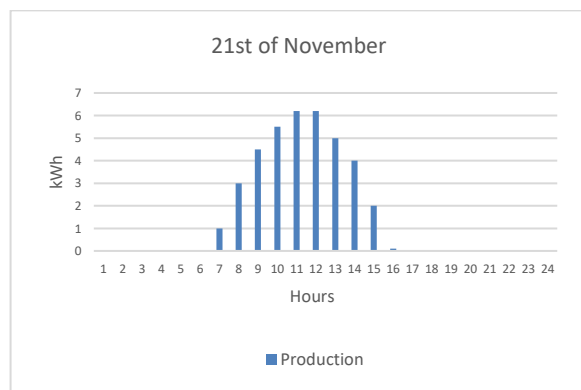
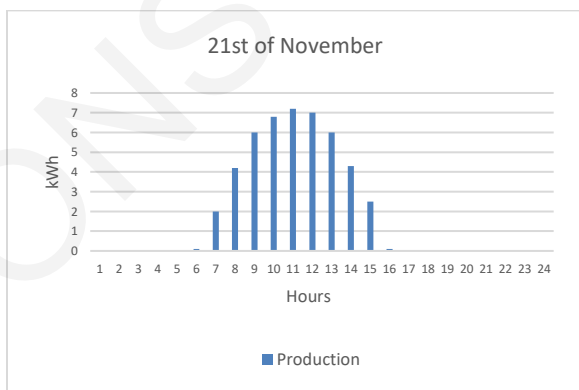
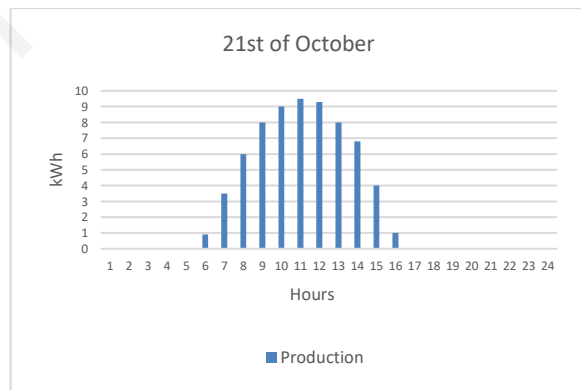
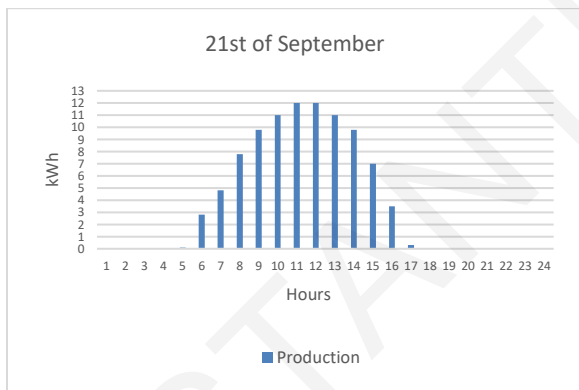
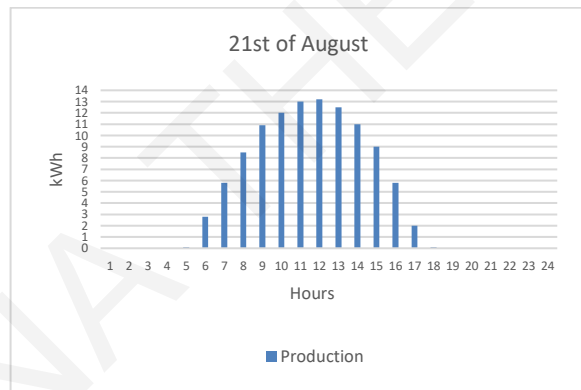
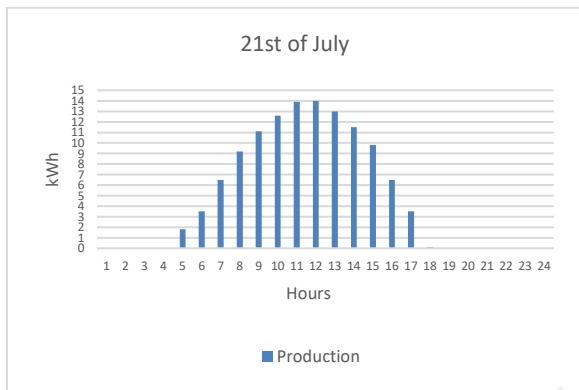
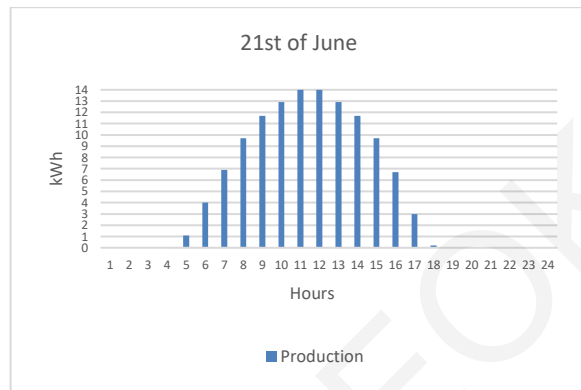
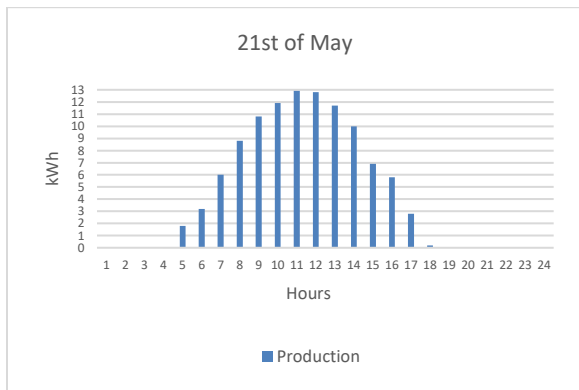


Month	Min Air Temperature	Max Air Temperature	Min Module Temperature	Max Module Temperature
January	9	15.5	1.5	3
February	8	16	1.5	4
March	9.8	16.5	1.5	4
April	11	21.5	1.5	5
May	17	24.5	2	6
June	20	28	2.5	7
July	23	31.5	3	7
August	23	33	4	7
September	20.5	29.5	3.5	6.5
October	17	25.5	2.5	5
November	14	22	2	4.5
December	10	17	1.5	3.5

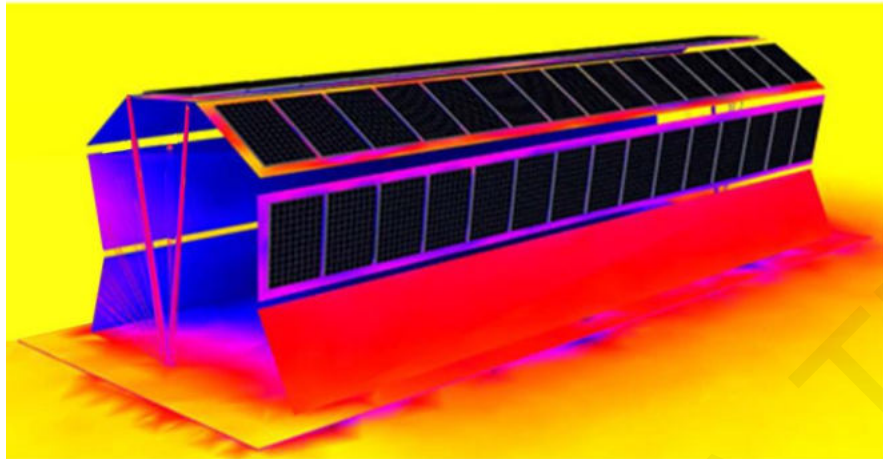


APPENDIX

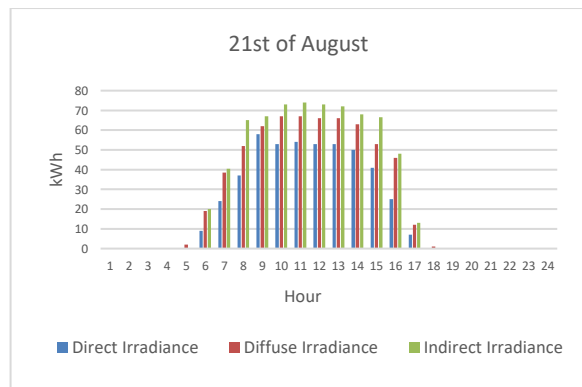
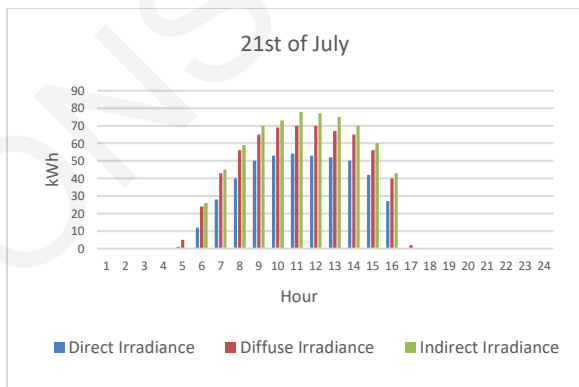
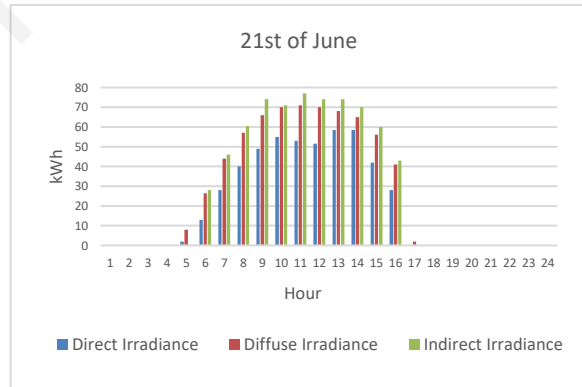
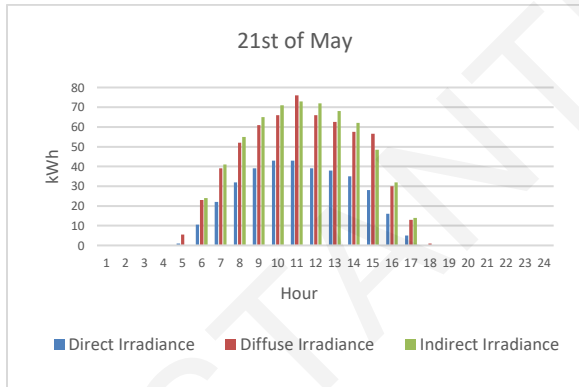
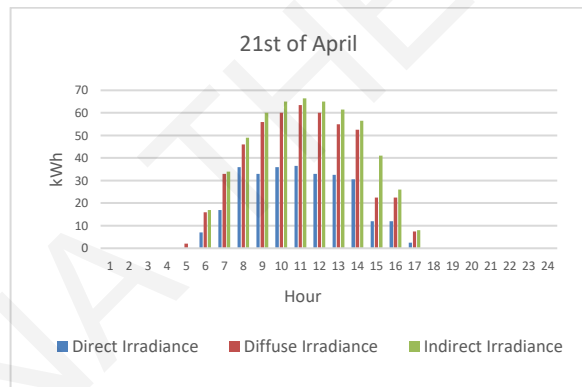
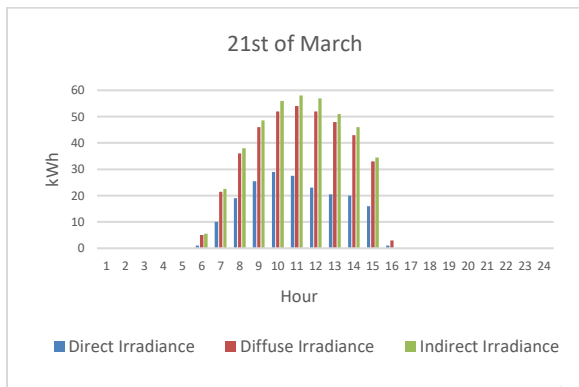
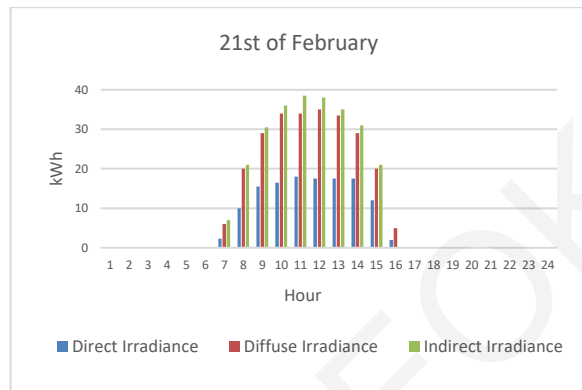
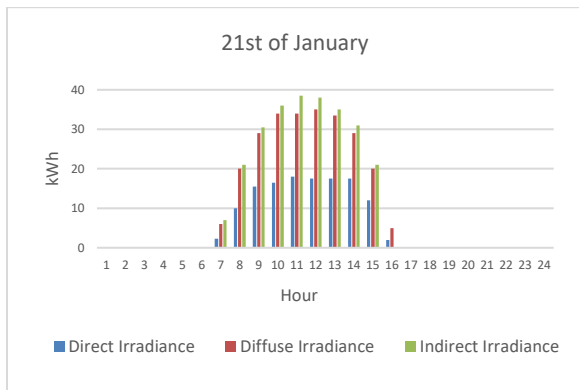


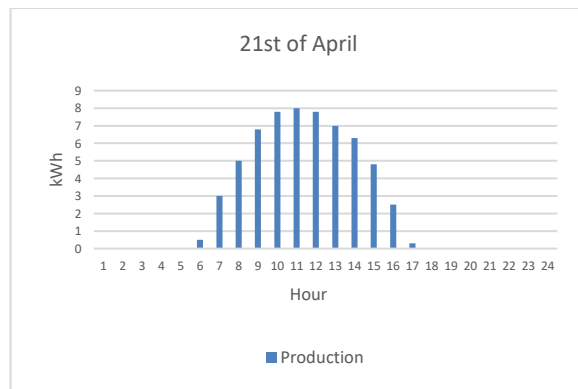
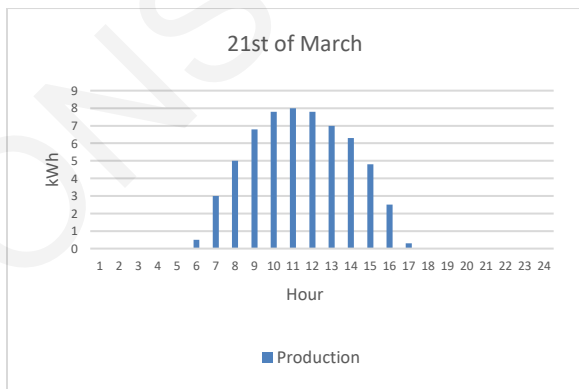
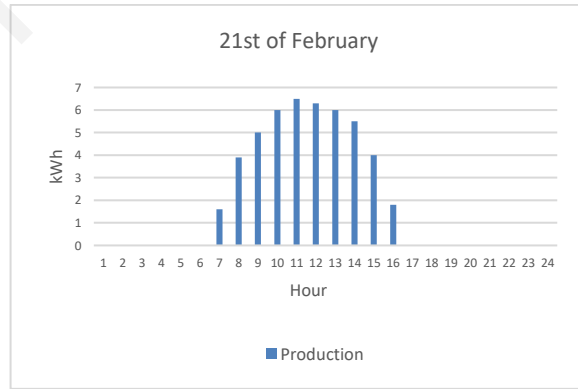
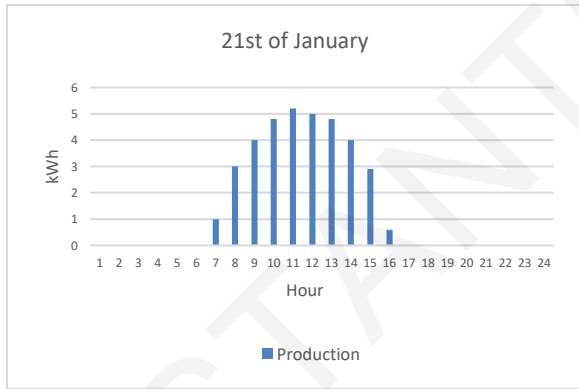
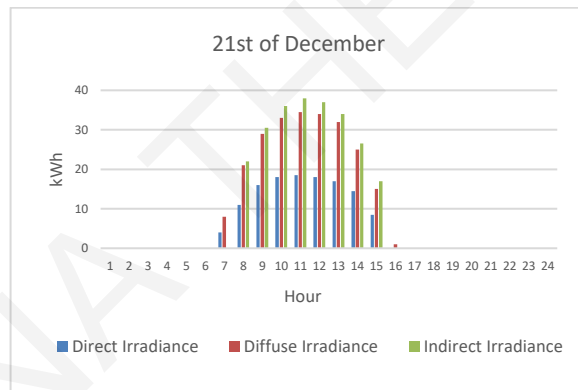
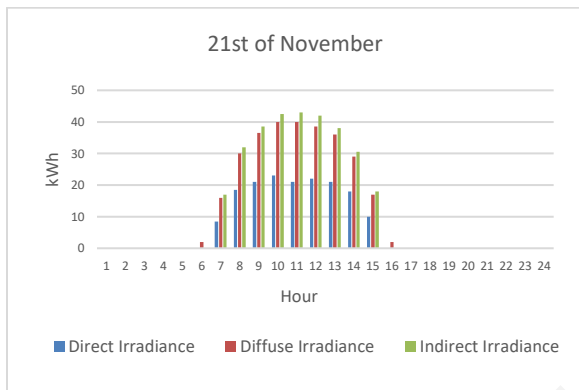
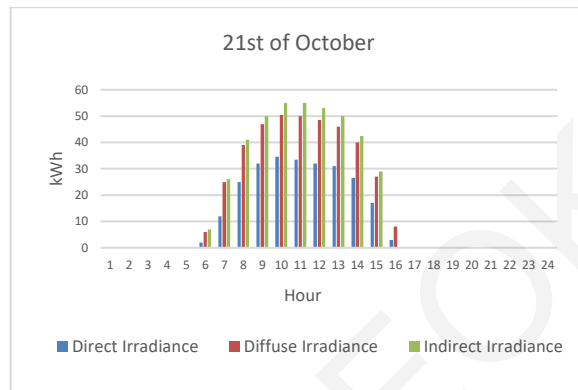
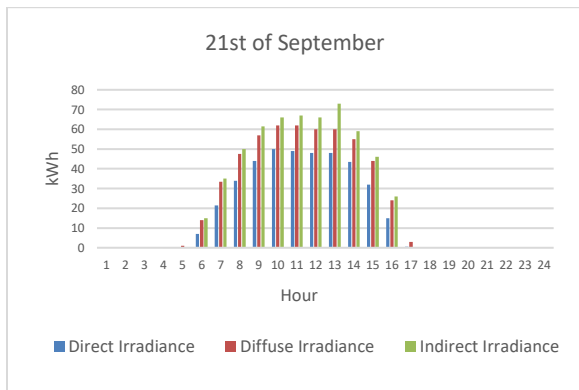


Target Position A

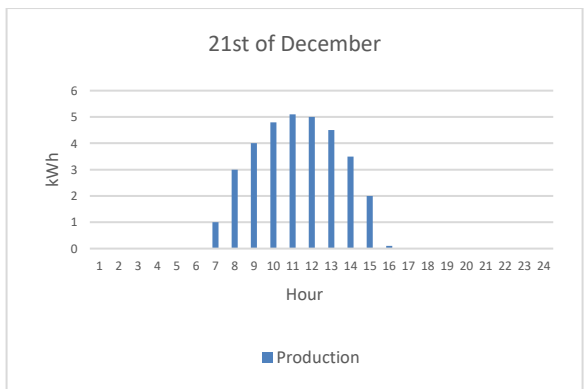
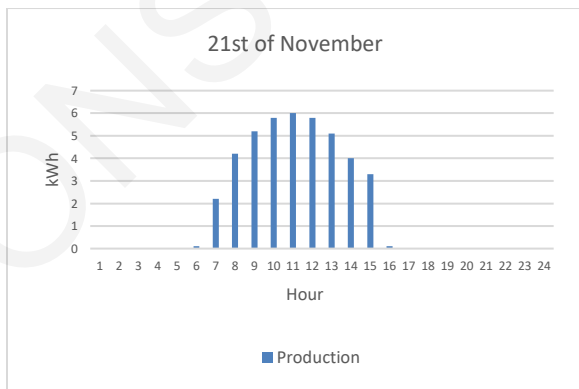
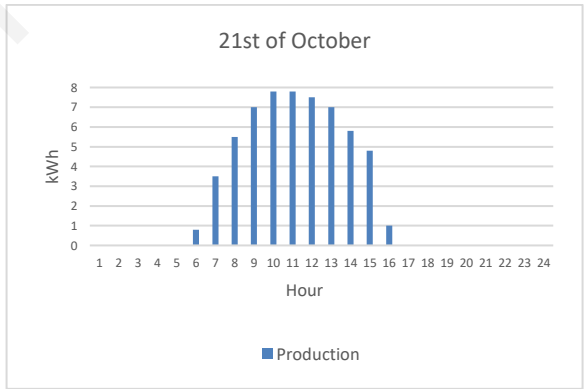
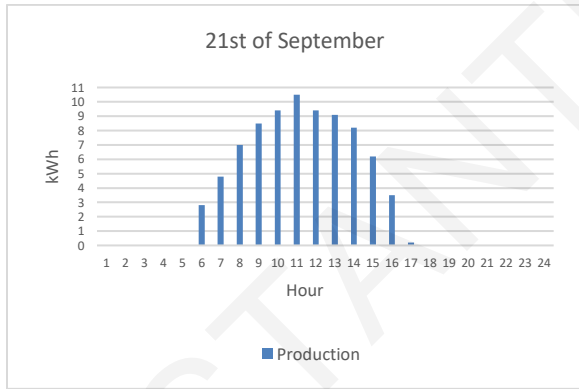
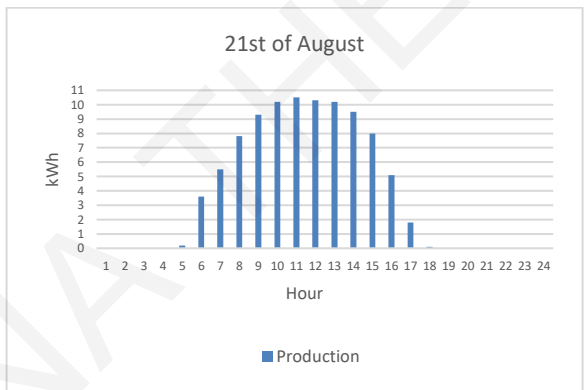
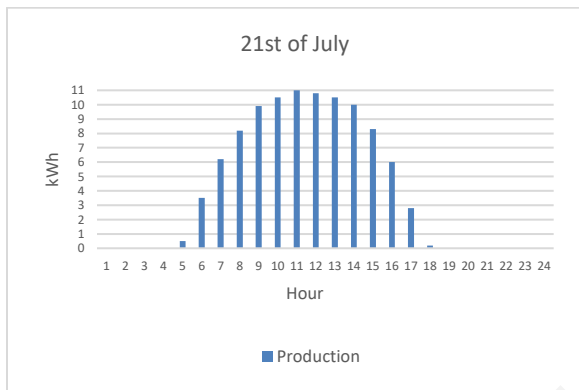
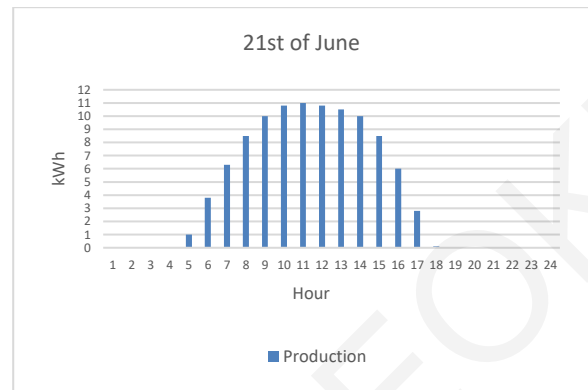
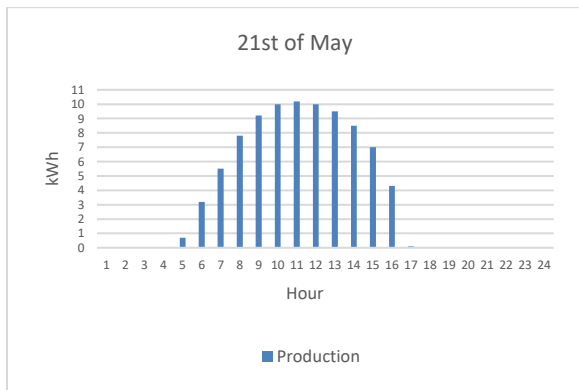


Month	Min Air Temperature	Max Air Temperature	Min Module Temperature	Max Module Temperature
January	9	15.5	2.5	5
February	8	16	2	5.5
March	10	16.5	2	6.5
April	12	21.5	2.5	8
May	17	24.5	4	9
June	20	28	4.5	10
July	23	32	5	10.5
August	23	32	5	11
September	20.5	29.5	4.5	10
October	17	26	4	8.5
November	14	22	3.5	7
December	10	17	2.5	6

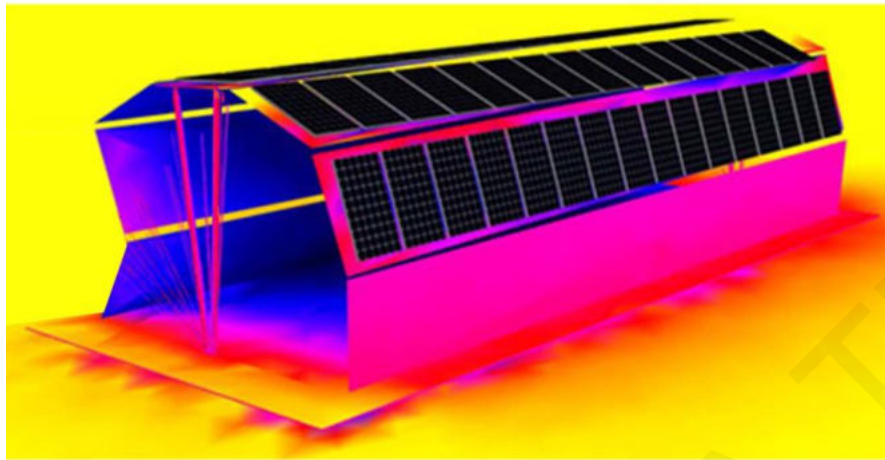




APPENDIX

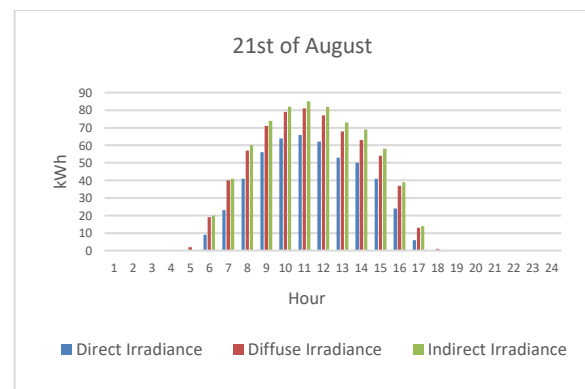
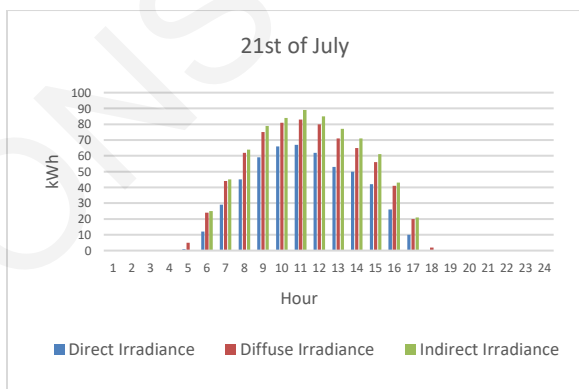
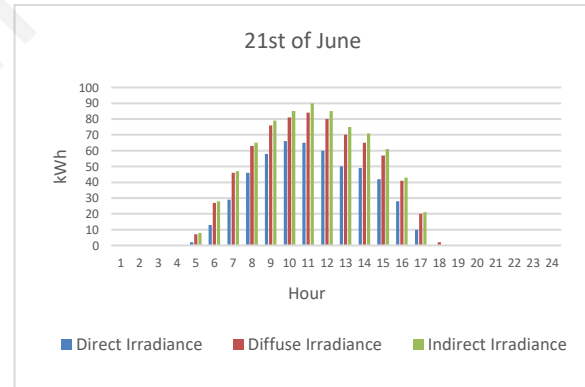
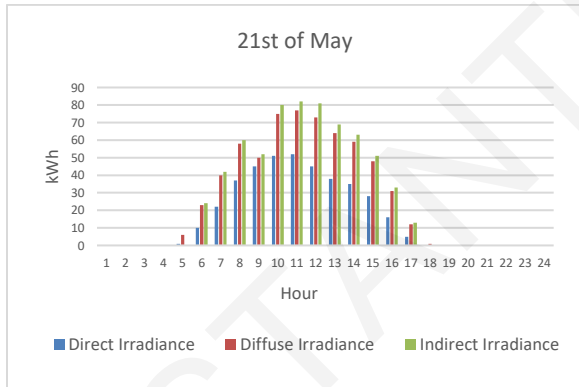
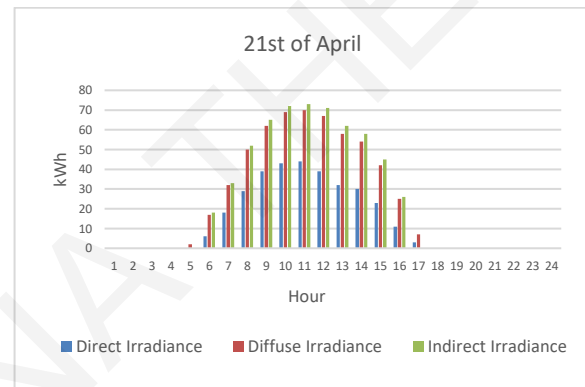
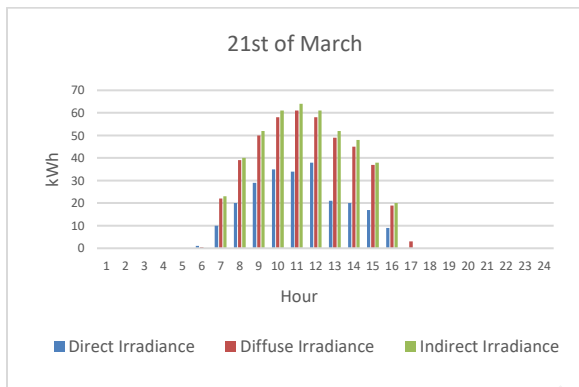
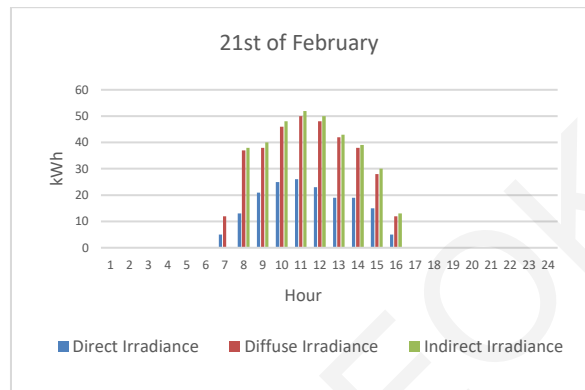
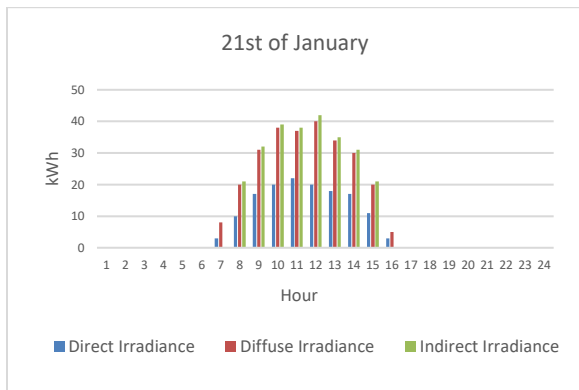


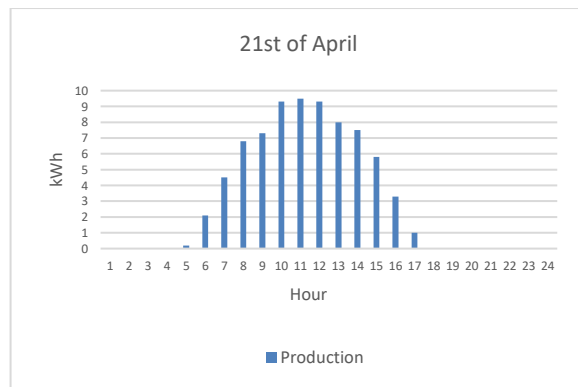
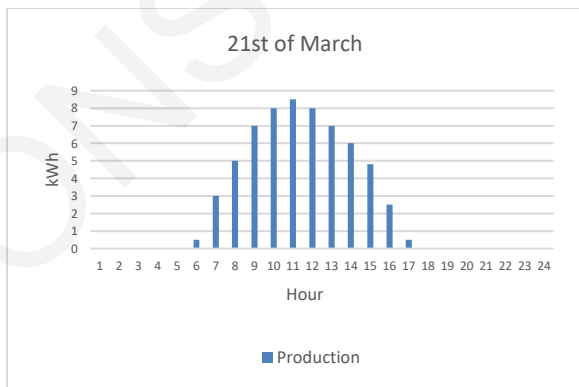
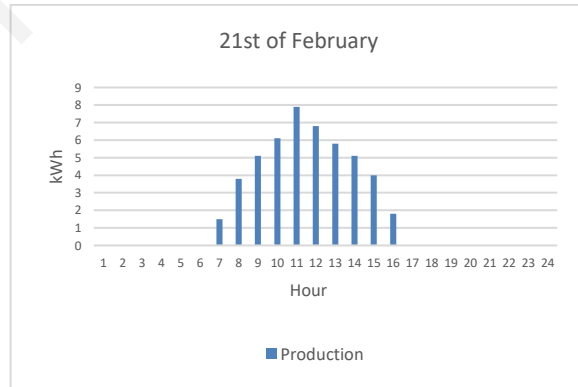
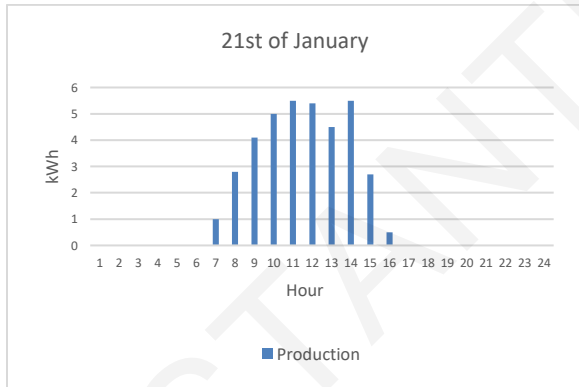
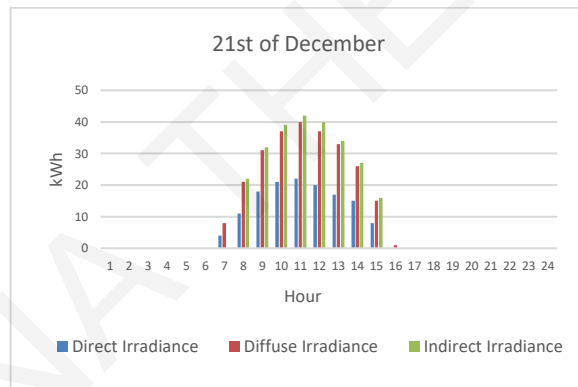
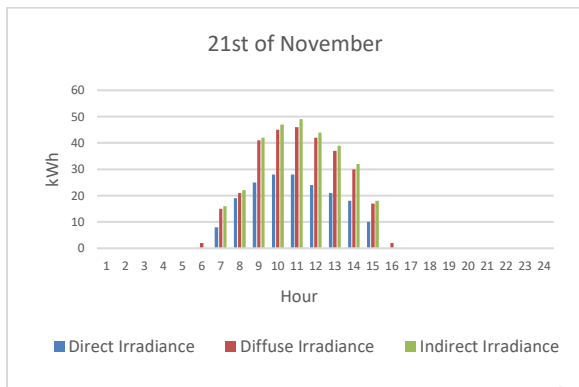
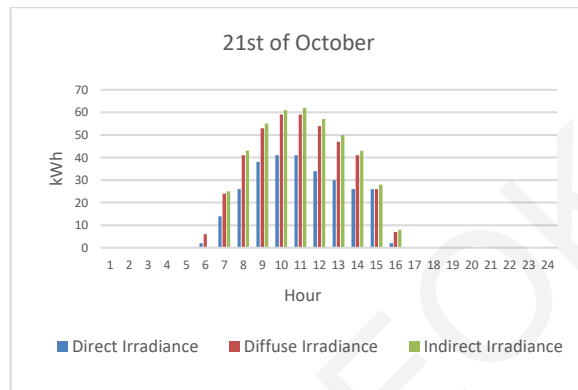
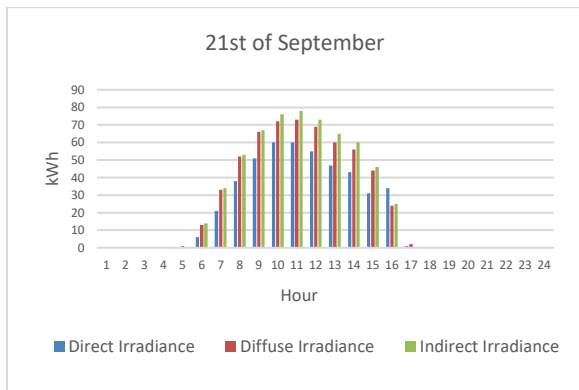
Target Position B

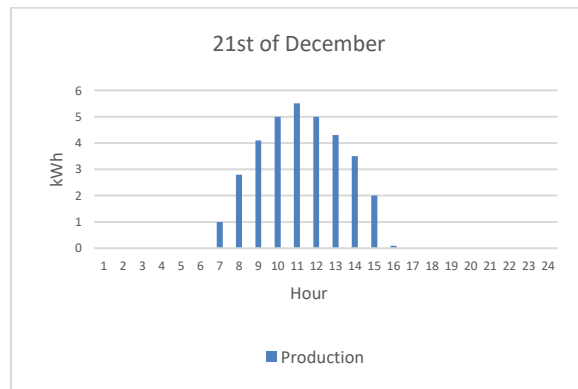
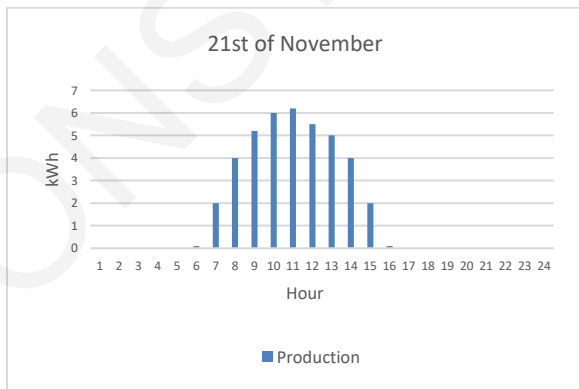
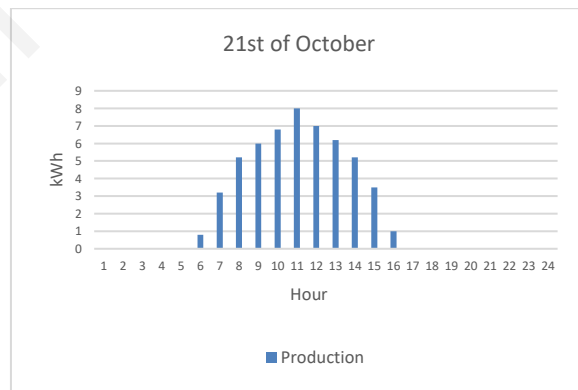
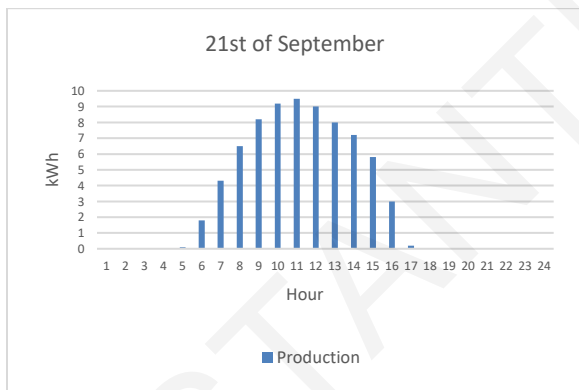
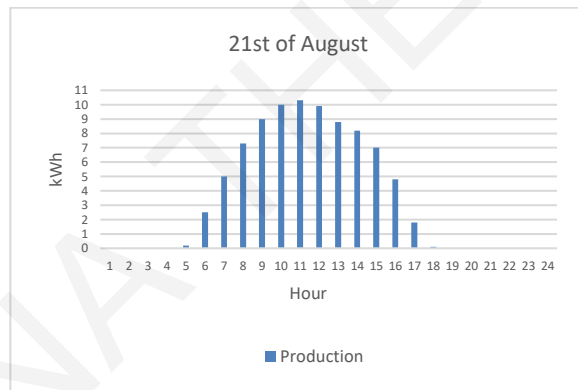
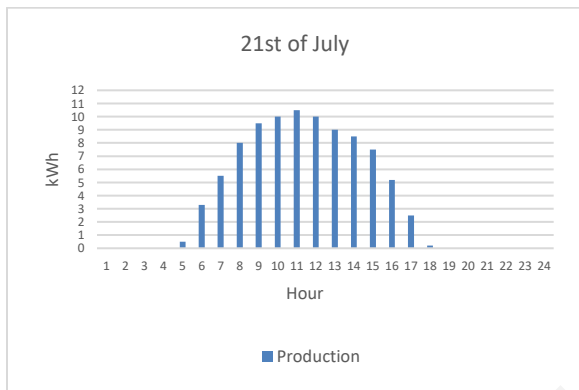
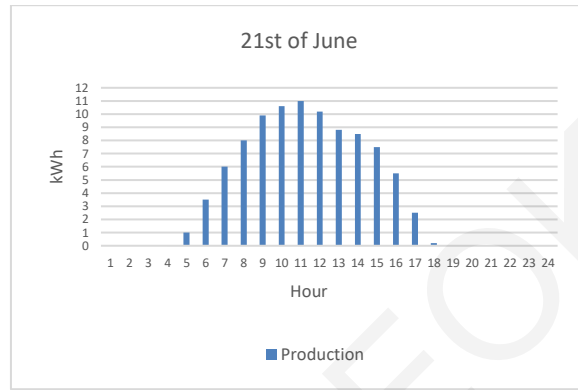
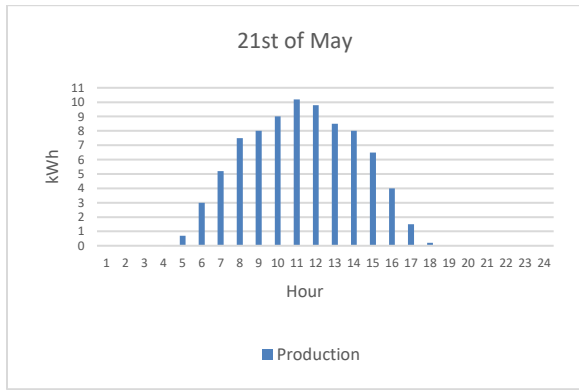


Month	Min Air Temperature	Max Air Temperature	Min Module Temperature	Max Module Temperature
January	9	15.5	3	8
February	8	16	3	9
March	9.8	16.5	4	9.8
April	12	21.5	4	12
May	17	24.5	6	13.5
June	20	28	4.5	15
July	23	31.5	8	16
August	23.5	33	8	16
September	20.5	29.5	7	15
October	17	25.5	6	13
November	14	22	4.5	10
December	10	17	3.5	9

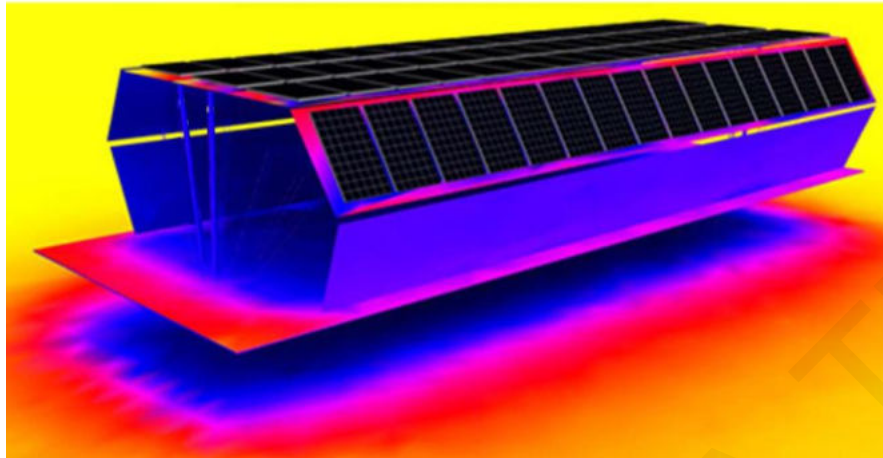
APPENDIX



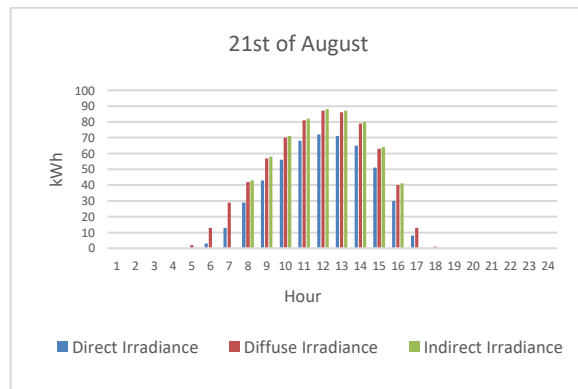
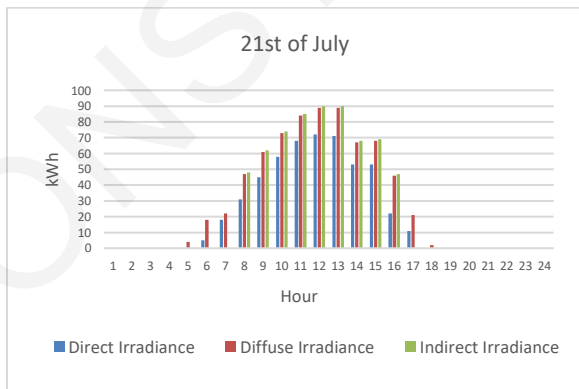
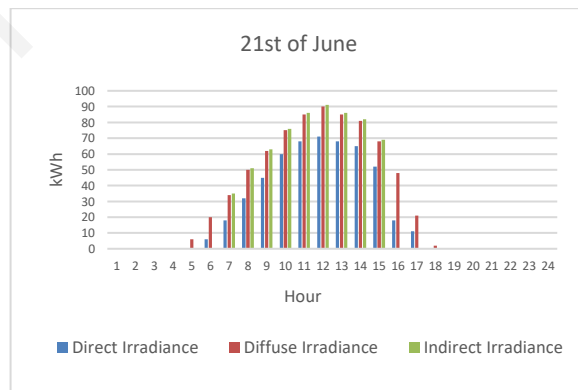
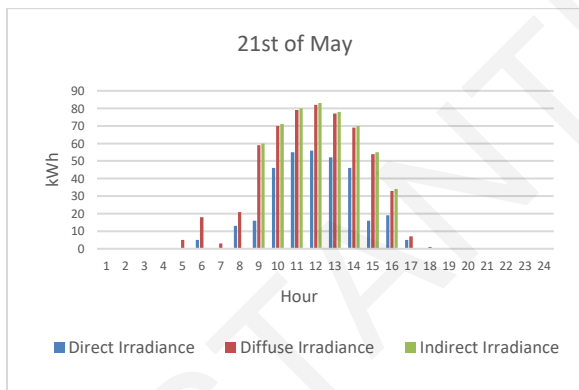
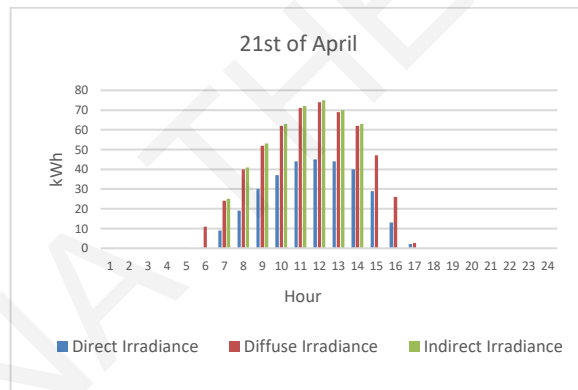
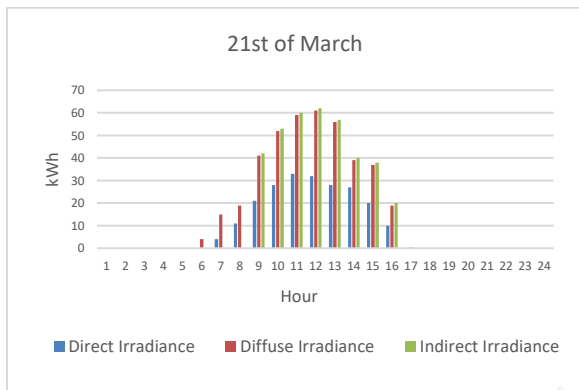
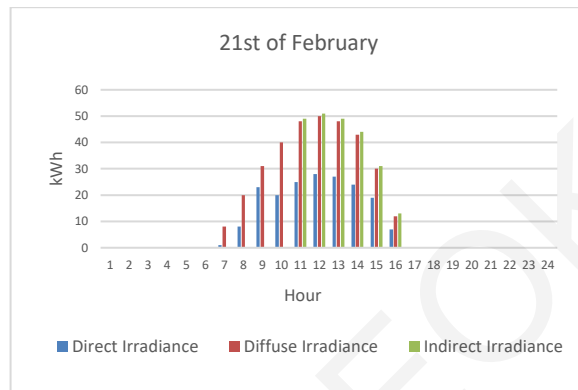
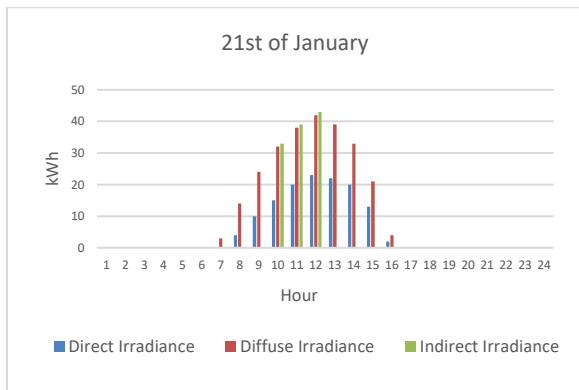


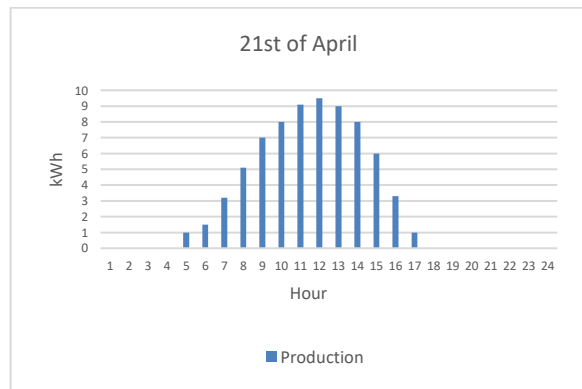
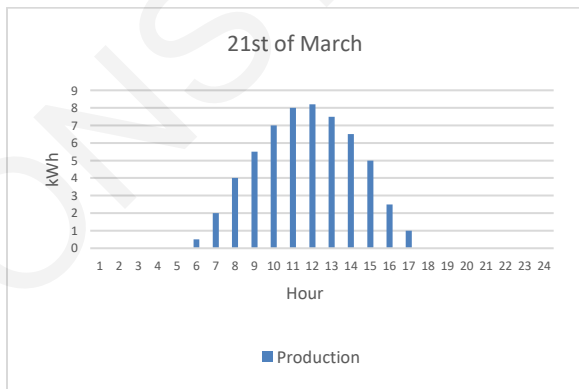
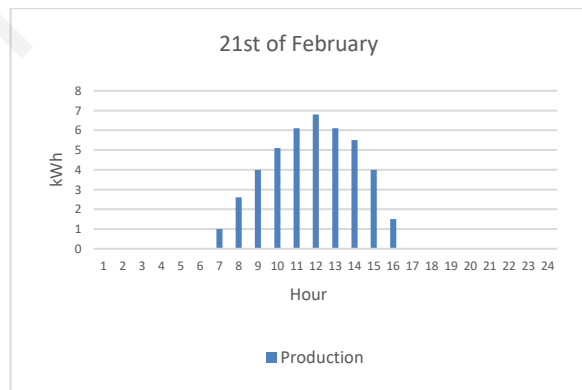
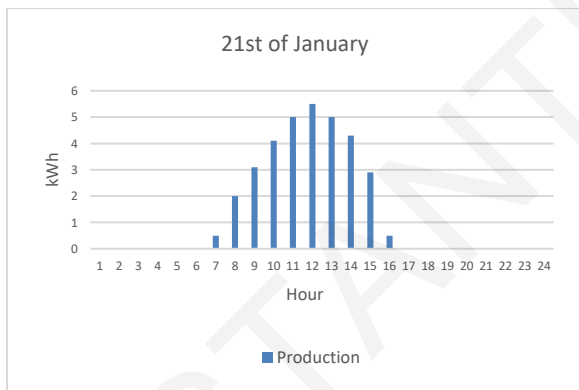
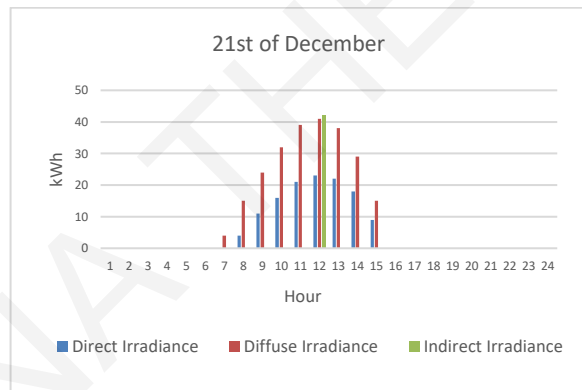
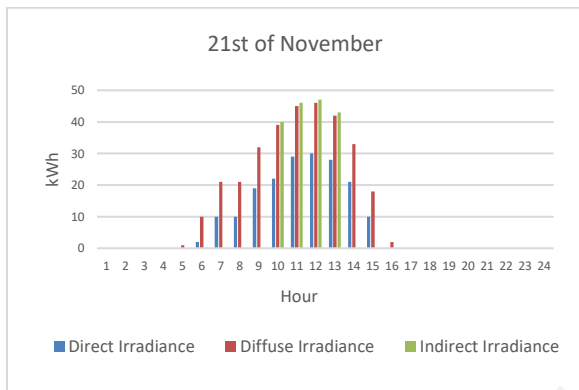
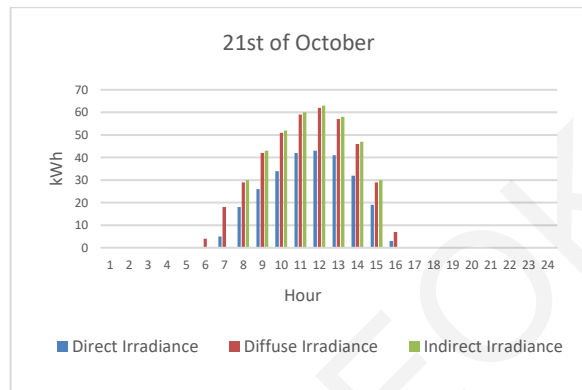
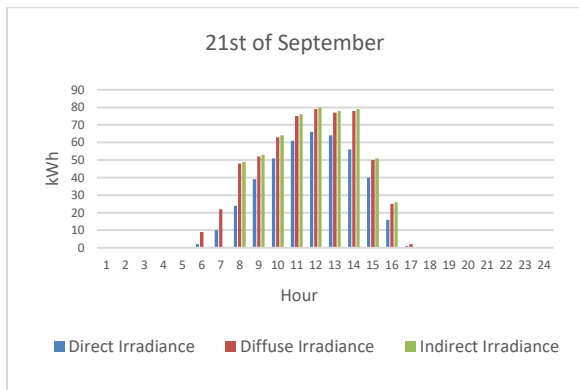


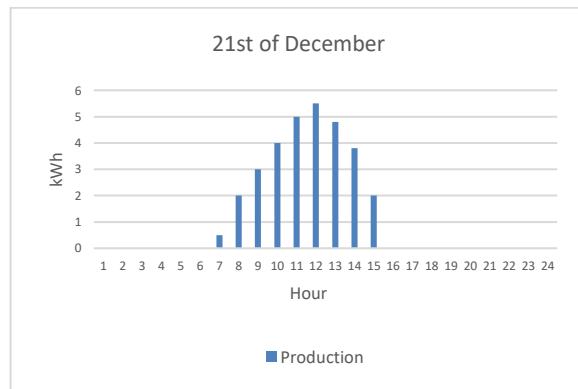
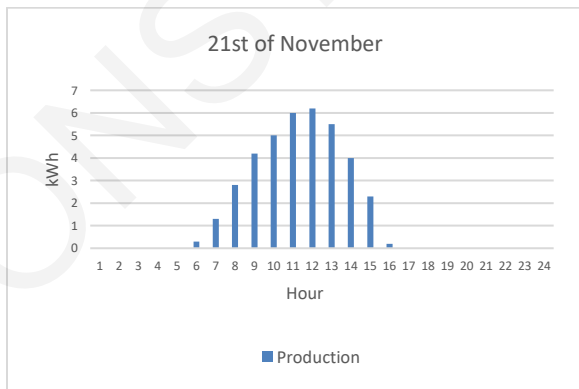
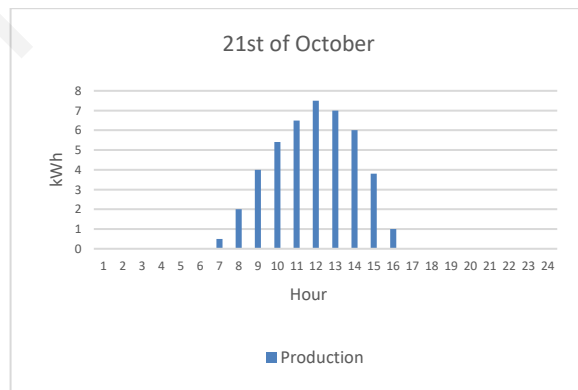
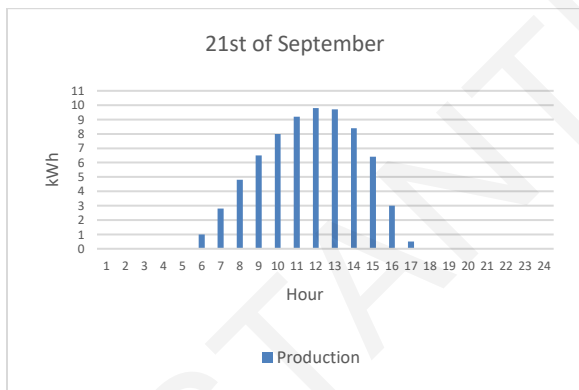
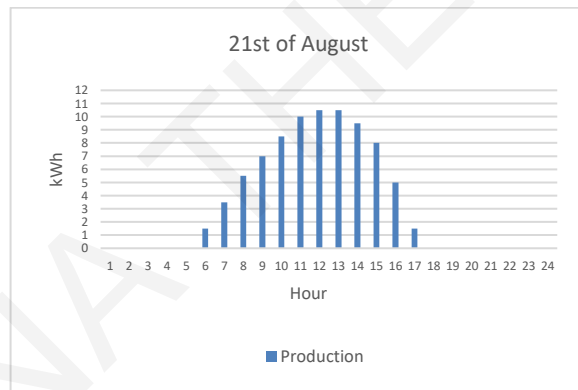
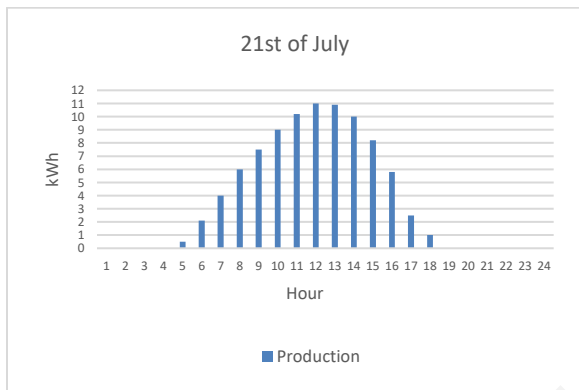
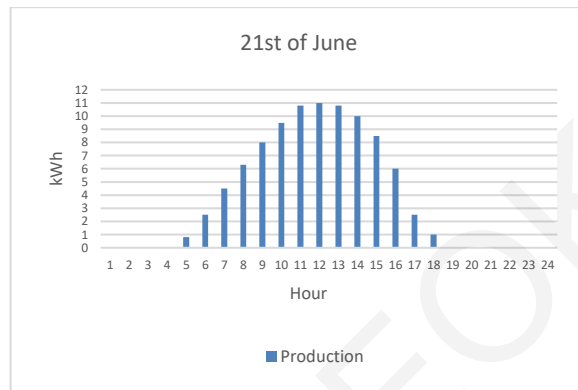
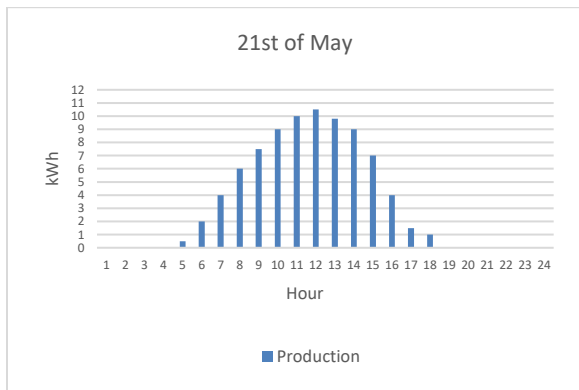
Target Position C

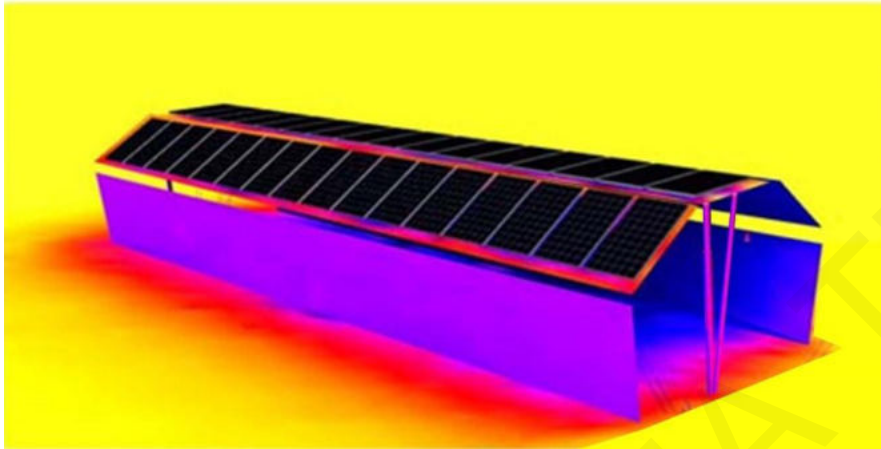


Month	Min Air Temperature	Max Air Temperature	Min Module Temperature	Max Module Temperature
January	9	15.5	4	10.5
February	8	16	3	11.5
March	9.8	16.5	4	13
April	12	22.5	5	16
May	17	24.5	6	18.5
June	20	28	8	20
July	23	32	9	21.5
August	23.5	33	9	22
September	20.5	29.5	8.5	20
October	17	25.5	7	16.5
November	14	22	5.5	13.5
December	10	18	4	11.5

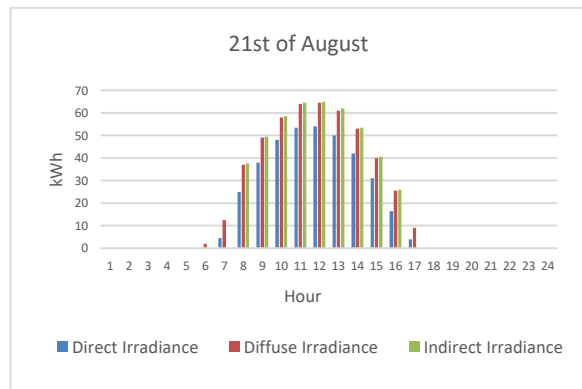
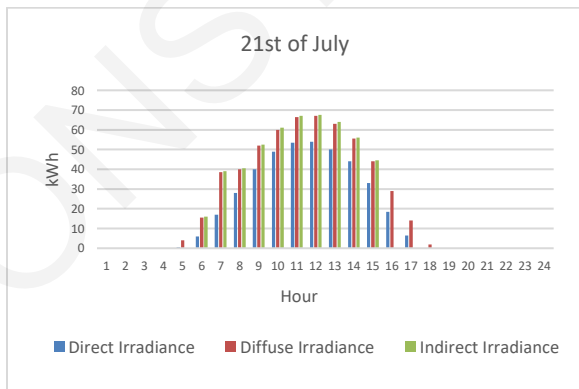
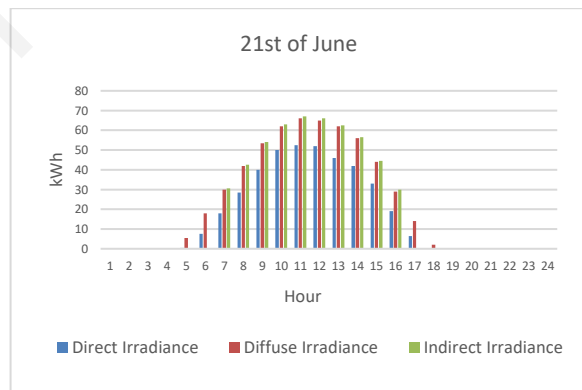
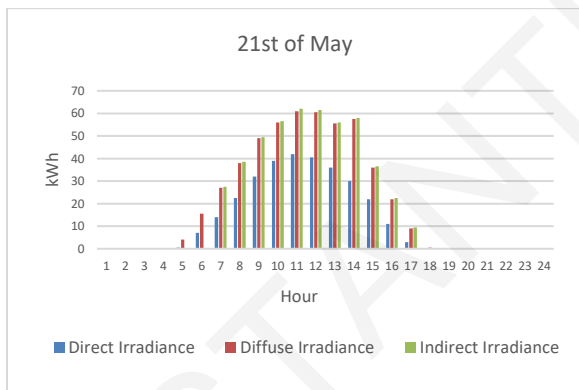
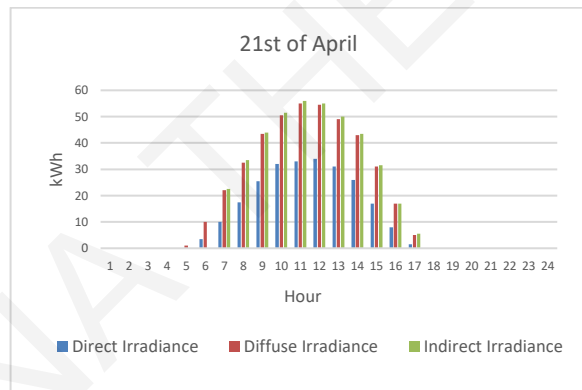
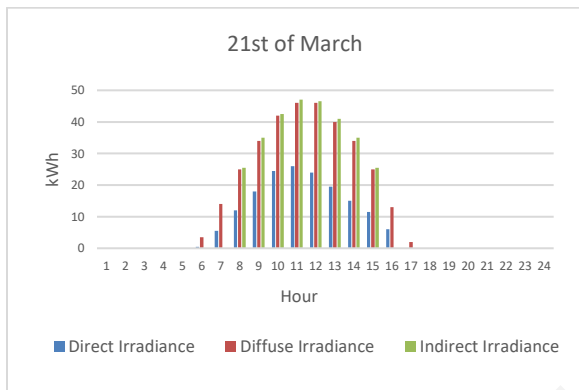
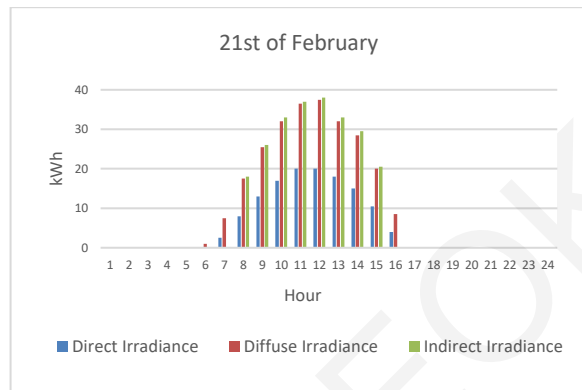
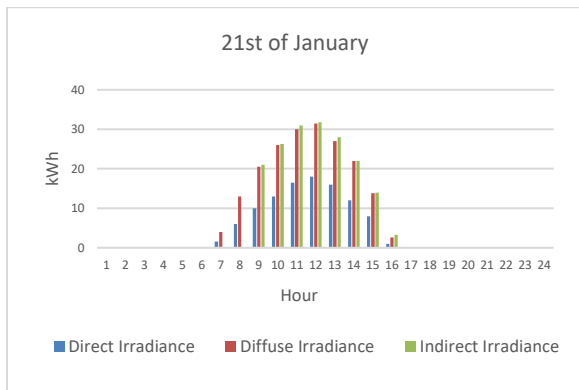


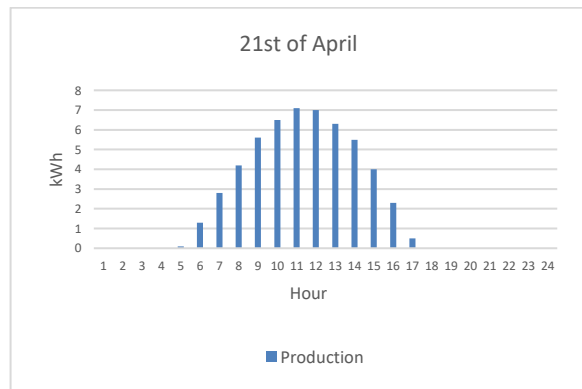
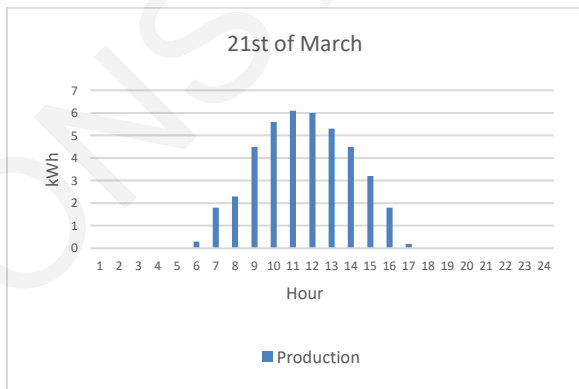
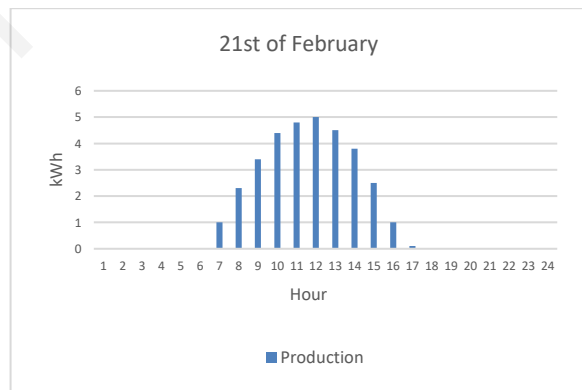
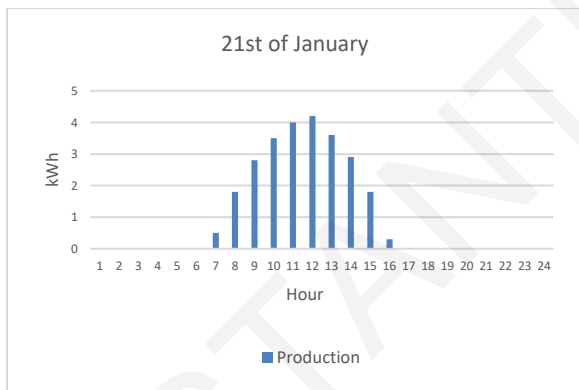
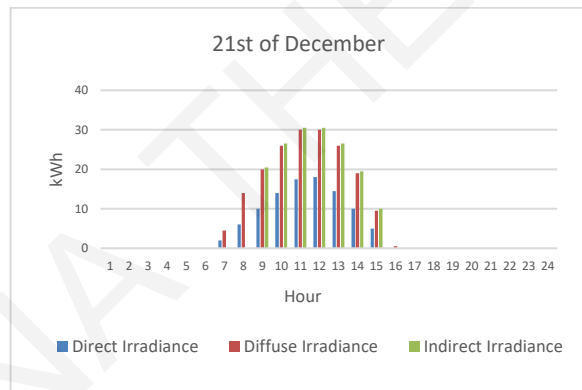
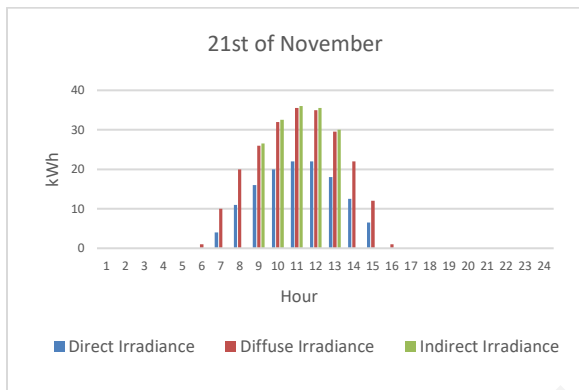
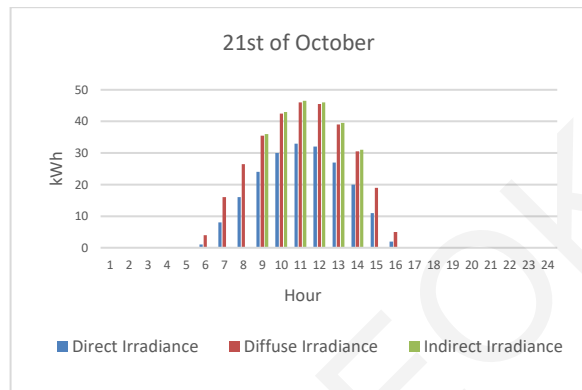
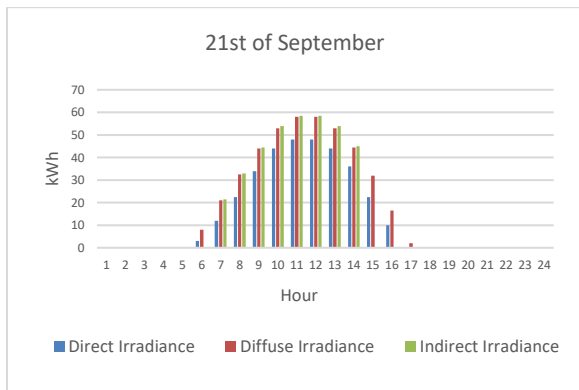


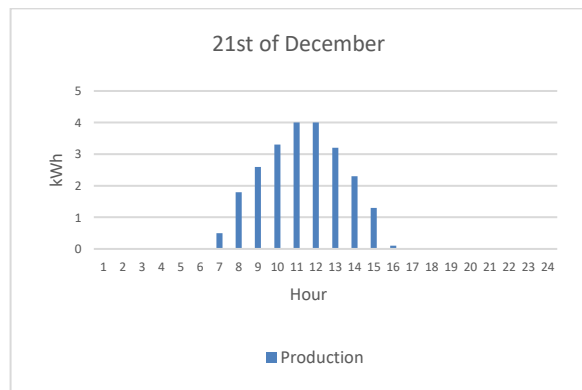
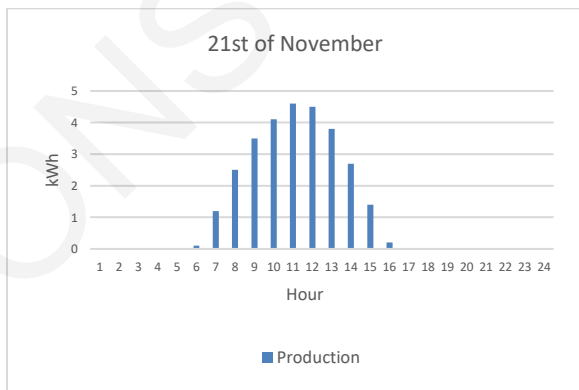
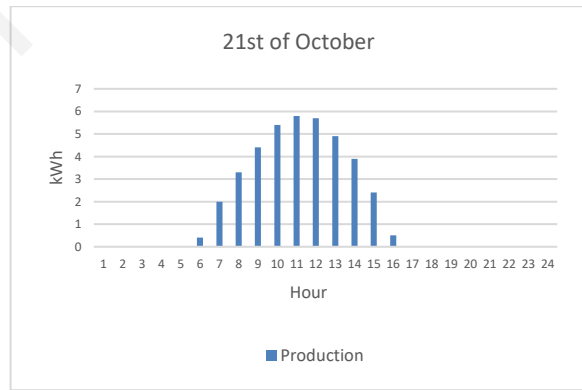
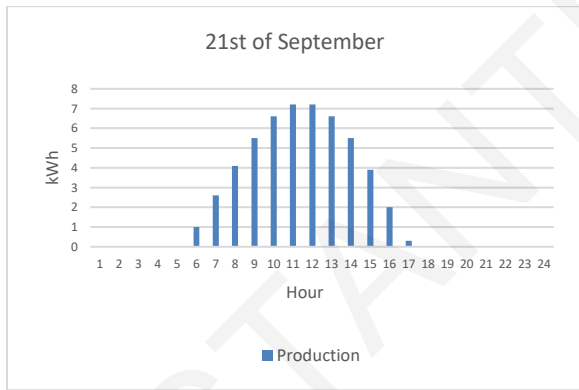
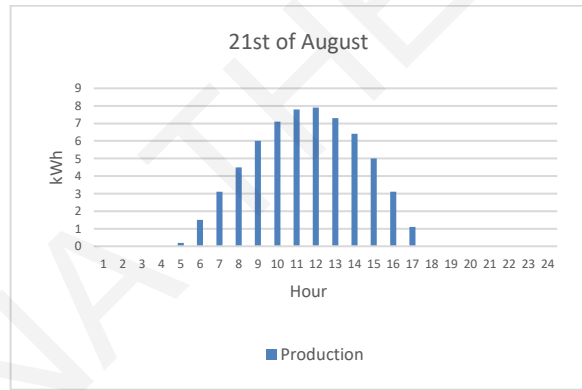
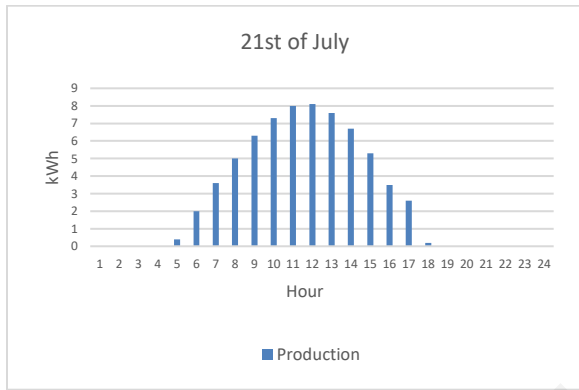
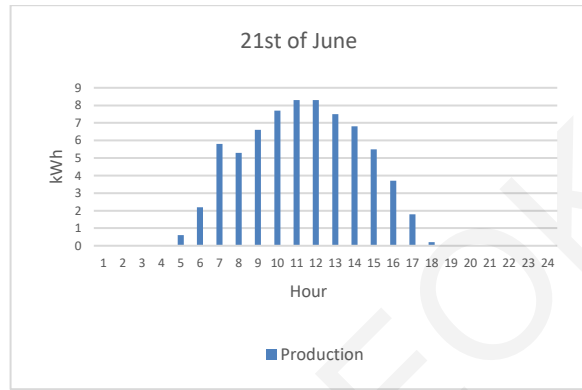
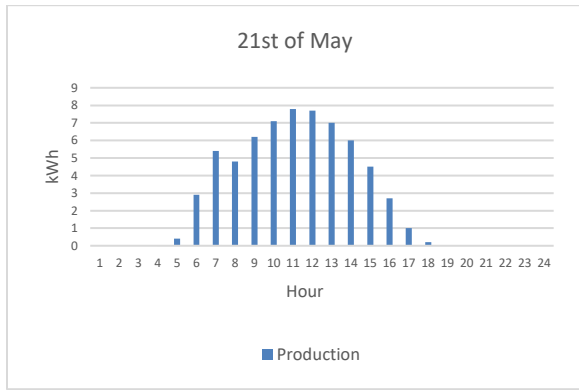


B. Site Location: Larnaca, Cyprus, Site Orientation 90°Initial Position

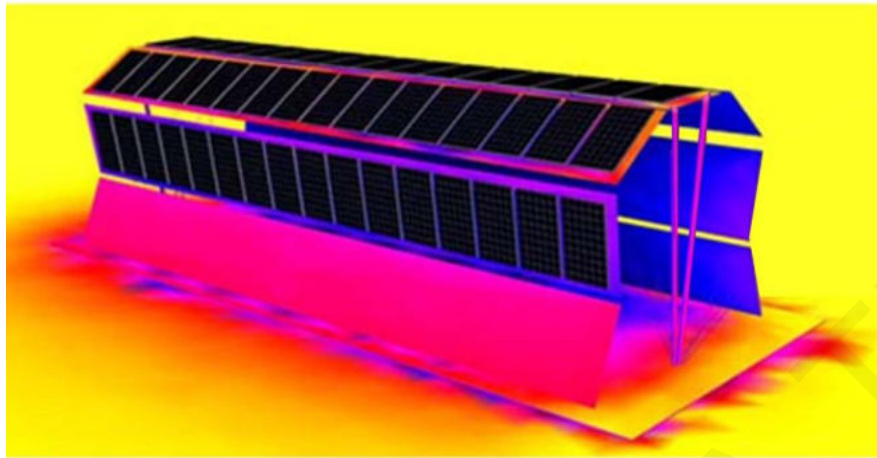
Month	Min Air Temperature	Max Air Temperature	Min Module Temperature	Max Module Temperature
January	9	15.5	4	10.5
February	8	16	3	11.5
March	9.8	16.5	4	13
April	12	22.5	5	16
May	17	24.5	6	18.5
June	20	28	8	20
July	23	32	9	21.5
August	23.5	33	9	22
September	20.5	29.5	8.5	20
October	17	25.5	7	16.5
November	14	22	5.5	13.5
December	10	18	4	11.5



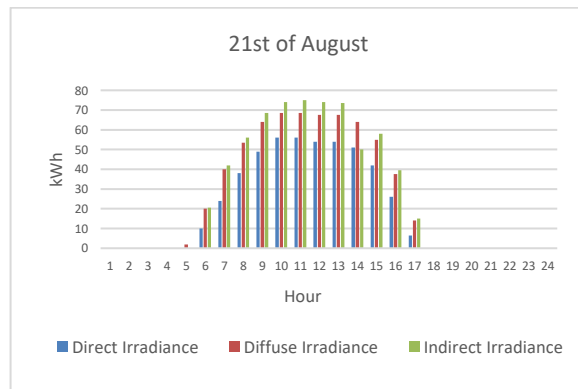
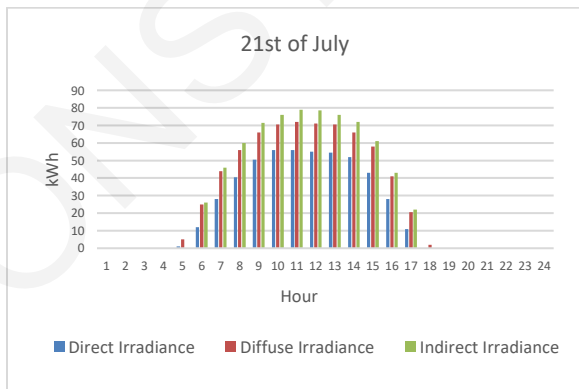
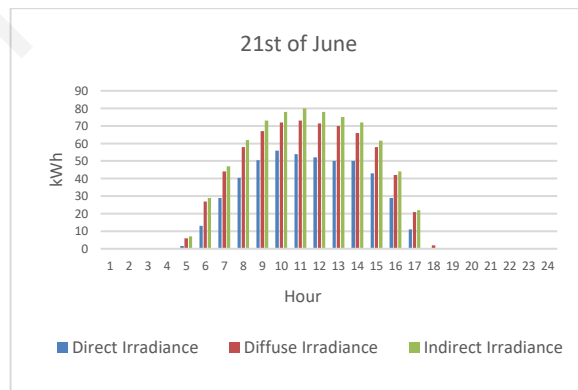
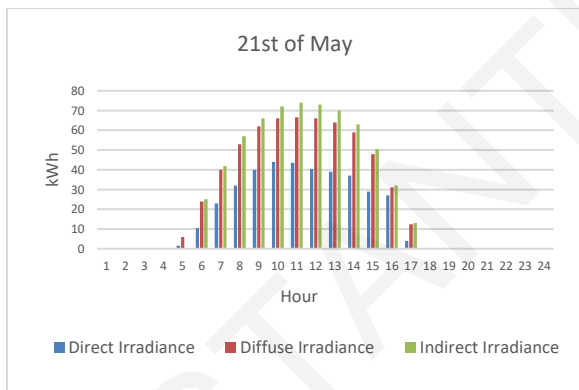
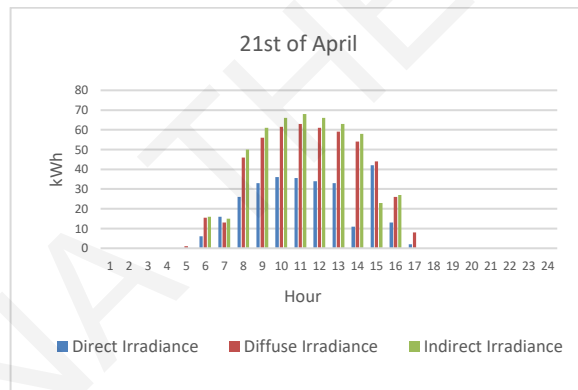
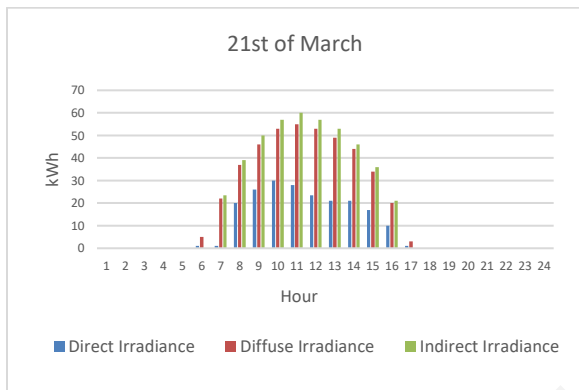
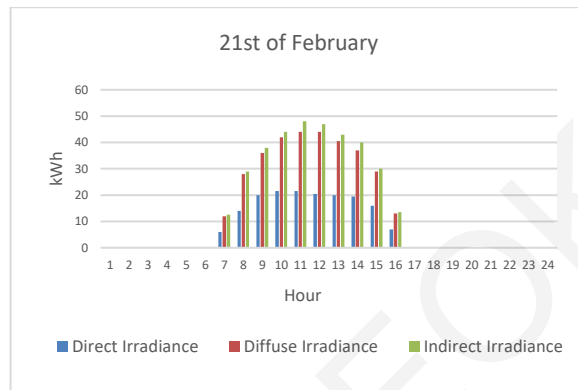
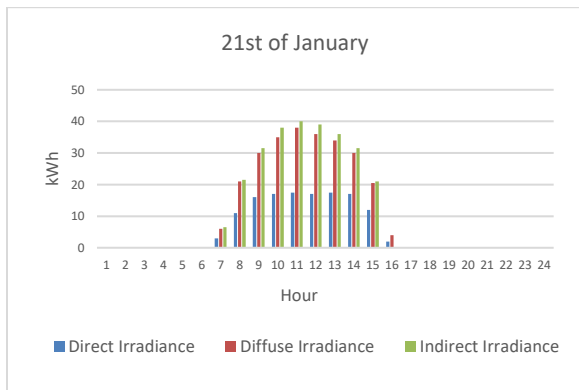


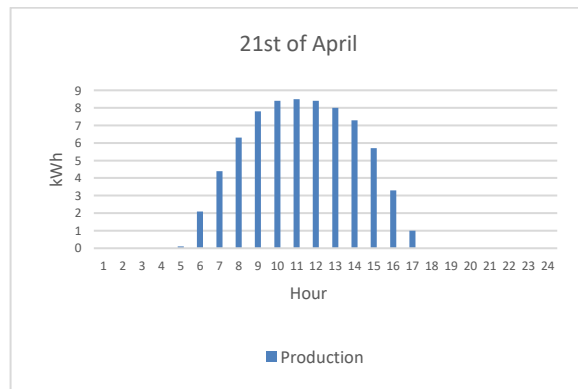
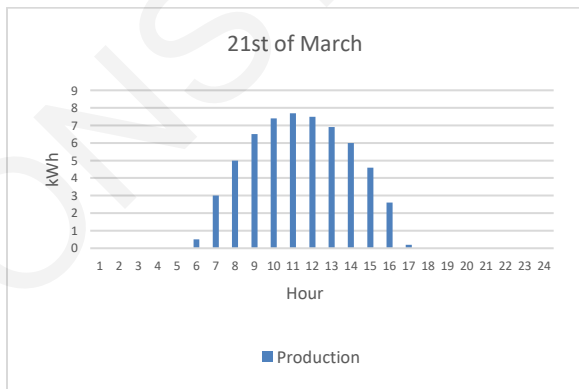
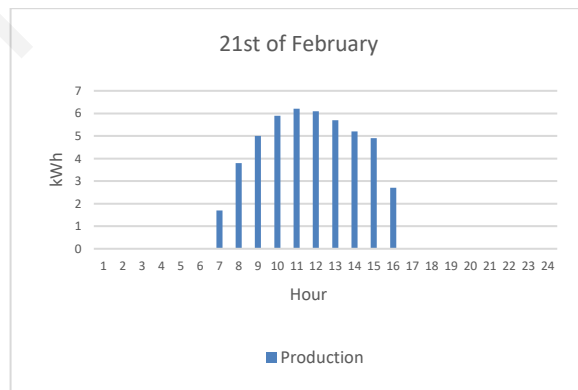
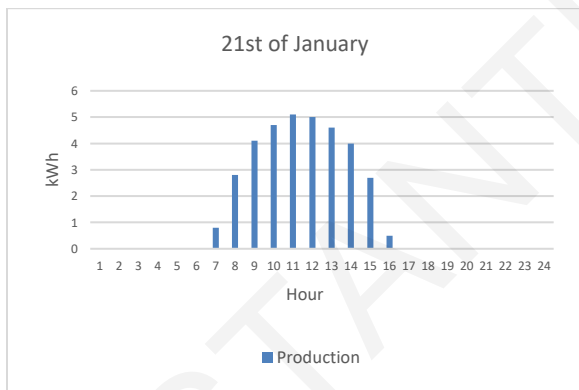
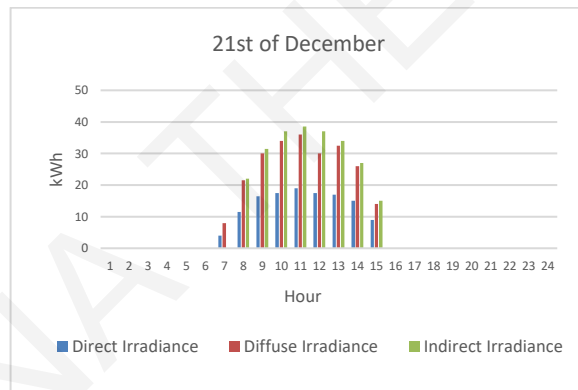
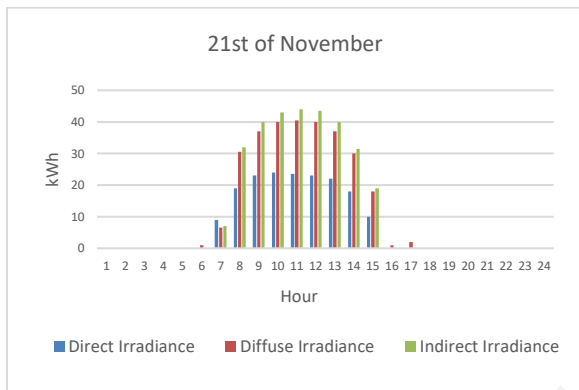
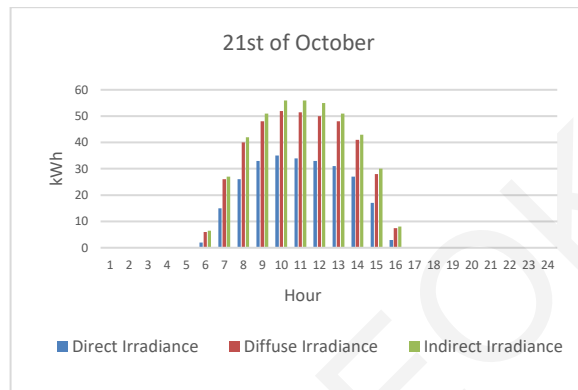
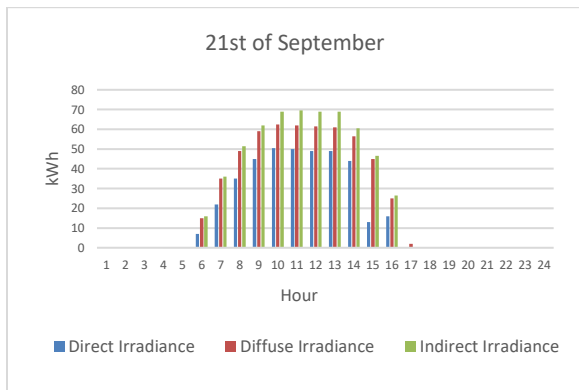


Target Position A

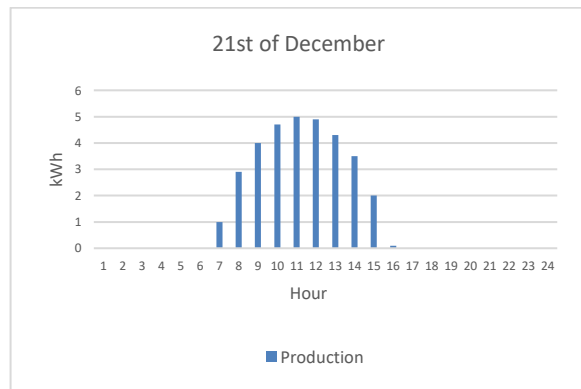
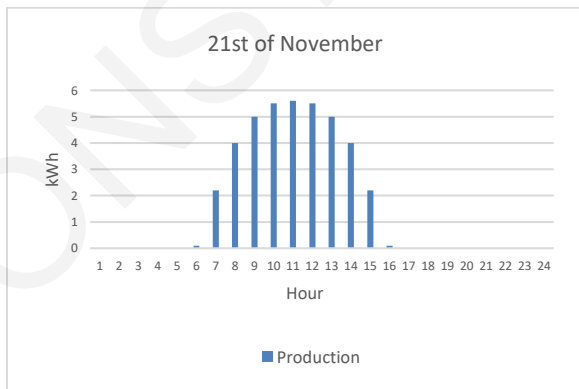
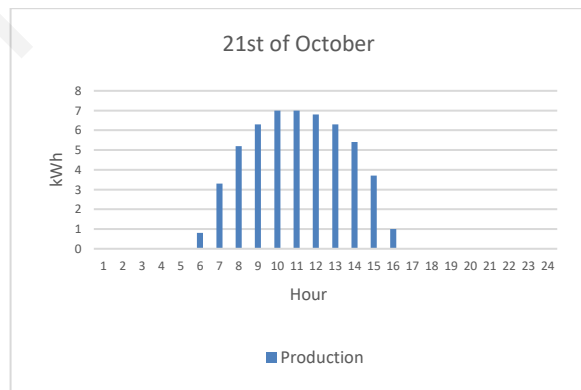
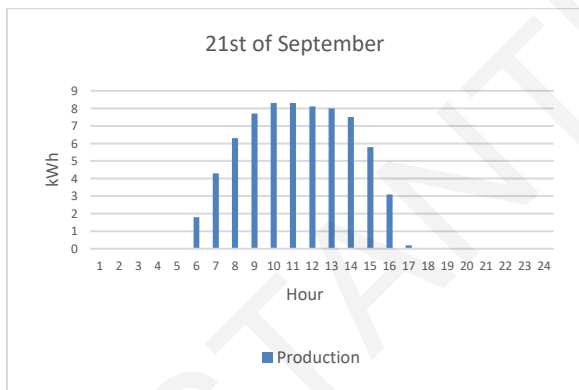
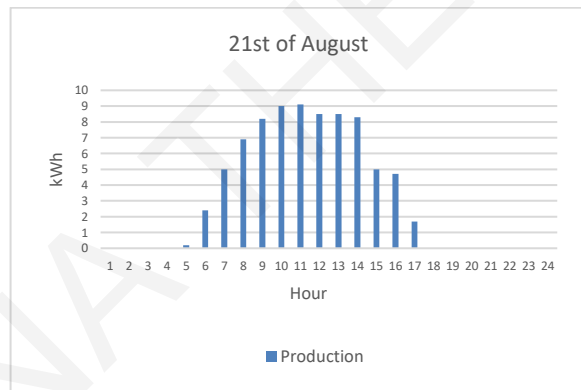
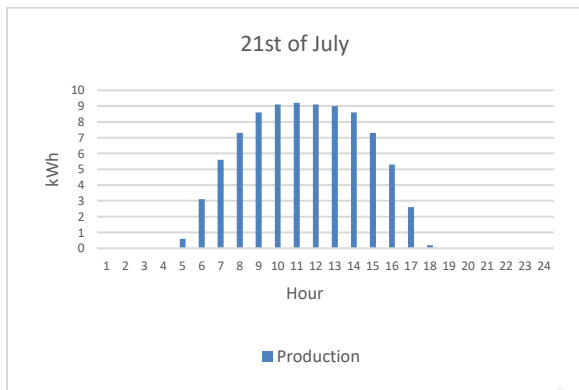
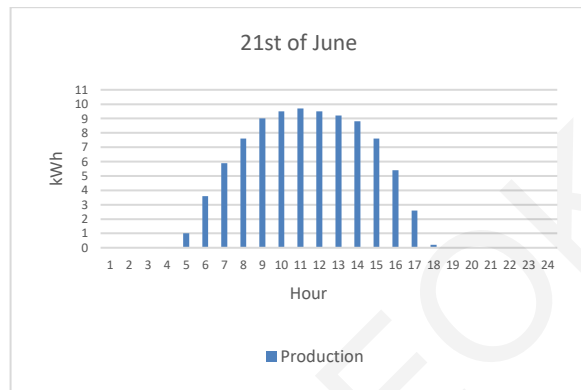
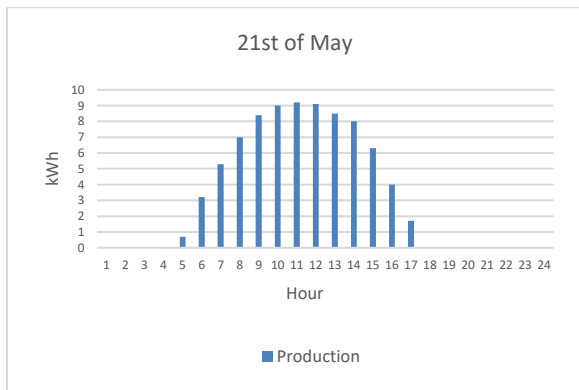


Month	Min Air Temperature	Max Air Temperature	Min Module Temperature	Max Module Temperature
January	10	15.5	3	8
February	8	16	3	8.5
March	10	16.5	3.5	9
April	12	21.5	4	12
May	17	24.5	5	13
June	20	28	6.5	14.5
July	23	32	8	15.5
August	23	32	8	15.5
September	20.5	29.5	7	14
October	17	26	6	12.5
November	14	22	5	10
December	10.5	18	3.5	8

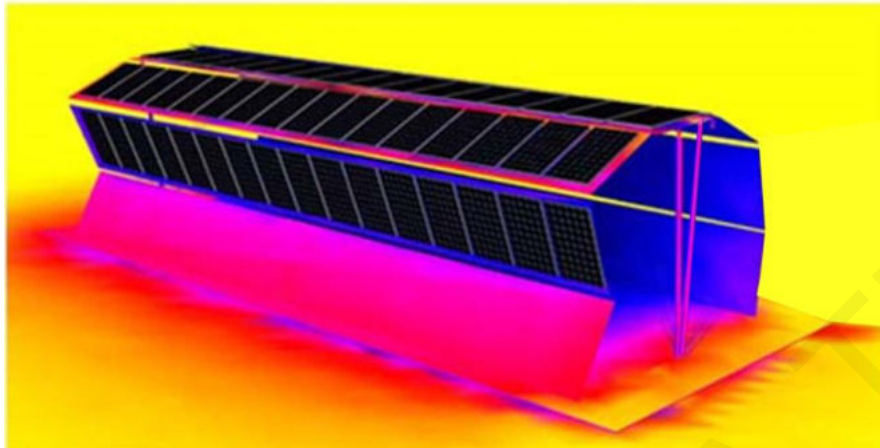
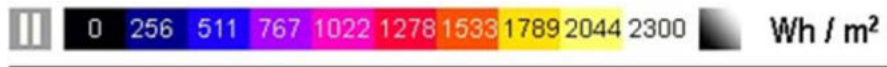




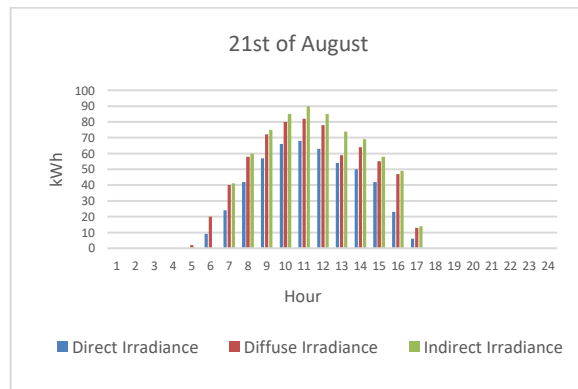
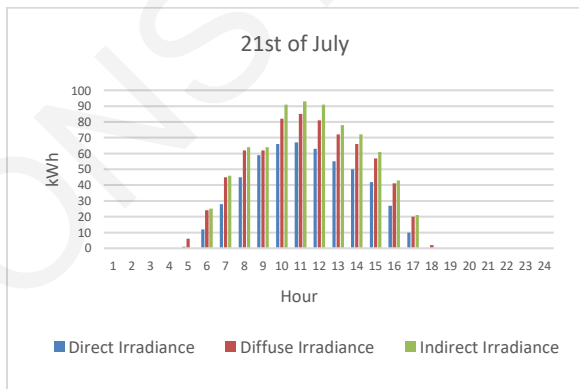
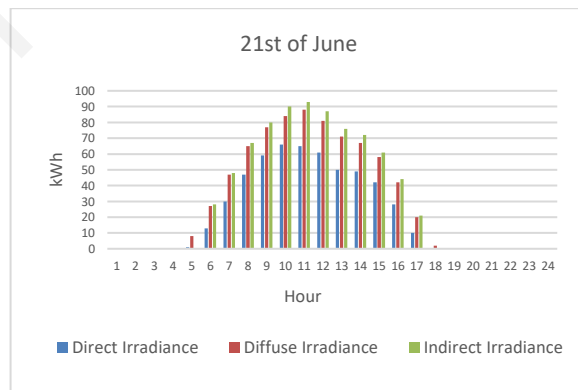
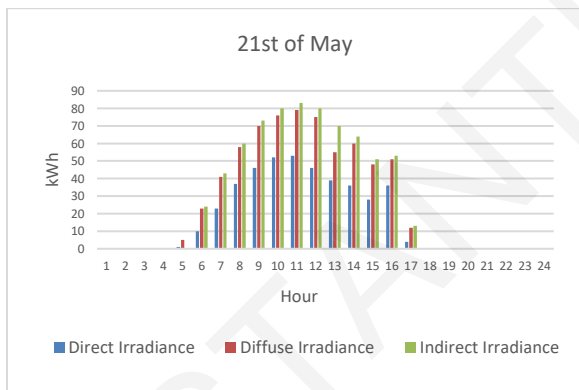
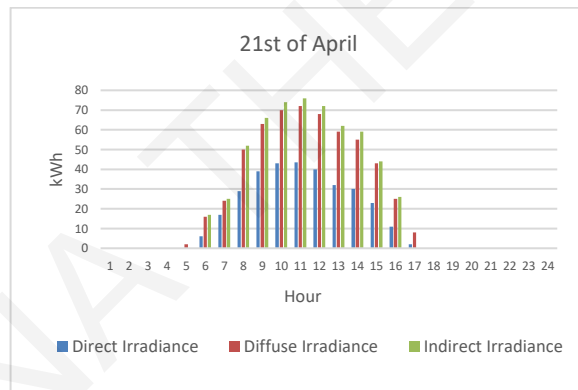
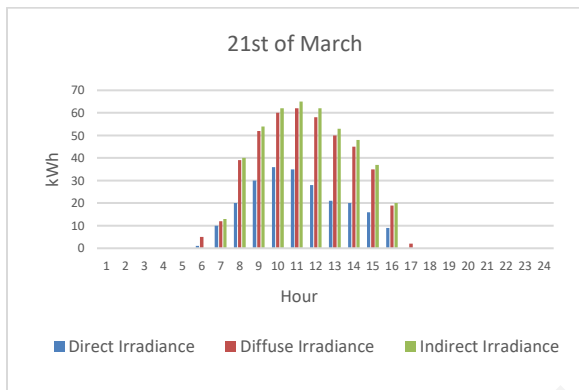
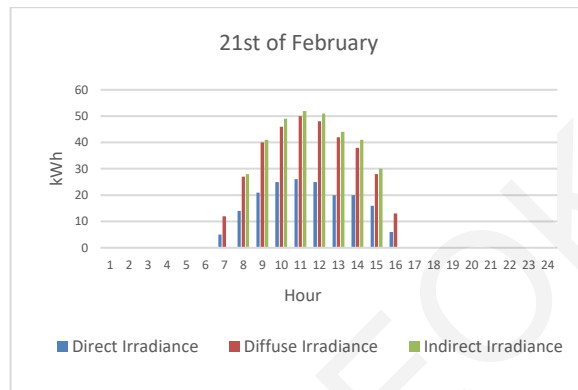
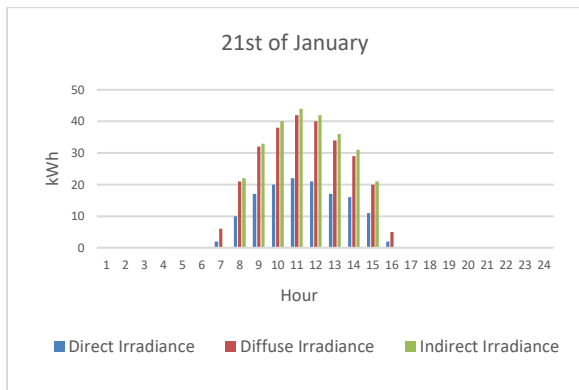
APPENDIX

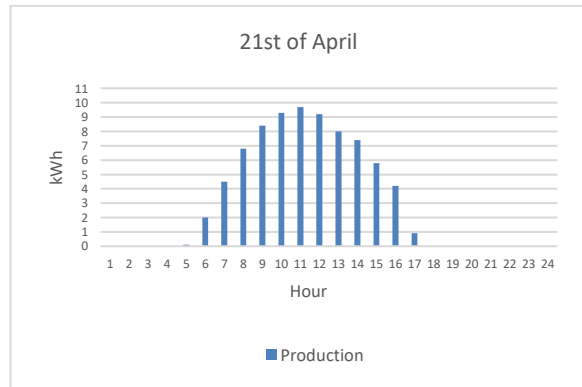
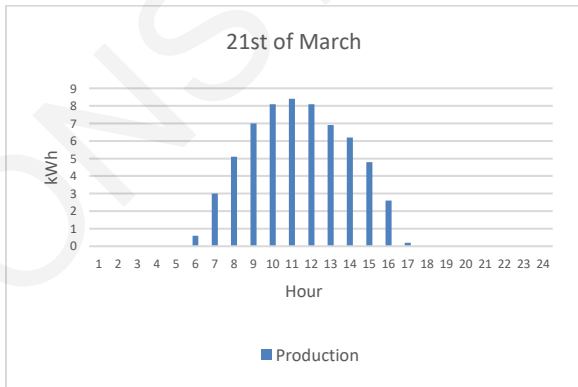
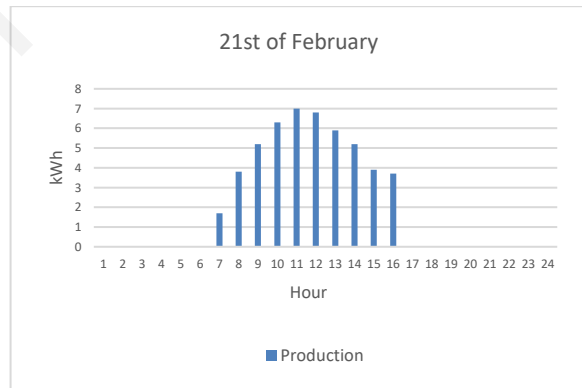
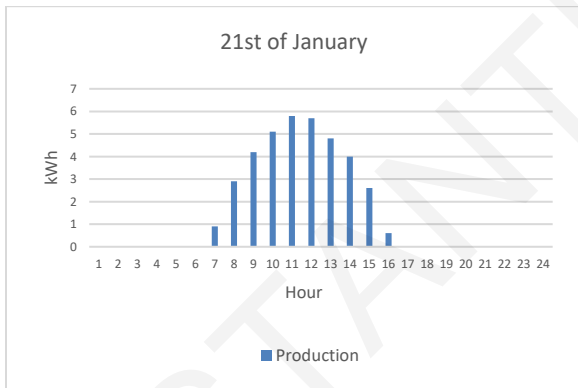
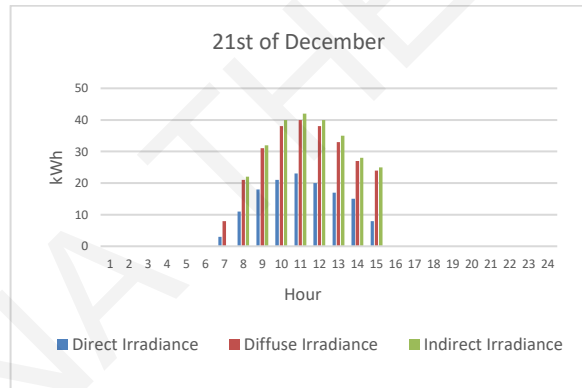
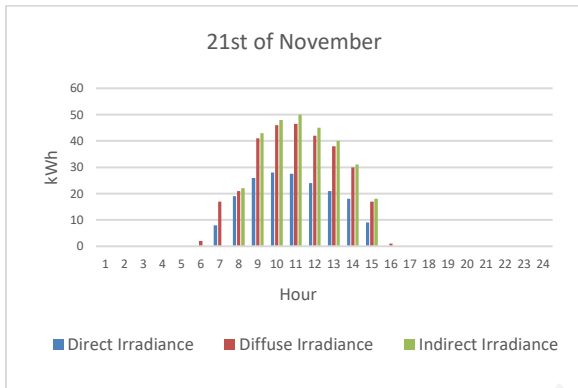
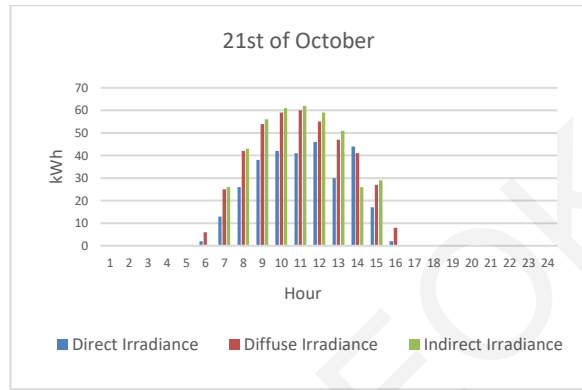
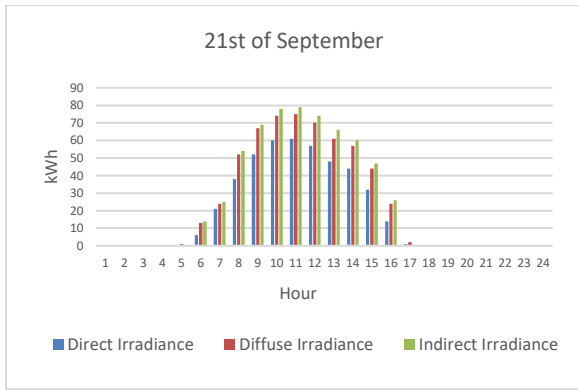


Target Position B

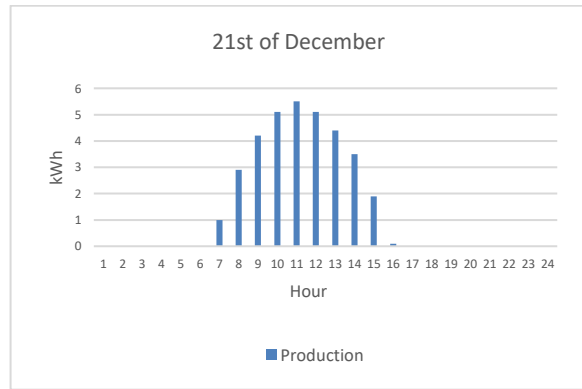
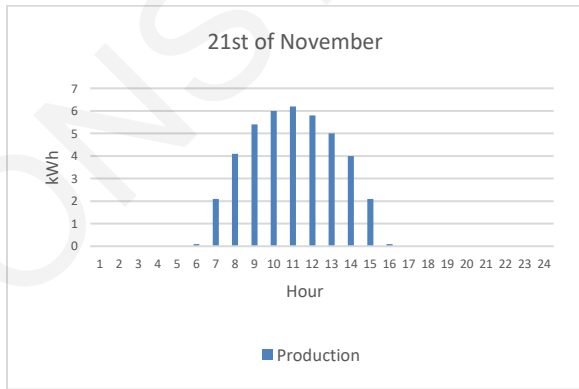
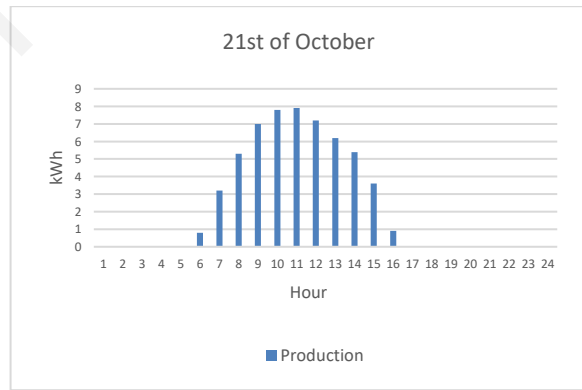
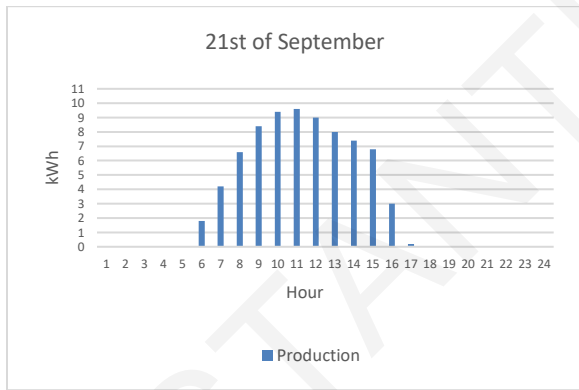
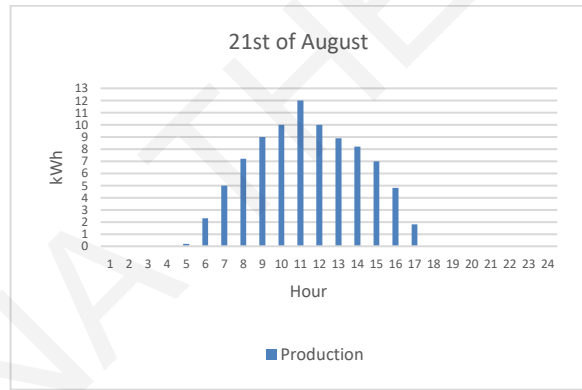
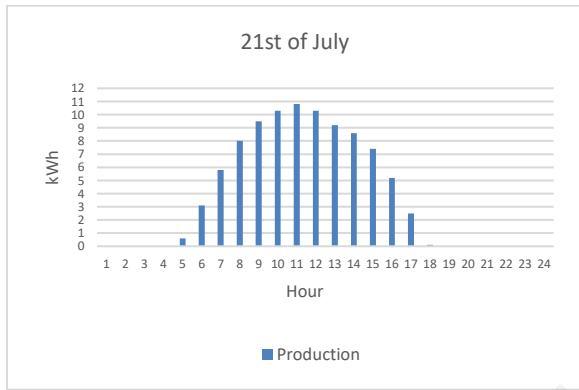
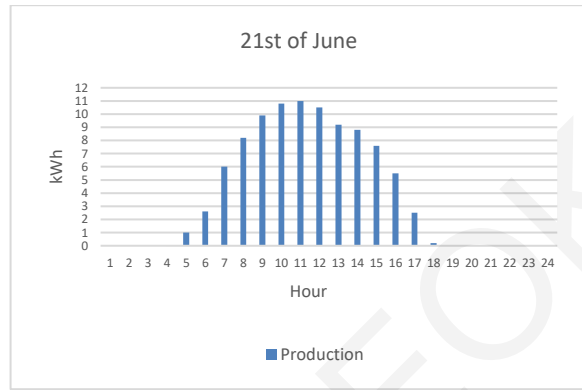
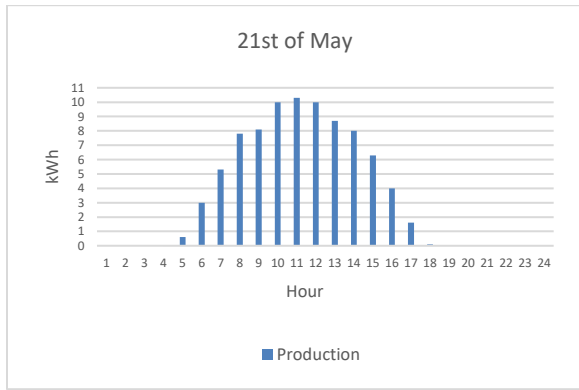


Month	Min Air Temperature	Max Air Temperature	Min Module Temperature	Max Module Temperature
January	10	15.5	3	8
February	8	16	3	8.5
March	10	16.5	3.5	9
April	12	21.5	4	12
May	17	24.5	5	13
June	20	28	6.5	14.5
July	23	32	8	15.5
August	23	32	8	15.5
September	20.5	29.5	7	14
October	17	26	6	12.5
November	14	22	5	10
December	10.5	18	3.5	8

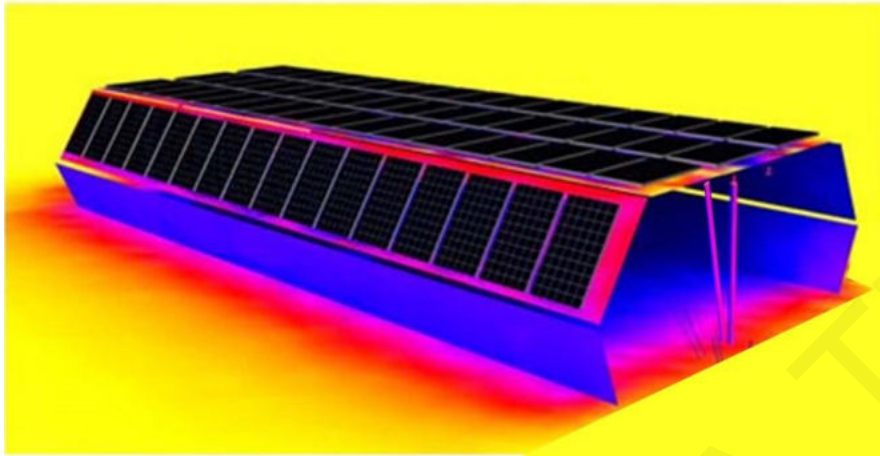




APPENDIX

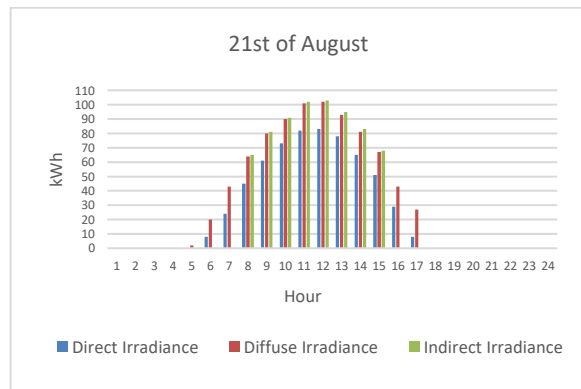
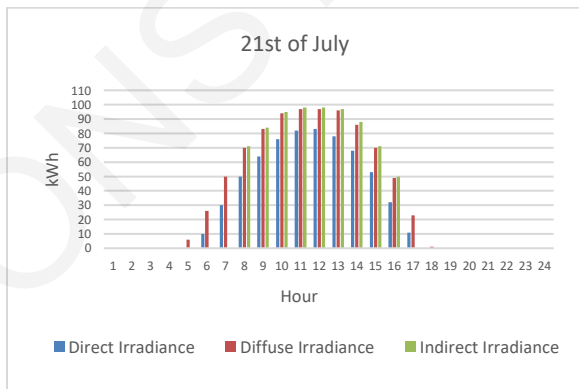
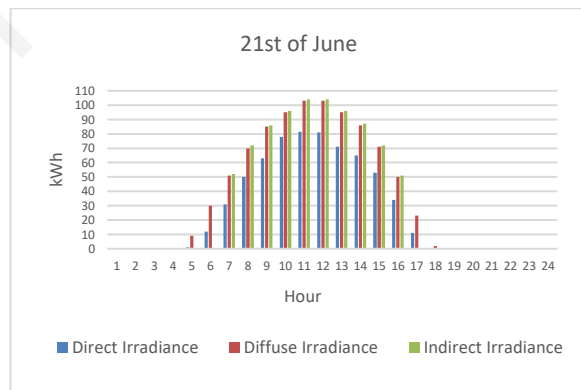
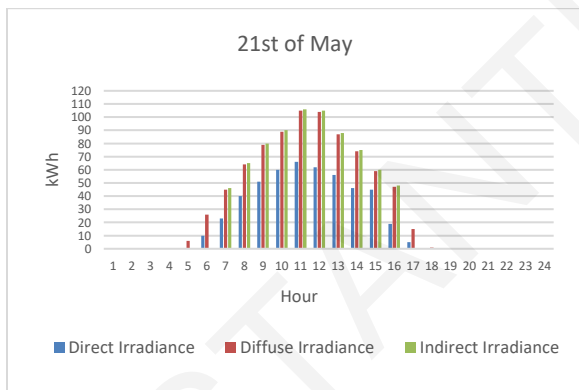
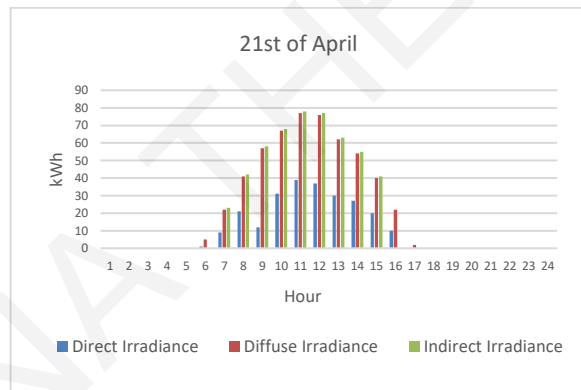
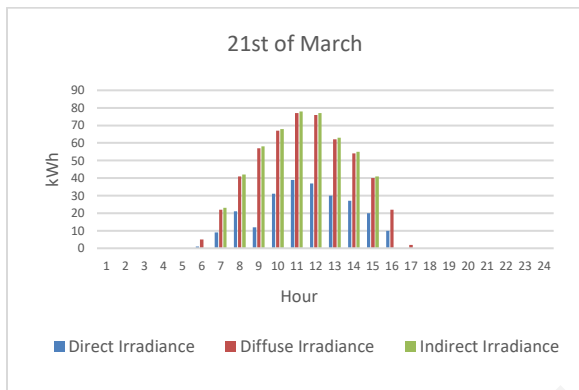
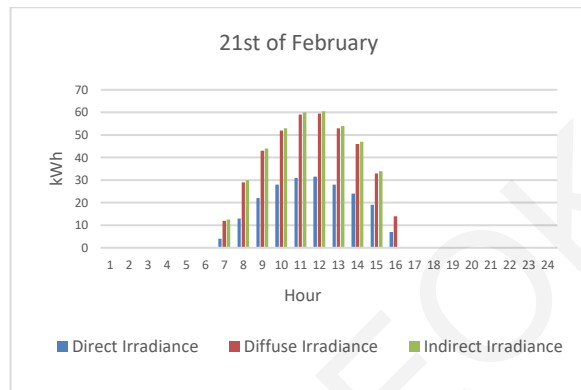
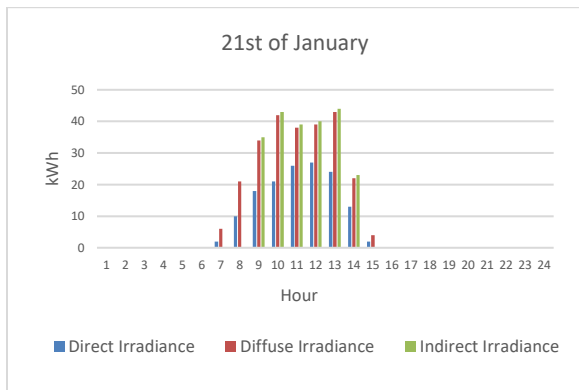


Target Position C

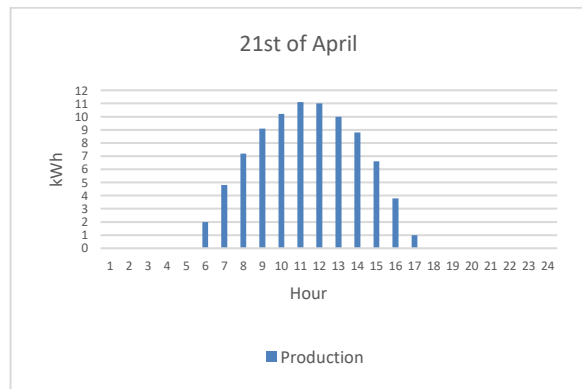
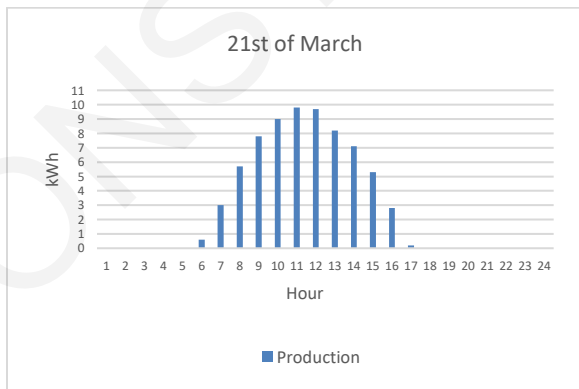
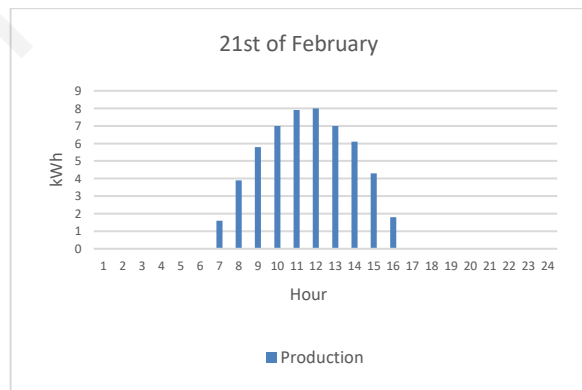
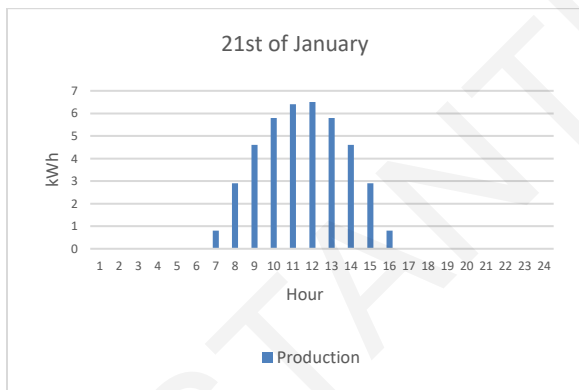
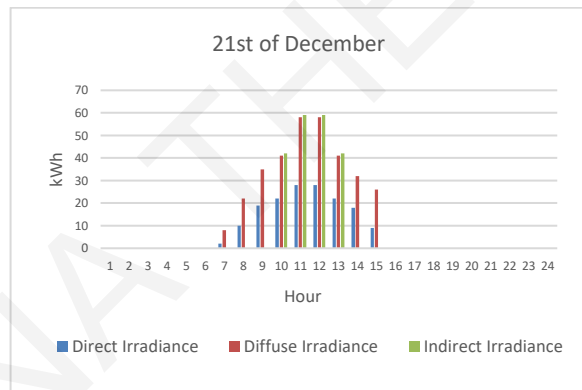
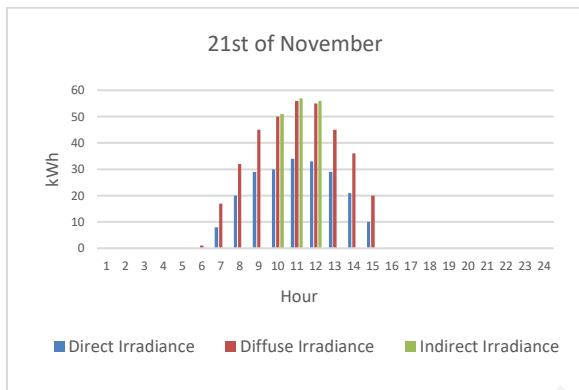
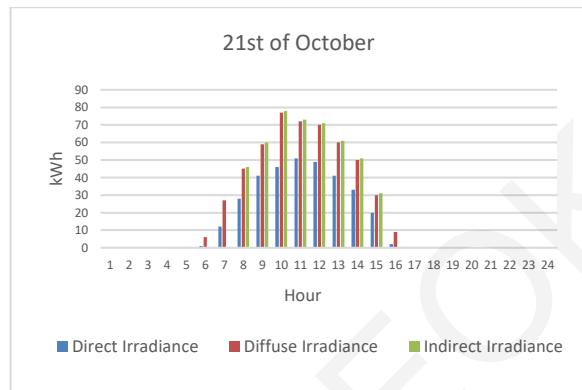
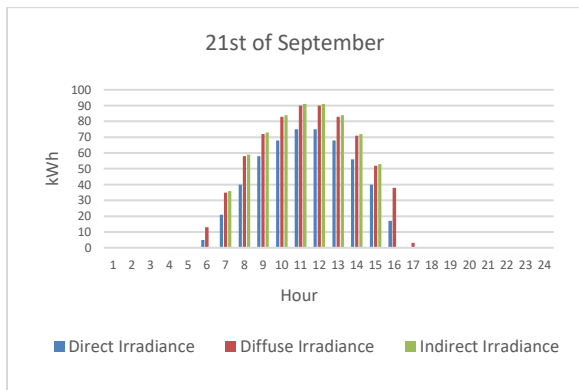


Month	Min Air Temperature	Max Air Temperature	Min Module Temperature	Max Module Temperature
January	10	15.5	3	8
February	8	16	3	8.5
March	10	16.5	3.5	9
April	12	21.5	4	12
May	17	24.5	5	13
June	20	28	6.5	14.5
July	23	32	8	15.5
August	23	32	8	15.5
September	20.5	29.5	7	14
October	17	26	6	12.5
November	14	22	5	10
December	10.5	18	3.5	8

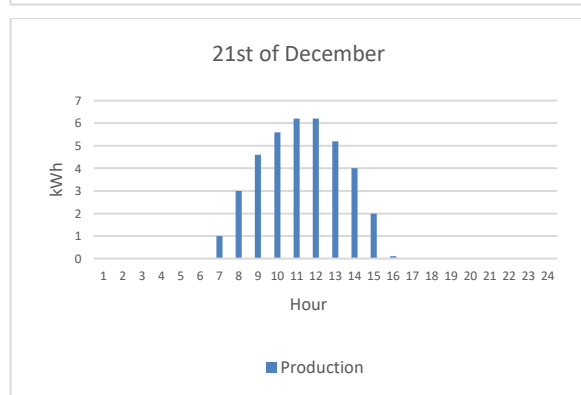
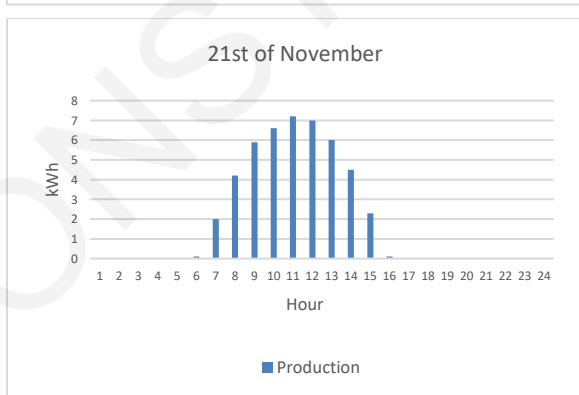
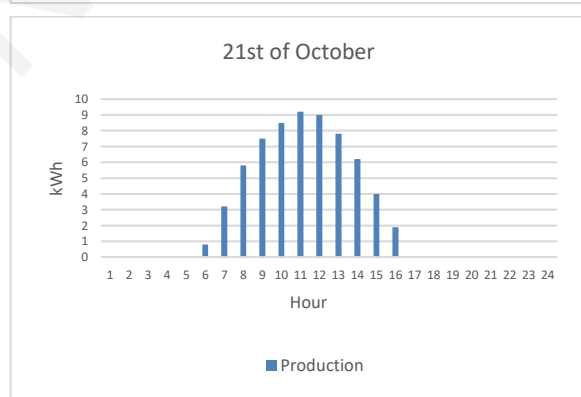
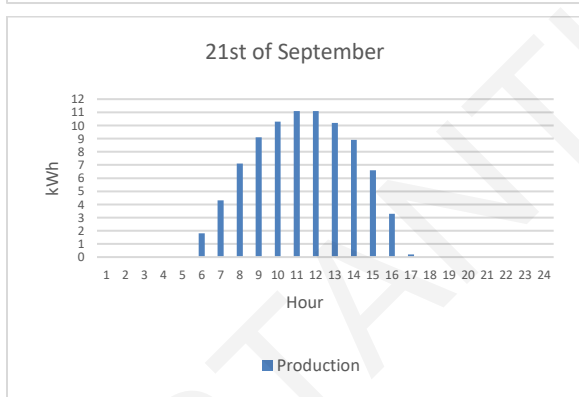
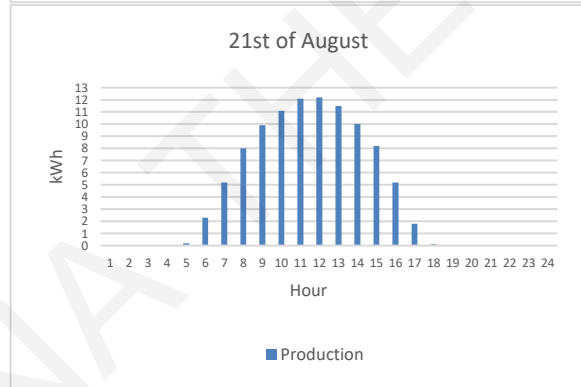
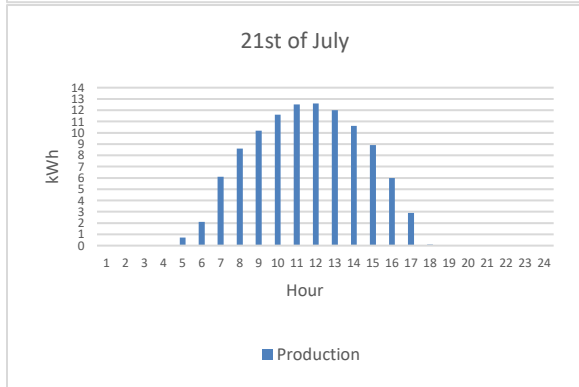
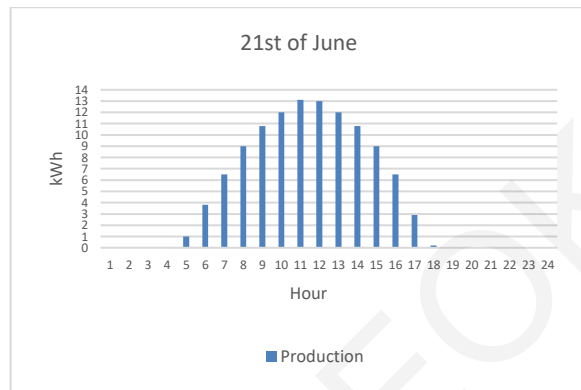
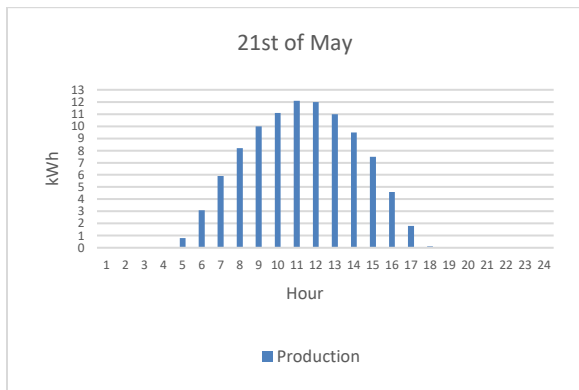
APPENDIX



APPENDIX

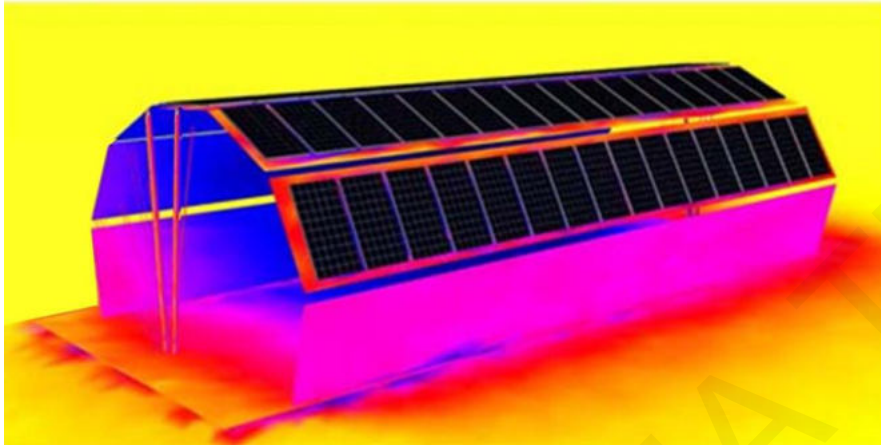


APPENDIX

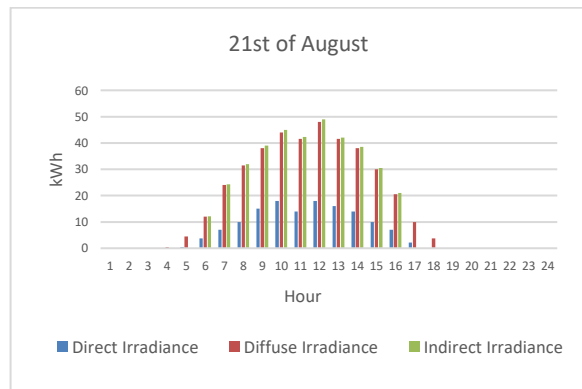
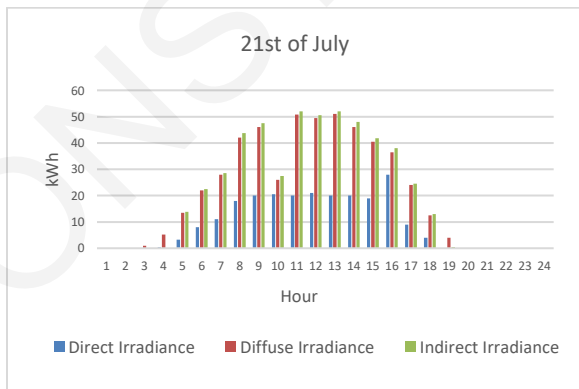
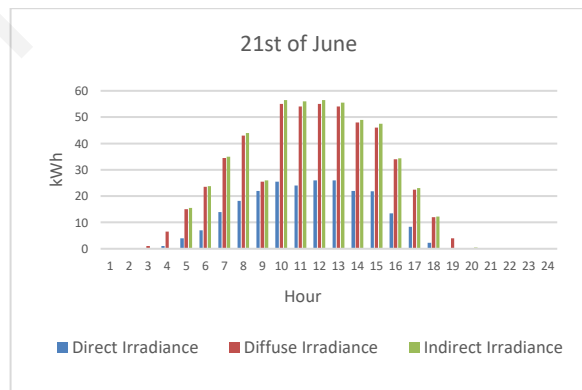
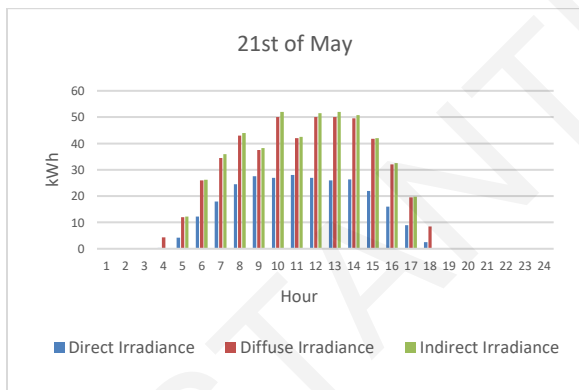
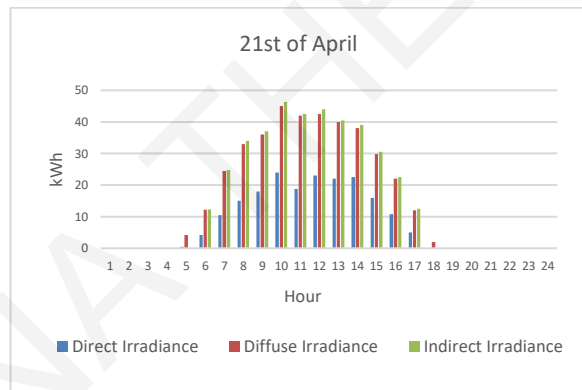
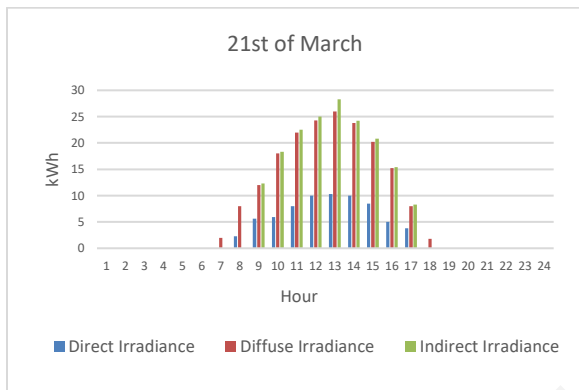
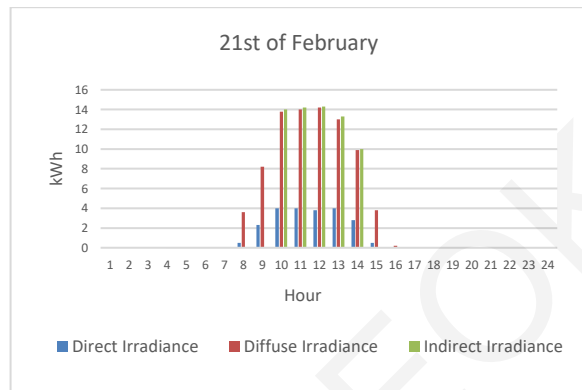
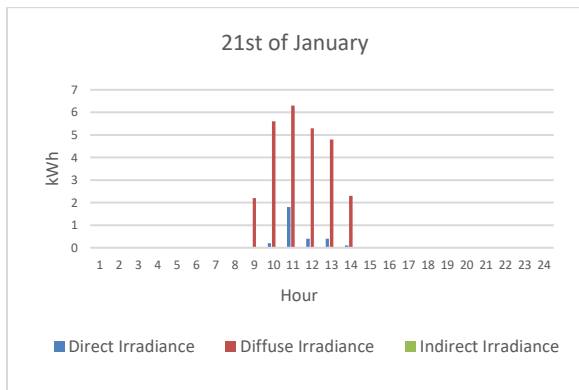


C. Site Location: Stockholm, Sweden, Site Orientation 0°

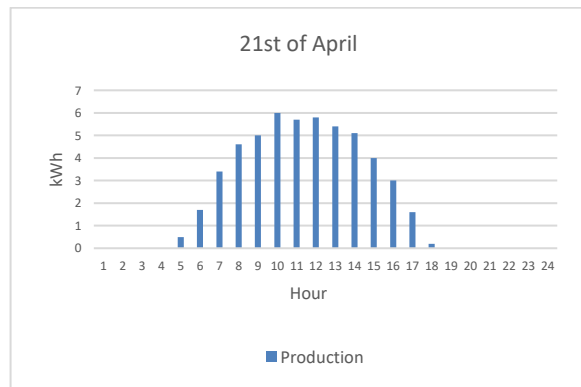
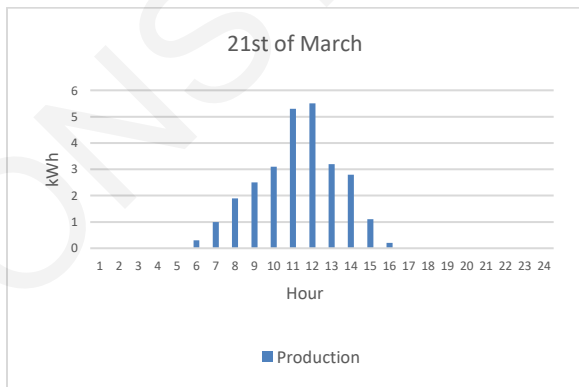
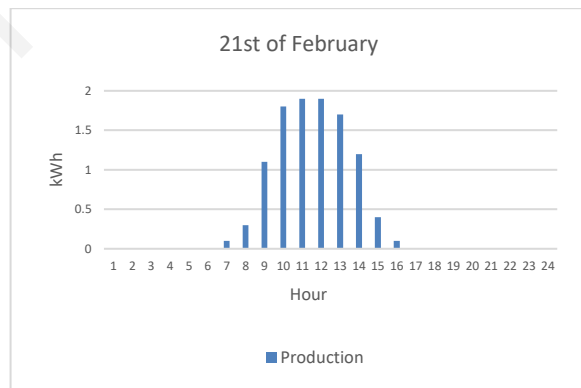
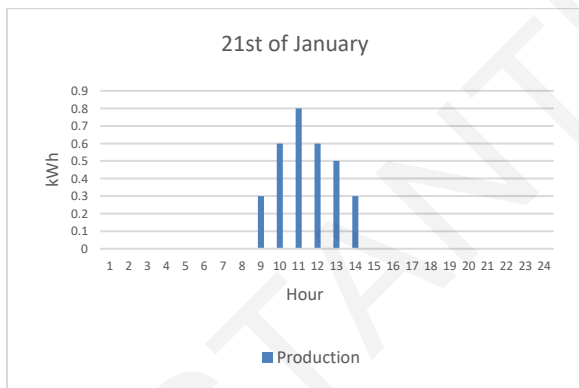
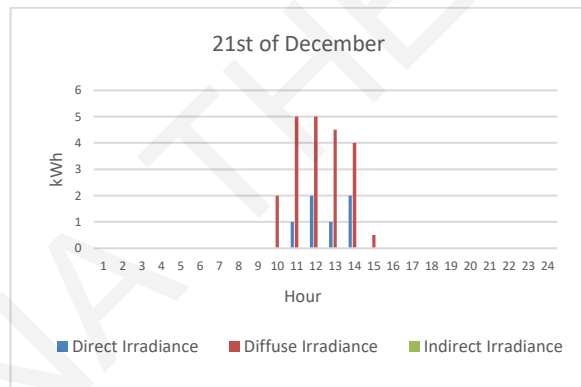
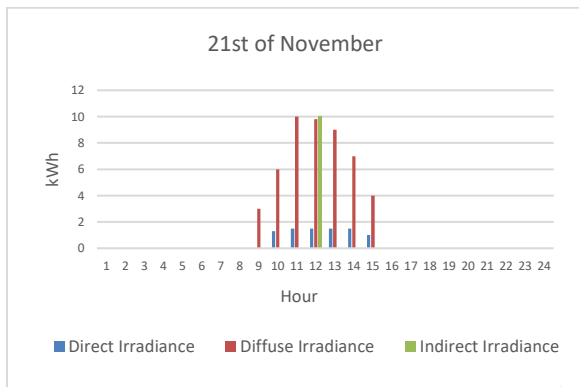
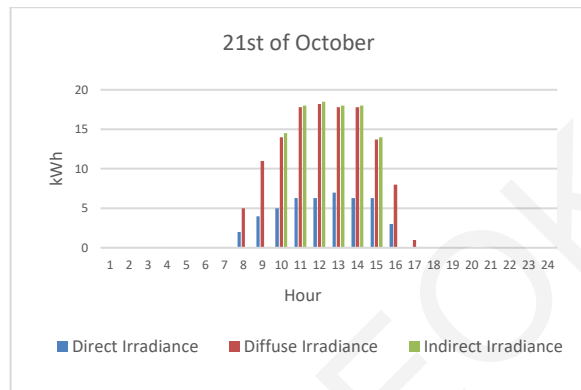
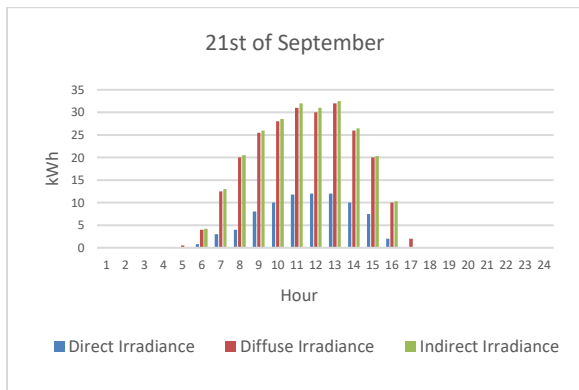
Initial Position



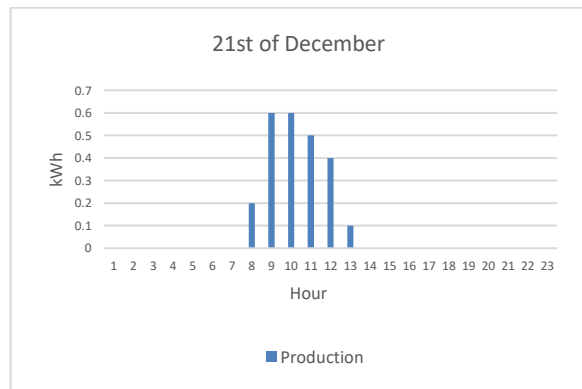
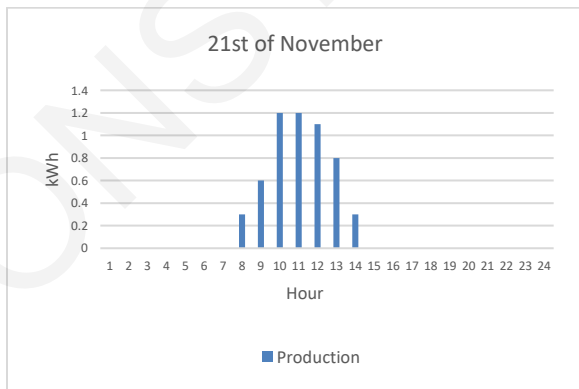
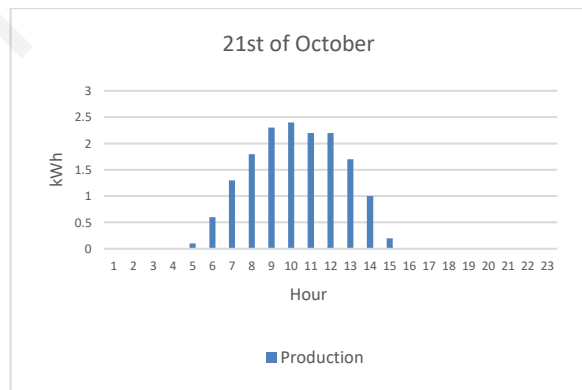
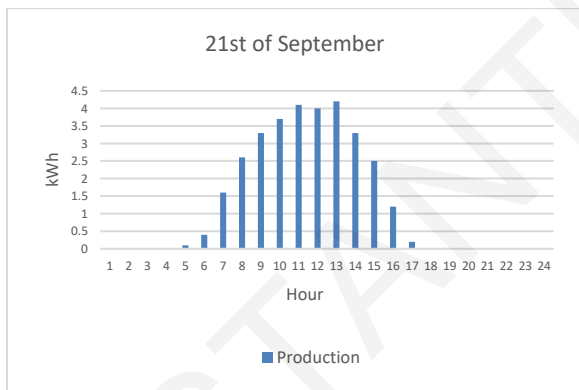
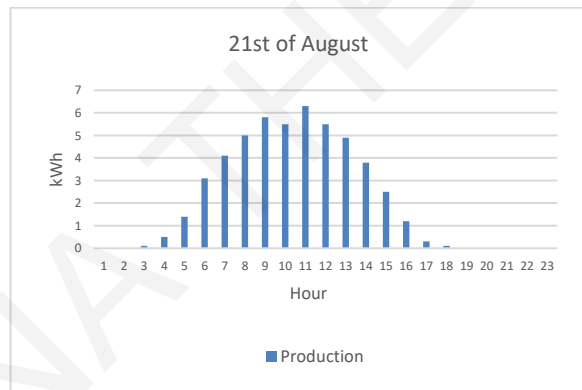
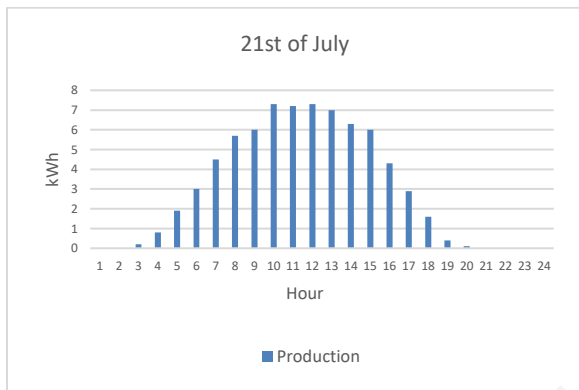
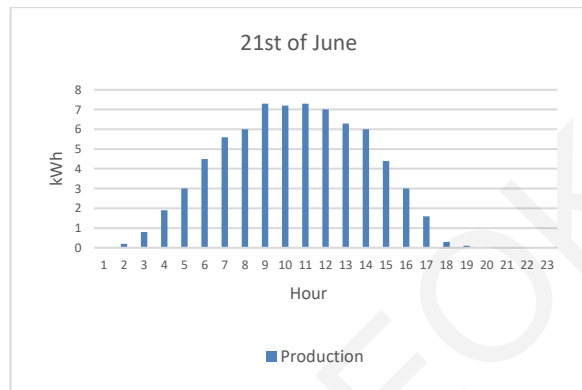
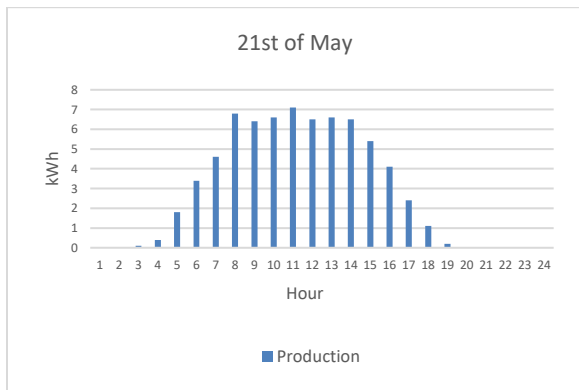
Month	Min Air Temperature	Max Air Temperature	Min Module Temperature	Max Module Temperature
January	-4	-2	-1	0
February	1.5	2	2	1.5
March	-2	2.5	-1	2.5
April	-1	8	0	6
May	6	5	1	8
June	10	18	4	10
July	14	20	4	10
August	2.5	19	4	9
September	9	14	2.5	6.5
October	4	8	2	4
November	1	3	0	3
December	-2	-0.5	-0.5	0



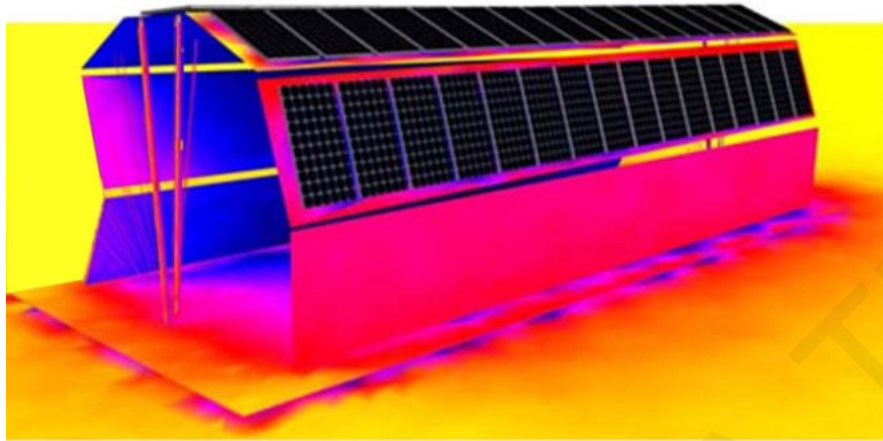
APPENDIX



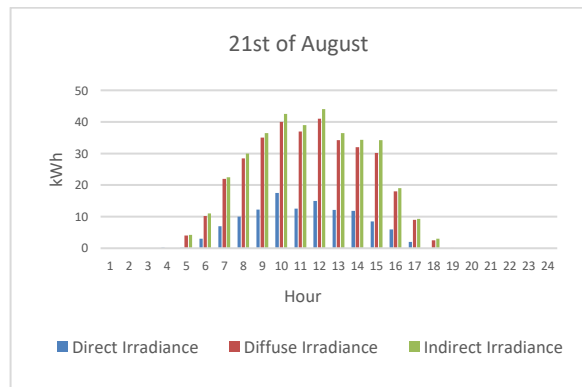
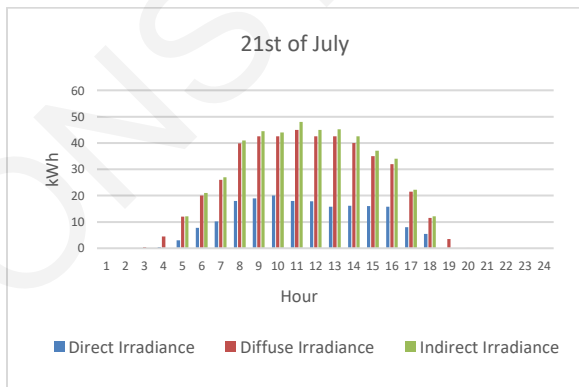
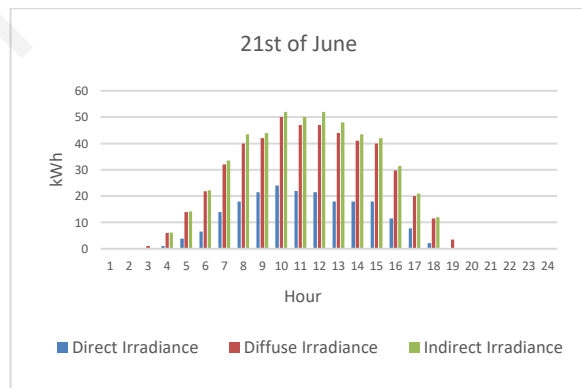
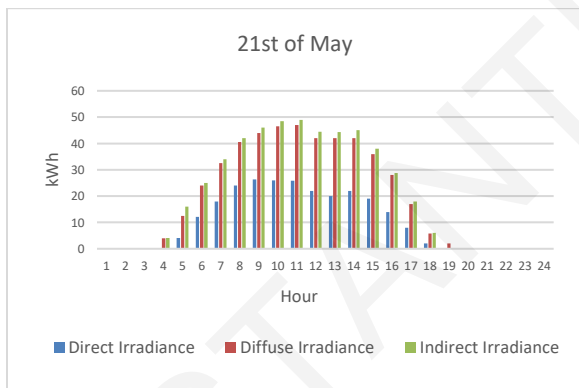
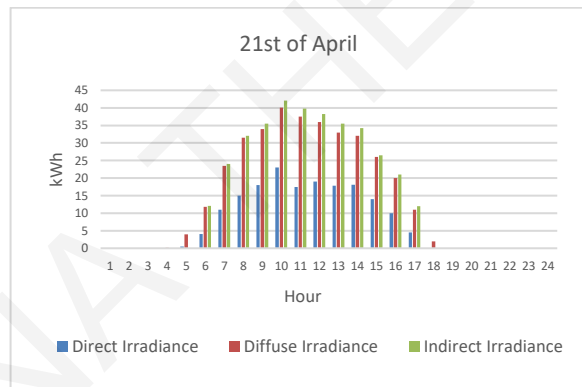
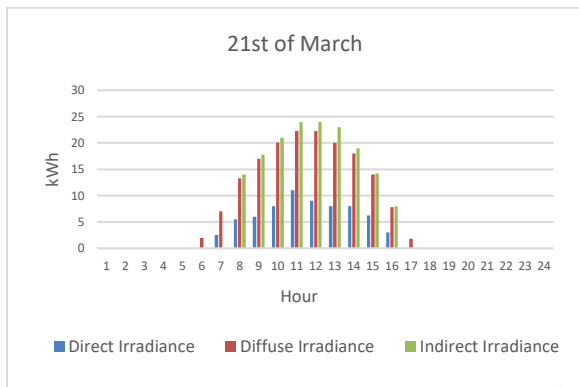
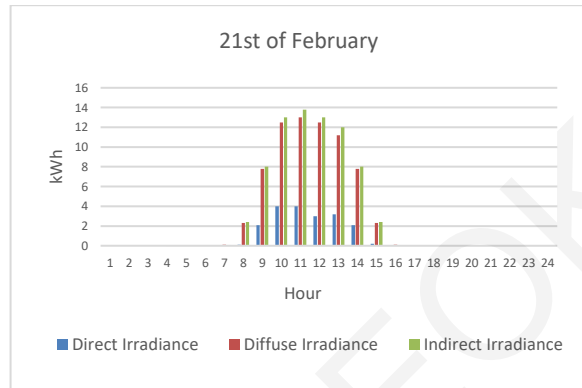
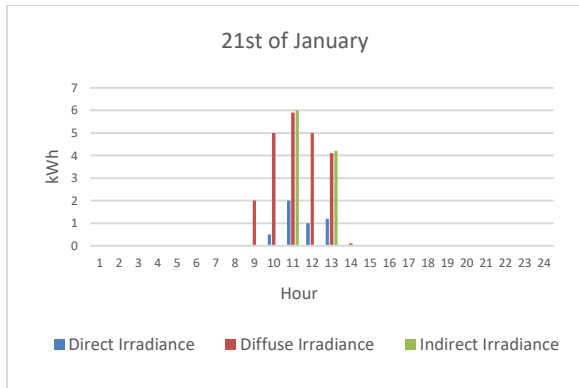
APPENDIX

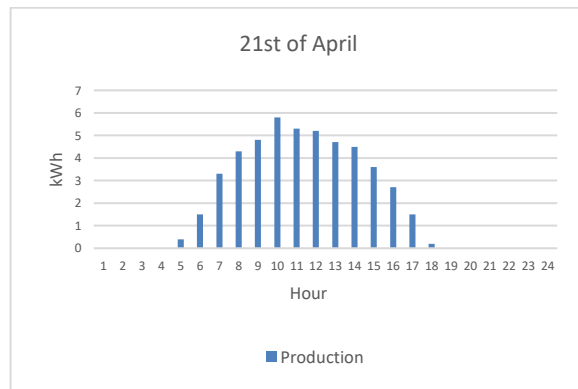
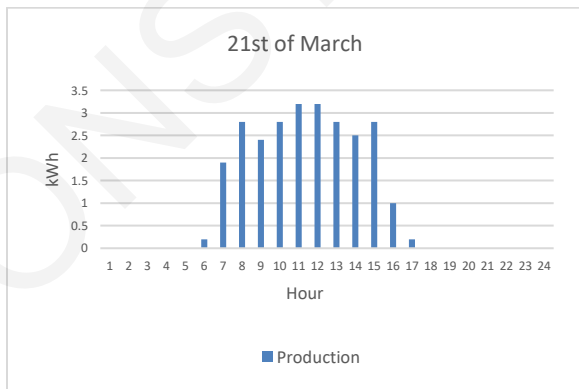
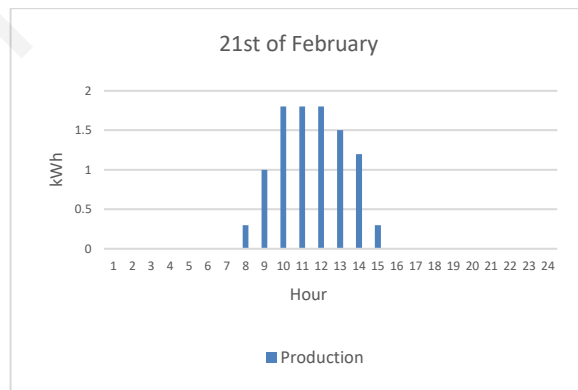
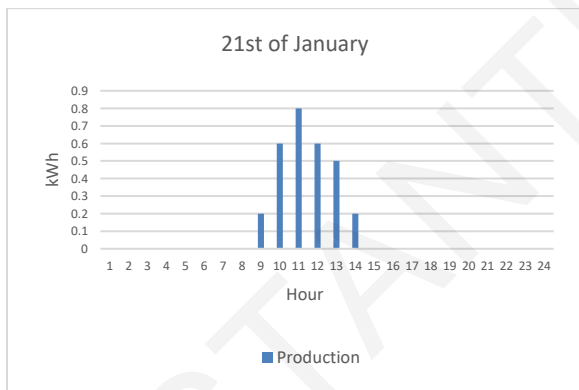
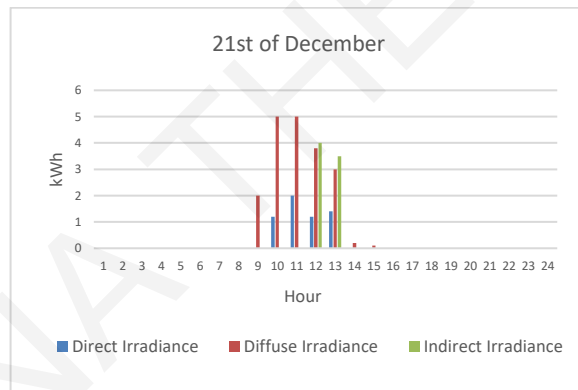
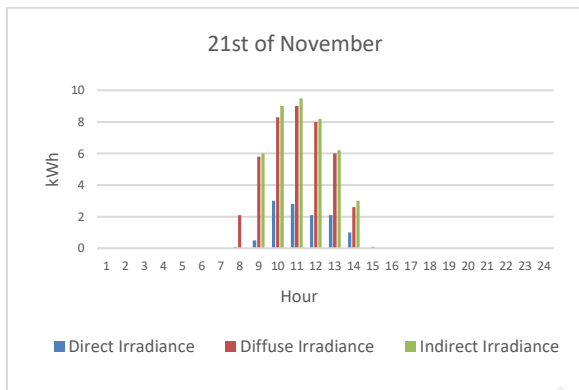
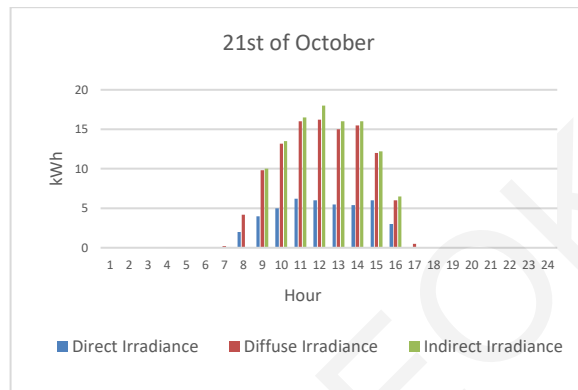
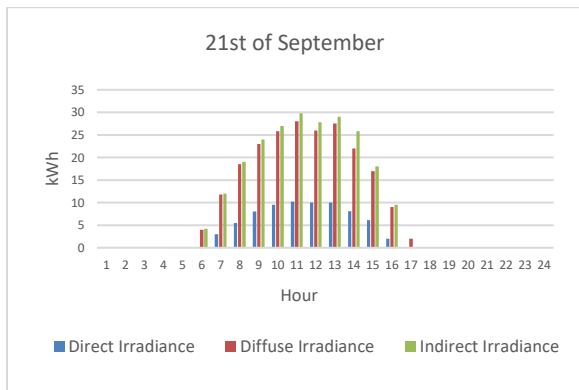


Target Position A

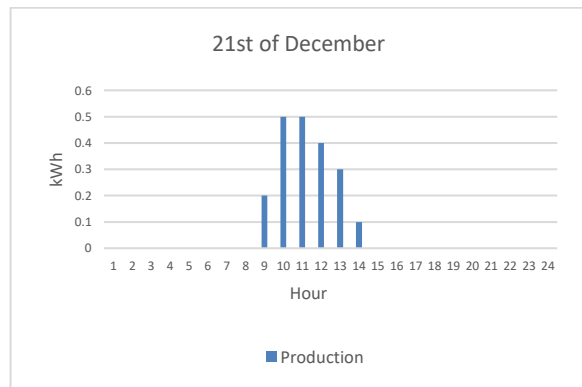
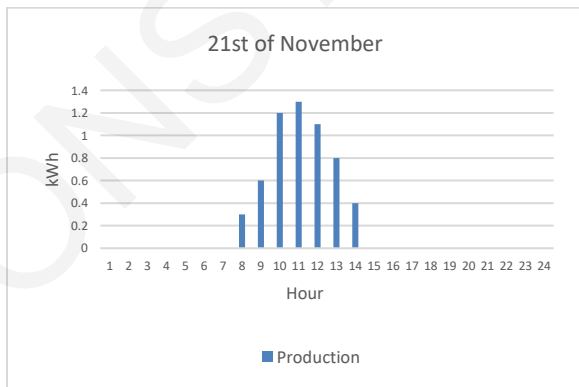
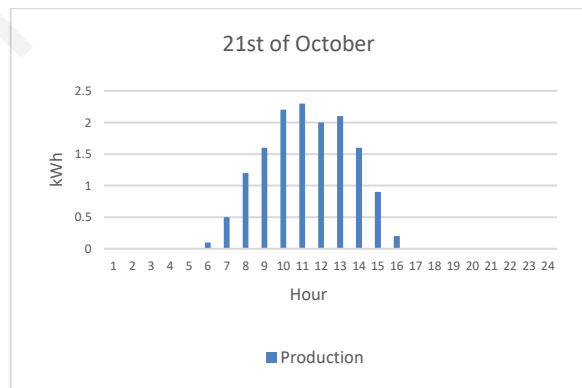
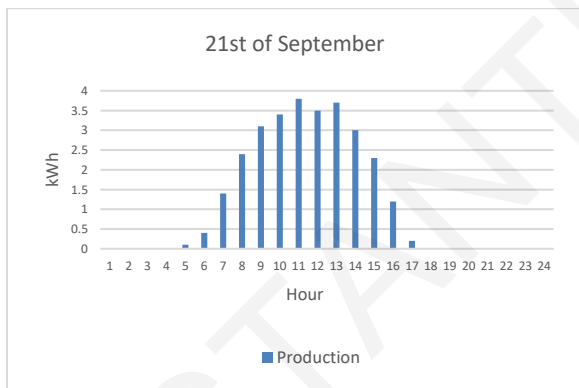
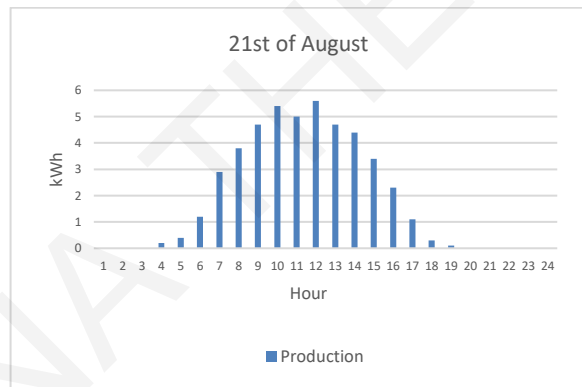
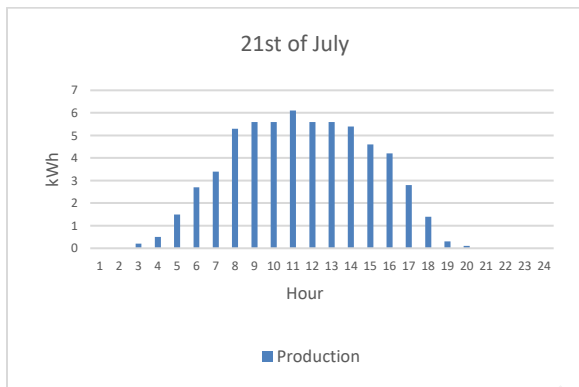
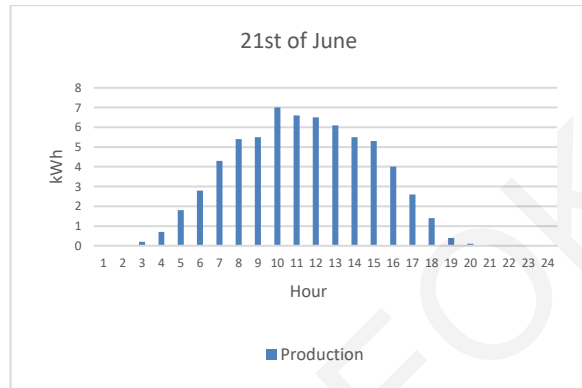
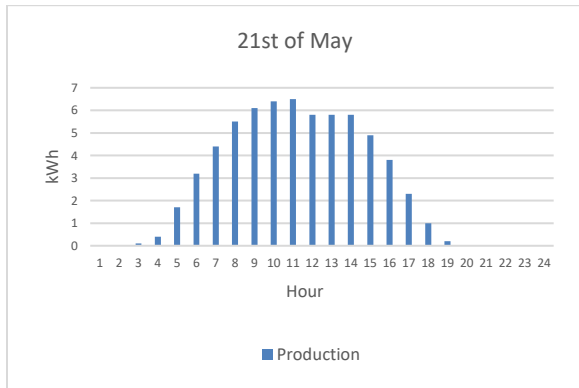


Month	Min Air Temperature	Max Air Temperature	Min Module Temperature	Max Module Temperature
January	-4	-2	-1	0
February	1.5	2	2	1.5
March	-2	2.5	-1	2.5
April	1	8	0	6
May	6	15	1	8
June	10	18	4	10
July	14	20	4	10
August	2	19	4	9
September	9	14	3	7
October	5	8	2	4
November	1	3	0	3
December	-2	-0.5	-0.5	0

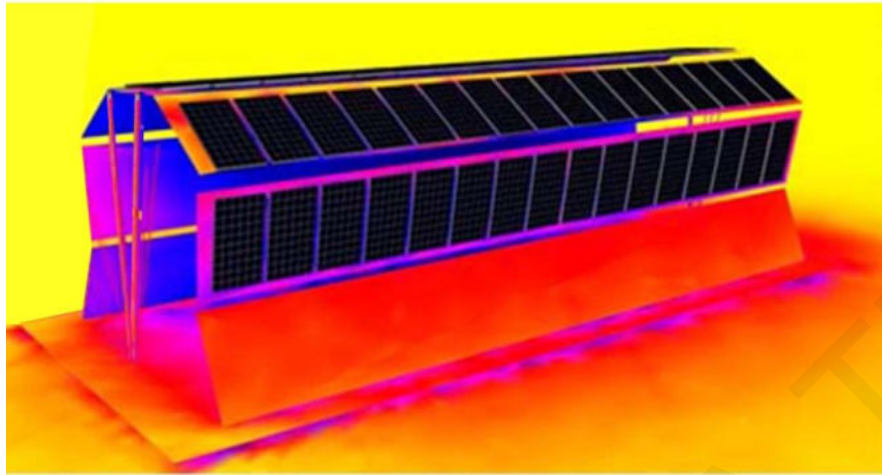
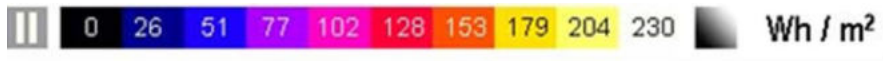




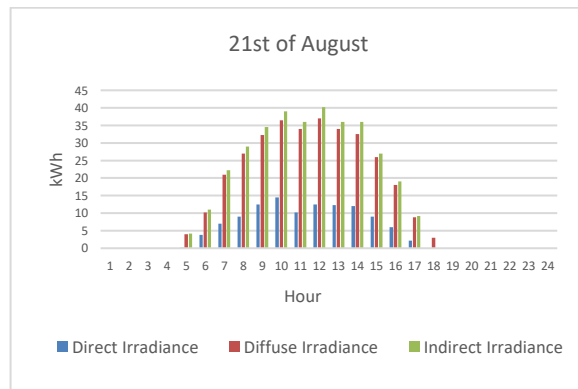
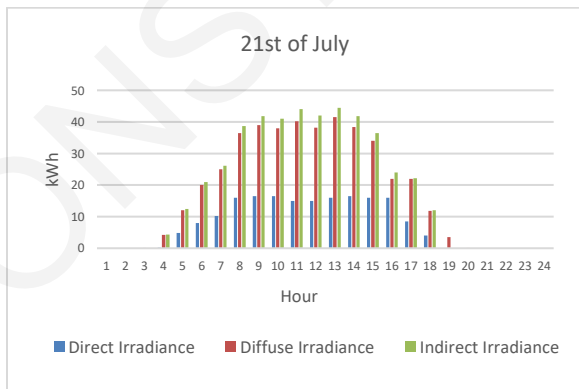
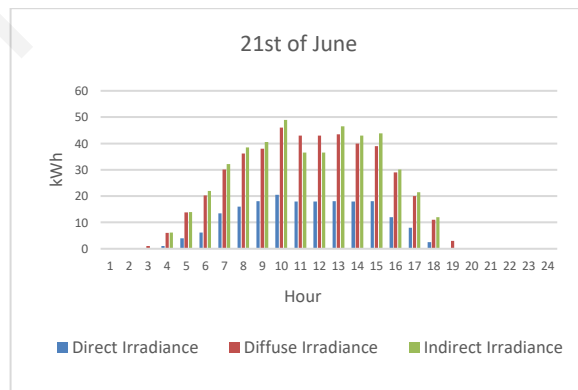
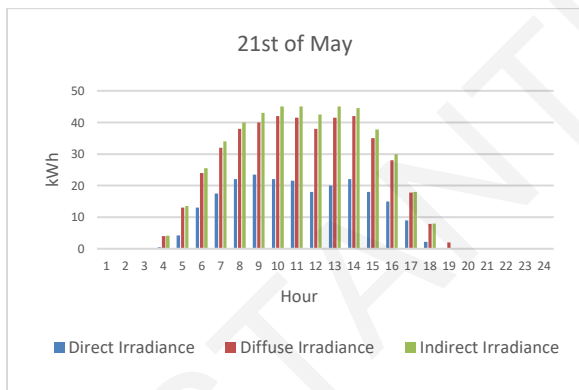
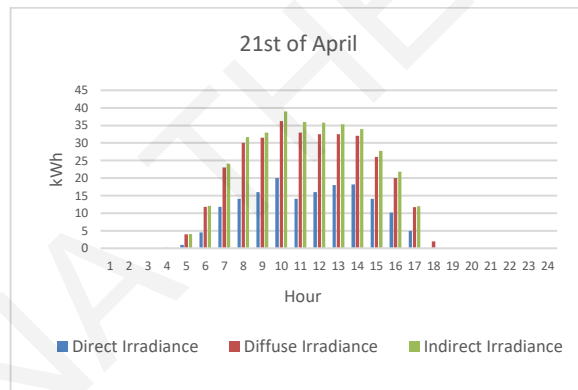
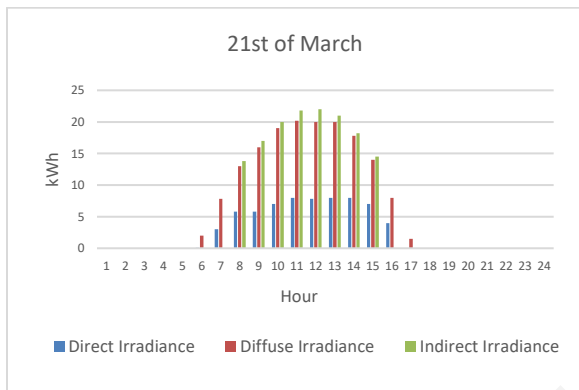
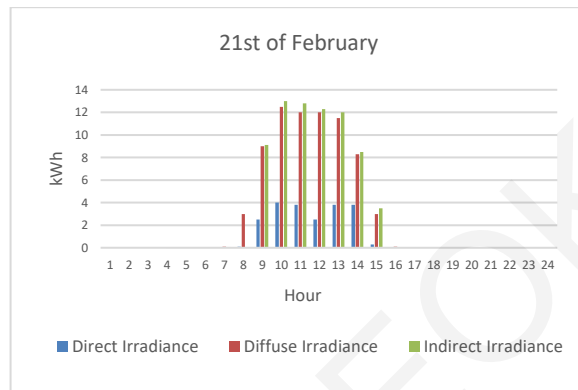
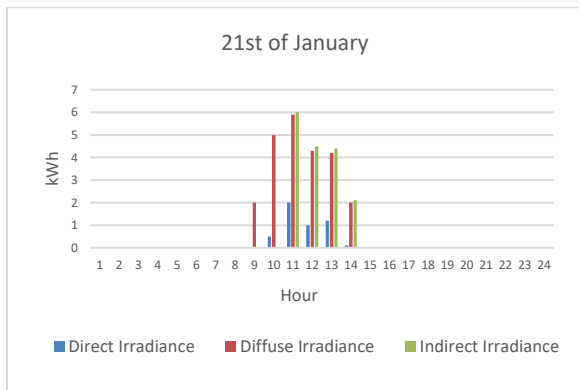
APPENDIX

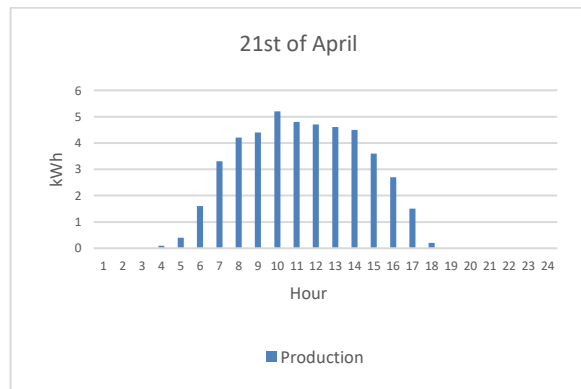
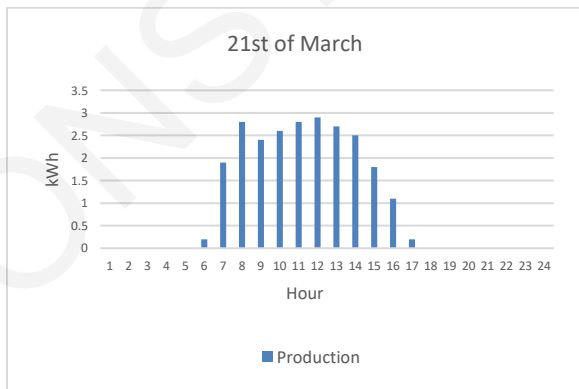
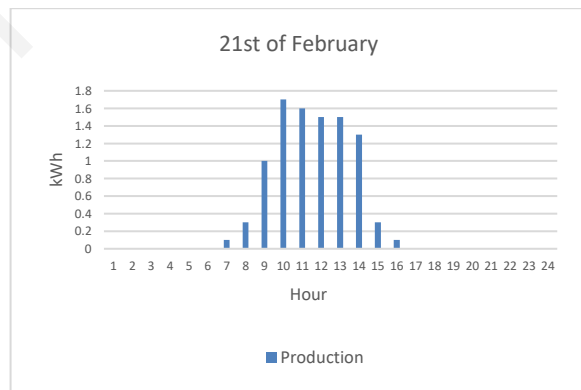
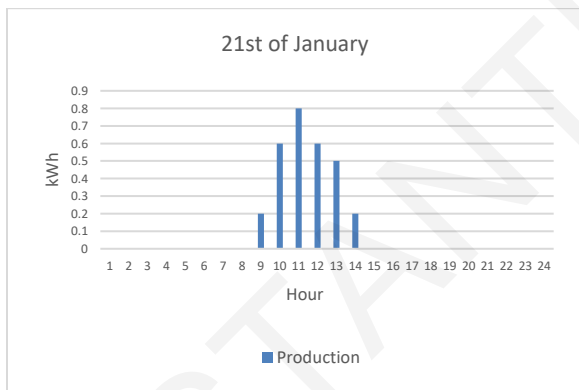
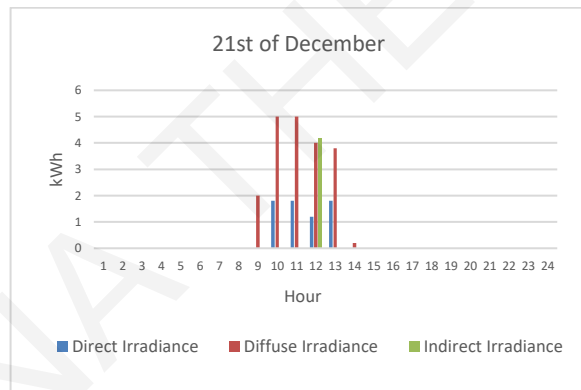
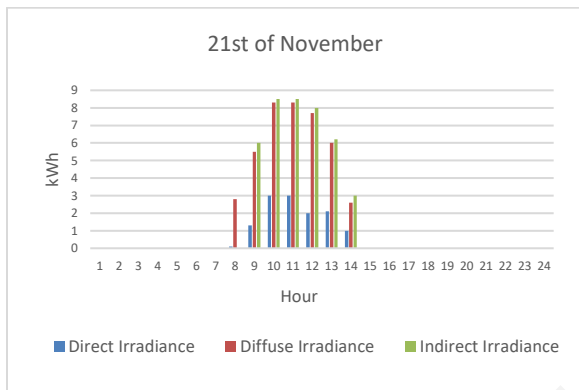
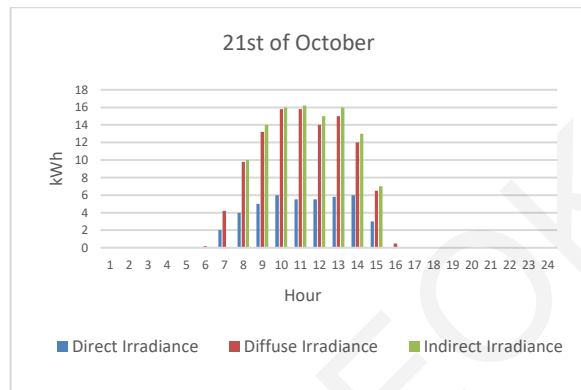
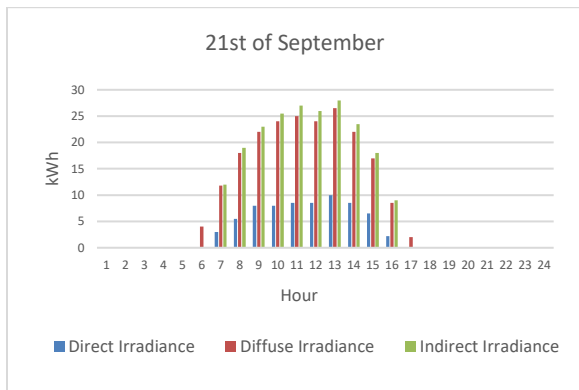


Target Position B

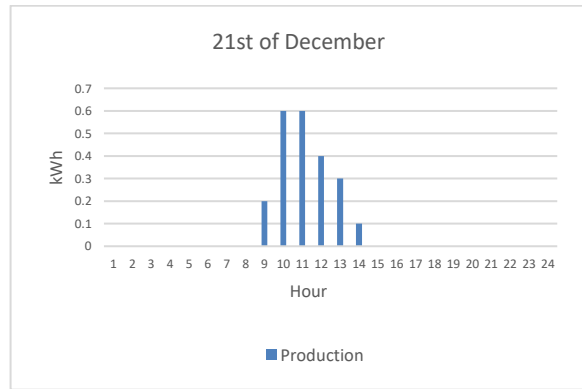
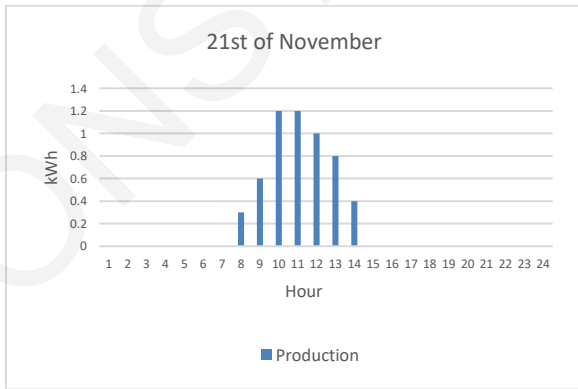
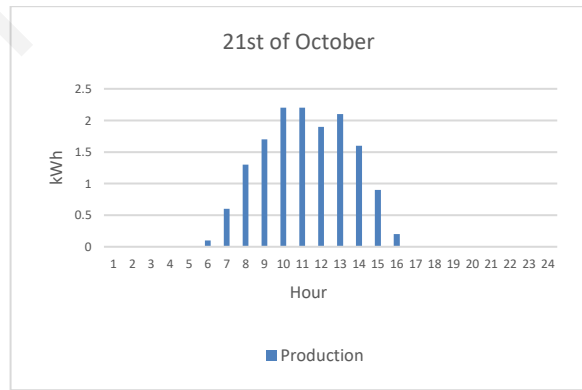
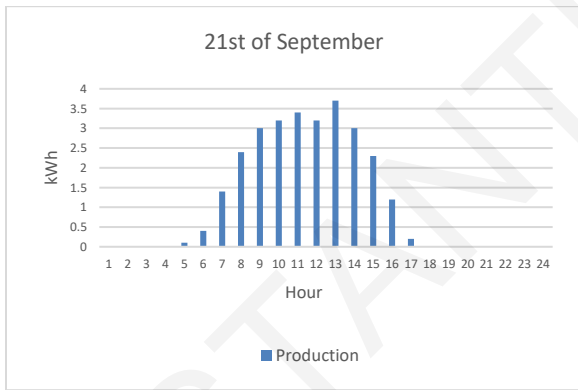
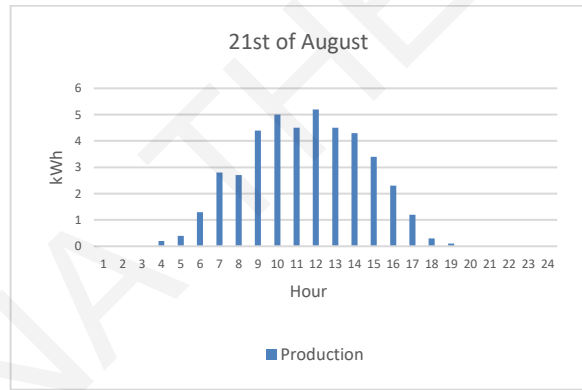
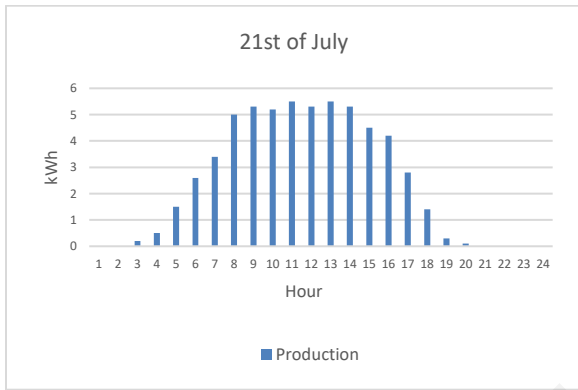
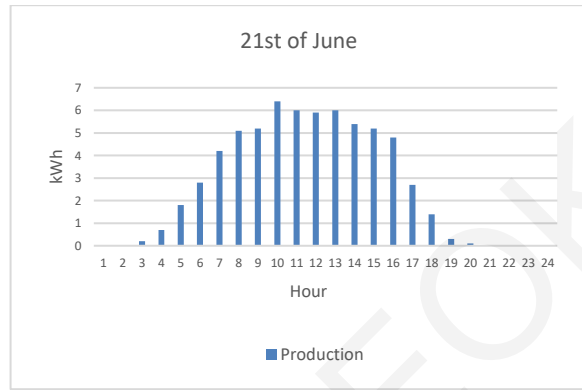
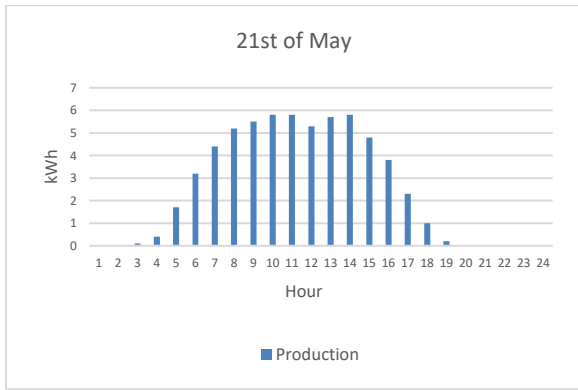


Month	Min Air Temperature	Max Air Temperature	Min Module Temperature	Max Module Temperature
January	-4	-2	-1	-0.5
February	2	1.5	1.5	-0.5
March	-1	2	-0.5	2.5
April	1	8	0	5
May	7	15	2	8
June	10	18	3.5	9
July	13.5	20	4	10
August	13	19	4	9
September	9	14	3	7
October	5	8.5	2	4
November	1	3	0	2
December	-2	-0.5	-0.5	0

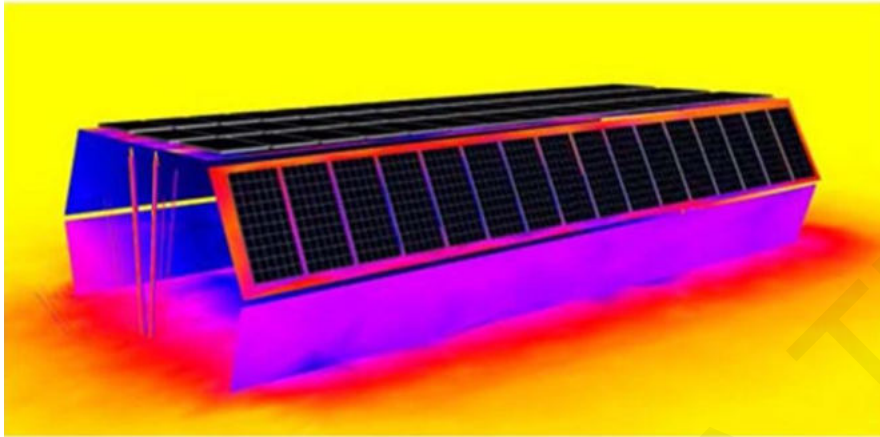
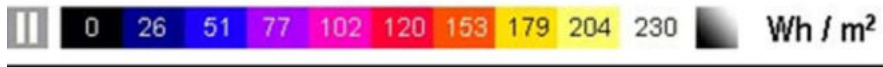




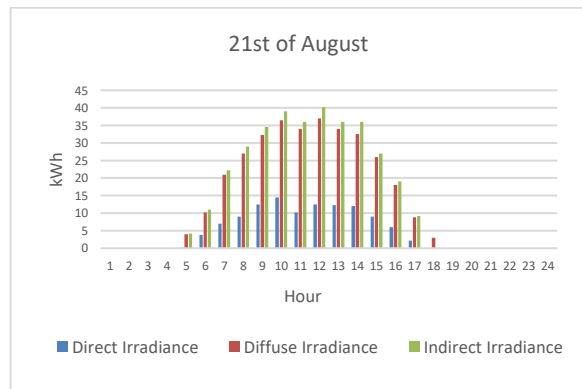
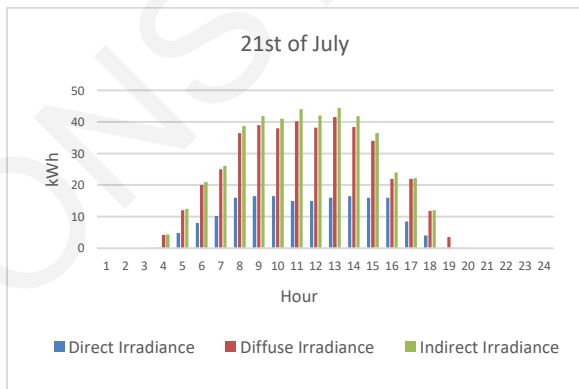
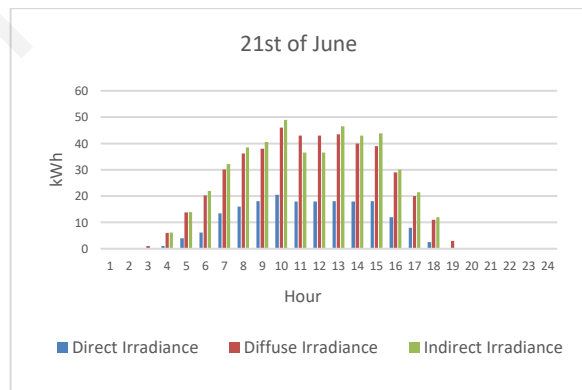
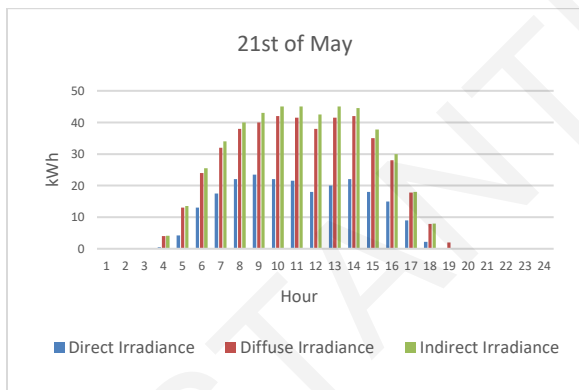
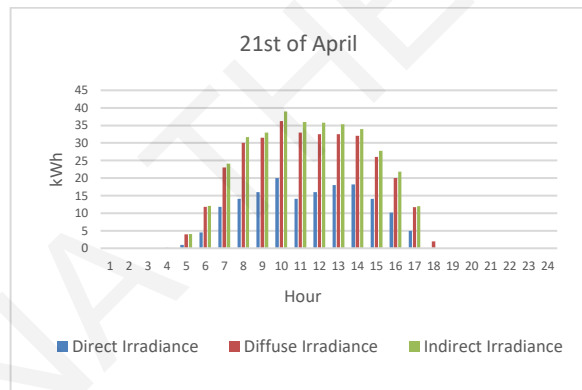
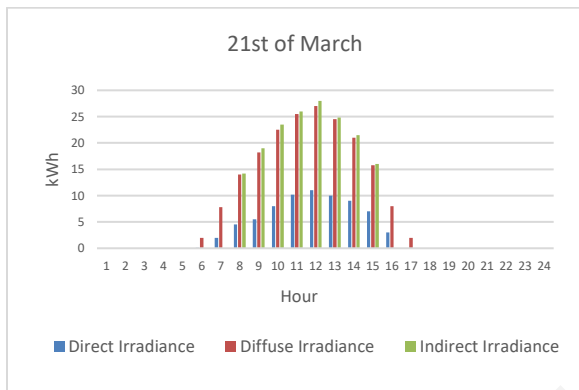
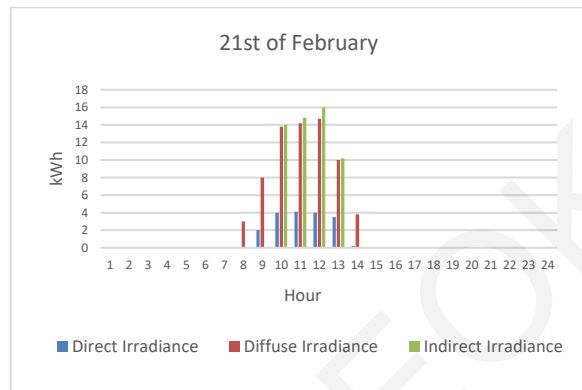
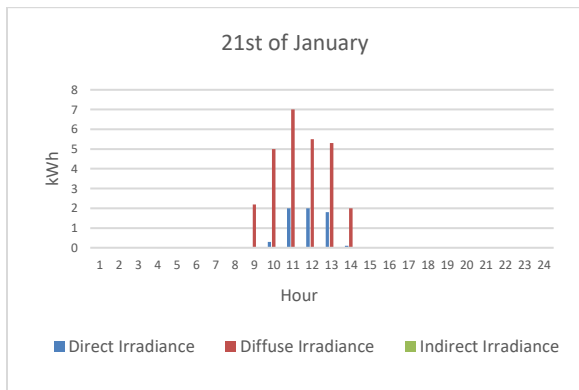
APPENDIX

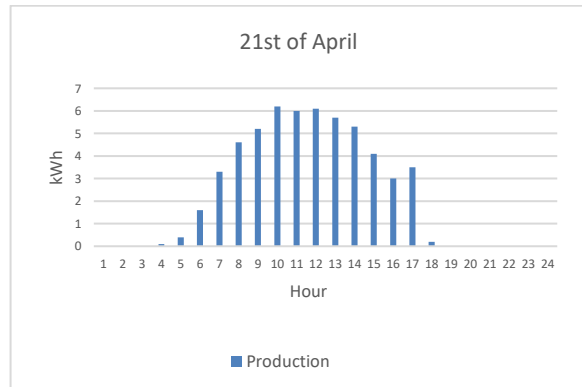
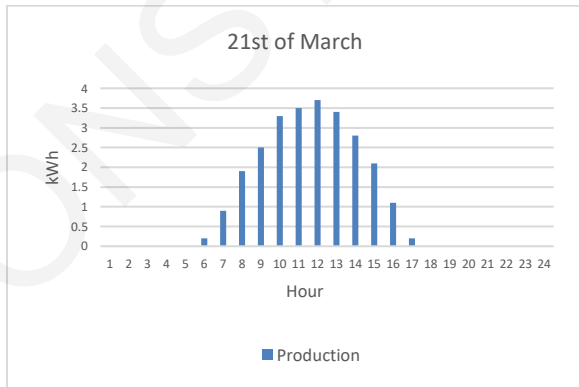
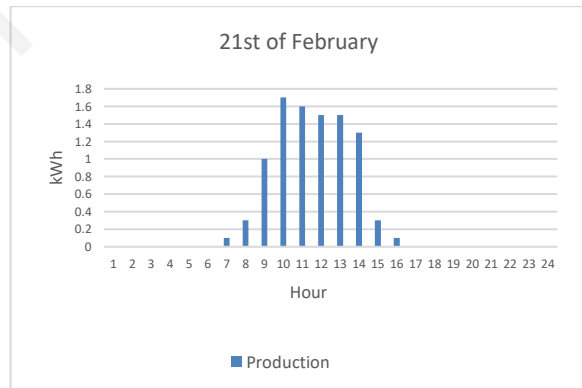
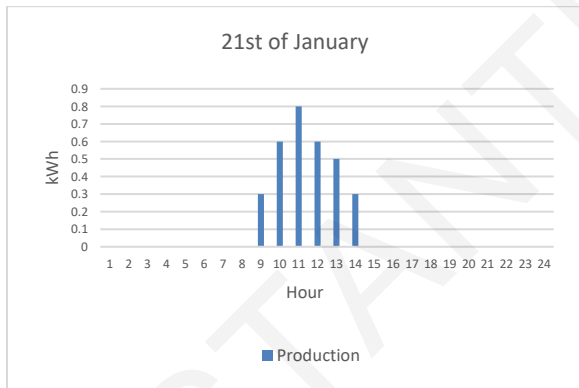
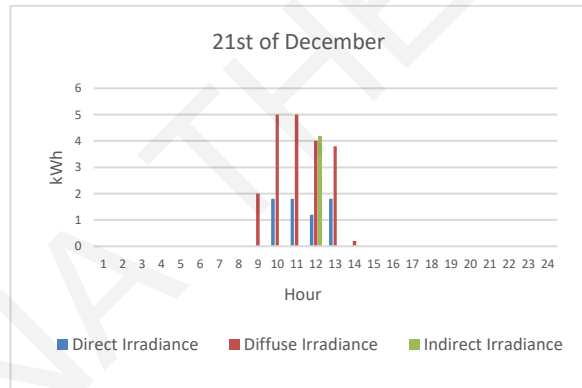
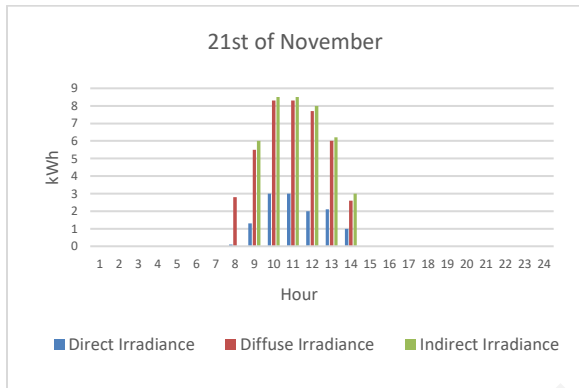
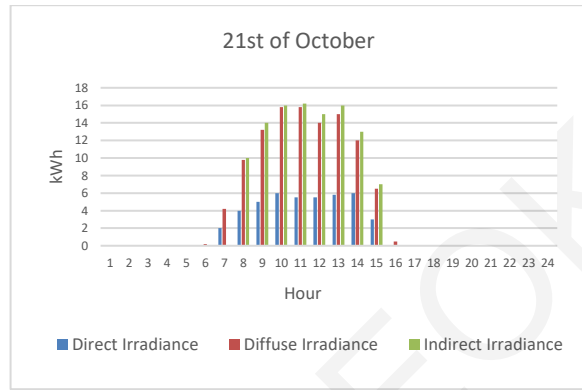
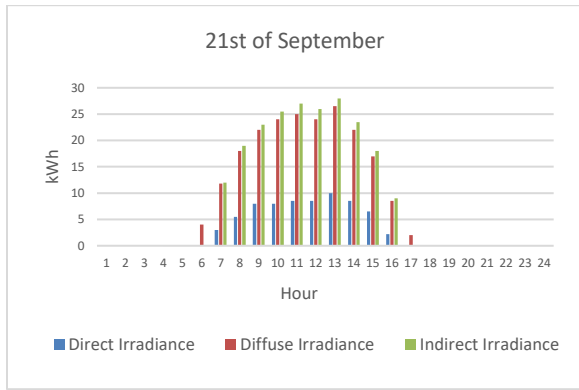


Target Position C

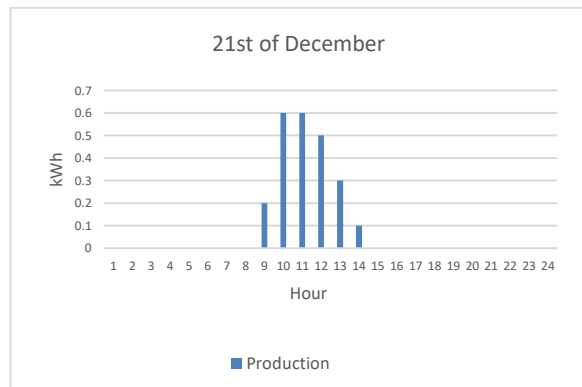
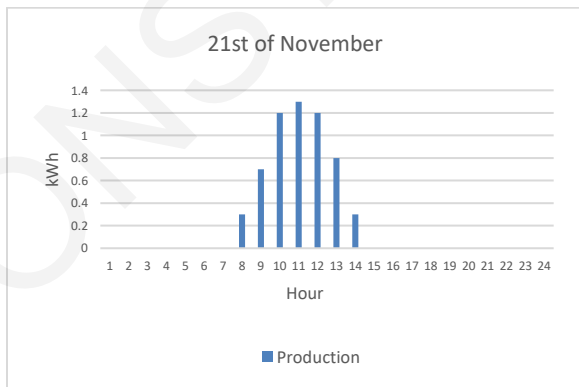
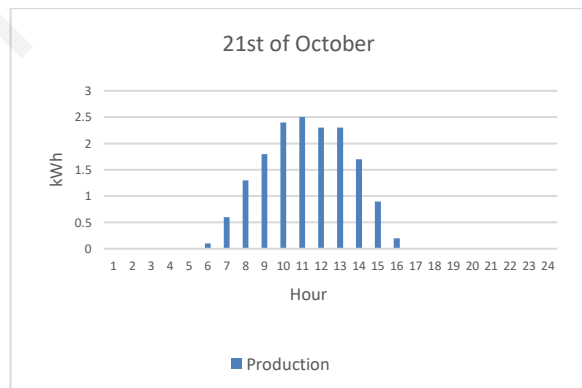
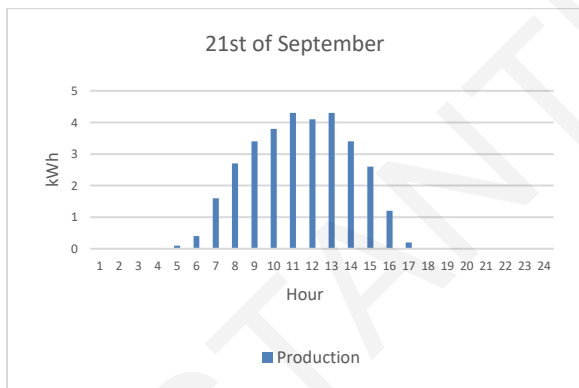
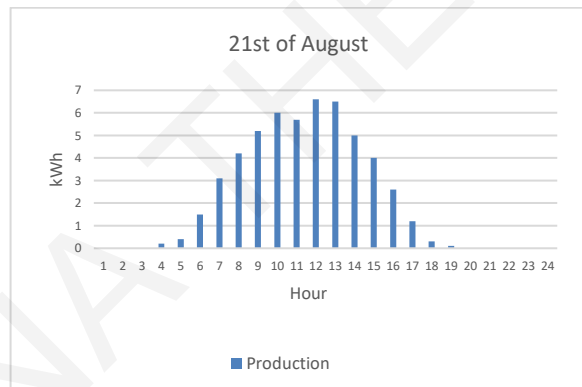
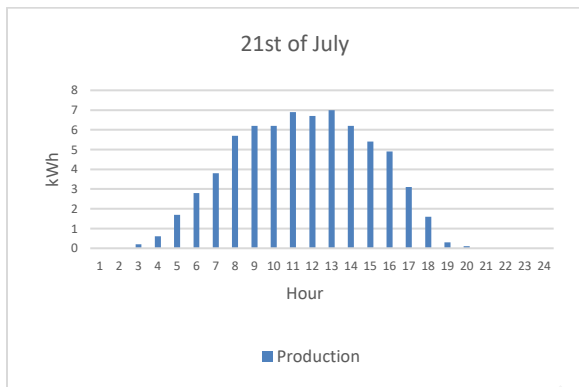
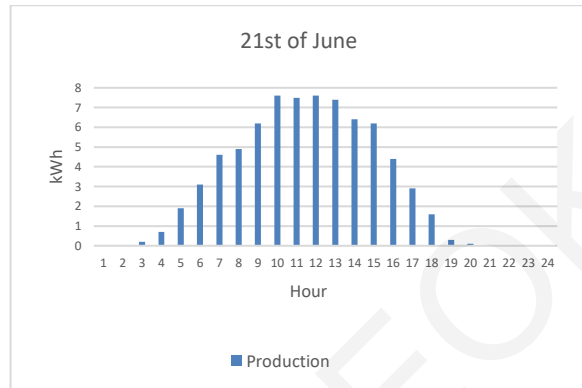
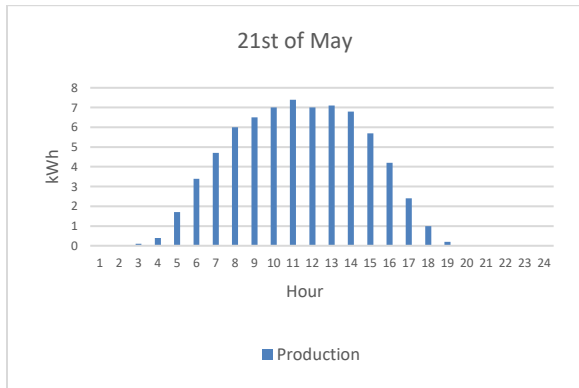


Month	Min Air Temperature	Max Air Temperature	Min Module Temperature	Max Module Temperature
January	-4	-2	-1	-0.5
February	2	1.5	1.5	-0.5
March	-1	2	-0.5	2.5
April	1	8	0	5
May	7	15	2	8
June	10	18	3.5	9
July	13.5	20	4	10
August	13	19	4	9
September	9	14	3	7
October	5	8.5	2	4
November	1	3	0	2
December	-2	-0.5	-0.5	0



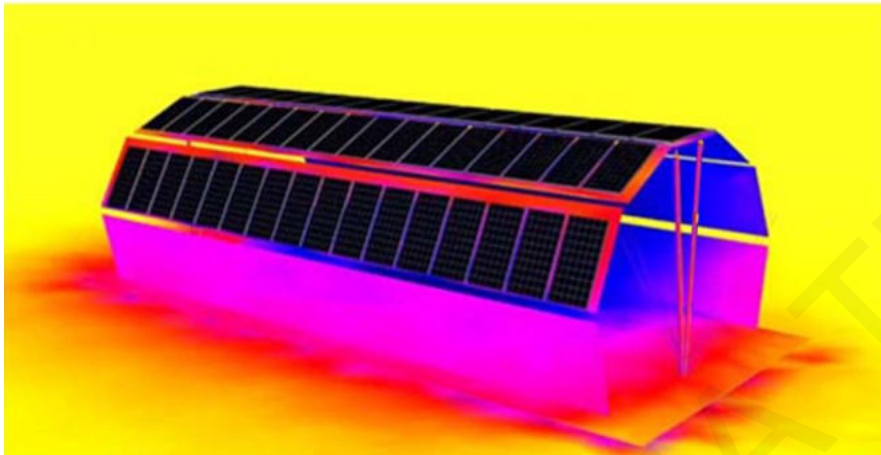


APPENDIX

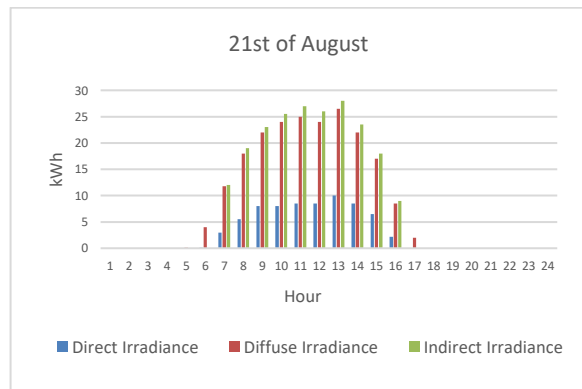
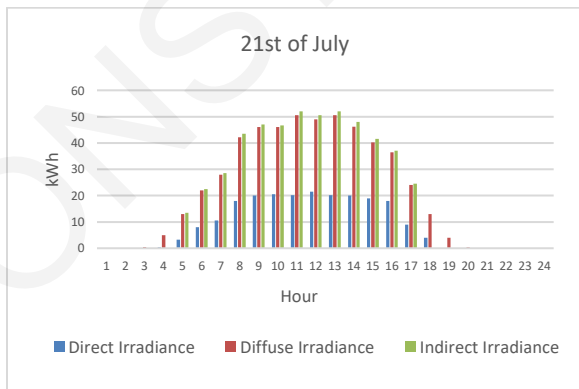
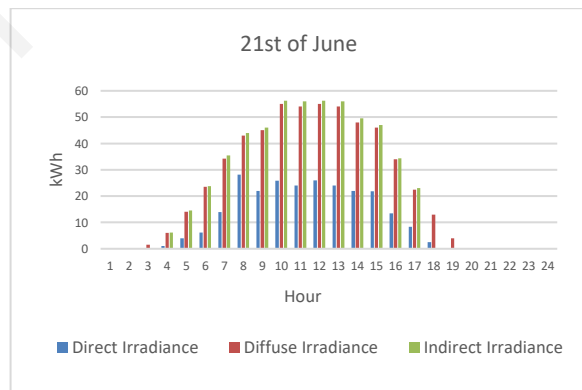
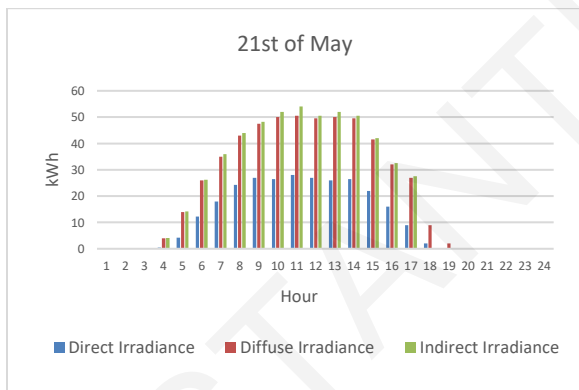
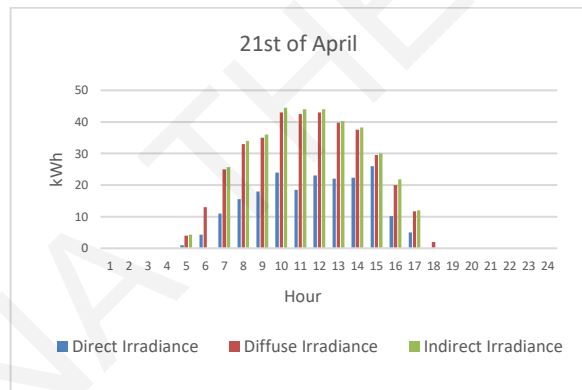
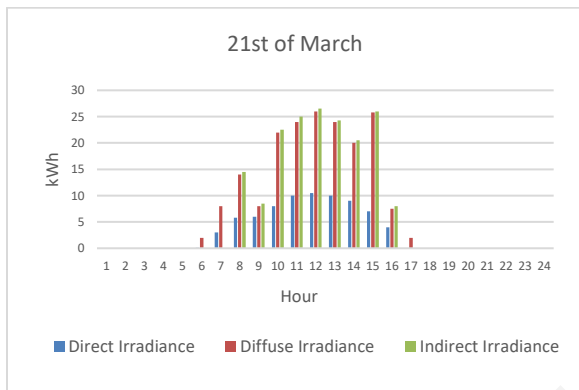
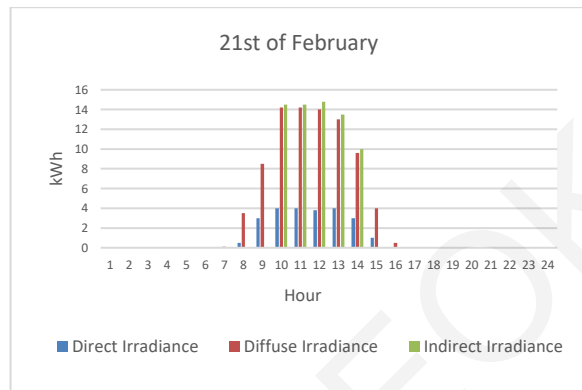
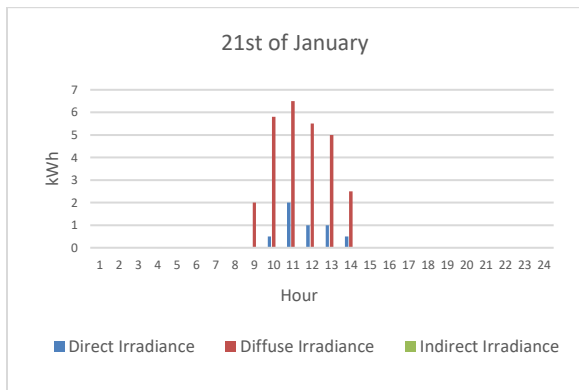


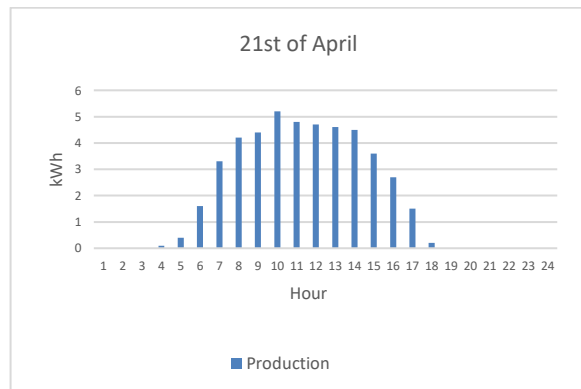
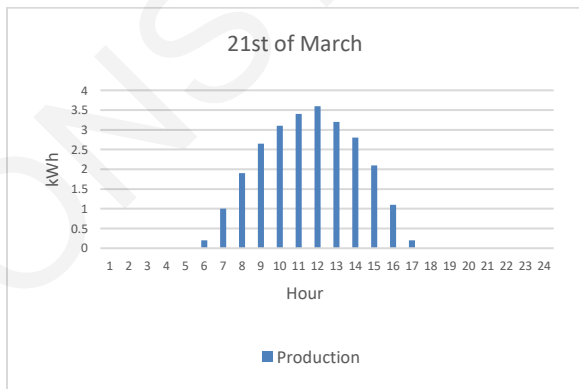
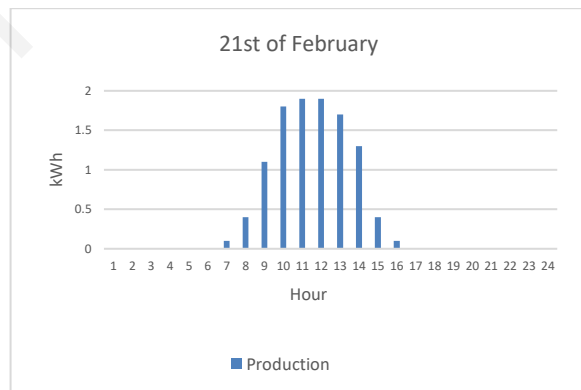
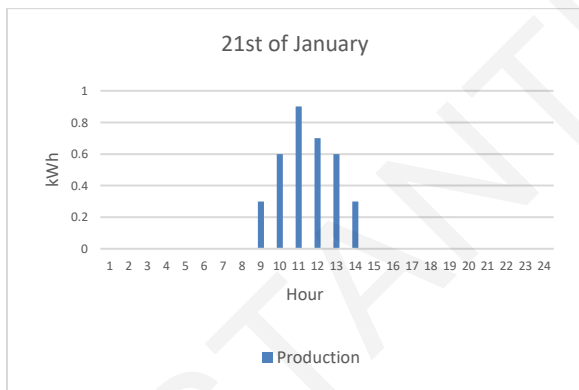
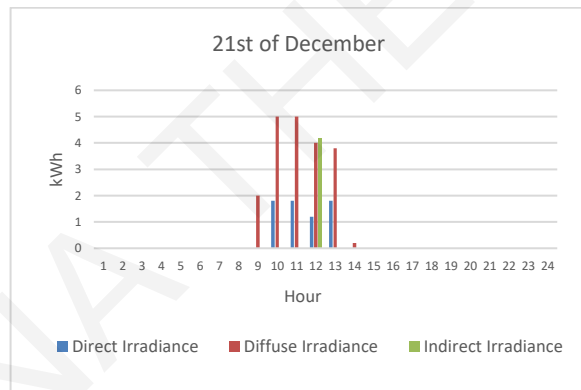
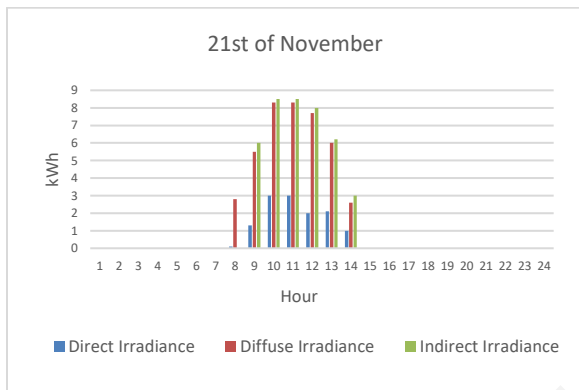
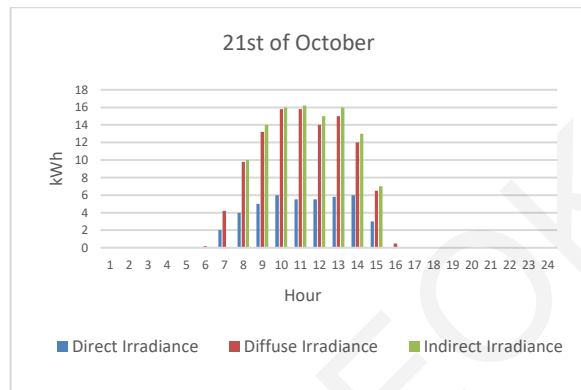
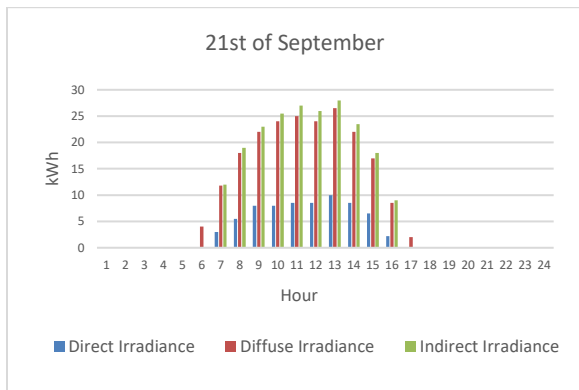
D. Site Location: Stockholm, Sweden, Site Orientation 90°

Initial Position

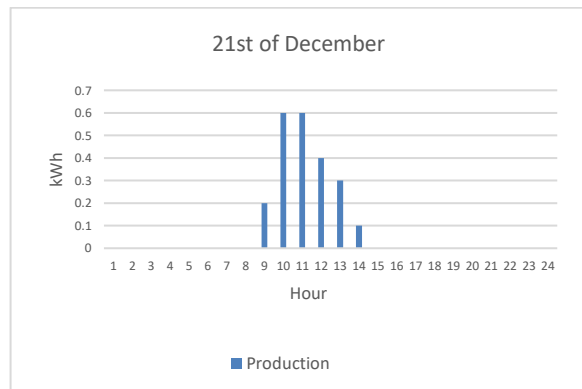
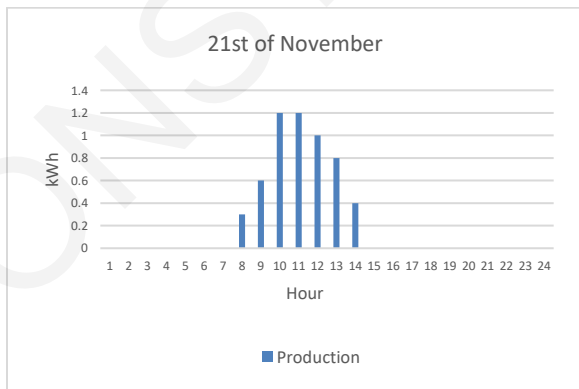
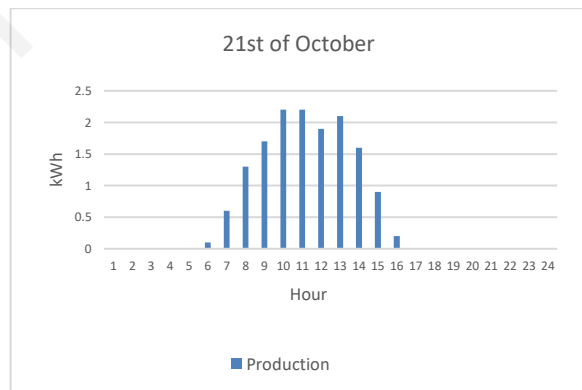
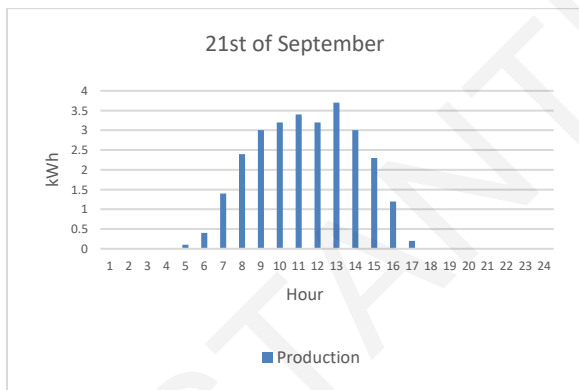
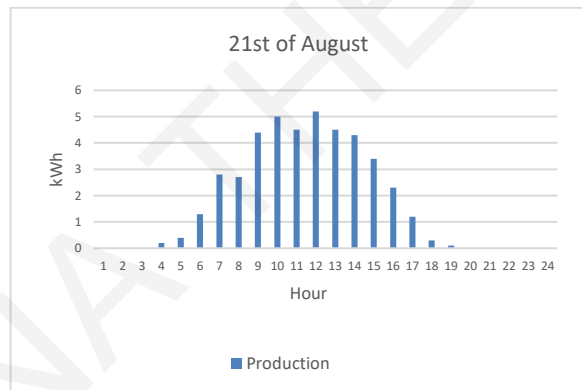
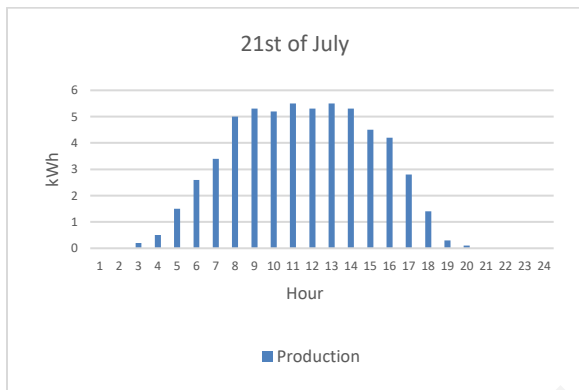
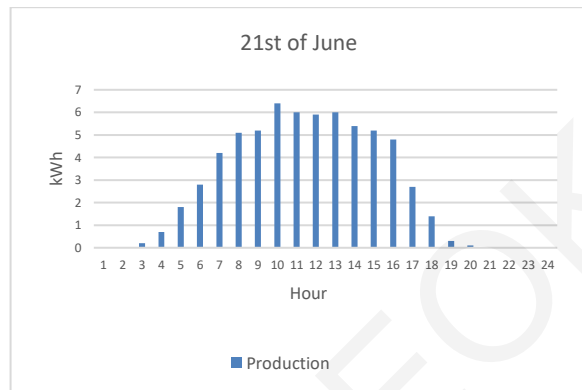
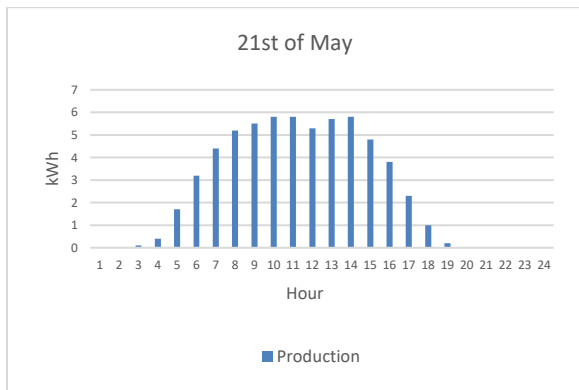


Month	Min Air Temperature	Max Air Temperature	Min Module Temperature	Max Module Temperature
January	-4	-2	-1	-0.5
February	2	1.5	1.5	-0.5
March	-1	2	-0.5	2.5
April	1	8	0	5
May	7	15	2	8
June	10	18	3.5	9
July	13.5	20	4	10
August	13	19	4	9
September	9	14	3	7
October	5	8.5	2	4
November	1	3	0	2
December	-2	-0.5	-0.5	0



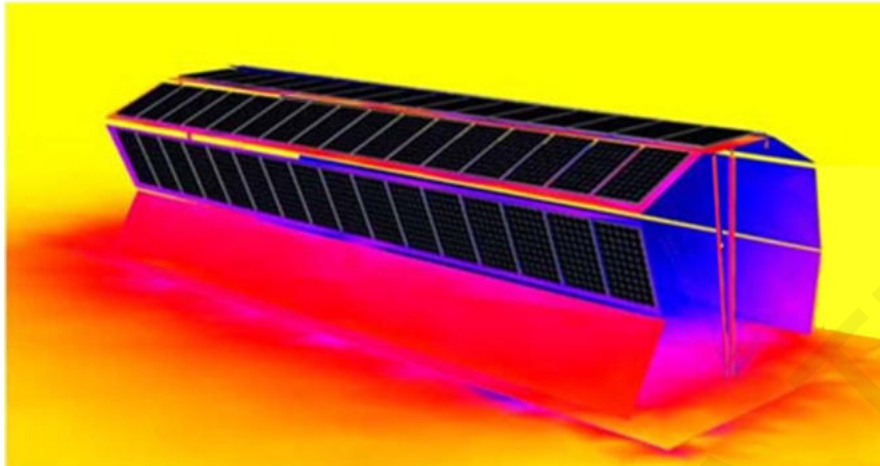


APPENDIX

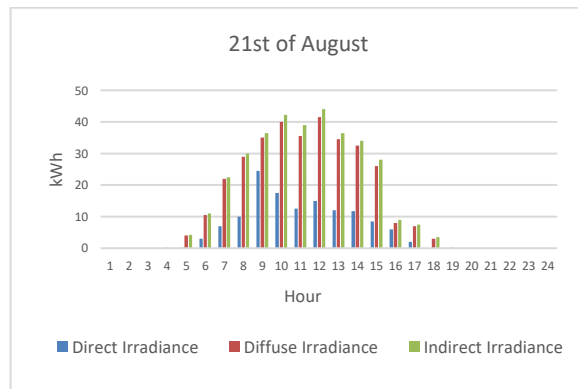
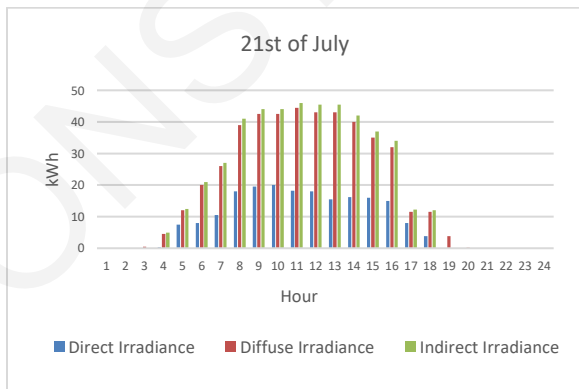
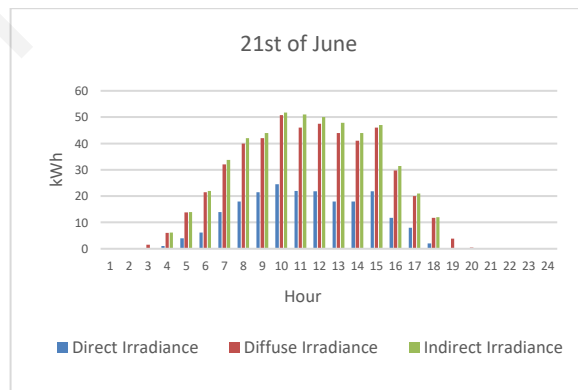
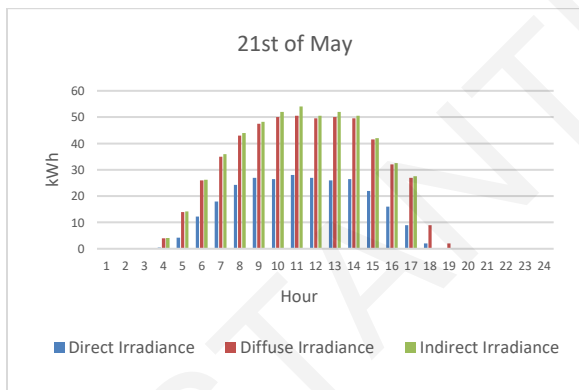
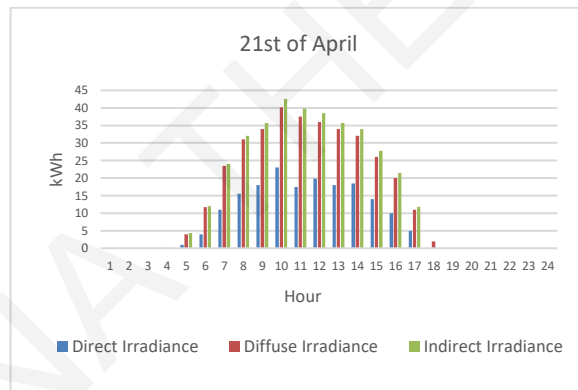
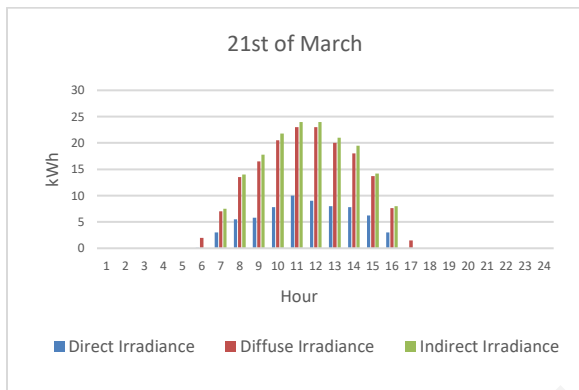
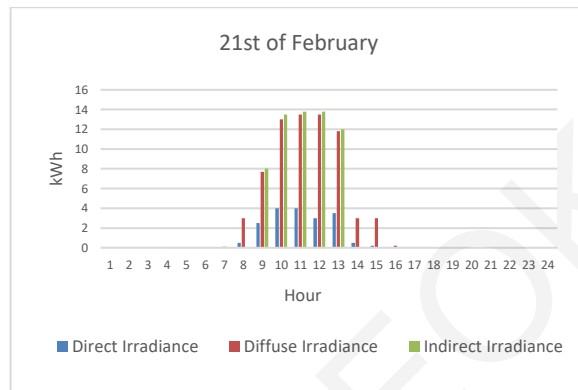
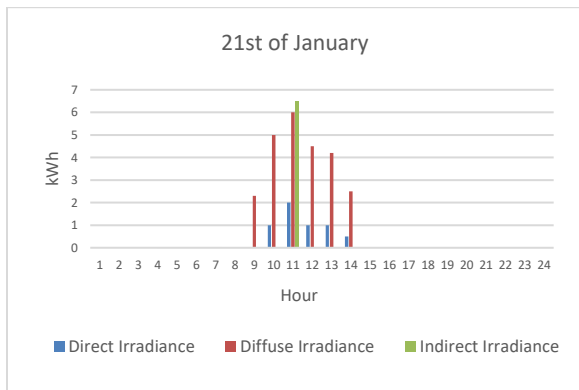


APPENDIX

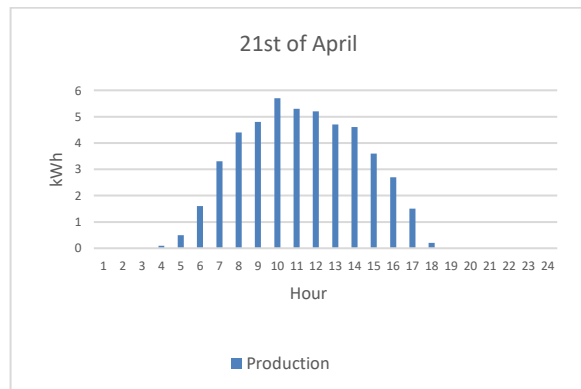
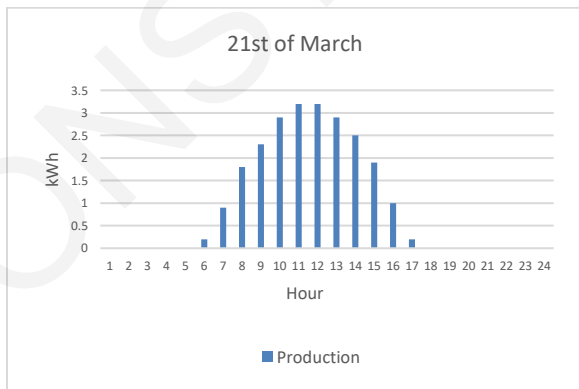
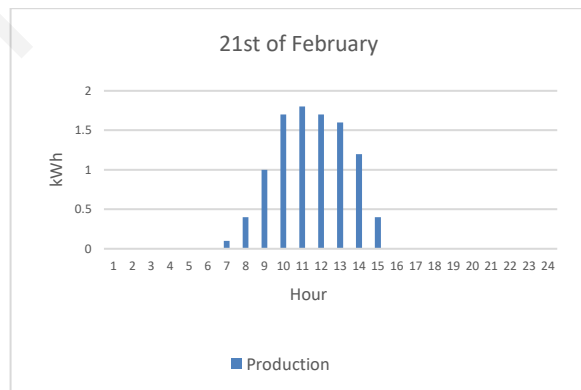
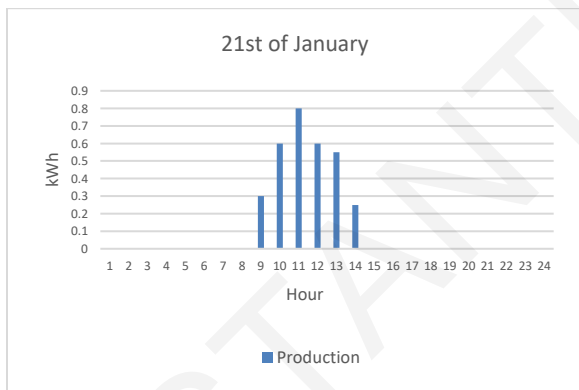
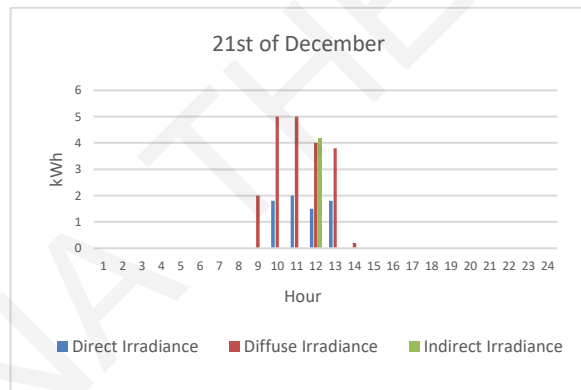
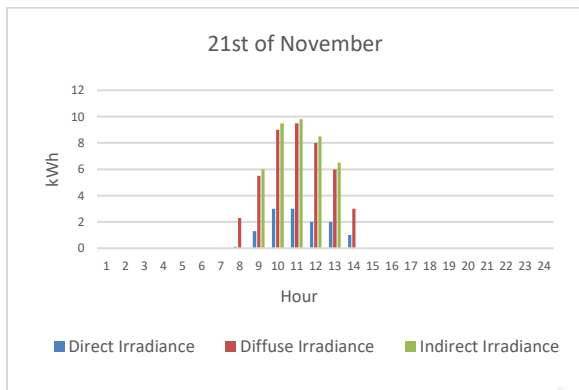
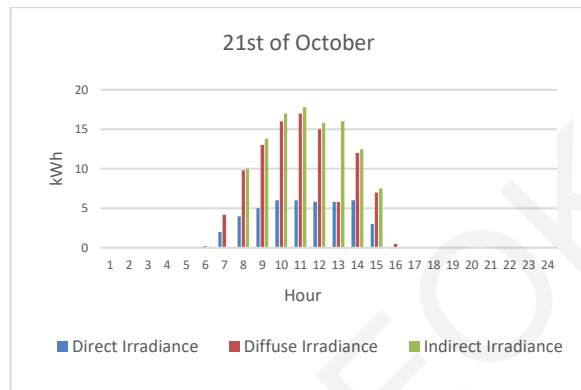
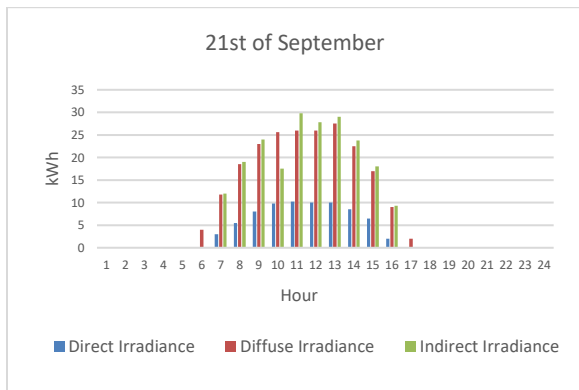
Target Position A



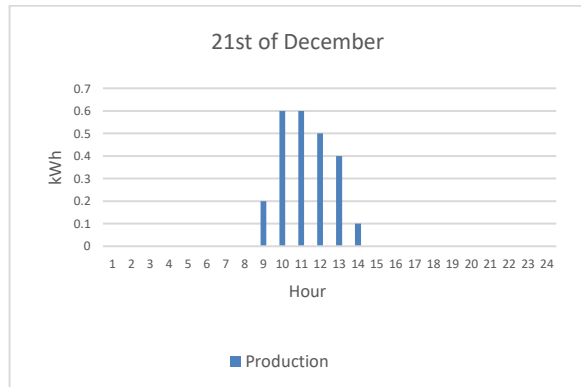
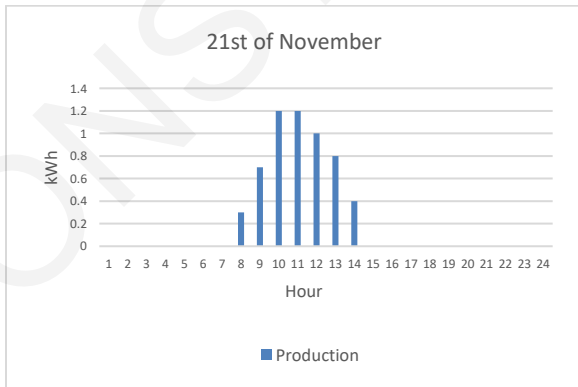
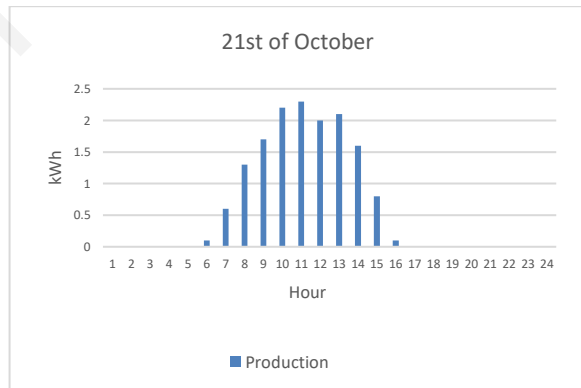
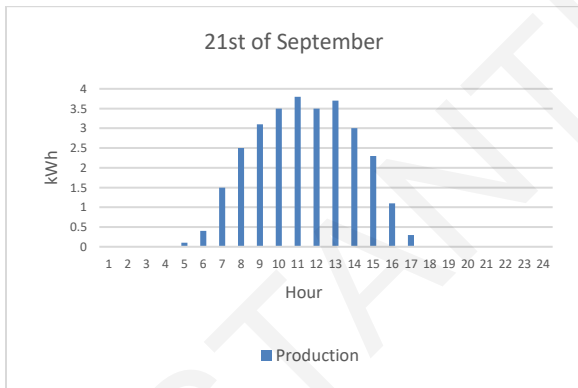
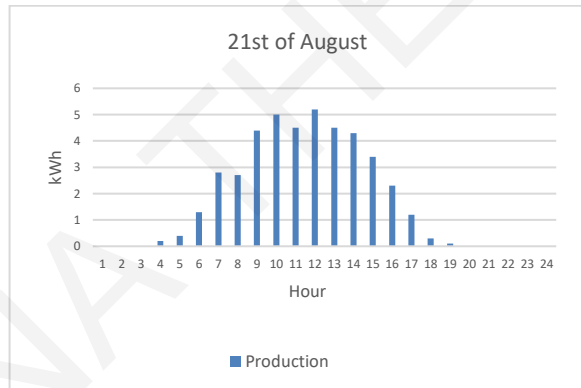
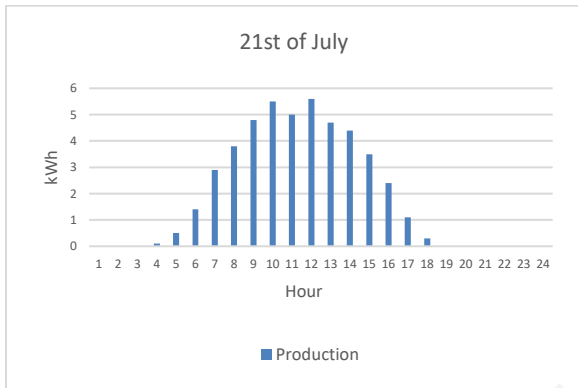
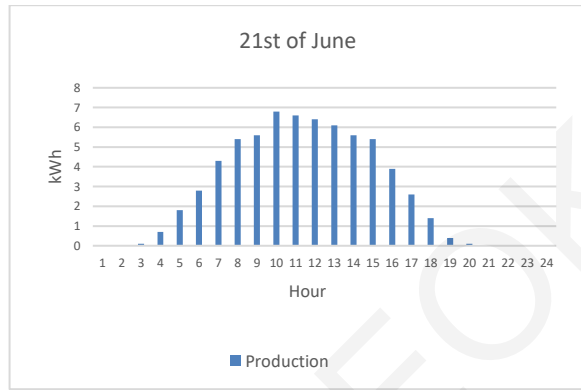
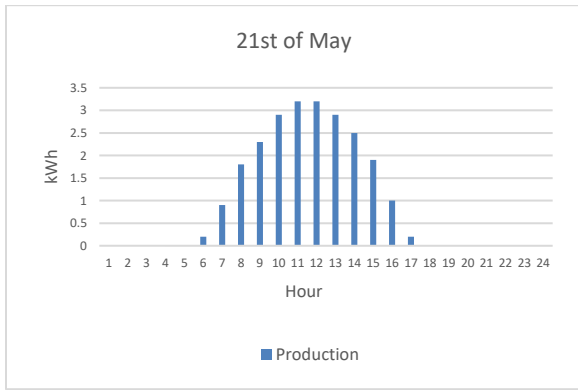
Month	Min Air Temperature	Max Air Temperature	Min Module Temperature	Max Module Temperature
January	-4	-2	-1	-0.5
February	2	1.5	1.5	-0.5
March	-1	2	-0.5	2.5
April	1	8	0	5
May	7	15	2	8
June	10	18	3.5	9
July	13.5	20	4	10
August	13	19	4	9
September	9	14	3	7
October	5	8.5	2	4
November	1	3	0	2
December	-2	-0.5	-0.5	0



APPENDIX

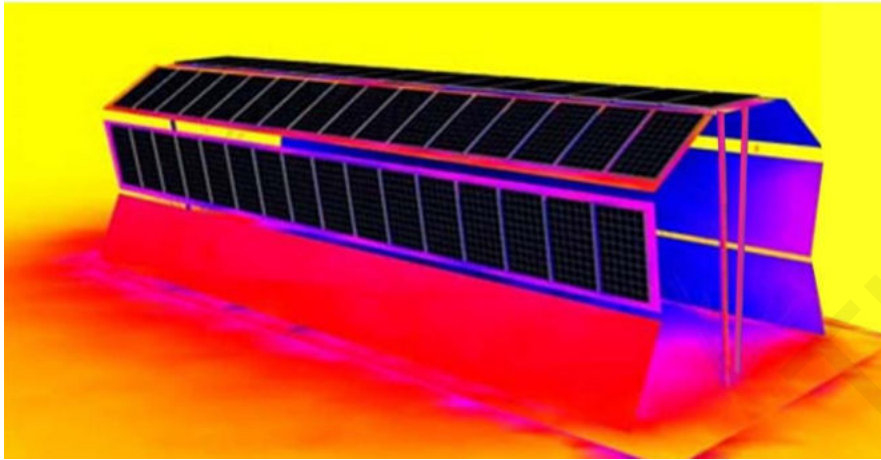
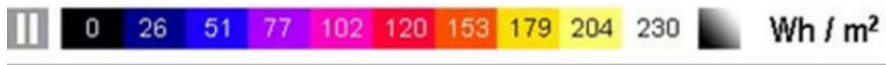


APPENDIX

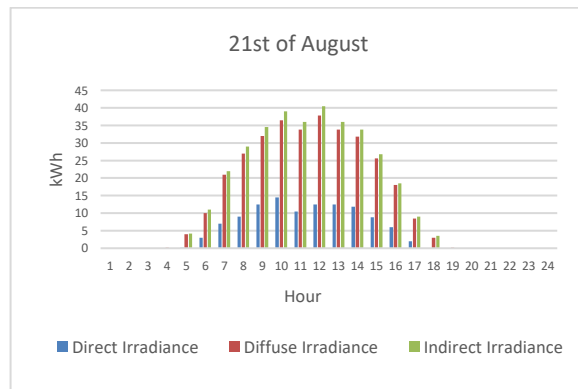
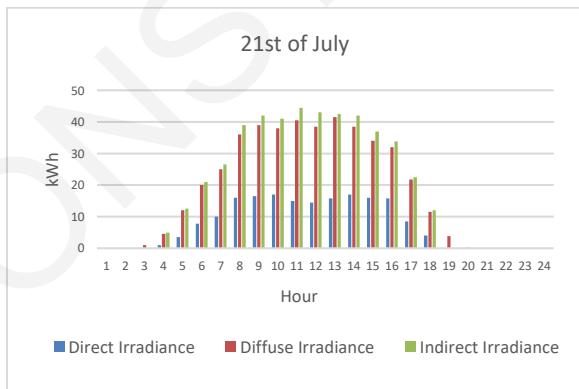
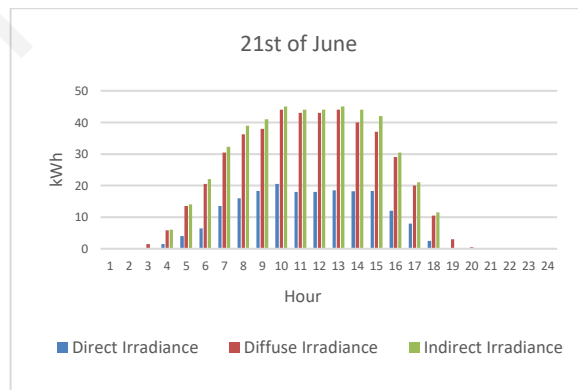
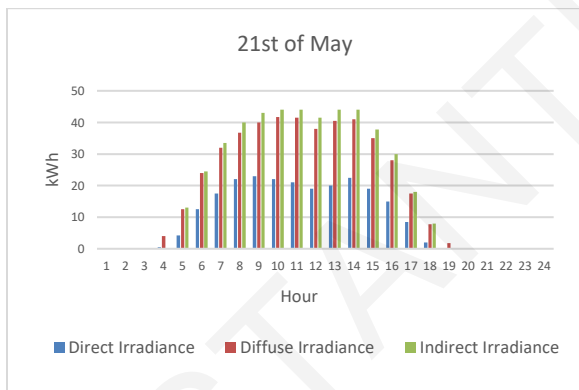
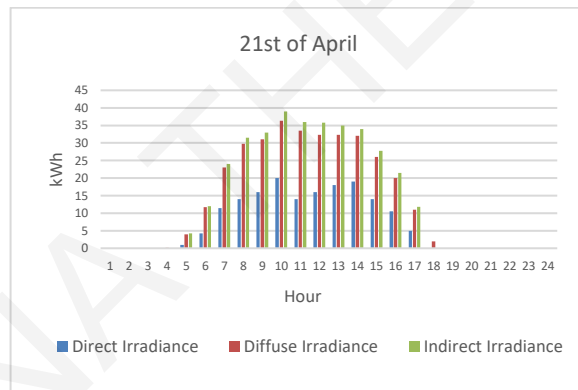
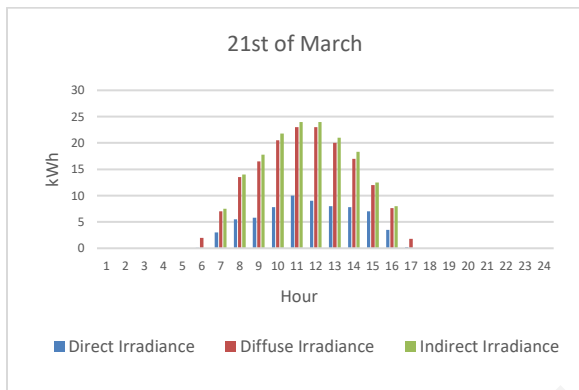
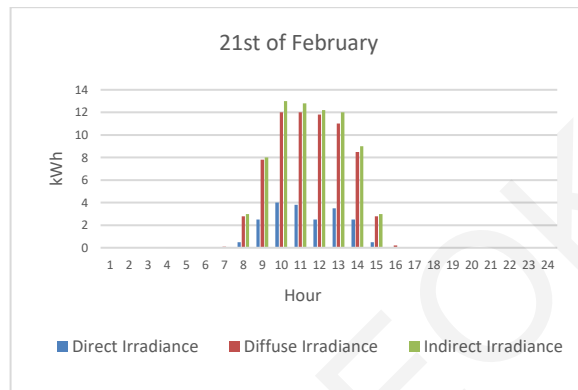
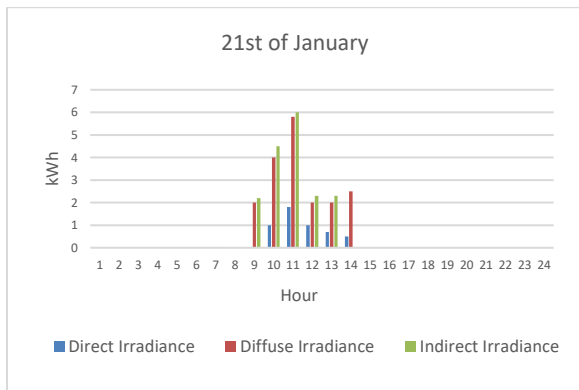


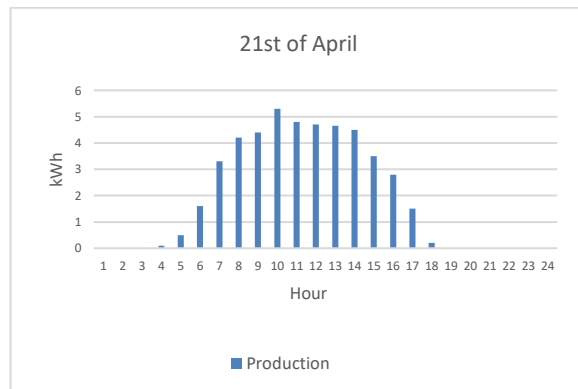
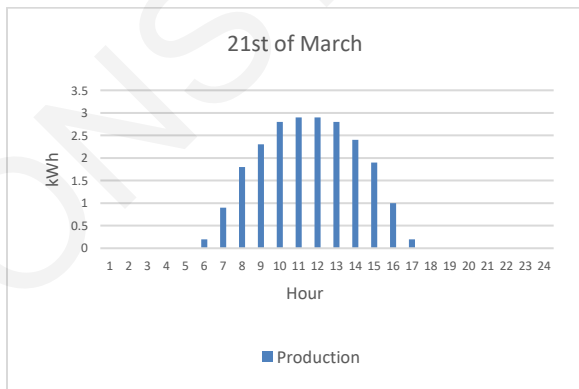
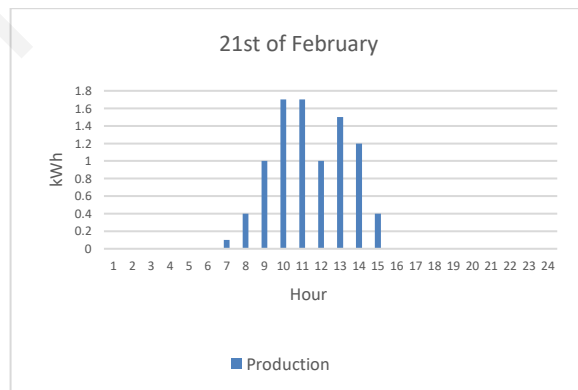
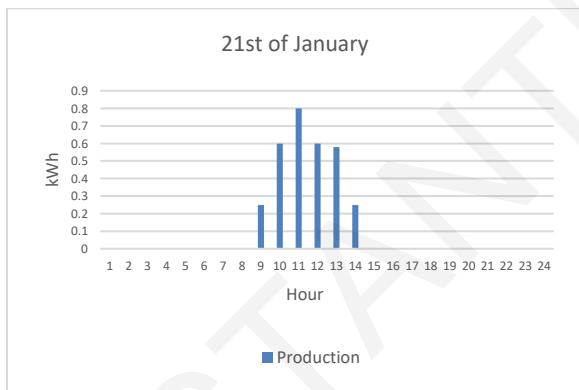
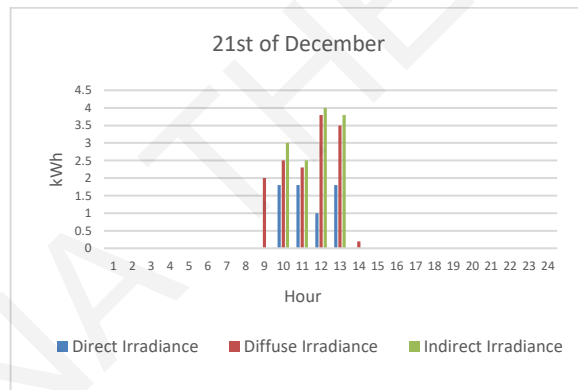
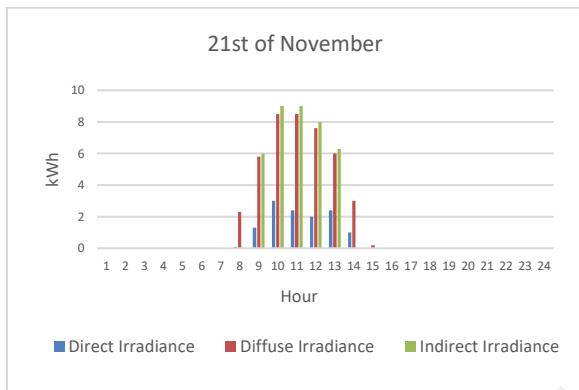
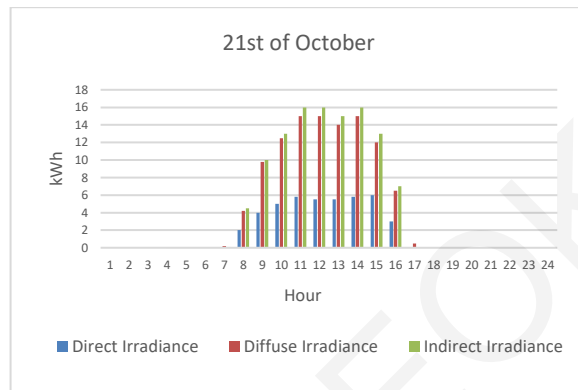
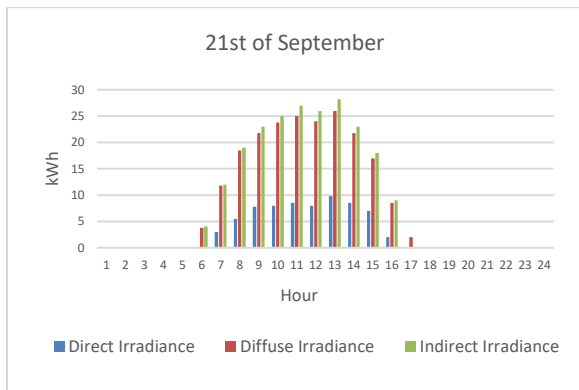
APPENDIX

Target Position B

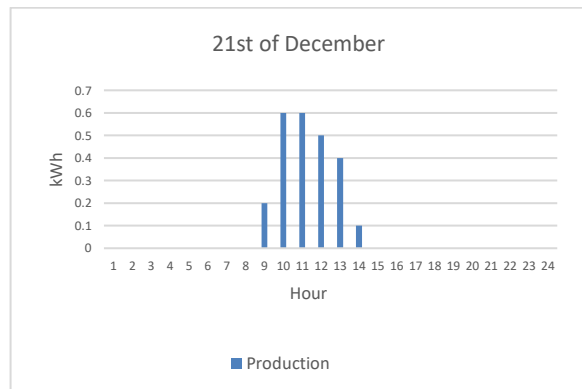
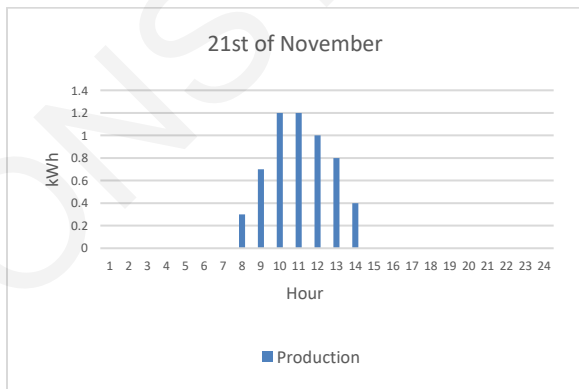
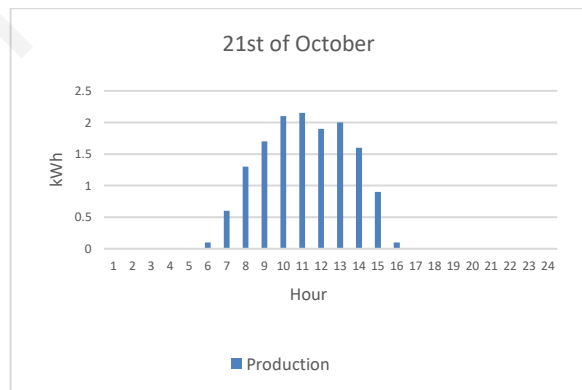
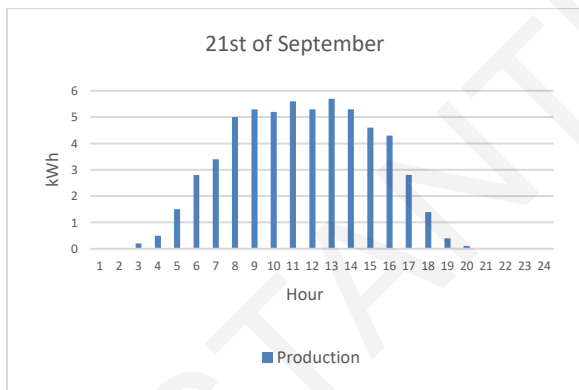
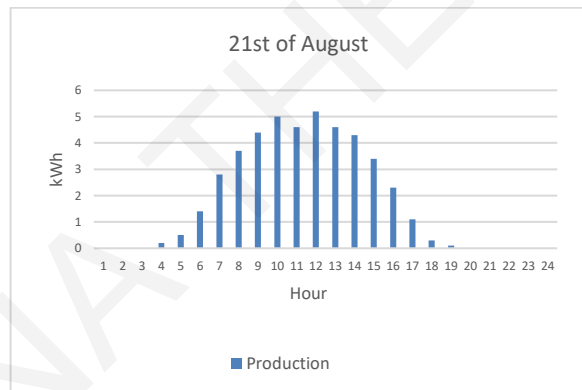
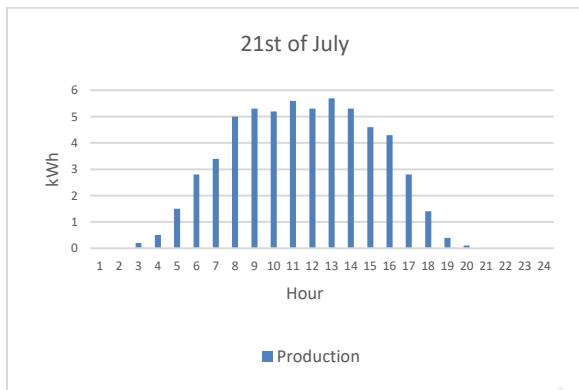
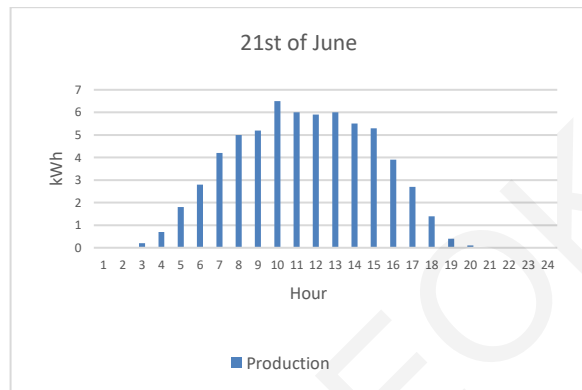
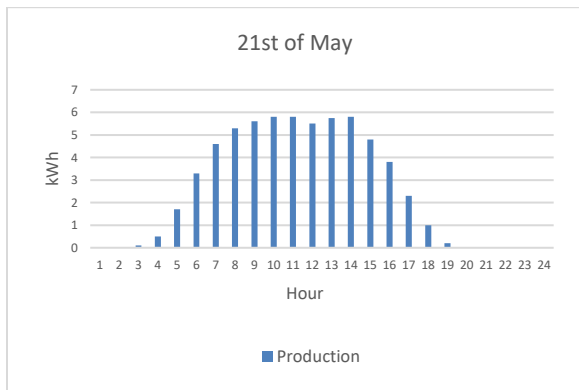


Month	Min Air Temperature	Max Air Temperature	Min Module Temperature	Max Module Temperature
January	-4	-2	-1	-0.5
February	2	1.5	1.5	-0.5
March	-1	2	-0.5	2.5
April	1	8	0	5
May	7	15	2	8
June	10	18	3.5	9
July	13.5	20	4	10
August	13	19	4	9
September	9	14	3	7
October	5	8.5	2	4
November	1	3	0	2
December	-2	-0.5	-0.5	0

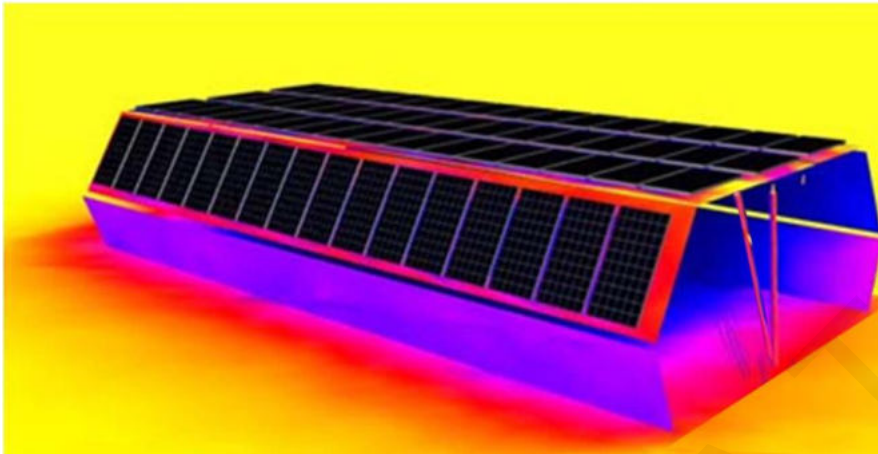




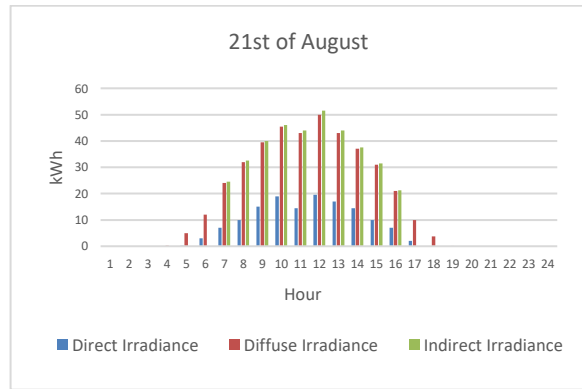
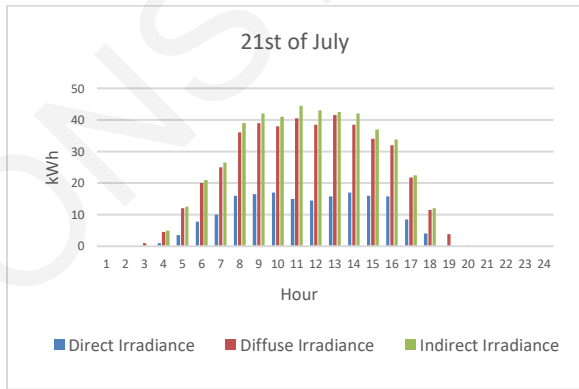
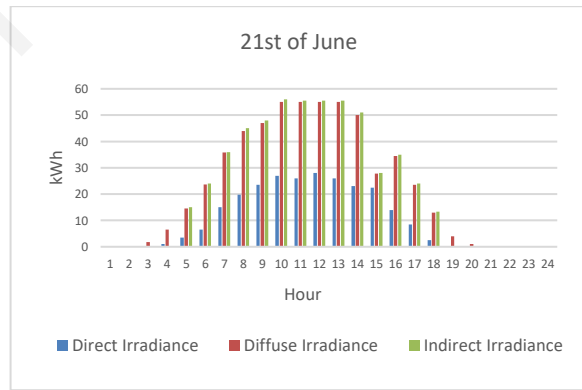
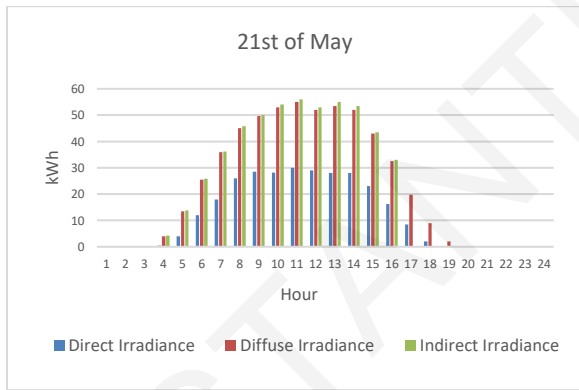
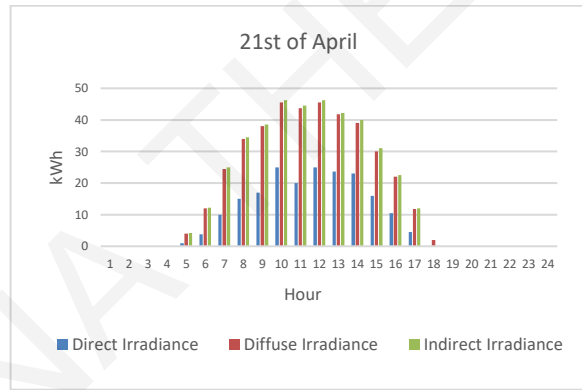
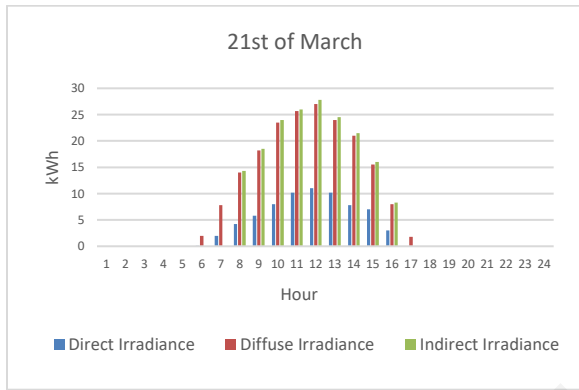
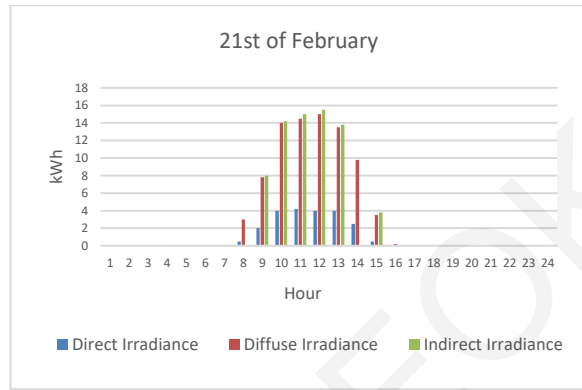
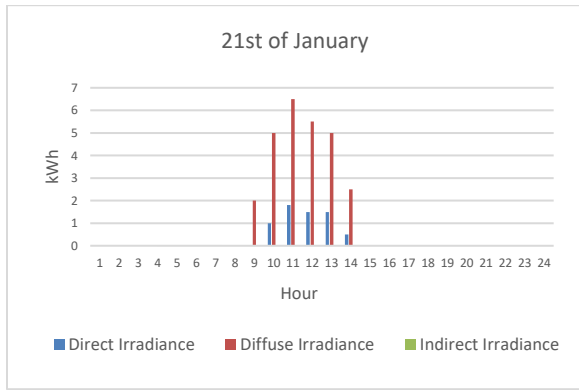
APPENDIX



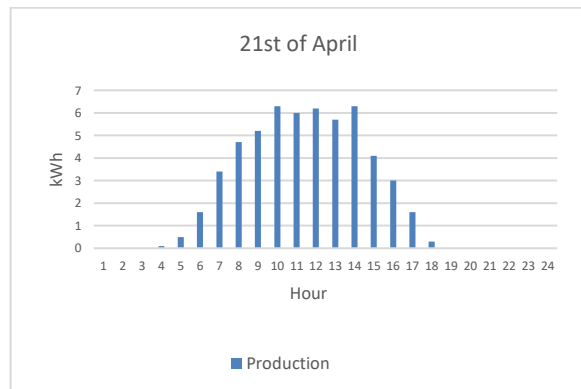
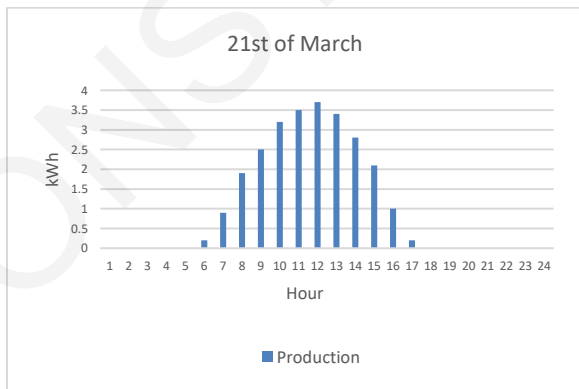
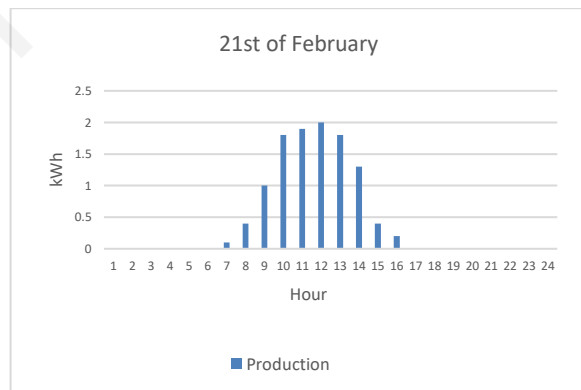
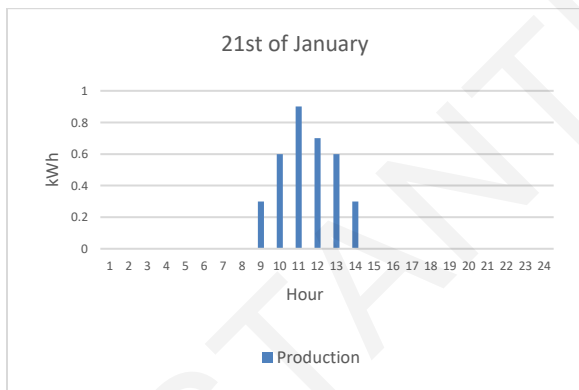
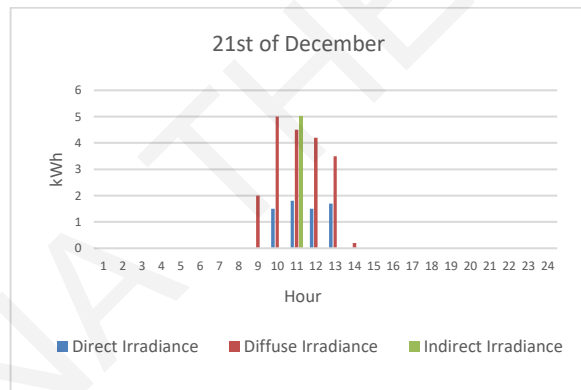
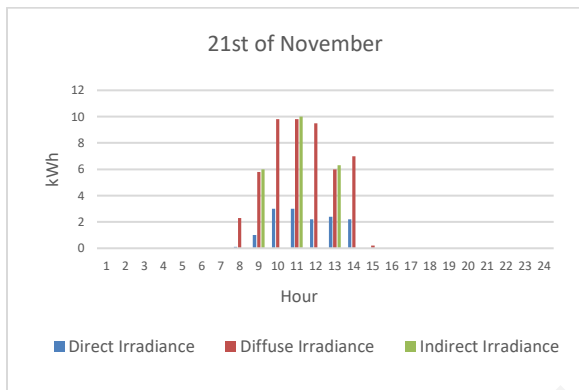
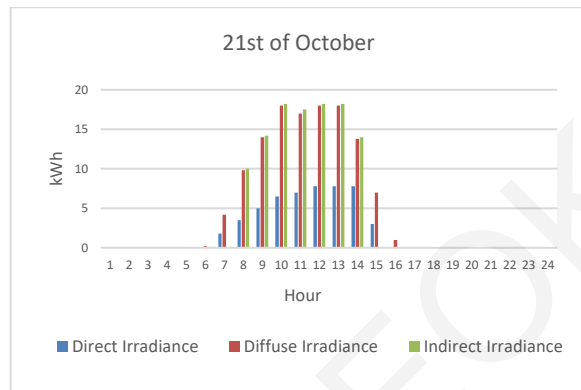
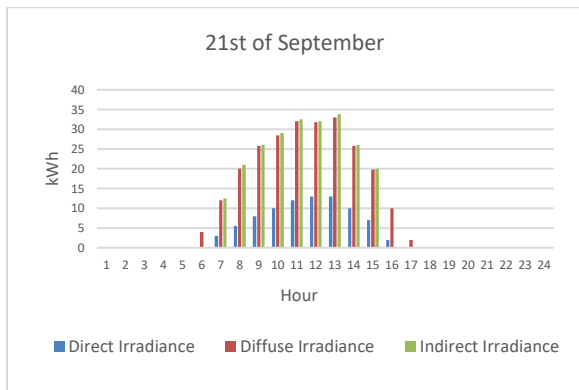
Target Position C



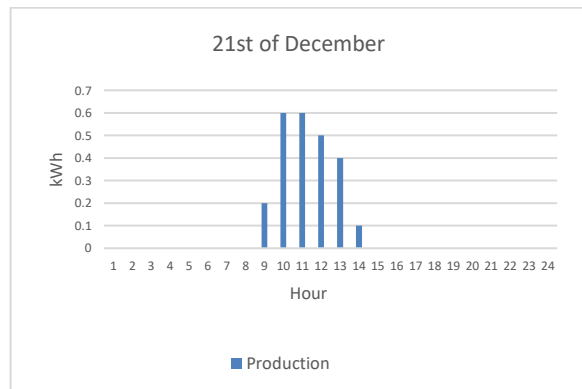
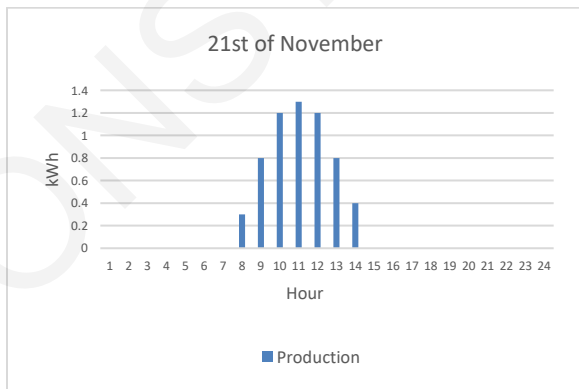
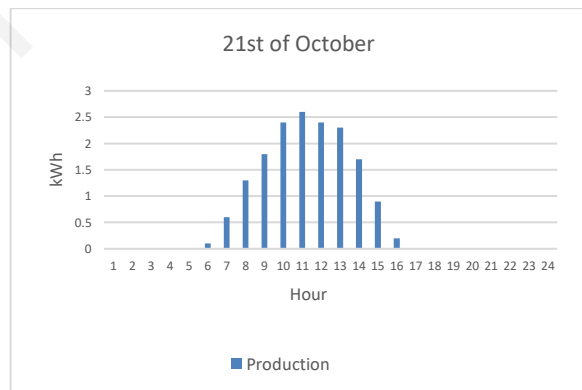
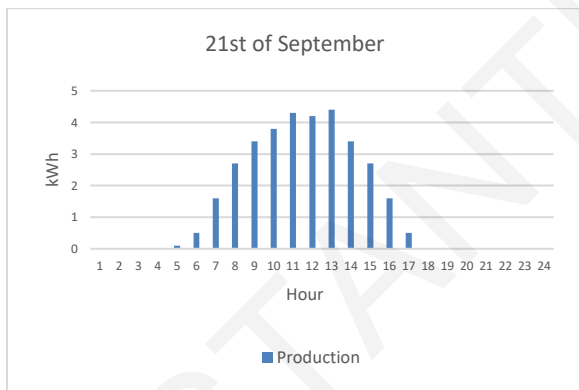
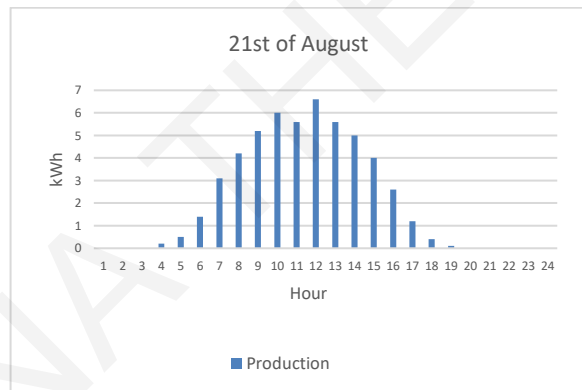
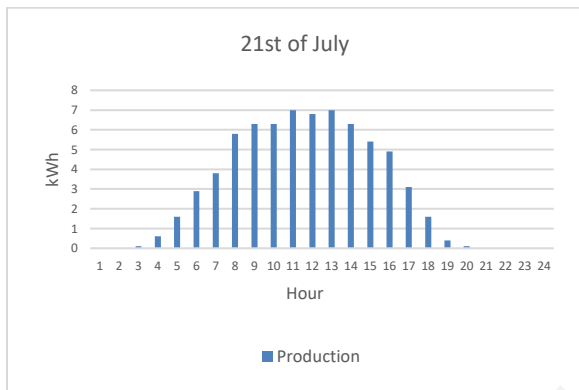
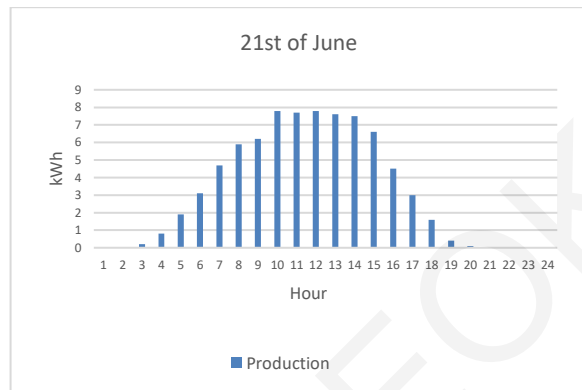
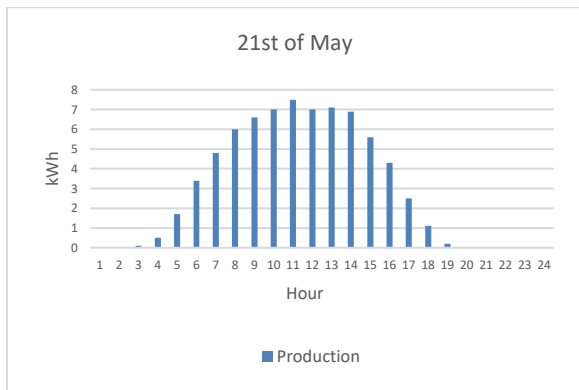
Month	Min Air Temperature	Max Air Temperature	Min Module Temperature	Max Module Temperature
January	-4	-2	-1	-0.5
February	2	1.5	1.5	-0.5
March	-1	2	-0.5	2.5
April	1	8	0	5
May	7	15	2	8
June	10	18	3.5	9
July	13.5	20	4	10
August	13	19	4	9
September	9	14	3	7
October	5	8.5	2	4
November	1	3	0	2
December	-2	-0.5	-0.5	0



APPENDIX



APPENDIX



REFERENCES**CHAPTER 1**

- [1.1] Rosenberg, D., Indeterminate architecture: Scissor-pair transformable structures. Footprint, Vol. 6, pp. 19-40, 2010
- [1.2] Rubio, F., Valero, F., Llopis-Albert, C., A review of mobile robots: Concepts, methods, theoretical framework, and applications. International Journal of Advanced Robotic Systems, Vol. 16, No 2, pp. 1-22, 2019
- [1.3] Matheou, M., Phocas, M.C., Christoforou, E.G., Müller, A., On the kinetics of reconfigurable hybrid structures, Building Engineering, Vol. 17, pp. 32-42, 2018
- [1.4] Duffy, J., Rooney, J., Knight, B., Crane, C., A review of a family of self-deploying tensegrity structures with elastic ties. The Shock and Vibration Digest, Vol. 32, No. 2, pp. 100-106, 2000
- [1.5] Akgun, Y., Gantes, J.C., Kalochairetis, K., Kiper, G., A novel concept of convertible roofs with high transformability consisting of planar scissor-hinge structures. Engineering Structures, Vol. 32, No. 9, pp. 2873-2883, 2010
- [1.6] Londono, N., Deployable stage: Proposal of an application with mobile structures. SMia, 23/04/2013
<https://smia-experimental.com/2013/04/23deployable-stage-proposal-of-an-application-with-mobile-structures-2/> Accessed: 04/2020
- [1.7] Dunnel, T., Rolling Bridge, London, England., Atlas Obscura,
<https://www.atlasobscura.com/places/rolling-bridge> Accessed 04/2020
- [1.8] Motro, R., Structural morphology of tensegrity systems. International Journal of Space Structures, Vol. 11, pp. 233-240, 2003
- [1.9] Fuller, B., Buckminster, R., Marks, R., The Dymaxion World of Buckminster Fuller. Doubleday Anchor Books, New York, 1973
- [1.10] Hanaor, A., Preliminary investigation of double-layer tensegrities, In: H. Topping (ed.), Proceedings of International Conference on the Design and Construction of Non-

- conventional Structures, Vol. 2, Edinburgh, Scotland: Civil-Comp press, pp. 757-769, 1987
- [1.11] Pugh A.: An Introduction to Tensegrity. University of California Press, Berkeley, California, 1976
- [1.12] Barbarigos, R.L., Motro, R., Smith, F.C.I., A transformable tensegrity-ring footbridge. IASS Symposium 2012: From Spatial Structures to Space Structures, Seoul, Korea, May 21-24, 2012
- [1.13] Adam, B., Smith, L, Active tensegrity: A control framework for an adaptive civil engineering structure. Computers & Structures, Vol. 86, No. 23-24, pp. 2215-2223, 2008
- [1.14] Phocas, M.C., Matheou, M., Christoforou, E.G., Design and Simulation analysis of a kinetic strut cable beam structure. In: C. Ripley, M. Asefi (eds), International Conference on Adaptation and Movement in Architecture, ICAMA 2013. Toronto, Ryerson University, pp. 224-236, 2013
- [1.15] Dimitriou, P., Phocas, M.C., Kontovourkis, O., Matheou, M., Christoforou, E.G., Deployment and reconfiguration approach of linkage structures. In: M. Gorgolewski, M. Asefi (eds), Proceedings of International Conference on Emerging Technologies in Architectural Design (ICETAD2019). Toronto, Canada, p. 1-8, 2019
- [1.16] Christoforou, E.G., Phocas, M.C., Matheou, M., Muller, A., Experimental implementation of the ‘effective 4 bar method’ on a reconfigurable articulated structure. Engineering Structures, Structures. Vol. 20, pp. 157-165, August 2019
- [1.17] Phocas, M.C., Christoforou, E.G., Matheou, M., Design motion planning and control of a reconfigurable hybrid structure. Engineering Structures, Vol. 101, No 29, pp. 376-385, 2015

CHAPTER 4

- [4.1] Knippers, J., Cremers, J., Gabler, M., Lienhard, J., Construction Manual for Polymers + Membranes. Institut für Internationale Architektur – Dokumentation, Munich, 2011.
- [4.2] LeCuyer, A., ETFE Technology and Design. Birkhäuser, June 2008

- [4.3] ETFE Architecture in Modern Design. <https://www.etfe-film.com/etfe-membrane>
Accessed 12/2020

CHAPTER 5

- [5.1] Burgess D., Thin-film solar cell, Encyclopedia Britannica.
<https://www.britannica.com/technology/thin-film-solar-cell> Accessed 12/2020
- [5.2] Athienitis, A.K., Barone, G., Buonomano, A., Palombo, A., Assessing active and passive effects of façade building integrated photovoltaics/thermal systems: Dynamic modelling and simulation. *Journal of Applied Energy*, Vol. 209, pp. 355-382, 2018
- [5.3] Thin film solar cell. Wikipedia Encyclopedia. https://en.wikipedia.org/wiki/Thin-film_solar_cell Accessed 11/2020
- [5.4] Brivio F., Walker A.B., Walsh A., Structural and electronic properties of hybrid perovskites for high-efficiency thin-film photovoltaics from first-principles.
<https://aip.scitation.org/doi/full/10.1063/1.4824147> Accessed 12/2020
- [5.5] PV Sites. <https://www.pvsites.eu/> Accessed 06/2019
- [5.6] EnergyPlus. <https://energyplus.net/> Accessed 01/2021
- [5.7] Department of Meteorology
http://www.moa.gov.cy/moa/ms/ms.nsf/DMLforecast_en/DMLforecast_en?OpenDocument Accessed 01/2021
- [5.8] Climate in Nicosia, Cyprus. <https://weather-and-climate.com/average-monthly-Rainfall-Temperature-Sunshine,larnaca,Cyprus> Accessed 01/2021
- [5.9] Swedish Meteorological and Hydrological Institute
<https://www.smhi.se/en/q/Paphos/146214> Accessed 01/2021
- [5.9] Muhammad, I., *An Introduction to Solar Radiation*, 1st ed. Academic Press, Don Mills, Ontario, Canada, pp. 1-28, 1983
- [5.10] Poudyal, K.N., Bhattarai, B.K., Sapkota, B.K., Kjeldstad, B., Karki, N.R., Estimation of global solar radiation using pyranometer and NILU-UV irradiance meter at Pokhara Valley in Nepal. *Journal of Institute of Engineering*. Vol. 9, pp. 69-78, 2014

- [5.11] Al-Addous, M., Dalala, Z., Class, C.B., Alawneh, F., Al-Taani, H., Performance analysis of off-grid PV systems in the Jordan valley. *Renewable Energy*, Vol. 113, pp. 930-941, 2017
- [5.12] Ma, W.W., Rasul, M.G., Liu, G., Li, M., Tan, X.H., Climate change impacts on techno-economic performance of roof PV solar system in Australia. *Renewable Energy*, Vol. 88, 430-438, 2016
- [5.13] Weather and Climate, <https://weather-and-climate.com/average-monthly-Rainfall-Temperature-Sunshine>, Stockholm, Sweden Accessed 01/2021